ILSB Report / ILSB-Arbeitsbericht 206
(supersedes CDL–FMD Report 3–1998)

A SHORT INTRODUCTION TO BASIC ASPECTS OF CONTINUUM MICROMECHANICS

Helmut J. Böhm

Institute of Lightweight Design and Structural Biomechanics (ILSB)
TU Wien, Vienna, Austria

updated: March 13, 2024

Contents

Notes on this Document

The present document is an expanded and updated version of the CDL–FMD report 3–1998, "A Short Introduction to Basic Aspects of Continuum Micromechanics", which, in turn, is based on lecture notes prepared for the European Advanced Summer Schools *Frontiers of Computational Micromechanics in Industrial and Engineering Materials* held in Galway, Ireland, in July 1998 and in August 2000. Related lecture notes were used for graduate courses in a Summer School held at Ameland, the Netherlands, in October 2000 and during the COMMAS Summer School held in September 2002 in Stuttgart, Germany. All of the above documents are related to the micromechanics section of the lecture notes for the course "Composite Engineering" (317.003) offered regularly at TU Wien.

The course notes "A Short Introduction to Continuum Micromechanics" (Böhm, 2004) for the CISM Course on *Mechanics of Microstructured Materials* held in July 2003 in Udine, Italy, may be regarded as a compact version of a precursor to the present report that employs a somewhat different notation. The course notes "Analytical and Numerical Methods for Modeling the Thermomechanical and Thermophysical Behavior of Microstructured Materials" (Böhm et al., 2009) are also related to the present report, but emphasize different aspects of continuum micromechanics, among them the thermal conduction behavior of inhomogeneous materials and the modeling of cellular materials.

The ILSB Report 206 is being updated periodically to reflect current developments in continuum micromechanics as seen by the author; its most recent version can be accessed via `https://www.ilsb.tuwien.ac.at/links/downloads/ilsbrep206.pdf`. Due to the dynamic nature of the document it is suggested that in citing it the time stamp should be given. A somewhat dated version of this report (August 12, 2015) can be accessed via the DOI: 10.13140/RG.2.1.3025.7127.

A type of Voigt/Nye notation is used for the mechanical variables in chapters 1 to 3. Tensors of order 4, such as elasticity, compliance, concentration and Eshelby tensors, are written as 6×6 (quasi-)matrices, and stress- as well as strain-like tensors of order 2 as 6-(quasi-)vectors. These 6-vectors are connected to index notation by the relations

$$\boldsymbol{\sigma} = \begin{pmatrix} \sigma_1 \\ \sigma_2 \\ \sigma_3 \\ \sigma_4 \\ \sigma_5 \\ \sigma_6 \end{pmatrix} \Leftrightarrow \begin{pmatrix} \sigma_{11} \\ \sigma_{22} \\ \sigma_{33} \\ \sigma_{12} \\ \sigma_{13} \\ \sigma_{23} \end{pmatrix} \qquad \boldsymbol{\varepsilon} = \begin{pmatrix} \varepsilon_1 \\ \varepsilon_2 \\ \varepsilon_3 \\ \varepsilon_4 \\ \varepsilon_5 \\ \varepsilon_6 \end{pmatrix} \Leftrightarrow \begin{pmatrix} \varepsilon_{11} \\ \varepsilon_{22} \\ \varepsilon_{33} \\ \gamma_{12} \\ \gamma_{13} \\ \gamma_{23} \end{pmatrix} \quad ,$$

where $\gamma_{ij} = 2\varepsilon_{ij}$ are the shear angles[1] ("engineering shear strains"). Tensors of order 4 are denoted by bold upper case letters, stress- and strain-like tensors of order 2 by bold lower case Greek letters, and 3-vectors by bold lower case letters. Conductivity-like tensors of order 2 are treated as 3×3 matrices and denoted by calligraphic upper case letters. All other variables are taken to be scalars.

In using the present notation it is assumed that the 4th-order tensors show orthotropic or higher symmetry and that the material axes are aligned with the coordinate system where appropriate. Details of the ordering of the components of $\boldsymbol{\varepsilon}$ and $\boldsymbol{\sigma}$ will not impact formulae. It is worth noting, however, that with a notation like the present one some coefficients of Eshelby tensors differ from their equivalents in index notation, compare Pedersen (1983).

The tensor product between two tensors of order 2 as well as the dyadic product between two vectors are denoted by the symbol "⊗", where $[\boldsymbol{\eta} \otimes \boldsymbol{\zeta}]_{ijkl} = \eta_{ij}\zeta_{kl}$, and $[\mathbf{a} \otimes \mathbf{b}]_{ij} = a_i b_j$, respectively. The contraction between a tensor of order 2 and a 3-vector is denoted by the symbol "∗", where $[\boldsymbol{\zeta} * \mathbf{n}]_i = \zeta_{ij} n_j$. Other products are defined implicitly by the types of quasi-matrices and quasi-vectors involved. A superscript $^{\mathrm{T}}$ denotes the transpose of a tensor, matrix or vector.

Constituents (phases) are denoted by superscripts, with $^{(\mathrm{p})}$ standing for a general phase, $^{(\mathrm{m})}$ for a matrix, $^{(\mathrm{i})}$ for inhomogeneities of general shape, and $^{(\mathrm{f})}$ for fibers. Axial and transverse properties of transversally isotropic materials are marked by subscripts $_A$ and $_T$, respectively, and effective (or apparent) properties are denoted by a superscript asterisk *.

The present use of phase volume fractions as microstructural parameters is valid for the microgeometries typically found in composite, porous and polycrystalline materials. Note that for penny shaped cracks a crack density parameter (O'Connell and Budiansky, 1974) is the proper choice.

[1] This notation allows strain energy densities to be obtained as the scalar product $U = \frac{1}{2}\boldsymbol{\sigma}^T\boldsymbol{\varepsilon}$.

Chapter 1

Introduction

In the present report some basic issues of and some of the modeling strategies used for studying static and quasistatic problems in continuum micromechanics of materials are discussed. The main emphasis is put on application related (or "engineering") aspects, and neither a comprehensive theoretical treatment nor a review of the pertinent literature are attempted. For more formal treatments of many of the concepts and methods discussed in the present work see, e.g., Mura (1987), Aboudi (1991), Nemat-Nasser and Hori (1993), Suquet (1997), Markov (2000), Bornert et al. (2001), Torquato (2002), Milton (2002), Qu and Cherkaoui (2006), Buryachenko (2007), Dvorak (2013), Kachanov and Sevostianov (2013), Kachanov and Sevostianov (2018) as well as Buryachenko (2022a); Yvonnet (2019) is specialized to numerical continuum micromechanics. Shorter overviews of continuum micromechanics were given, e.g., by Hashin (1983), Zaoui (2002) and Kanouté et al. (2009). Discussions of the history of the development of the field can be found in Markov (2000) and Zaoui (2002).

Due to the author's research interests, more room is given to the thermomechanical behavior of two-phase materials showing a matrix–inclusion topology ("solid dispersions") rather than to materials with other phase topologies or phase geometries.

1.1 Inhomogeneous Materials

Many industrial and engineering materials as well as the majority of biological materials are inhomogeneous, i.e., they consist of dissimilar constituents ("phases") that are distinguishable at some (small) length scale(s). Each constituent shows different material properties and/or material orientations and may itself be inhomogeneous at some smaller length scale(s). Inhomogeneous materials (also referred to as microstructured, heterogeneous or complex materials) play important roles in materials science and technology. Well-known examples of such materials are composites, concrete, polycrystalline materials, porous and cellular materials, functionally graded materials, wood, and bone.

The behavior of inhomogeneous materials is determined, on the one hand, by the relevant material properties of the constituents and, on the other hand, by their volume fractions, geometries and topologies (the "phase arrangement"). Obviously, the availability of information on these counts determines the accuracy of any model or theoretical description. The behavior of inhomogeneous materials can be studied at a number of

length scales ranging from sub-atomic scales, which are dominated by quantum effects, to scales for which continuum descriptions are best suited. The present report concentrates on continuum models for heterogeneous materials, the pertinent research field being customarily referred to as continuum micromechanics of materials. The use of continuum models puts a lower limit on the length scales that can be covered in a relatively carefree way with the methods discussed here, which typically may be taken as being of the order of 1 μm (Forest et al., 2002).

As will be discussed in Section 1.2, an important aim of bridging length scales for inhomogeneous materials lies in deducing their overall ("effective" or "apparent") behavior[2] (e.g., macroscopic stiffness, thermal expansion and strength properties, heat conduction and related transport properties, electrical and magnetic properties, electromechanical properties, etc.) from the corresponding material behavior of the constituents (as well as that of the interfaces between them) and from the geometrical arrangement of the phases. Such scale transitions from lower (finer) to higher (coarser) length scales aim at achieving a marked reduction in the number of degrees of freedom describing the system. The continuum methods discussed in this report are most suitable for (but not restricted to) handling scale transitions from length scales in the low micrometer range to macroscopic samples, components or structures with sizes of millimeters to meters.

In what follows, the main focus will be put on describing the thermomechanical behavior of inhomogeneous two-phase materials. Most of the discussed modeling approaches can, however, be extended to multi-phase materials (albeit with restrictions), and there is a large body of literature applying analogous or related continuum methods to other physical properties of inhomogeneous materials, compare, e.g., Hashin (1983), Torquato (2002) as well as Milton (2002), and see Sections 2.10 and 6.9 of the present report.

The most basic classification criterion for inhomogeneous materials is aimed at the microscopic phase topology. In matrix–inclusion arrangements ("solid suspensions", as found in particulate and fibrous materials, such as "typical" composite materials, in porous materials, and in closed-cell foams[3]) only the matrix shows a connected topology and the constituents play clearly distinct roles. In interpenetrating (interwoven, co-continuous, skeletal) phase arrangements (as found, e.g., in open-cell foams, in certain composites, or in many functionally graded materials) and in typical polycrystals ("granular materials"), in contrast, the phases cannot be readily distinguished topologically.

Obviously, an important parameter in continuum micromechanics is the level of inhomogeneity of the constituents' behavior, which is often described by a phase contrast. For example, a scalar elastic contrast of a two-phase composite may be defined in terms of the the Young's moduli of matrix and inhomogeneities (or reinforcements), $E^{(\mathrm{i})}$ and $E^{(\mathrm{m})}$, as

[2]The designator "effective material properties" is typically reserved for describing the macroscopic responses of bulk materials, whereas the term "apparent material properties" is used for the properties of finite-sized samples (Huet, 1990), for which boundary effects play a role.

[3]With respect to their thermomechanical behavior, porous and cellular materials can usually be treated as inhomogeneous materials in which one constituent shows vanishing stiffness, thermal expansion, conductivity, etc., compare Section 6.7.

$$c_{\mathrm{el}} = \frac{E^{(\mathrm{i})}}{E^{(\mathrm{m})}} \quad . \tag{1.1}$$

Analogous scalar contrasts may be defined in terms of other material parameters; for a more sophisticated elastic contrast tensor see, e.g., Sevostianov and Kachanov (2014).

Length Scales

In the present context the lowest length scale described by a given micromechanical model is termed the microscale, of characteristic length ℓ, the largest one the macroscale, of characteristic length L, and intermediate ones are called mesoscales[4]. The fields describing the behavior of an inhomogeneous material, i.e., in mechanics the stresses $\boldsymbol{\sigma}(\mathbf{x})$, strains $\boldsymbol{\varepsilon}(\mathbf{x})$ and displacements $\mathbf{u}(\mathbf{x})$, are split into contributions corresponding to the different length scales, which are referred to as micro-, macro- and mesofields, respectively. The phase geometries on the meso- and microscales are denoted as meso- and microgeometries.

Micromechanical models are based on the assumption that the length scales in a given inhomogeneous material are well separated, i.e., $\ell \ll L$. This is understood to imply that for each micro–macro pair of scales, on the one hand, the fluctuating contributions to the fields at the smaller length scale ("fast variables") influence the behavior at the larger length scale only via their volume averages. On the other hand, gradients of the fields as well as compositional gradients at the larger length scale ("slow variables") are taken to be insignificant at the smaller length scale, where these fields appear to be locally constant and can be described in terms of uniform "applied fields" or "far fields". Formally, this splitting of the strain and stress fields into slow and fast contributions can be written as

$$\boldsymbol{\varepsilon}(\mathbf{x}) = \langle \boldsymbol{\varepsilon} \rangle + \boldsymbol{\varepsilon}'(\mathbf{x}) \qquad \text{and} \qquad \boldsymbol{\sigma}(\mathbf{x}) = \langle \boldsymbol{\sigma} \rangle + \boldsymbol{\sigma}'(\mathbf{x}) \qquad , \tag{1.2}$$

where $\langle \boldsymbol{\varepsilon} \rangle$ and $\langle \boldsymbol{\sigma} \rangle$ are the macroscopic, averaged fields, whereas $\boldsymbol{\varepsilon}'(\mathbf{x})$ and $\boldsymbol{\sigma}'(\mathbf{x})$ stand for the microscopic fluctuations.

Unless specifically stated otherwise, in the present report the above conditions on the slow and fast variables are assumed to be met. If this is not the case to a sufficient degree (e.g., in the cases of insufficient separation of the length scales, of the presence of marked compositional or load gradients, of regions in the vicinity of free surfaces of inhomogeneous materials, or of macroscopic interfaces adjoined by at least one inhomogeneous material), embedding schemes, compare Chapter 8, or special analysis methods must be applied. The latter may take the form of second-order homogenization schemes that explicitly account for deformation gradients on the microscale (Kouznetsova et al., 2004) and result in nonlocal homogenized behavior, see, e.g., Feyel (2003).

Length scales below a given microscale are not necessarily amenable to continuum mechanical descriptions; for an overview of pertinent methods see, e.g., Raabe (1998).

[4]The nomenclature with respect to "micro", "meso" and "macro" is far from universal, the naming of the length scales of inhomogeneous materials being notoriously inconsistent even in literature dealing specifically with continuum micromechanics. In a more neutral way, the smaller length scale may be referred to as the "fine-grained" and the larger one as the "coarse-grained" length scale.

1.2 Homogenization and Localization

The two central aims of continuum micromechanics can be stated to be, on the one hand, the bridging of length scales and, on the other hand, studying the structure–property relationships of inhomogeneous materials.

The first of the above issues, the bridging of length scales, involves two main tasks. On the one hand, the behavior at some larger length scale (the macroscale) must be estimated or bounded by using information from a smaller length scale (the microscale), i.e., homogenization problems must be solved. The most important applications of homogenization are materials characterization, i.e., simulating the overall material response under simple loading conditions such as uniaxial tensile tests, and constitutive modeling, where the responses to general loads, load paths and loading sequences must be described. Homogenization (also referred to as "upscaling" or "coarse graining") may be interpreted as describing the behavior of a material that is inhomogeneous at some lower length scale in terms of a (fictitious) energetically equivalent, homogeneous reference material, which is sometimes referred to as the homogeneous equivalent medium (HEM). Since homogenization links the phase arrangement at the microscale to the macroscopic behavior, it will, in general, provide microstructure–property relationships. On the other hand, the local responses at the smaller length scale may be deduced from the loading conditions (and, where appropriate, from the load histories) on the larger length scale. This task, which corresponds to "zooming in" on the local fields in an inhomogeneous material, is referred to as localization, downscaling or fine graining. In either case the main inputs are the geometrical arrangement and the material behaviors of the constituents at the microscale. In many continuum micromechanical methods, homogenization is less demanding than localization because the local fields tend to show a much more marked dependence on details of the local geometry of the constituents.

For a volume element Ω_s of an inhomogeneous material that is sufficiently large, contains no significant gradients of composition, and shows no significant variations in the applied loads, homogenization relations take the form of volume averages of some variable $f(\mathbf{x})$,

$$\langle f \rangle = \frac{1}{\Omega_\mathrm{s}} \int_{\Omega_\mathrm{s}} f(\mathbf{x}) \, \mathrm{d}\Omega \qquad . \tag{1.3}$$

Accordingly, the homogenization relations for the stress and strain tensors can be expressed as

$$\begin{aligned} \langle \boldsymbol{\varepsilon} \rangle &= \frac{1}{\Omega_\mathrm{s}} \int_{\Omega_\mathrm{s}} \boldsymbol{\varepsilon}(\mathbf{x}) \, \mathrm{d}\Omega = \frac{1}{2\Omega_\mathrm{s}} \int_{\Gamma_\mathrm{s}} \left[\mathbf{u}(\mathbf{x}) \otimes \mathbf{n}_\Gamma(\mathbf{x}) + \mathbf{n}_\Gamma(\mathbf{x}) \otimes \mathbf{u}(\mathbf{x}) \right] \mathrm{d}\Gamma \\ \langle \boldsymbol{\sigma} \rangle &= \frac{1}{\Omega_\mathrm{s}} \int_{\Omega_\mathrm{s}} \boldsymbol{\sigma}(\mathbf{x}) \, \mathrm{d}\Omega = \frac{1}{\Omega_\mathrm{s}} \int_{\Gamma_\mathrm{s}} \mathbf{t}(\mathbf{x}) \otimes \mathbf{x} \, \mathrm{d}\Gamma \qquad , \end{aligned} \tag{1.4}$$

where Γ_s stands for surface of the volume element Ω_s, $\mathbf{u}(\mathbf{x})$ is the displacement vector, $\mathbf{t}(\mathbf{x}) = \boldsymbol{\sigma}(\mathbf{x}) * \mathbf{n}_\Gamma(\mathbf{x})$ is the surface traction vector, and $\mathbf{n}_\Gamma(\mathbf{x})$ is the surface normal vector. Equations (1.4) are known as the average strain and average stress theorems, and the surface integral formulation for $\boldsymbol{\varepsilon}$ given above pertains to the small strain regime and to continuous displacements. Under the latter conditions the mean strains and stresses in a

control volume, $\langle\boldsymbol{\varepsilon}\rangle$ and $\langle\boldsymbol{\sigma}\rangle$, are fully determined by the surface displacements and tractions. If the displacements show discontinuities, e.g., due to imperfect interfaces between the constituents or due to (micro) cracks, correction terms involving the displacement jumps across imperfect interfaces or cracks must be introduced, compare Nemat-Nasser and Hori (1993). In the absence of body forces the microstresses $\boldsymbol{\sigma}(\mathbf{x})$ are self-equilibrated (but in general not zero). In the above form, eqn. (1.4) applies to linear elastic behavior, but it can be modified to cover the thermoelastic regime and extended into the nonlinear range, e.g., to elastoplastic materials described by secant or incremental plasticity models, compare Section 2.9. For a discussion of averaging techniques and related results for finite deformation regimes see, e.g., Nemat-Nasser (1999).

The microscopic strain and stress fields, $\boldsymbol{\varepsilon}(\mathbf{x})$ and $\boldsymbol{\sigma}(\mathbf{x})$, in a given volume element Ω_s are formally linked to the corresponding macroscopic responses, $\langle\boldsymbol{\varepsilon}\rangle$ and $\langle\boldsymbol{\sigma}\rangle$, by localization (or projection) relations of the type

$$\boldsymbol{\varepsilon}(\mathbf{x}) = \mathbf{A}(\mathbf{x})\langle\boldsymbol{\varepsilon}\rangle \qquad \text{and} \qquad \boldsymbol{\sigma}(\mathbf{x}) = \mathbf{B}(\mathbf{x})\langle\boldsymbol{\sigma}\rangle \qquad . \tag{1.5}$$

$\mathbf{A}(\mathbf{x})$ and $\mathbf{B}(\mathbf{x})$ are known as mechanical strain and stress concentration tensors (or influence functions (Hill, 1963), influence function tensors, interaction tensors), respectively. When these are known the localization problem is solved.

Equations (1.2) and (1.4) imply that the volume averages of fluctuations vanish for sufficiently large integration volumes,

$$\langle\boldsymbol{\varepsilon}'\rangle = \frac{1}{\Omega_\mathrm{s}}\int_{\Omega_\mathrm{s}} \boldsymbol{\varepsilon}'(\mathbf{x})\,\mathrm{d}\Omega = \mathbf{o} \qquad \text{and} \qquad \langle\boldsymbol{\sigma}'\rangle = \frac{1}{\Omega_\mathrm{s}}\int_{\Omega_\mathrm{s}} \boldsymbol{\sigma}'(\mathbf{x})\,\mathrm{d}\Omega = \mathbf{o} \qquad . \tag{1.6}$$

Similarly, surface integrals over the microscopic fluctuations of the field variables tend to zero for appropriate volume elements[5].

For suitable volume elements of inhomogeneous materials that show sufficient separation between the length scales and for suitable boundary conditions the relation

$$\frac{1}{2}\langle\widetilde{\boldsymbol{\sigma}}^\mathrm{T}\,\widetilde{\boldsymbol{\varepsilon}}\rangle = \frac{1}{2\Omega}\int_\Omega \widetilde{\boldsymbol{\sigma}}^\mathrm{T}(\mathbf{x})\;\widetilde{\boldsymbol{\varepsilon}}(\mathbf{x})\,\mathrm{d}\Omega = \frac{1}{2}\langle\widetilde{\boldsymbol{\sigma}}\rangle^\mathrm{T}\,\langle\widetilde{\boldsymbol{\varepsilon}}\rangle \tag{1.7}$$

must hold for general statically admissible stress fields $\widetilde{\boldsymbol{\sigma}}$ and kinematically admissible strain fields $\widetilde{\boldsymbol{\varepsilon}}$, compare Hill (1967) and Mandel (1972). This equation is known as Hill's macrohomogeneity condition, the Hill–Mandel condition or the energy equivalence condition, compare Nemat-Nasser (1999), Bornert (2001) and Zaoui (2001). Equation (1.7) states that the strain energy density of the microfields equals the strain energy density of the macrofields, making the microscopic and macroscopic descriptions energetically equivalent. Interestingly, the fluctuations of the microfields do not contribute to the macroscopic strain energy, i.e.,

$$\langle\boldsymbol{\sigma}'^\mathrm{T}\,\boldsymbol{\varepsilon}'\rangle = 0 \qquad . \tag{1.8}$$

[5]Whereas volume and surface integrals over products of slow and fast variables vanish, integrals over products of fluctuating variables ("correlations"), e.g., $\langle\boldsymbol{\varepsilon}'^2\rangle$, remain finite in general.

The Hill–Mandel condition forms the basis of the interpretation of homogenization procedures in the thermoelastic regime[6] in terms of a homogeneous comparison material (or "reference medium") that is energetically equivalent to a given inhomogeneous material.

1.3 Volume Elements

The second central issue of continuum micromechanics, studying the structure–property relationships of inhomogeneous materials, obviously requires suitable descriptions of their structure at the appropriate length scale, i.e., within the present context, their microgeometries.

The microgeometries of real inhomogeneous materials are at least to some extent random and, in the majority of cases of practical relevance, their detailed phase arrangements are highly complex. As a consequence, exact expressions for $\mathbf{A}(\mathbf{x})$, $\mathbf{B}(\mathbf{x})$, $\boldsymbol{\varepsilon}(\mathbf{x})$, $\boldsymbol{\sigma}(\mathbf{x})$, etc., in general cannot be given with reasonable effort, and approximations have to be introduced. Typically, these approximations are based on the ergodic hypothesis, i.e., the heterogeneous material is assumed to be statistically homogeneous. This implies that sufficiently large volume elements selected at random positions within a sample have statistically equivalent phase arrangements and give rise to the same averaged material properties[7]. As mentioned above, such material properties are referred to as the overall or effective material properties of the inhomogeneous material.

Ideally, the homogenization volume should be chosen to be a proper representative volume element (RVE) as defined by Hill (1963), which essentially is a subvolume of Ω_s of sufficient size to contain all information necessary for describing the behavior of the composite. Representative volume elements have been defined, on the one hand, by requiring them to be statistically representative of a given microgeometry in terms of purely geometry-based descriptors, the resulting "geometrical RVEs" being independent of the physical property to be studied. On the other hand, their definition can be based on the requirement that the overall responses with respect to some given physical behavior do not depend on the actual position of the RVE nor on the boundary conditions applied to it[8]. The size of such "physical RVEs" depends not only on the microgeometry, but also on the physical property considered. Bornert (2001) argued that, for given microgeometries, geometrically representative volumes are always smaller than mechanically (and thus

[6] For a discussion of the Hill–Mandel condition for finite deformations and related issues see, e.g., Khisaeva and Ostoja-Starzewski (2006).

[7] Some inhomogeneous materials are not statistically homogeneous by design, e.g., functionally graded materials in the direction(s) of the gradient(s), and, consequently, may require nonstandard treatment. For such materials it is not possible to define effective material properties in the sense of eqn. (1.10). Deviations from statistical homogeneity may also be introduced into inhomogeneous materials as side effects of manufacturing processes.

[8] These two approaches emphasize different aspects of the original definition of Hill (1963), which requires the RVE of an inhomogeneous material to be (a) "entirely typical of the whole mixture on average" and to contain (b) "a sufficient number of inclusions for the apparent properties to be independent of the surface values of traction and displacement, so long as these values are macroscopically uniform".
Alternatively, less stringent definitions were proposed, e.g., regarding an RVE as the "smallest possible structure that could sufficiently capture the macroscopic response" of an inhomogeneous material (Firooz et al., 2019).

physically) representative ones. For alternative definitions of RVEs see, e.g., Bouhfid et al. (2019).

Within either definition, an RVE must be sufficiently large to allow a meaningful sampling of the microscopic fields and sufficiently small for the influence of macroscopic gradients to be negligible. In addition, it must be smaller than typical samples or components[9]. For further discussion of microgeometries and homogenization volumes see Section 5.1. For methods involving the analysis of discrete volume elements, the latter must, in addition, be sufficiently small for an analysis of the microfields to be feasible.

The fields in a constituent $^{(\mathrm{p})}$ can be split into phase averages and fluctuations by analogy to eqn. (1.2) as

$$\boldsymbol{\varepsilon}^{(\mathrm{p})}(\mathbf{x}) = \langle\boldsymbol{\varepsilon}\rangle^{(\mathrm{p})} + \boldsymbol{\varepsilon}^{(\mathrm{p})\prime}(\mathbf{x}) \qquad \text{and} \qquad \boldsymbol{\sigma}^{(\mathrm{p})}(\mathbf{x}) = \langle\boldsymbol{\sigma}\rangle^{(\mathrm{p})} + \boldsymbol{\sigma}^{(\mathrm{p})\prime}(\mathbf{x}) \qquad . \tag{1.9}$$

The $\boldsymbol{\varepsilon}^{(\mathrm{p})\prime}(\mathbf{x})$ and $\boldsymbol{\sigma}^{(\mathrm{p})\prime}(\mathbf{x})$ are referred to as intra-phase fluctuations, whereas differences between the $\langle\boldsymbol{\varepsilon}\rangle^{(\mathrm{p})}$ and $\langle\boldsymbol{\sigma}\rangle^{(\mathrm{p})}$ describe the inter-phase heterogeneity of the fields. In the case of materials with matrix–inclusion topology the variations of the fields between the individual particles or fibers making up the inhomogeneity phase, the inter-particle or inter-fiber fluctuations, and the field gradients within individual inhomogeneities, the intra-particle or intra-fiber fluctuations, may also be of interest.

Needless to say, volume elements should be chosen to be as simple possible in order to limit the modeling effort, but their level of complexity must be sufficient for covering the aspects of their behavior targeted by a given study, compare, e.g., the examples given by Forest et al. (2002).

1.4 Overall Behavior, Material Symmetries

The homogenized strain and stress fields of an elastic inhomogeneous material as obtained by eqn. (1.4), $\langle\boldsymbol{\varepsilon}\rangle$ and $\langle\boldsymbol{\sigma}\rangle$, can be linked by effective elastic tensors $\mathbf{E}^*$ and $\mathbf{C}^*$ as

$$\langle\boldsymbol{\sigma}\rangle = \mathbf{E}^*\langle\boldsymbol{\varepsilon}\rangle \qquad \text{and} \qquad \langle\boldsymbol{\varepsilon}\rangle = \mathbf{C}^*\langle\boldsymbol{\sigma}\rangle \qquad , \tag{1.10}$$

which may be viewed as the elasticity tensor (or "tensor of elastic moduli") and compliance tensor, respectively, of an appropriate, energetically equivalent homogeneous material, with $\mathbf{C}^* = \mathbf{E}^{*-1}$. Using eqns. (1.4) and (1.5) these effective elastic tensors can be obtained from the local elastic tensors, $\mathbf{E}(\mathbf{x})$ and $\mathbf{C}(\mathbf{x})$, and the concentration tensors, $\mathbf{A}(\mathbf{x})$ and $\mathbf{B}(\mathbf{x})$, by volume averaging

$$\begin{aligned} \mathbf{E}^* &= \frac{1}{\Omega_\mathrm{s}} \int_{\Omega_\mathrm{s}} \mathbf{E}(\mathbf{x})\mathbf{A}(\mathbf{x})\mathrm{d}\Omega \\ \mathbf{C}^* &= \frac{1}{\Omega_\mathrm{s}} \int_{\Omega_\mathrm{s}} \mathbf{C}(\mathbf{x})\mathbf{B}(\mathbf{x})\mathrm{d}\Omega \qquad , \end{aligned} \tag{1.11}$$

[9] This requirement was symbolically denoted as MICRO≪MESO≪MACRO by Hashin (1983), where MICRO and MACRO have their "usual" meanings and MESO stands for the length scale of the homogenization volume. As noted by Nemat-Nasser (1999) it is the dimension relative to the microstructure relevant for a given problem that is important for the size of an RVE.

Other effective properties of inhomogeneous materials, e.g., tensors describing their thermophysical behavior, can be evaluated in an analogous way.

The resulting homogenized behavior of many multi-phase materials can be idealized as being statistically isotropic or quasi-isotropic (e.g., for composites reinforced with spherical particles, randomly oriented particles of general shape or randomly oriented fibers, many polycrystals, many porous and cellular materials, random mixtures of two phases) or statistically transversally isotropic (e.g., for composites reinforced with aligned fibers or platelets, composites reinforced with nonaligned reinforcements showing a planar random or other axisymmetric orientation distribution function, etc.), compare (Hashin, 1983). Of course, lower material symmetries of the homogenized response may also be found, e.g., in textured polycrystals or in composites containing reinforcements with orientation distributions of low symmetry, compare Allen and Lee (1990).

Statistically isotropic multi-phase materials show the same overall behavior in all directions, and their effective elasticity tensors and thermal expansion tensors take the forms

$$\mathbf{E}^* = \begin{pmatrix} E^*_{11} & E^*_{12} & E^*_{12} & 0 & 0 & 0 \\ E^*_{12} & E^*_{11} & E^*_{12} & 0 & 0 & 0 \\ E^*_{12} & E^*_{12} & E^*_{11} & 0 & 0 & 0 \\ 0 & 0 & 0 & E^*_{44} & 0 & 0 \\ 0 & 0 & 0 & 0 & E^*_{44} & 0 \\ 0 & 0 & 0 & 0 & 0 & E^*_{44} = \frac{1}{2}(E^*_{11} - E^*_{12}) \end{pmatrix} \qquad \boldsymbol{\alpha}^* = \begin{pmatrix} \alpha^* \\ \alpha^* \\ \alpha^* \\ 0 \\ 0 \\ 0 \end{pmatrix} \tag{1.12}$$

in Voigt/Nye notation. Two independent parameters are sufficient for describing isotropic overall linear elastic behavior (e.g., the effective Young's modulus $E^* = E^*_{11} - 2{E^*_{12}}^2/(E^*_{11} + E^*_{12})$, the effective Poisson's ratio $\nu^* = E^*_{12}/(E^*_{11} + E^*_{12})$, the effective shear modulus $G^* = E^*_{44} = E^*/2(1+\nu^*)$, the effective bulk modulus $K^* = (E^*_{11}+2E^*_{12})/3 = (E^*/3(1-2\nu^*)$, or the effective Lamé constants) and one is required for the effective thermal expansion behavior in the linear range (the effective coefficient of thermal expansion $\alpha^* = \alpha^*_{11}$).

The effective elasticity and thermal expansion tensors for statistically transversally isotropic materials have the structure

$$\mathbf{E}^* = \begin{pmatrix} E^*_{11} & E^*_{12} & E^*_{12} & 0 & 0 & 0 \\ E^*_{12} & E^*_{22} & E^*_{23} & 0 & 0 & 0 \\ E^*_{12} & E^*_{23} & E^*_{22} & 0 & 0 & 0 \\ 0 & 0 & 0 & E^*_{44} & 0 & 0 \\ 0 & 0 & 0 & 0 & E^*_{44} & 0 \\ 0 & 0 & 0 & 0 & 0 & E^*_{66} = \frac{1}{2}(E^*_{22} - E^*_{23}) \end{pmatrix} \qquad \boldsymbol{\alpha}^* = \begin{pmatrix} \alpha^*_{\mathrm{A}} \\ \alpha^*_{\mathrm{T}} \\ \alpha^*_{\mathrm{T}} \\ 0 \\ 0 \\ 0 \end{pmatrix} \quad , \tag{1.13}$$

where 1 is the axial direction and 2–3 is the transverse plane of isotropy. Generally, the thermoelastic behavior of transversally isotropic materials is described by five independent elastic constants and two independent coefficients of thermal expansion. Appropriate elasticity parameters in this context are, e.g., the axial and transverse effective Young's moduli, $E^*_{\mathrm{A}} = E^*_{11} - \frac{2E^{*2}_{12}}{E^*_{22}+E^*_{23}}$ and $E^*_{\mathrm{T}} = E^*_{22} - \frac{E^*_{11}E^{*2}_{23}+E^*_{22}E^{*2}_{12}-2E^*_{23}E^{*2}_{12}}{E^*_{11}E^*_{22}-E^{*2}_{12}}$, the axial and transverse effective shear moduli, $G^*_{\mathrm{A}} = E^*_{44}$ and $G^*_{\mathrm{T}} = E^*_{66}$, the axial and transverse effective Poisson's

ratios, $\nu_{\rm A}^*{=}\nu_{12}{=}\frac{E_{12}^*}{E_{22}^*+E_{23}^*}$ and $\nu_{\rm T}^*{=}\nu_{23}{=}\frac{E_{11}^*E_{23}^*-E_{12}^{*2}}{E_{11}^*E_{22}^*-E_{12}^{*2}}$, as well as the effective transverse (plane strain) bulk modulus $K_{\rm T}^* = (E_{22}^*+E_{23}^*)/2 = E_{\rm A}^*/2[(1-\nu_{\rm T}^*)(E_{\rm A}^*/E_{\rm T}^*)-2\nu_{\rm A}^{*\,2}]$. The transverse ("in-plane") properties are related via $G_{\rm T}^* = E_{\rm T}^*/2(1+\nu_{\rm T}^*)$, but there is no general linkage between the axial properties $E_{\rm A}^*$, $G_{\rm A}^*$ and $\nu_{\rm A}^*$ beyond the above definition of $K_{\rm T}^*$. For the special case of materials consisting of aligned phases that are continuous in the 1-direction, however, the Hill (1964) connections,

$$\begin{aligned} E_{\rm A}^* &= \xi E_{\rm A}^{(\rm f)} + (1-\xi)E^{(\rm m)} + \frac{4(\nu_{\rm A}^{(\rm f)}-\nu^{(\rm m)})^2}{(1/K_{\rm T}^{(\rm f)}-1/K_{\rm T}^{(\rm m)})^2}\left(\frac{\xi}{K_{\rm T}^{(\rm f)}}+\frac{1-\xi}{K_{\rm T}^{(\rm m)}}-\frac{1}{K_{\rm T}^*}\right) \\ \nu_{\rm A}^* &= \xi \nu_{\rm A}^{(\rm f)} + (1-\xi)\nu^{(\rm m)} + \frac{\nu_{\rm A}^{(\rm f)}-\nu^{(\rm m)}}{1/K_{\rm T}^{(\rm f)}-1/K_{\rm T}^{(\rm m)}}\left(\frac{\xi}{K_{\rm T}^{(\rm f)}}+\frac{1-\xi}{K_{\rm T}^{(\rm m)}}-\frac{1}{K_{\rm T}^*}\right) \quad , \end{aligned} \tag{1.14}$$

allow the effective moduli $E_{\rm A}^*$ and $\nu_{\rm A}^*$ to be expressed by $K_{\rm T}^*$, some constituent properties, and the fiber volume fraction $\xi = \Omega^{(\rm f)}/\Omega$; see also Milton (2002). Analogous relations hold for unidirectionally reinforced composites of tetragonal macroscopic symmetry (Berggren et al., 2003). Both an axial and a transverse effective coefficient of thermal expansion, $\alpha_{\rm A}^* = \alpha_{11}^*$ and $\alpha_{\rm T}^* = \alpha_{22}^*$, are required for transversally isotropic materials.

The overall material symmetries of inhomogeneous materials and their effect on various physical properties can be treated in full analogy to the symmetries of crystals as discussed, e.g., by Nye (1957). Accordingly, deviations of predicted elastic tensors from macroscopically isotropic elastic symmetry can be assessed via a Zener (1948) anisotropy ratio, $Z = 2E_{66}^*/(E_{22}^*-E_{23}^*)$, or other anisotropy parameters, see, e.g., Kanit et al. (2006).

The influence of the overall symmetry of the phase arrangement on the overall mechanical behavior of inhomogeneous materials can be marked[10], especially in nonlinear regimes. Accordingly, it is good practice to aim at approximating the symmetry of the actual material as closely as possible in any modeling effort.

1.5 Major Modeling Strategies in Continuum Micromechanics of Materials

All micromechanical methods described in the present report can be used to carry out materials characterization, i.e., simulating the overall material response under simple loading conditions such as uniaxial tensile tests. Many homogenization procedures can also be employed directly to provide micromechanically based constitutive material models at higher length scales. This implies that they allow evaluating the full homogenized stress and strain tensors for any pertinent loading condition and for any pertinent loading history[11].

[10] Overall properties described by tensors or lower rank, e.g., thermal expansion and thermal conduction, are less sensitive to material symmetry effects than are mechanical responses, compare Nye (1957).

[11] The overall thermomechanical behavior of homogenized materials is often richer than that of the constituents, i.e., the effects of the interaction of the constituents in many cases cannot be satisfactorily described by simply adapting material parameters without changing the functional relationships in the constitutive laws of the constituents. For example, a composite consisting of a matrix that follows J_2 plasticity and elastic reinforcements shows some pressure dependence in its macroscopic plastic behavior,

This task is obviously much more demanding than materials characterization. Compared to semi-empirical constitutive laws, as proposed, e.g., by Davis (1996), micromechanically based constitutive models have both a clear physical basis and an inherent capability for "zooming in" on the local phase stresses and strains by using localization procedures.

Evaluating the local responses of the constituents (in the ideal case, at any material point) for a given macroscopic state of a sample or structure, i.e., localization, is of special interest for identifying local deformation mechanisms and for studying as well as assessing local strength relevant behavior, such as the onset and progress of plastic yielding or of damage, which, of course, can have major repercussions on the macroscopic behavior. For valid descriptions of local strength-relevant responses details of the microgeometry tend to be of major importance and may, in fact, determine the macroscopic response, an extreme case being the mechanical strength of brittle inhomogeneous materials.

Because for realistic phase distributions an exact analysis of the spatial variations of the microfields in large volume elements tends to be beyond present capabilities[12] suitable approximations must be introduced. For convenience, the majority of the resulting modeling approaches may be treated as falling into two groups. The first of these comprises methods that describe interactions, e.g., between phases or between individual reinforcements, in a collective way, its main representatives being

- Mean-Field Approaches (MFAs) and related methods (see Chapter 2): Highly idealized microgeometries are used (compare, e.g., fig 2.1) and the microfields within each constituent are approximated by their phase averages $\langle\boldsymbol{\varepsilon}\rangle^{(\mathrm{p})}$ and $\langle\boldsymbol{\sigma}\rangle^{(\mathrm{p})}$, i.e., phase-wise uniform stress and strain fields are employed. The phase geometry enters these models, sometimes implicitly, via statistical descriptors, such as volume fractions, macroscopic symmetry, phase topology, reinforcement aspect ratios, etc. In MFAs the localization relations take the form

$$\begin{aligned} \langle\boldsymbol{\varepsilon}\rangle^{(\mathrm{p})} &= \bar{\mathbf{A}}^{(\mathrm{p})}\langle\boldsymbol{\varepsilon}\rangle \\ \langle\boldsymbol{\sigma}\rangle^{(\mathrm{p})} &= \bar{\mathbf{B}}^{(\mathrm{p})}\langle\boldsymbol{\sigma}\rangle \end{aligned} \tag{1.15}$$

  and the homogenization relations can be written as

$$\begin{aligned} \langle\boldsymbol{\varepsilon}\rangle^{(\mathrm{p})} &= \frac{1}{\Omega^{(\mathrm{p})}}\int_{\Omega^{(\mathrm{p})}} \boldsymbol{\varepsilon}(\mathbf{x})\,\mathrm{d}\Omega \qquad \text{with} \qquad \langle\boldsymbol{\varepsilon}\rangle = \sum\nolimits_{\mathrm{p}} V^{(\mathrm{p})}\langle\boldsymbol{\varepsilon}\rangle^{(\mathrm{p})} \\ \langle\boldsymbol{\sigma}\rangle^{(\mathrm{p})} &= \frac{1}{\Omega^{(\mathrm{p})}}\int_{\Omega^{(\mathrm{p})}} \boldsymbol{\sigma}(\mathbf{x})\,\mathrm{d}\Omega \qquad \text{with} \qquad \langle\boldsymbol{\sigma}\rangle = \sum\nolimits_{\mathrm{p}} V^{(\mathrm{p})}\langle\boldsymbol{\sigma}\rangle^{(\mathrm{p})} \end{aligned} \quad , \tag{1.16}$$

  where $^{(\mathrm{p})}$ denotes a given phase of the material, $\Omega^{(\mathrm{p})}$ is the volume occupied by this phase, and $V^{(\mathrm{p})}{=}\Omega^{(\mathrm{p})}/\sum_{\mathrm{k}}\Omega^{(\mathrm{k})}{=}\Omega^{(\mathrm{p})}/\Omega_{\mathrm{s}}$ is the volume fraction of the phase. In contrast to eqn. (1.5) the phase concentration tensors $\bar{\mathbf{A}}$ and $\bar{\mathbf{B}}$ used in MFAs are

and the macroscopic flow behavior of inhomogeneous materials can lose normality even though that of each of the constituents is associated (Li and Ostoja-Starzewski, 2006). Also, two dissimilar constituents following Maxwell-type linear viscoelastic behavior do not necessarily give rise to a macroscopic Maxwell behavior (Barello and Lévesque, 2008).

[12] Exact predictions of the effective properties would require an infinite set of correlation functions for statistically characterizing the inhomogeneous microstructure, compare Torquato et al. (1999).

not functions of the spatial coordinates[13].
Mean-field approaches tend to be formulated (and provide estimates for effective properties) in terms of the phase concentration tensors, they pose low computational requirements, and they have been highly successful in describing the thermoelastic response of inhomogeneous materials. Their use in modeling nonlinear composites continues to be a subject of active research. Their most important representatives are effective-field and effective-medium approximations.

- Bounding Methods (see Chapter 3): Variational principles are used to obtain upper and (in many cases) lower bounds on the overall elastic tensors, elastic moduli, secant moduli, and other physical properties of inhomogeneous materials the microgeometries of which are described by statistical parameters. Many analytical bounds are obtained on the basis of phase-wise constant stress polarization fields, making them closely related to MFAs. Bounds — in addition to their intrinsic value — are tools of vital importance in assessing other models of inhomogeneous materials. Furthermore, in most cases one of the bounds provides useful estimates for the physical property under consideration, even if the bounds are rather slack (Torquato, 1991).

Because they do not explicitly account for pair-wise or multi-particle interactions mean-field approaches have sometimes been referred to as "non-interacting approximations" in the literature. This designator, however, is best limited to the dilute regime in the sense of Section 2.2, collective interactions being explicitly incorporated into mean-field models for non-dilute volume fractions. MFA and bounding methods implicitly postulate the existence of a representative volume element.

The second group of approximations are based on studying discrete microgeometries, for which they aim at evaluating the microfields at high resolution, thus fully accounting for the interactions between phases within the "simulation box". It includes the following groups of models, compare the sketches in fig. 1.1.

- Periodic Microfield Approaches (PMAs), often referred to as periodic homogenization schemes and sometimes as unit cell methods, see Chapter 6. In such models the inhomogeneous material is approximated by an infinitely extended model material with a periodic phase arrangement. The resulting periodic microfields are usually evaluated by analyzing a repeating volume element (which may describe microgeometries ranging from rather simplistic to highly complex ones) via analytical or numerical methods. Such approaches are often used for performing materials characterization of inhomogeneous materials in the nonlinear range, but they can also be employed as micromechanically based constitutive models. The high resolution of the microfields provided by PMAs can be very useful in studying the initiation of damage at the microscale. However, because they inherently give rise to periodic configurations of damage and patterns of cracks, PMAs typically are not a good choice for investigating phenomena such as the interaction of the microgeometry with macroscopic cracks.
Periodic microfield approaches can give detailed information on the local stress and

[13]Surface integral formulations analogous to eqn. (1.4) may be used to evaluate consistent expressions for $\langle \boldsymbol{\varepsilon} \rangle^{(\mathrm{p})}$ for void-like and $\langle \boldsymbol{\sigma} \rangle^{(\mathrm{p})}$ for rigid inhomogeneities embedded in a matrix.

strain fields within a given unit cell, but they tend to be relatively expensive computationally. Among the methods in the present group they are the only ones that do not intrinsically give rise to boundary layers in the microfields.

- Windowing Approaches (see Chapter 7): Subregions ("windows") — usually, but not necessarily, of rectangular or hexahedral shape — are randomly chosen from a given phase arrangement and subjected to boundary conditions that guarantee energy equivalence between the micro- and macroscales. Accordingly, windowing methods describe the behavior of individual inhomogeneous samples rather than of inhomogeneous materials and typically give rise to apparent rather than effective macroscopic responses. For the special cases of macrohomogeneous stress and strain boundary conditions, respectively, lower and upper estimates for and bounds on the overall behavior of the inhomogeneous material can be obtained. In addition, mixed homogeneous boundary conditions can be applied in order to generate estimates.

- Embedded Cell or Embedding Approaches (ECAs; see Chapter 8): The inhomogeneous material is approximated by a model consisting of a "core" containing a discrete phase arrangement that is embedded within some outer region showing smeared-out material behavior; far-field loads are applied to this outer region. The material properties of the embedding layer may be described by some macroscopic constitutive law, they can be determined self-consistently or quasi-self-consistently from the behavior of the core, or the embedding region may take the form of a coarse description and/or discretization of the phase arrangement. ECAs can be used for materials characterization, and they are usually the best choice for studying regions of special interest in inhomogeneous materials, such as the surroundings of tips of macroscopic cracks. Like PMAs, embedded cell approaches can resolve local stress and strain fields in the core region at high detail, but tend to be computationally expensive.

- Other homogenization approaches employing discrete microgeometries, such as submodeling techniques (on which some remarks are given in Chapter 8), or the statistics-based non-periodic homogenization scheme of Li and Cui (2005).

Because the above group of methods explicitly study mesodomains as defined by Hashin (1983) they are sometimes referred to as "Mesoscale Approaches". Their ability of highly resolving the microfields underlies the designation "Full Field Models" and their reliance on numerical methods led to the name "Direct Numerical Simulations". Figure 1.1 shows a sketch of a volume element as well as PMA, ECA and windowing approaches applied to it.

Some further descriptions that have been applied to studying the macroscopic thermomechanical behavior of inhomogeneous materials, such as isostrain and isostress models (the former being known as the "rules of mixture") and the Halpin–Tsai equations[14] are

[14]For certain moduli of composites reinforced by particles or by continuous aligned fibers the Halpin–Tsai equations can be obtained from the estimates of Kerner (1956) and Hermans (1967), respectively. Following the procedures outlined in Halpin and Kardos (1976) these models, together with Hill's connections, eqns. (1.14), and some minor approximations, yield sets of specific "Halpin–Tsai-parameters" which, however, do not appear to have been used widely in practice. In most cases, instead, the Halpin–Tsai equations were applied in a semi-empirical way to other moduli or to other composite geometries, or were used with other sets of parameters of various provenience.

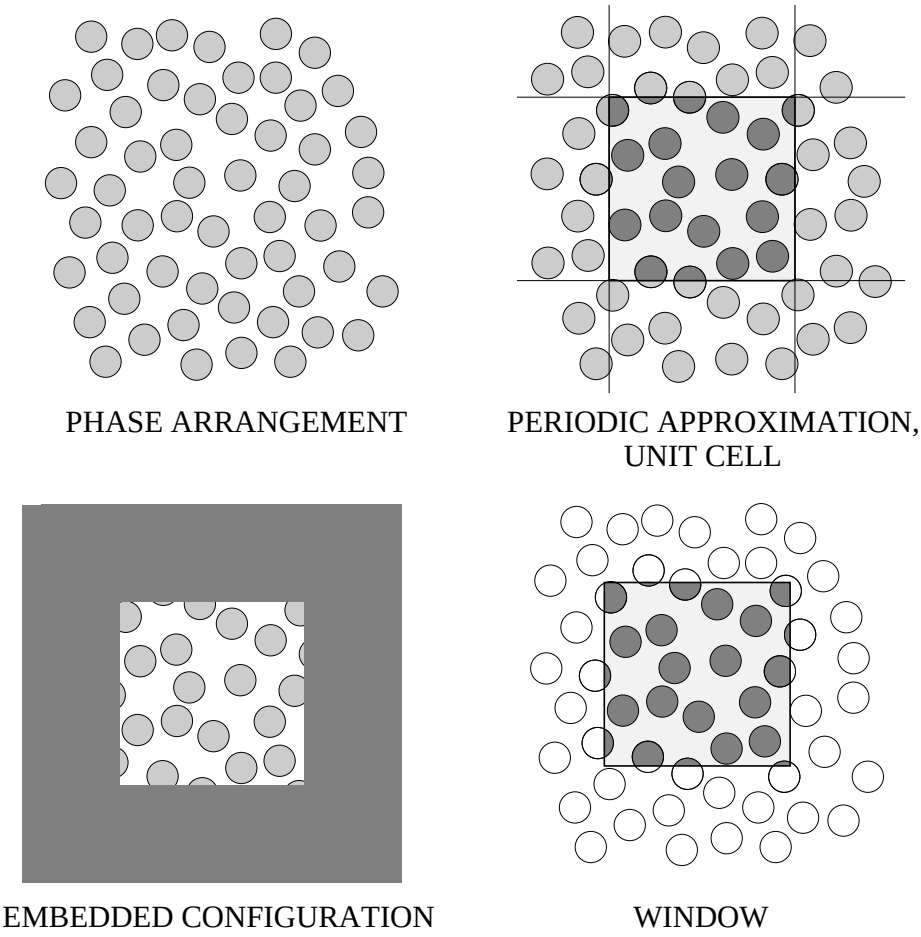

Figure 1.1: Schematic sketch of a random matrix–inclusion microstructure and of the volume elements used by a periodic microfield method (which employs a slightly different periodic "model" microstructure), an embedding scheme and a windowing approach to studying this inhomogeneous material.

not discussed here because, with the exception of special cases, their connection to actual microgeometries is not very strong, limiting their predictive capabilities. For brevity, a number of micromechanical models with solid physical basis, such as expressions for self-similar composite sphere assemblages (CSA, Hashin (1962)) and composite cylinder assemblages (CCA, Hashin and Rosen (1964)), are not covered within the present discussion, either.

For studying materials that are inhomogeneous at a number of (sufficiently widely spread) length scales (e.g., materials in which well defined clusters of inhomogeneities are present), hierarchical procedures that use homogenization at more than one level are a natural extension of the above concepts. Such multi-scale or sequential homogenization models are the subject of a short discussion in Chapter 9.

A final group of models used for studying inhomogeneous materials is the direct numerical simulation of microstructured structures or samples. Until fairly recently, computational requirements restricted such modeling approaches to configurations exceeding the size of the microscale by less than, say, one or two orders of magnitude, see, e.g.,

Papka and Kyriakides (1994), Silberschmidt and Werner (2001), Luxner et al. (2005) or Tekoğlu et al. (2011). However, improvements in computing power have allowed extending this type of model to larger structures, compare, e.g., Bishop et al. (2015). Even though the geometries considered may appear similar to the ones used in windowing approaches, compare Chapter 7, models of the above type by design aim at describing the behavior of small structures rather than that of materials. As a consequence, they are typically subjected to boundary conditions and load cases that are pertinent to structural (among them bending or indentation loads), but not to material behavior. The effects of these boundary conditions as well as the sample's size in terms of the characteristic length of the inhomogeneities, ℓ, tend to play considerable roles in the mechanical behavior of such inhomogeneous structures, which is typically evaluated in terms of force vs. displacement rather than stress vs. strain curves. Arguably, such structural models are not part of the "core tool set" of micromechanics, because they do not involve scale transitions.

1.6 Model Verification and Validation

Micromechanical approaches aim at generating predictive models for the behavior of inhomogeneous materials. Obviously, model verification, i.e., monitoring a model's correct setup and implementation, as well as validation, i.e., assessing the accuracy of a model's representation of the targeted material behavior, play important roles in this context. Of course, both model verification and validation in continuum micromechanics require keeping tabs on the consistency and plausibility of modeling assumptions and results throughout a given study.

For verification, it is often possible to compare predictions obtained with different, unrelated micromechanical methods that pertain to a given geometrical configuration and employ the same constitutive models as well as material parameters. In such a setting, finding good agreement over sets of markedly different material parameters is a strong indicator (but definitely not a guarantee) that the models involved successfully capture the physics of the problem.

Bounding methods, see Chapter 3, play an especially important role in verification studies: When it comes to studying the linear elastic (or conduction) responses of inhomogeneous materials, in many cases appropriate bounds are available, compare Section 3. Analytical or numerical models that violate the Hashin–Shtrikman bounds pertaining to the macroscopic symmetry and microscopic geometrical configuration of the material in the linear regime by more than trivial differences (which may be due to, e.g., roundoff errors), must be viewed as at least potentially flawed[15]. In such verification assessments the value of an estimate relative to the pertinent bounds may provide additional information: it is well known that stiff inhomogeneities in a compliant matrix give rise to effective moduli closer to the lower and compliant inhomogeneities in a stiff matrix to estimates closer to the upper bound (Torquato, 1991), with analogous relationships holding for conduction problems. It is good practice to assess linear versions of models intended for studying nonlinear behavior against the appropriate bounds — this essentially provides a check if a given

[15]If data from measurements do not comply with the pertinent Hashin–Shtrikman bounds the most common reason is inaccurate data for the constituent behavior or the volume fractions.

model is capable of producing a physically valid partitioning of the stress (flux) and strain (gradient) fields between the target material's phases in a fairly well understood regime. Issues cropping up with linear behavior tend not to disappear, but rather to become more marked in the more complex nonlinear setting. For generality of the results it typically makes sense to carry out verification analyses for parameter combinations that "stress" the methods involved, which in the context of continuum micromechanics often means phase contrasts that differ clearly from unity and high inhomogeneity volume fractions.

In the case of modeling efforts making use of discretizing numerical engineering methods for evaluating position dependent fields in a volume element, convergence studies involving successively finer discretizations are an important part of verification. In this context it is worth noting that convergence in terms of the macroscopic responses does not guarantee convergence in terms of the microscopic fields, and, especially, of the latters' minimum and maximum values. For full field simulations convergence studies in terms of the size of volume elements may also be of considerable interest.

The validation of micromechanical models against experimental data is obviously highly important, but may be tricky in practice due to the considerable number of potential sources of discrepancies — on the modeling side they include the representativeness of the volume elements used, the quality of the material models employed for the constituents, the accuracy of the material parameters prescribed to these constitutive models as well as errors in the implementation or application of the model. Obtaining perfect or near-perfect agreement between measurements and predictions without "tuning" input parameters in general is not the most probable of outcomes, especially when damage and failure modeling are involved. Accordingly, even highly successful validation against some set of experimental data does not remove the need for model verification as defined above. Specifically, a model giving predictions that are close to experimental results but fall outside the pertinent bounds in the linear range cannot be treated as verified — after all, even good agreement with measurements may be due to the canceling of different errors arising from the above issues. In a similar vein, obtaining responses close to experimental results from a model that takes major liberties in terms of the microgeometry constitutes neither verification nor proper validation.

Obtaining reliable values for material parameters pertinent to the microscale tends to be a major challenge in micromechanics, especially when a model involves damage. A fairly common way of dealing with this problem is carrying out parameter identification via inverse procedures built around the micromechanical model and available experimental results. When following such a strategy, using the same set of experimental data for both parameter identification and model verification must be avoided — in such a setting "overspecialization" of the parameters to that data set may occur, which makes model and parameters unsuitable for generalization to other situations. In a common scenario of this type the nonlinear macroscopic behavior of a composite is to be studied and experimental data are limited to results from uniaxial tensile tests. In such a case even a perfect match of predictions with the above experimental results is far from guaranteeing that load cases involving other macroscopic triaxialities, e.g., shear, or complex stress trajectories will be described reasonably well by the model.

Chapter 2

Mean-Field Methods

In this chapter mean-field methods are discussed mainly in the context of two-phase materials. Special emphasis is put on effective-field methods of the Mori–Tanaka type, which may be viewed as the simplest mean-field approaches to modeling inhomogeneous materials that encompass the full physical range of phase volume fractions[16]. Unless specifically stated otherwise, the material behavior of both reinforcements and matrix is taken to be linear (thermo)elastic, both strains and temperature changes being assumed to be small. Perfect bonding between the constituents is assumed in all cases. There is an extensive body of literature covering relevant mean-field approaches, so that the following treatment is far from complete.

2.1 General Relations between Mean Fields in Thermoelastic Two-Phase Materials

Throughout this report additive decomposition of strains is used. For example, for the case of thermoelastoplastic material behavior the total strain tensor can be written in this approximation as

$$\boldsymbol{\varepsilon} = \boldsymbol{\varepsilon}_{\mathrm{el}} + \boldsymbol{\varepsilon}_{\mathrm{pl}} + \boldsymbol{\varepsilon}_{\mathrm{th}} \quad , \tag{2.1}$$

where $\boldsymbol{\varepsilon}_{\mathrm{el}}$, $\boldsymbol{\varepsilon}_{\mathrm{pl}}$ and $\boldsymbol{\varepsilon}_{\mathrm{th}}$ denote the elastic, plastic and thermal strains, respectively. The strain and stress tensors may be split into volumetric/hydrostatic and deviatoric contributions

$$\begin{aligned} \boldsymbol{\varepsilon} &= \boldsymbol{\varepsilon}_{\mathrm{vol}} + \boldsymbol{\varepsilon}_{\mathrm{dev}} = \mathbf{O}_{\mathrm{vol}}\,\boldsymbol{\varepsilon} + \mathbf{O}_{\mathrm{dev}}\,\boldsymbol{\varepsilon} \\ \boldsymbol{\sigma} &= \boldsymbol{\sigma}_{\mathrm{hyd}} + \boldsymbol{\sigma}_{\mathrm{dev}} = \mathbf{O}_{\mathrm{vol}}\,\boldsymbol{\sigma} + \mathbf{O}_{\mathrm{dev}}\,\boldsymbol{\sigma} \quad , \end{aligned} \tag{2.2}$$

$\mathbf{O}_{\mathrm{vol}}$ and $\mathbf{O}_{\mathrm{dev}}$ being volumetric and deviatoric projection tensors.

For thermoelastic inhomogeneous materials, the macroscopic stress–strain relations can be written in the form

$$\begin{aligned} \langle\boldsymbol{\sigma}\rangle &= \mathbf{E}^*\langle\boldsymbol{\varepsilon}\rangle + \boldsymbol{\lambda}^*\Delta T \\ \langle\boldsymbol{\varepsilon}\rangle &= \mathbf{C}^*\langle\boldsymbol{\sigma}\rangle + \boldsymbol{\alpha}^*\Delta T \quad . \end{aligned} \tag{2.3}$$

[16] Because Eshelby and Mori–Tanaka methods are specifically suited for matrix–inclusion-type microtopologies, the expression "composite" is often used in the present chapter instead of the more general designation "inhomogeneous material".

Here the expression $\boldsymbol{\alpha}^*\Delta T$ corresponds to the macroscopic thermal strain tensor, $\boldsymbol{\lambda}^* = -\mathbf{E}^*\boldsymbol{\alpha}^*$ is the macroscopic specific thermal stress tensor (i.e., the overall stress response of a fully constrained material to a purely thermal unit load, also known as the tensor of thermal stress coefficients), and ΔT stands for the (spatially homogeneous) temperature difference with respect to some (stress-free) reference temperature. The constituents, here a matrix $^{(\mathrm{m})}$ and inhomogeneities $^{(\mathrm{i})}$, are also assumed to behave thermoelastically, so that

$$\begin{aligned} \langle\boldsymbol{\sigma}\rangle^{(\mathrm{m})} &= \mathbf{E}^{(\mathrm{m})}\langle\boldsymbol{\varepsilon}\rangle^{(\mathrm{m})} + \boldsymbol{\lambda}^{(\mathrm{m})}\Delta T & \qquad \langle\boldsymbol{\sigma}\rangle^{(\mathrm{i})} &= \mathbf{E}^{(\mathrm{i})}\langle\boldsymbol{\varepsilon}\rangle^{(\mathrm{i})} + \boldsymbol{\lambda}^{(\mathrm{i})}\Delta T \\ \langle\boldsymbol{\varepsilon}\rangle^{(\mathrm{m})} &= \mathbf{C}^{(\mathrm{m})}\langle\boldsymbol{\sigma}\rangle^{(\mathrm{m})} + \boldsymbol{\alpha}^{(\mathrm{m})}\Delta T & \qquad \langle\boldsymbol{\varepsilon}\rangle^{(\mathrm{i})} &= \mathbf{C}^{(\mathrm{i})}\langle\boldsymbol{\sigma}\rangle^{(\mathrm{i})} + \boldsymbol{\alpha}^{(\mathrm{i})}\Delta T \end{aligned} \quad , \tag{2.4}$$

where the relations $\boldsymbol{\lambda}^{(\mathrm{m})} = -\mathbf{E}^{(\mathrm{m})}\boldsymbol{\alpha}^{(\mathrm{m})}$ and $\boldsymbol{\lambda}^{(\mathrm{i})} = -\mathbf{E}^{(\mathrm{i})}\boldsymbol{\alpha}^{(\mathrm{i})}$ hold.

From the definition of phase averaging, eqn. (1.16), relations between the phase averaged fields in the form

$$\begin{aligned} \langle\boldsymbol{\varepsilon}\rangle &= \xi\langle\boldsymbol{\varepsilon}\rangle^{(\mathrm{i})} + (1-\xi)\langle\boldsymbol{\varepsilon}\rangle^{(\mathrm{m})} &= \boldsymbol{\varepsilon}^{\mathrm{a}} \\ \langle\boldsymbol{\sigma}\rangle &= \xi\langle\boldsymbol{\sigma}\rangle^{(\mathrm{i})} + (1-\xi)\langle\boldsymbol{\sigma}\rangle^{(\mathrm{m})} &= \boldsymbol{\sigma}^{\mathrm{a}} \end{aligned} \tag{2.5}$$

follow immediately, where $\xi = V^{(\mathrm{i})} = \Omega^{(\mathrm{i})}/\Omega_{\mathrm{s}}$ stands for the volume fraction of the reinforcements and $1-\xi = V^{(\mathrm{m})} = \Omega^{(\mathrm{m})}/\Omega_{\mathrm{s}}$ for the volume fraction of the matrix. $\boldsymbol{\varepsilon}^{\mathrm{a}}$ and $\boldsymbol{\sigma}^{\mathrm{a}}$ denote far-field ("applied") homogeneous stress and strain tensors, respectively, with $\boldsymbol{\varepsilon}^{\mathrm{a}} = \mathbf{C}^*\boldsymbol{\sigma}^{\mathrm{a}}$. Perfect interfaces between the phases are assumed in expressing the macroscopic strain of the composite as the weighted sum of the phase averaged strains.

The phase averaged strains and stresses can be related to the overall strains and stresses by the phase averaged strain and stress concentration (or localization) tensors $\bar{\mathbf{A}}$, $\bar{\boldsymbol{\beta}}$, $\bar{\mathbf{B}}$, and $\bar{\boldsymbol{\kappa}}$ (Hill, 1963), respectively, which are defined for thermoelastic inhomogeneous materials by the expressions

$$\begin{aligned} \langle\boldsymbol{\varepsilon}\rangle^{(\mathrm{m})} &= \bar{\mathbf{A}}^{(\mathrm{m})}\langle\boldsymbol{\varepsilon}\rangle + \bar{\boldsymbol{\beta}}^{(\mathrm{m})}\Delta T & \qquad \langle\boldsymbol{\varepsilon}\rangle^{(\mathrm{i})} &= \bar{\mathbf{A}}^{(\mathrm{i})}\langle\boldsymbol{\varepsilon}\rangle + \bar{\boldsymbol{\beta}}^{(\mathrm{i})}\Delta T \\ \langle\boldsymbol{\sigma}\rangle^{(\mathrm{m})} &= \bar{\mathbf{B}}^{(\mathrm{m})}\langle\boldsymbol{\sigma}\rangle + \bar{\boldsymbol{\kappa}}^{(\mathrm{m})}\Delta T & \qquad \langle\boldsymbol{\sigma}\rangle^{(\mathrm{i})} &= \bar{\mathbf{B}}^{(\mathrm{i})}\langle\boldsymbol{\sigma}\rangle + \bar{\boldsymbol{\kappa}}^{(\mathrm{i})}\Delta T \end{aligned} \quad , \tag{2.6}$$

see eqn. (1.15) for the purely elastic case. $\bar{\mathbf{A}}$ and $\bar{\mathbf{B}}$ are referred to as the mechanical or (elastic) phase stress and strain concentration tensors, respectively, and $\bar{\boldsymbol{\beta}}$ as well as $\bar{\boldsymbol{\kappa}}$ are the corresponding thermal concentration tensors. In contrast to the elastic tensors $\mathbf{E}$ and $\mathbf{C}$, the concentration tensors $\bar{\mathbf{A}}$ and $\bar{\mathbf{B}}$ are not necessarily symmetric.

By using eqns. (2.5) and (2.6), the strain and stress concentration tensors can be shown to fulfill the relations

$$\begin{aligned} \xi\bar{\mathbf{A}}^{(\mathrm{i})} + (1-\xi)\bar{\mathbf{A}}^{(\mathrm{m})} &= \mathbf{I} & \qquad \xi\bar{\boldsymbol{\beta}}^{(\mathrm{i})} + (1-\xi)\bar{\boldsymbol{\beta}}^{(\mathrm{m})} &= \mathbf{o} \\ \xi\bar{\mathbf{B}}^{(\mathrm{i})} + (1-\xi)\bar{\mathbf{B}}^{(\mathrm{m})} &= \mathbf{I} & \qquad \xi\bar{\boldsymbol{\kappa}}^{(\mathrm{i})} + (1-\xi)\bar{\boldsymbol{\kappa}}^{(\mathrm{m})} &= \mathbf{o} \end{aligned} \quad , \tag{2.7}$$

where $\mathbf{I}$ stands for the symmetric rank 4 identity tensor and $\mathbf{o}$ for the rank 2 null tensor.

The effective elasticity and compliance tensors of a two-phase composite can be obtained from the properties of the constituents and from the mechanical concentration tensors as

$$\begin{aligned} \mathbf{E}^* &= \xi\mathbf{E}^{(\mathrm{i})}\bar{\mathbf{A}}^{(\mathrm{i})} + (1-\xi)\mathbf{E}^{(\mathrm{m})}\bar{\mathbf{A}}^{(\mathrm{m})} \\ &= \mathbf{E}^{(\mathrm{m})} + \xi[\mathbf{E}^{(\mathrm{i})} - \mathbf{E}^{(\mathrm{m})}]\bar{\mathbf{A}}^{(\mathrm{i})} = \mathbf{E}^{(\mathrm{i})} + (1-\xi)[\mathbf{E}^{(\mathrm{m})} - \mathbf{E}^{(\mathrm{i})}]\bar{\mathbf{A}}^{(\mathrm{m})} \end{aligned} \tag{2.8}$$

$$\begin{aligned} \mathbf{C}^* &= \xi \mathbf{C}^{(\mathrm{i})} \bar{\mathbf{B}}^{(\mathrm{i})} + (1-\xi) \mathbf{C}^{(\mathrm{m})} \bar{\mathbf{B}}^{(\mathrm{m})} \\ &= \mathbf{C}^{(\mathrm{m})} + \xi [\mathbf{C}^{(\mathrm{i})} - \mathbf{C}^{(\mathrm{m})}] \bar{\mathbf{B}}^{(\mathrm{i})} = \mathbf{C}^{(\mathrm{i})} + (1-\xi) [\mathbf{C}^{(\mathrm{m})} - \mathbf{C}^{(\mathrm{i})}] \bar{\mathbf{B}}^{(\mathrm{m})} \quad , \end{aligned} \tag{2.9}$$

compare eqn. (1.11).

The tensor of effective thermal expansion coefficients, $\boldsymbol{\alpha}^*$, and the specific thermal stress tensor, $\boldsymbol{\lambda}^*$, can be related to the thermoelastic phase behavior and the thermal concentration tensors as

$$\begin{aligned} \boldsymbol{\alpha}^* &= \xi [\mathbf{C}^{(\mathrm{i})} \bar{\boldsymbol{\kappa}}^{(\mathrm{i})} + \boldsymbol{\alpha}^{(\mathrm{i})}] + (1-\xi) [\mathbf{C}^{(\mathrm{m})} \bar{\boldsymbol{\kappa}}^{(\mathrm{m})} + \boldsymbol{\alpha}^{(\mathrm{m})}] \\ &= \xi \boldsymbol{\alpha}^{(\mathrm{i})} + (1-\xi) \boldsymbol{\alpha}^{(\mathrm{m})} + (1-\xi) [\mathbf{C}^{(\mathrm{m})} - \mathbf{C}^{(\mathrm{i})}] \bar{\boldsymbol{\kappa}}^{(\mathrm{m})} \\ &= \xi \boldsymbol{\alpha}^{(\mathrm{i})} + (1-\xi) \boldsymbol{\alpha}^{(\mathrm{m})} + \xi [\mathbf{C}^{(\mathrm{i})} - \mathbf{C}^{(\mathrm{m})}] \bar{\boldsymbol{\kappa}}^{(\mathrm{i})} \quad . \end{aligned} \tag{2.10}$$

$$\begin{aligned} \boldsymbol{\lambda}^* &= \xi [\mathbf{E}^{(\mathrm{i})} \bar{\boldsymbol{\beta}}^{(\mathrm{i})} + \boldsymbol{\lambda}^{(\mathrm{i})}] + (1-\xi) [\mathbf{E}^{(\mathrm{m})} \bar{\boldsymbol{\beta}}^{(\mathrm{m})} + \boldsymbol{\lambda}^{(\mathrm{m})}] \\ &= \xi \boldsymbol{\lambda}^{(\mathrm{i})} + (1-\xi) \boldsymbol{\lambda}^{(\mathrm{m})} + (1-\xi) [\mathbf{E}^{(\mathrm{m})} - \mathbf{E}^{(\mathrm{i})}] \bar{\boldsymbol{\beta}}^{(\mathrm{m})} \\ &= \xi \boldsymbol{\lambda}^{(\mathrm{i})} + (1-\xi) \boldsymbol{\lambda}^{(\mathrm{m})} + \xi [\mathbf{E}^{(\mathrm{i})} - \mathbf{E}^{(\mathrm{m})}] \bar{\boldsymbol{\beta}}^{(\mathrm{i})} \quad . \end{aligned} \tag{2.11}$$

The above expressions can be derived by inserting eqns. (2.4) and (2.6) into eqns. (2.5) and comparing with eqns. (2.3). Alternatively, the effective thermal expansion coefficient and specific thermal stress coefficient tensors of multi-phase materials can be obtained as

$$\begin{aligned} \boldsymbol{\alpha}^* &= \sum_{(\mathrm{p})} \xi^{(\mathrm{p})} (\bar{\mathbf{B}}^{(\mathrm{p})})^{\mathrm{T}} \boldsymbol{\alpha}^{(\mathrm{p})} \\ \boldsymbol{\lambda}^* &= \sum_{(\mathrm{p})} \xi^{(\mathrm{p})} (\bar{\mathbf{A}}^{(\mathrm{p})})^{\mathrm{T}} \boldsymbol{\lambda}^{(\mathrm{p})} \quad , \end{aligned} \tag{2.12}$$

compare (Mandel, 1965; Levin, 1967), where the sums run over all phases $^{(\mathrm{p})}$. The above expression for $\boldsymbol{\alpha}^*$ being known as the Mandel–Levin formula. If the effective compliance tensor of a two-phase material is known, eqn. (2.7) can be inserted into eqn. (2.12) to give the overall coefficients of thermal expansion as

$$\boldsymbol{\alpha}^* = (\mathbf{C}^* - \mathbf{C}^{(\mathrm{m})})(\mathbf{C}^{(\mathrm{i})} - \mathbf{C}^{(\mathrm{m})})^{-1} \boldsymbol{\alpha}^{(\mathrm{i})} - (\mathbf{C}^* - \mathbf{C}^{(\mathrm{i})})(\mathbf{C}^{(\mathrm{i})} - \mathbf{C}^{(\mathrm{m})})^{-1} \boldsymbol{\alpha}^{(\mathrm{m})} \quad . \tag{2.13}$$

The mechanical stress and strain concentration tensors for a given phase are linked by expressions of the type

$$\bar{\mathbf{A}}^{(\mathrm{p})} = \mathbf{C}^{(\mathrm{p})} \bar{\mathbf{B}}^{(\mathrm{p})} \mathbf{E}^* \qquad \text{and} \qquad \bar{\mathbf{B}}^{(\mathrm{p})} = \mathbf{E}^{(\mathrm{p})} \bar{\mathbf{A}}^{(\mathrm{p})} \mathbf{C}^* \quad , \tag{2.14}$$

from which $\mathbf{E}^*$ and $\mathbf{C}^*$ may be eliminated via eqn. (2.79). For two-phase materials the concentration tensors can be evaluated from the effective and the phase-level elastic tensors, e.g.,

$$\begin{aligned} (1-\xi) \bar{\mathbf{A}}^{(\mathrm{m})} &= (\mathbf{E}^{(\mathrm{m})} - \mathbf{E}^{(\mathrm{i})})^{-1} (\mathbf{E}^* - \mathbf{E}^{(\mathrm{i})}) \\ \xi \bar{\mathbf{B}}^{(\mathrm{i})} &= (\mathbf{C}^{(\mathrm{i})} - \mathbf{C}^{(\mathrm{m})})^{-1} (\mathbf{C}^* - \mathbf{C}^{(\mathrm{m})}) \quad . \end{aligned} \tag{2.15}$$

on the basis of eqns. (2.7) and (2.7). Furthermore, by invoking the principle of virtual work Benveniste and Dvorak (1990) developed relations that the thermal strain concentration tensors, $\bar{\boldsymbol{\beta}}^{(\mathrm{p})}$, to the mechanical strain concentration tensors, $\bar{\mathbf{A}}^{(\mathrm{p})}$, and the thermal stress concentration tensors, $\bar{\boldsymbol{\kappa}}^{(\mathrm{p})}$, to the mechanical stress concentration tensors, $\bar{\mathbf{B}}^{(\mathrm{p})}$, respectively, as

$$\begin{aligned}
\bar{\boldsymbol{\beta}}^{(\mathrm{m})} &= [\mathbf{I} - \bar{\mathbf{A}}^{(\mathrm{m})}][\mathbf{E}^{(\mathrm{i})} - \mathbf{E}^{(\mathrm{m})}]^{-1}[\boldsymbol{\lambda}^{(\mathrm{m})} - \boldsymbol{\lambda}^{(\mathrm{i})}] \\
\bar{\boldsymbol{\beta}}^{(\mathrm{i})} &= [\mathbf{I} - \bar{\mathbf{A}}^{(\mathrm{i})}][\mathbf{E}^{(\mathrm{m})} - \mathbf{E}^{(\mathrm{i})}]^{-1}[\boldsymbol{\lambda}^{(\mathrm{i})} - \boldsymbol{\lambda}^{(\mathrm{m})}] \\
\bar{\boldsymbol{\kappa}}^{(\mathrm{m})} &= [\mathbf{I} - \bar{\mathbf{B}}^{(\mathrm{m})}][\mathbf{C}^{(\mathrm{i})} - \mathbf{C}^{(\mathrm{m})}]^{-1}[\boldsymbol{\alpha}^{(\mathrm{m})} - \boldsymbol{\alpha}^{(\mathrm{i})}] \\
\bar{\boldsymbol{\kappa}}^{(\mathrm{i})} &= [\mathbf{I} - \bar{\mathbf{B}}^{(\mathrm{i})}][\mathbf{C}^{(\mathrm{m})} - \mathbf{C}^{(\mathrm{i})}]^{-1}[\boldsymbol{\alpha}^{(\mathrm{i})} - \boldsymbol{\alpha}^{(\mathrm{m})}] \quad .
\end{aligned} \tag{2.16}$$

From eqns. (2.9) to (2.16) it is evident that the knowledge of one elastic phase concentration tensor is sufficient for describing the full thermoelastic behavior of two-phase inhomogeneous materials within the mean-field framework. It is worth mentioning that a fair number of additional relations between phase averaged tensors have been reported in the literature.

An additional set of useful concentration tensors are the partial strain and stress concentration tensors, $\bar{\mathbf{T}}^{(\mathrm{p,q})}$ and $\bar{\mathbf{W}}^{(\mathrm{p,q})}$, defined by

$$\begin{aligned}
\boldsymbol{\varepsilon}^{(\mathrm{p})} &= \bar{\mathbf{T}}^{(\mathrm{p,q})}\boldsymbol{\varepsilon}^{(\mathrm{q})} \\
\boldsymbol{\sigma}^{(\mathrm{p})} &= \bar{\mathbf{W}}^{(\mathrm{p,q})}\boldsymbol{\sigma}^{(\mathrm{q})} \quad ,
\end{aligned} \tag{2.17}$$

which connect the fields in phases $^{(\mathrm{p})}$ and $^{(\mathrm{q})}$, compare, e.g., Dvorak et al. (1992). For two-phase composites with matrix–inclusion topology the partial concentration tensors $\bar{\mathbf{T}}^{(\mathrm{i,m})}$ and $\bar{\mathbf{W}}^{(\mathrm{i,m})}$ are linked to the "standard" phase averaged concentration tensors by the relations

$$\begin{aligned}
\bar{\mathbf{A}}^{(\mathrm{m})} &= \left[\xi\bar{\mathbf{T}}^{(\mathrm{i,m})} + (1-\xi)\mathbf{I}\right]^{-1} \\
\bar{\mathbf{B}}^{(\mathrm{m})} &= \left[\xi\bar{\mathbf{W}}^{(\mathrm{i,m})} + (1-\xi)\mathbf{I}\right]^{-1} \\
\bar{\mathbf{A}}^{(\mathrm{i})} &= \bar{\mathbf{T}}^{(\mathrm{i,m})}\left[\xi\bar{\mathbf{T}}^{(\mathrm{i,m})} + (1-\xi)\mathbf{I}\right]^{-1} \\
\bar{\mathbf{B}}^{(\mathrm{i})} &= \bar{\mathbf{W}}^{(\mathrm{i,m})}\left[\xi\bar{\mathbf{W}}^{(\mathrm{i,m})} + (1-\xi)\mathbf{I}\right]^{-1} \quad ;
\end{aligned} \tag{2.18}$$

The inverse of the partial inhomogeneity stress concentration tensor $[\bar{\mathbf{W}}^{(\mathrm{i,m})}]^{-1} = \bar{\mathbf{W}}^{\mathrm{m,i}}$ was referred to as the "bridging tensor" by Huang (2000).

Equations (2.3) to (2.18) do not account for temperature dependence of the thermoelastic moduli. For a mean-field framework capable of handling temperature dependent moduli for finite temperature excursions and small strains see, e.g., Boussaa (2011).

Alternatively to using concentration tensors most analytical micromechanical models may be formulated in terms of contribution tensors, which were introduced by Horii and Nemat-Nasser (1985), elaborated by Kachanov et al. (1994) for porous materials, extended to composite materials by Sevostianov and Kachanov (1999) as well as Eroshkin and Tsukrov (2005) and further modified by Sevostianov and Kachanov (2011). Contribution tensors are defined via the differences between the effective compliance and elasticity

tensors caused by the presence of inhomogeneities $^{(\mathrm{i})}$ and the corresponding elastic tensors of the reinforcement-free matrix, $^{(\mathrm{m})}$, as

$$\begin{aligned} \mathbf{H}^{(\mathrm{i})} &= \frac{1}{\xi}(\mathbf{C}^{*} - \mathbf{C}^{(\mathrm{m})}) \\ \mathbf{N}^{(\mathrm{i})} &= \frac{1}{\xi}(\mathbf{E}^{*} - \mathbf{E}^{(\mathrm{m})}) \end{aligned} \quad . \tag{2.19}$$

The compliance contribution tensors $\mathbf{H}^{(\mathrm{i})}$ and elasticity contribution tensor $\mathbf{N}^{(\mathrm{i})}$ can be shown to be connected to the phase averaged strain and stress concentration tensors, $\bar{\mathbf{A}}^{(\mathrm{i})}$ and $\bar{\mathbf{B}}^{(\mathrm{i})}$, by the relations

$$\begin{aligned} \mathbf{H}^{(\mathrm{i})} &= (\mathbf{C}^{(\mathrm{i})} - \mathbf{C}^{(\mathrm{m})})\bar{\mathbf{B}}^{(\mathrm{i})} \\ \mathbf{N}^{(\mathrm{i})} &= (\mathbf{E}^{(\mathrm{i})} - \mathbf{E}^{(\mathrm{m})})\bar{\mathbf{A}}^{(\mathrm{i})} \end{aligned} \tag{2.20}$$

and they are linked to each other via the expressions

$$\begin{aligned} \mathbf{H}^{(\mathrm{i})} &= -\mathbf{C}^{(\mathrm{m})}\mathbf{N}^{(\mathrm{i})}\big(\mathbf{E}^{(\mathrm{m})} + \xi\mathbf{N}^{(\mathrm{i})}\big)^{-1} \\ \mathbf{N}^{(\mathrm{i})} &= -\mathbf{E}^{(\mathrm{m})}\mathbf{H}^{(\mathrm{i})}\big(\mathbf{C}^{(\mathrm{m})} + \xi\mathbf{H}^{(\mathrm{i})}\big)^{-1} \end{aligned} \tag{2.21}$$

In contrast to concentration tensors the contribution tensors $\mathbf{H}^{(\mathrm{i})}$ and $\mathbf{N}^{(\mathrm{i})}$ are symmetric, as is evident from eqns. (2.19).

2.2 Eshelby Tensor and Dilute Matrix–Inclusion Composites

Eshelby's Eigenstrain Problem

A large percentage of the mean-field descriptions used in continuum micromechanics of materials have been based on the work of Eshelby, who initially studied the stress and strain distributions in homogeneous media that contain a subregion ("inclusion") that spontaneously changes its shape and/or size ("undergoes a transformation") so that it no longer fits into its previous space in the "parent medium". Eshelby's results show that if an elastic homogeneous ellipsoidal inclusion (i.e., an inclusion consisting of the same material as the matrix) in an infinite matrix is subjected to a homogeneous strain $\boldsymbol{\varepsilon}_{\mathrm{t}}$ (called the "stress-free strain", "unconstrained strain", "polarization strain", "eigenstrain", or "transformation strain"), the stress and strain states in the constrained inclusion are uniform[17], i.e., $\boldsymbol{\sigma}^{(\mathrm{i})} = \langle\boldsymbol{\sigma}\rangle^{(\mathrm{i})}$ and $\boldsymbol{\varepsilon}^{(\mathrm{i})} = \langle\boldsymbol{\varepsilon}\rangle^{(\mathrm{i})}$. The uniform strain in the constrained inclusion (the "constrained strain"), $\boldsymbol{\varepsilon}^{(\mathrm{i})} = \boldsymbol{\varepsilon}_{\mathrm{c}}$, is related to the stress-free strain $\boldsymbol{\varepsilon}_{\mathrm{t}}$ by the expression (Eshelby, 1957)

$$\boldsymbol{\varepsilon}_{\mathrm{c}} = \mathbf{S}\boldsymbol{\varepsilon}_{\mathrm{t}} \quad , \tag{2.22}$$

where $\mathbf{S}$ is referred to as the (interior-point) Eshelby tensor. For eqn. (2.22) to hold, $\boldsymbol{\varepsilon}_{\mathrm{t}}$ may be any kind of eigenstrain that is uniform over the inclusion (e.g., a thermal strain or

[17]This "Eshelby property" or "Eshelby uniformity" is limited to inclusions and inhomogeneities of ellipsoidal shape (Lubarda and Markenscoff, 1998; Kang and Milton, 2008). However, hyperboloidal domains will (Franciosi, 2020) and certain non-dilute periodic arrangements of non-ellipsoidal inclusions can (Liu et al., 2007) also give rise to homogeneous fields.

a strain due to some phase transformation involving no changes in the elastic constants of the inclusion).

The Eshelby tensor $\mathbf{S}$ depends only on the material properties of the parent medium (in many cases the matrix) and on the specific shape of the ellipsoidal inclusions. Eshelby tensors for inclusions of general shape can be obtained as

$$\mathbf{S}^{(\mathrm{i},0)}(\mathbf{x}) = \int_{\Omega^{(\mathrm{i})}} \widehat{\mathbf{G}}^{(0)}(\mathbf{x}-\mathbf{x}')\,\mathbf{E}^{(0)}\,\mathrm{d}\Omega' = \mathbf{P}^{(\mathrm{i},0)}(\mathbf{x})\mathbf{E}^{(0)} \qquad , \tag{2.23}$$

compare, e.g., Kachanov and Sevostianov (2018). Here $\widehat{\mathbf{G}}^{(0)}$ and $\mathbf{E}^{(0)}$ stand for the modified Green's tensor and the elasticity tensor of the parent medium $^{(0)}$, respectively. $\mathbf{P}^{(\mathrm{i},0)}$ is known as the Hill tensor, mean polarization factor tensor or shape tensor. Here, the superscripts in $\mathbf{S}^{(\mathrm{i},0)}(\mathbf{x})$ and $\mathbf{P}^{(\mathrm{i},0)}(\mathbf{x})$ explicitly denote evaluation with respect to the parent medium $^{(0)}$ and the shape of inclusion $^{(\mathrm{i})}$. The so-called first Eshelby problem consists in finding solutions for the above integral.

Closed form expressions for the Eshelby tensor of spheroidal inclusions in an isotropic matrix are available as functions of the aspect ratio (eccentricity) a, see, e.g., Pedersen (1983), Tandon and Weng (1984), Mura (1987) or Clyne and Withers (1993), the formulae resulting for continuous fibers of circular cross-section ($a \to \infty$), spherical inclusions ($a = 1$), and thin circular disks or layers ($a \to 0$) being rather simple. Analogous expressions for the Eshelby tensor have also been reported for spheroidal inclusions in a matrix of transversally isotropic material symmetry (Withers, 1989; Parnell and Calvo-Jurado, 2015), provided the material axes of the matrix are aligned with the orientations of non-spherical inclusions. Expressions for the Eshelby tensors of general ellipsoidal inclusions in an isotropic matrix in terms of incomplete elliptic integrals (which, in general, must be evaluated numerically) can be found, e.g., in Mura (1987). Instead of evaluating the Eshelby tensor for a given configuration, the Hill tensor, $\mathbf{P}^{(\mathrm{i,m})} = \mathbf{S}\mathbf{C}^{(\mathrm{m})}$ (where $\mathbf{S}$ denotes $\mathbf{S}^{(\mathrm{i,m})}$), may be solved for instead, compare, e.g., Masson (2008) or Barthélémy (2020). For detailed discussion of Eshelby and Hill tensors pertaining to ellipsoidal inclusions see Parnell (2016); information on position-dependent and averaged Eshelby tensors for polyhedral inhomogeneities embedded in an isotropic matrix is provided, e.g., by Kachanov and Sevostianov (2018).

For materials of low elastic symmetry the modified Green's function tensor $\widehat{\mathbf{G}}^{(0)}$ as required in eqn. (2.23) is not available. However, the problem can be transformed into a surface integral in Fourier space (Mura, 1987), where the modified Green's tensors are known explicitly for all material symmetries. Approximations to the Eshelby tensors of ellipsoids embedded in matrices of general elastic symmetry can then be obtained by using numerical quadrature for the back transformation, compare Gavazzi and Lagoudas (1990).

Eshelby's Inhomogeneity Problem

For mean-field descriptions of dilute matrix–inclusion composites, the main interest lies on the stress and strain fields in inhomogeneous inclusions ("inhomogeneities") that are embedded in a matrix. The case where the inhomogeneities do not interact with each other can be handled on the basis of Eshelby's theory for homogeneous inclusions, eqn. (2.22),

by introducing the concept of an equivalent homogeneous inclusion. This approach involves replacing an actual perfectly bonded inhomogeneity, which has different material properties than the matrix and which is subjected to a given unconstrained eigenstrain $\boldsymbol{\varepsilon}_\mathrm{t}$, with a (fictitious) "equivalent" homogeneous inclusion on which a (fictitious) "equivalent" eigenstrain $\boldsymbol{\varepsilon}_\tau$ is made to act. This equivalent eigenstrain is chosen in such a way that the inhomogeneous inclusion and the equivalent homogeneous inclusion attain the same stress state $\boldsymbol{\sigma}^{(\mathrm{i})}$ as well as the same constrained strain $\boldsymbol{\varepsilon}_\mathrm{c}$ (Eshelby, 1957; Withers et al., 1989). When $\boldsymbol{\sigma}^{(\mathrm{i})}$ is expressed in terms of the elastic strain in the inhomogeneity or inclusion, this condition translates into the equality

$$\boldsymbol{\sigma}^{(\mathrm{i})} = \mathbf{E}^{(\mathrm{i})}[\boldsymbol{\varepsilon}_\mathrm{c} - \boldsymbol{\varepsilon}_\mathrm{t}] = \mathbf{E}^{(\mathrm{m})}[\boldsymbol{\varepsilon}_\mathrm{c} - \boldsymbol{\varepsilon}_\tau] \qquad . \tag{2.24}$$

Here $\boldsymbol{\varepsilon}_\mathrm{c} - \boldsymbol{\varepsilon}_\mathrm{t}$ and $\boldsymbol{\varepsilon}_\mathrm{c} - \boldsymbol{\varepsilon}_\tau$ are the elastic strains in the inhomogeneous inclusion and the equivalent homogeneous inclusion, respectively. Obviously, in the general case the stress-free strains will be different for the equivalent inclusion and the real inhomogeneity, $\boldsymbol{\varepsilon}_\mathrm{t} \neq \boldsymbol{\varepsilon}_\tau$. Plugging the result of applying eqn. (2.22) to the equivalent eigenstrain, $\boldsymbol{\varepsilon}_\mathrm{c} = \mathbf{S}\boldsymbol{\varepsilon}_\tau$, into eqn. (2.24) leads to the relationship

$$\boldsymbol{\sigma}^{(\mathrm{i})} = \mathbf{E}^{(\mathrm{i})}[\mathbf{S}\boldsymbol{\varepsilon}_\tau - \boldsymbol{\varepsilon}_\mathrm{t}] = \mathbf{E}^{(\mathrm{m})}[\mathbf{S} - \mathbf{I}]\boldsymbol{\varepsilon}_\tau \qquad , \tag{2.25}$$

which can be rearranged to obtain the equivalent eigenstrain as a function of the known stress-free eigenstrain $\boldsymbol{\varepsilon}_\mathrm{t}$ of the inhomogeneous inclusion as

$$\boldsymbol{\varepsilon}_\tau = [(\mathbf{E}^{(\mathrm{i})} - \mathbf{E}^{(\mathrm{m})})\mathbf{S} + \mathbf{E}^{(\mathrm{m})}]^{-1}\mathbf{E}^{(\mathrm{i})}\boldsymbol{\varepsilon}_\mathrm{t} \qquad . \tag{2.26}$$

This, in turn, allows the stress in the inhomogeneity, $\boldsymbol{\sigma}^{(\mathrm{i})}$, to be expressed explicitly as

$$\boldsymbol{\sigma}^{(\mathrm{i})} = \mathbf{E}^{(\mathrm{m})}(\mathbf{S} - \mathbf{I})[(\mathbf{E}^{(\mathrm{i})} - \mathbf{E}^{(\mathrm{m})})\mathbf{S} + \mathbf{E}^{(\mathrm{m})}]^{-1}\mathbf{E}^{(\mathrm{i})}\boldsymbol{\varepsilon}_\mathrm{t} \qquad . \tag{2.27}$$

The concept of the equivalent homogeneous inclusion can be extended to the "inhomogeneity problem", where a uniform mechanical strain $\boldsymbol{\varepsilon}^\mathrm{a}$ or stress $\boldsymbol{\sigma}^\mathrm{a}$ is applied to a system consisting of a perfectly bonded inhomogeneous elastic inclusion in an infinite matrix. Here, the strain in the inhomogeneity, $\boldsymbol{\varepsilon}^{(\mathrm{i})}$, is a superposition of the applied strain and of a term $\boldsymbol{\varepsilon}_\mathrm{c}$ that accounts for the constraint effects of the surrounding matrix. Well-known expressions for dilute, non-interacting elastic concentration tensors based on the above considerations were proposed by Hill (1965b) and elaborated by Benveniste (1987). For deriving them, the conditions of equal stresses and strains in the actual inhomogeneity (elasticity tensor $\mathbf{E}^{(\mathrm{i})}$) and the equivalent inclusion (elasticity tensor $\mathbf{E}^{(\mathrm{m})}$) under an applied far-field strain $\boldsymbol{\varepsilon}^\mathrm{a}$ take the form

$$\boldsymbol{\sigma}^{(\mathrm{i})} = \mathbf{E}^{(\mathrm{i})}[\boldsymbol{\varepsilon}^\mathrm{a} + \boldsymbol{\varepsilon}_\mathrm{c}] = \mathbf{E}^{(\mathrm{m})}[\boldsymbol{\varepsilon}^\mathrm{a} + \boldsymbol{\varepsilon}_\mathrm{c} - \boldsymbol{\varepsilon}_\tau] \tag{2.28}$$

and

$$\boldsymbol{\varepsilon}^{(\mathrm{i})} = \boldsymbol{\varepsilon}^\mathrm{a} + \boldsymbol{\varepsilon}_\mathrm{c} = \boldsymbol{\varepsilon}^\mathrm{a} + \mathbf{S}\boldsymbol{\varepsilon}_\tau \qquad , \tag{2.29}$$

respectively, where eqn. (2.22) is used to describe the constrained strain of the equivalent homogeneous inclusion. On the basis of these relationships the strain in the inhomogeneity can be expressed as

$$\boldsymbol{\varepsilon}^{(\mathrm{i})} = [\mathbf{I} + \mathbf{S}\mathbf{C}^{(\mathrm{m})}(\mathbf{E}^{(\mathrm{i})} - \mathbf{E}^{(\mathrm{m})})]^{-1}\boldsymbol{\varepsilon}^\mathrm{a} \qquad . \tag{2.30}$$

Because the strain in the inhomogeneity is homogeneous, $\boldsymbol{\varepsilon}^{(\mathrm{i})} = \langle\boldsymbol{\varepsilon}\rangle^{(\mathrm{i})}$, the strain concentration tensor for dilute inhomogeneities follows directly from eqn. (2.30) as

$$\bar{\mathbf{A}}^{(\mathrm{i})}_{\mathrm{dil}} = [\mathbf{I} + \mathbf{S}\mathbf{C}^{(\mathrm{m})}(\mathbf{E}^{(\mathrm{i})} - \mathbf{E}^{(\mathrm{m})})]^{-1} \quad . \tag{2.31}$$

By using $\langle\boldsymbol{\varepsilon}\rangle^{(\mathrm{i})} = \mathbf{C}^{(\mathrm{i})}\langle\boldsymbol{\sigma}\rangle^{(\mathrm{i})}$ as well as $\boldsymbol{\varepsilon}^{\mathrm{a}} \approxeq \mathbf{C}^{(\mathrm{m})}\boldsymbol{\sigma}^{\mathrm{a}}$, the dilute stress concentration tensor for the inhomogeneities is found from eqn. (2.30) as

$$\begin{aligned} \bar{\mathbf{B}}^{(\mathrm{i})}_{\mathrm{dil}} &= \mathbf{E}^{(\mathrm{i})}[\mathbf{I} + \mathbf{S}\mathbf{C}^{(\mathrm{m})}(\mathbf{E}^{(\mathrm{i})} - \mathbf{E}^{(\mathrm{m})})]^{-1}\mathbf{C}^{(\mathrm{m})} \\ &= [\mathbf{I} + \mathbf{E}^{(\mathrm{m})}(\mathbf{I} - \mathbf{S})(\mathbf{C}^{(\mathrm{i})} - \mathbf{C}^{(\mathrm{m})})]^{-1} \quad . \end{aligned} \tag{2.32}$$

For the dilute case the "standard" and partial inhomogeneity concentration tensors coincide, i.e.,

$$\bar{\mathbf{T}}^{(\mathrm{i,m})}_{\mathrm{dil}} = \bar{\mathbf{A}}^{(\mathrm{i})}_{\mathrm{dil}} \qquad \text{and} \qquad \bar{\mathbf{W}}^{(\mathrm{i,m})}_{\mathrm{dil}} = \bar{\mathbf{B}}^{(\mathrm{i})}_{\mathrm{dil}} \quad , \tag{2.33}$$

so that the dilute partial concentration tensors for an inhomogeneity $^{(\mathrm{p})}$ embedded in a medium $^{(\mathrm{q})}$ result as

$$\begin{aligned} \bar{\mathbf{T}}^{(\mathrm{p,q})}_{\mathrm{dil}} &= [\mathbf{I} + \mathbf{S}^{(\mathrm{p,q})}\mathbf{C}^{(\mathrm{q})}(\mathbf{E}^{(\mathrm{p})} - \mathbf{E}^{(\mathrm{q})})]^{-1} = [\mathbf{I} + \mathbf{P}^{(\mathrm{p,q})}(\mathbf{E}^{(\mathrm{p})} - \mathbf{E}^{(\mathrm{q})})]^{-1} \\ \bar{\mathbf{W}}^{(\mathrm{p,q})}_{\mathrm{dil}} &= [\mathbf{I} + \mathbf{E}^{(\mathrm{q})}(\mathbf{I} - \mathbf{S}^{(\mathrm{p,q})})(\mathbf{C}^{(\mathrm{p})} - \mathbf{C}^{(\mathrm{q})})]^{-1} \quad . \end{aligned} \tag{2.34}$$

The dilute elasticity and compliance contribution tensors can be obtained from eqns. (2.31) and (2.32) via eqns. (2.19) as

$$\begin{aligned} \mathbf{N}^{(\mathrm{i})}_{\mathrm{dil}} &= (\mathbf{E}^{(\mathrm{i})} - \mathbf{E}^{(\mathrm{m})})\bar{\mathbf{A}}^{(\mathrm{i})}_{\mathrm{dil}} = \left[(\mathbf{E}^{(\mathrm{i})} - \mathbf{E}^{(\mathrm{m})})^{-1} + \mathbf{S}\mathbf{C}^{(\mathrm{m})}\right]^{-1} \\ \mathbf{H}^{(\mathrm{i})}_{\mathrm{dil}} &= (\mathbf{C}^{(\mathrm{i})} - \mathbf{C}^{(\mathrm{m})})\bar{\mathbf{B}}^{(\mathrm{i})}_{\mathrm{dil}} = \left[(\mathbf{C}^{(\mathrm{i})} - \mathbf{C}^{(\mathrm{m})})^{-1} + \mathbf{E}^{(\mathrm{m})}(\mathbf{I} - \mathbf{S})\right]^{-1} \quad . \end{aligned} \tag{2.35}$$

It is worth noting that in eqns. (2.24) to (2.35) the Eshelby tensor always refers to the equivalent homogeneous inclusion and is independent of the material symmetry and elastic properties of the actual inhomogeneities.

Dilute thermal concentration tensors can be generated from eqns. (2.31) and (2.32) by using eqns. (2.7) and (2.16). Alternative, but fully equivalent expressions for dilute mechanical and thermal inhomogeneity concentration tensors were given, e.g., by Mura (1987), Wakashima et al. (1988) and Clyne and Withers (1993). All of the above relations were derived under the assumption that the inhomogeneities are dilutely dispersed in the matrix and thus do not "feel" any effects of their neighbors (i.e., they are loaded by the unperturbed applied stress $\boldsymbol{\sigma}^{\mathrm{a}}$ or applied strain $\boldsymbol{\varepsilon}^{\mathrm{a}}$, the so-called dilute or non-interacting case). Accordingly, the resulting inhomogeneity concentration tensors are independent of the reinforcement volume fraction ξ. The corresponding matrix concentration tensors can be obtained via eqns. (2.7) and, accordingly, depend on ξ.

Following, e.g., Dederichs and Zeller (1973) or Kachanov and Sevostianov (2018) the strain field in an inhomogeneity of general shape can be given as

$$\boldsymbol{\varepsilon}^{(\mathrm{i})}(\mathbf{x}) = \langle\boldsymbol{\varepsilon}\rangle^{(0)} + (\mathbf{E}^{(\mathrm{i})} - \mathbf{E}^{(\mathrm{m})}) \int_{V^{(\mathrm{i})}} \widehat{\mathbf{G}}^{(0)}(\mathbf{x} - \mathbf{x}')\, \boldsymbol{\varepsilon}(\mathbf{x}')\, \mathrm{d}\Omega' \quad . \tag{2.36}$$

Solutions of eqn. (2.23), i.e., Hill or Eshelby tensors, in general hold for eqn. (2.36) only if $\boldsymbol{\varepsilon}$ is constant within the inhomogeneity, a condition that is fulfilled solely for ellipsoids. The integral equation (2.36) is a Lippmann–Schwinger equation and describes the so-called second Eshelby problem[18].

The stress and strain fields outside an inhomogeneity or a transformed homogeneous inclusion in an infinite matrix are not uniform on the microscale[19] (Eshelby, 1959). Within the framework of mean-field approaches, which aim to link the average fields in matrix and inhomogeneities with the overall response of inhomogeneous materials, however, it is only the average matrix stresses and strains that are of interest. For dilute composites, such expressions follow directly by combining eqns. (2.31) and (2.32) with eqn. (2.7), with the dilute matrix concentration tensors fulfilling $\bar{\mathbf{A}}_{\mathrm{dil}}^{(\mathrm{m})} \to \mathbf{I}$ and $\bar{\mathbf{B}}_{\mathrm{dil}}^{(\mathrm{m})} \to \mathbf{I}$. Expressions for the overall elastic and thermal expansion tensors can be obtained in a straightforward way from the dilute concentration tensors $\bar{\mathbf{A}}_{\mathrm{dil}}^{(\mathrm{i})}$ and $\bar{\mathbf{B}}_{\mathrm{dil}}^{(\mathrm{i})}$ by using eqns. (2.8) to (2.16), typical results being

$$\begin{aligned} \mathbf{E}_{\mathrm{NI}}^{*} &= \mathbf{E}^{(\mathrm{m})} + \xi(\mathbf{E}^{(\mathrm{i})} - \mathbf{E}^{(\mathrm{m})})\bar{\mathbf{A}}_{\mathrm{dil}}^{(\mathrm{i})} = \mathbf{E}^{(\mathrm{m})} + \xi\mathbf{N}_{\mathrm{dil}}^{(\mathrm{i})} \\ \mathbf{C}_{\mathrm{NI}}^{*} &= \mathbf{C}^{(\mathrm{m})} + \xi(\mathbf{C}^{(\mathrm{i})} - \mathbf{C}^{(\mathrm{m})})\bar{\mathbf{B}}_{\mathrm{dil}}^{(\mathrm{i})} = \mathbf{C}^{(\mathrm{m})} + \xi\mathbf{H}_{\mathrm{dil}}^{(\mathrm{i})} \quad . \end{aligned} \tag{2.37}$$

Such models are often referred to as Non-Interacting Approximations (NIA). It must be kept in mind that all mean-field expressions of this type are strictly valid only for vanishingly small inhomogeneity volume fractions[20].

2.3 Mean-Field Methods for Two-Phase Thermoelastic Composites with Aligned Reinforcements

Models for the overall thermoelastic behavior of composites with reinforcement volume fractions of more than a few percent must explicitly account for interactions between inhomogeneities, i.e., for the effects of all surrounding reinforcements on the stress and strain fields experienced by a given fiber or particle. Within the mean-field framework such interaction effects as well as the concomitant perturbations of the stress and strain fields in the matrix are typically accounted for in a collective way via approximations that are phase-wise constant. Beyond such "background" effects, at non-trivial volume fractions interactions between individual reinforcements give rise to, on the one hand, inhomogeneous stress and strain fields within each inhomogeneity as well as in the matrix. Such

[18] Eshelby tensors in the strict sense are solutions to the integral, eqn. (2.23). Tensors obtained by solving the integral equation (2.36) and then using eqn. (2.30) to extract $\mathbf{S}$ coincide with the proper Eshelby tensor only if the inhomogeneity is of ellipsoidal shape.
It may be noted that Eshelby (1957) did not proceed via eqns. (2.23) and (2.36).

[19] The fields outside a single inclusion can be described via the exterior-point Eshelby tensor, see, e.g., Mura (1987), Ju and Sun (1999), Meng et al. (2012) or Jin et al. (2016). From the (constant) interior-point fields and the (position dependent) exterior-point fields the stress and strain jumps at the interface between inclusion and matrix can be evaluated.

[20] With growing inhomogeneity volume fraction the predictions of dilute approximations deviate increasingly from solutions accounting for interactions between inhomogeneities and phase arrangement effects become more and more pronounced. The detailed behavior depends on the elastic contrast between the phases; as a rule of thumb, reasonably dependable results from non-interacting models cannot be expected for $\xi \lessapprox 0.1$.

intra-particle, intra-fiber and intra-matrix fluctuations cannot be resolved by mean-field approaches. On the other hand, the interactions cause the levels of the average stresses and strains in individual inhomogeneities to differ, i.e., inter-particle and inter-fiber fluctuations are present. These are not resolved by most mean-field-type methods, either; for an exception see, e.g., El Mouden and Molinari (2000).

Two main strategies are available for handling non-dilute reinforcement volume fractions within mean-field methods in continuum micromechanics: Either non-interacting inhomogeneities are subjected to suitably modified stress or strain fields (rather than to the corresponding far fields) or they are embedded into a suitably selected, fictitious medium (rather than into the matrix). This way the Eshelby-based apparatus for non-interacting reinforcements discussed in section 2.2 can be directly leveraged into the non-dilute regime. The above two strategies are commonly referred to as effective-field and as effective-medium approaches, respectively. Figure 2.1 schematically compares the material and loading configurations underlying non-interacting (NIA or "dilute Eshelby") models, an effective-field scheme and two effective-medium approaches.

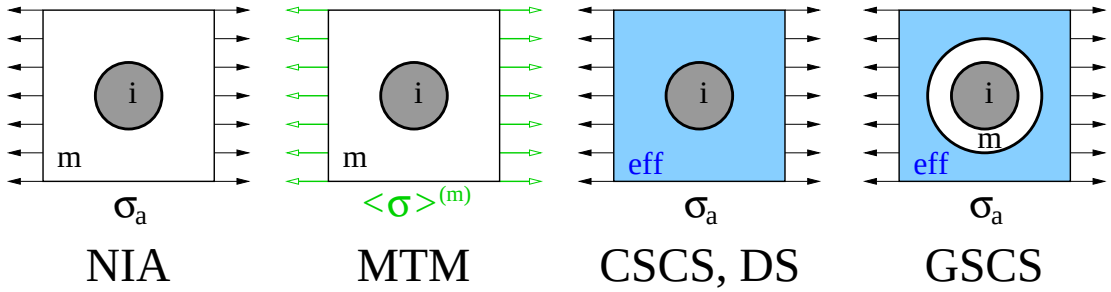

Figure 2.1: Schematic comparison of the Eshelby method in the non-interacting approximation (NIA), Mori–Tanaka approaches (MTM), differential schemes (DS) and classical (CSCS) as well as generalized self-consistent (GSCS) schemes.

2.3.1 Effective-Field Approaches

One way of introducing collective interactions between inhomogeneities into mean-field models consists of approximating the stresses acting on an inhomogeneity, which may be viewed as perturbation stresses caused by the presence of other inhomogeneities ("image stresses", "background stresses") superimposed on the applied far-field stress, by a suitable uniform effective stress, $\boldsymbol{\sigma}_{\mathrm{E}}$. On the basis of analogous considerations the far-field strain may be replaced by an effective strain $\boldsymbol{\varepsilon}_{\mathrm{E}}$. Following this concept of effective fields, which was introduced by Mossotti (1850), the the phase averaged strain and stress in an inhomogeneity are described as

$$\begin{aligned} \langle\boldsymbol{\varepsilon}\rangle^{(\mathrm{i})} &= \bar{\mathbf{A}}^{(\mathrm{i})}_{\mathrm{dil}}\,\boldsymbol{\varepsilon}_{\mathrm{E}} = \bar{\mathbf{A}}^{(\mathrm{i})}_{\mathrm{dil}}\mathbf{A}^{(\mathrm{i})}_{\mathrm{cic}}\,\langle\boldsymbol{\varepsilon}\rangle \\ \langle\boldsymbol{\sigma}\rangle^{(\mathrm{i})} &= \bar{\mathbf{B}}^{(\mathrm{i})}_{\mathrm{dil}}\,\boldsymbol{\sigma}_{\mathrm{E}} = \bar{\mathbf{B}}^{(\mathrm{i})}_{\mathrm{dil}}\mathbf{B}^{(\mathrm{i})}_{\mathrm{cic}}\,\langle\boldsymbol{\sigma}\rangle \end{aligned} \tag{2.38}$$

(Sevostianov and Kachanov, 2014). Here the tensors $\mathbf{A}^{(\mathrm{i})}_{\mathrm{cic}}$ and $\mathbf{B}^{(\mathrm{i})}_{\mathrm{cic}}$ link the the effective and the macroscopic fields, providing corrections for collective interactions. What remains, of course, is the task of finding suitable expressions for the effective fields, $\boldsymbol{\varepsilon}_{\mathrm{E}}$ and/or $\boldsymbol{\sigma}_{\mathrm{E}}$.

Mori–Tanaka-Type Estimates

The idea of choosing the matrix fields as the effective fields goes back to Brown and Stobbs (1971) as well as Mori and Tanaka (1973); such effective-field approaches are generically referred to as Mori–Tanaka methods. Benveniste (1987) based his treatment of Mori–Tanaka approaches on the relationships

$$\begin{aligned} \langle\boldsymbol{\varepsilon}\rangle^{(\mathrm{i})} &= \bar{\mathbf{T}}_{\mathrm{dil}}^{(\mathrm{i,m})}\langle\boldsymbol{\varepsilon}\rangle^{(\mathrm{m})} = \bar{\mathbf{A}}_{\mathrm{dil}}^{(\mathrm{i})}\langle\boldsymbol{\varepsilon}\rangle^{(\mathrm{m})} \\ \langle\boldsymbol{\sigma}\rangle^{(\mathrm{i})} &= \bar{\mathbf{W}}_{\mathrm{dil}}^{(\mathrm{i,m})}\langle\boldsymbol{\varepsilon}\rangle^{(\mathrm{m})} = \bar{\mathbf{B}}_{\mathrm{dil}}^{(\mathrm{i})}\langle\boldsymbol{\sigma}\rangle^{(\mathrm{m})} \end{aligned} \tag{2.39}$$

or, equivalently,

$$\begin{aligned} \bar{\mathbf{A}}^{(\mathrm{i})} &= \bar{\mathbf{A}}_{\mathrm{dil}}^{(\mathrm{i})}\bar{\mathbf{A}}^{(\mathrm{m})} \\ \bar{\mathbf{B}}^{(\mathrm{i})} &= \bar{\mathbf{B}}_{\mathrm{dil}}^{(\mathrm{i})}\bar{\mathbf{B}}^{(\mathrm{m})} \end{aligned} \quad , \tag{2.40}$$

which literally transcribe the above assumptions, compare also Fig. 2.1. Consistent expressions for $\langle\boldsymbol{\varepsilon}\rangle^{(\mathrm{m})}$ and/or $\langle\boldsymbol{\sigma}\rangle^{(\mathrm{m})}$ can be obtained by inserting eqn. (2.39) into eqn. (2.5), leading to the relations

$$\begin{aligned} \langle\boldsymbol{\varepsilon}\rangle^{(\mathrm{m})} &= [(1-\xi)\mathbf{I} + \xi\bar{\mathbf{A}}_{\mathrm{dil}}^{(\mathrm{i})}]^{-1}\langle\boldsymbol{\varepsilon}\rangle \\ \langle\boldsymbol{\sigma}\rangle^{(\mathrm{m})} &= [(1-\xi)\mathbf{I} + \xi\bar{\mathbf{B}}_{\mathrm{dil}}^{(\mathrm{i})}]^{-1}\langle\boldsymbol{\sigma}\rangle \end{aligned} \quad . \tag{2.41}$$

These, in turn, allow the Mori–Tanaka strain and stress concentration tensors for matrix and inhomogeneities to be written in terms of the dilute concentration tensors as[21]

$$\begin{aligned} \bar{\mathbf{A}}_{\mathrm{MT}}^{(\mathrm{m})} &= [(1-\xi)\mathbf{I} + \xi\bar{\mathbf{A}}_{\mathrm{dil}}^{(\mathrm{i})}]^{-1} & \bar{\mathbf{A}}_{\mathrm{MT}}^{(\mathrm{i})} &= \bar{\mathbf{A}}_{\mathrm{dil}}^{(\mathrm{i})}[(1-\xi)\mathbf{I} + \xi\bar{\mathbf{A}}_{\mathrm{dil}}^{(\mathrm{i})}]^{-1} \\ \bar{\mathbf{B}}_{\mathrm{MT}}^{(\mathrm{m})} &= [(1-\xi)\mathbf{I} + \xi\bar{\mathbf{B}}_{\mathrm{dil}}^{(\mathrm{i})}]^{-1} & \bar{\mathbf{B}}_{\mathrm{MT}}^{(\mathrm{i})} &= \bar{\mathbf{B}}_{\mathrm{dil}}^{(\mathrm{i})}[(1-\xi)\mathbf{I} + \xi\bar{\mathbf{B}}_{\mathrm{dil}}^{(\mathrm{i})}]^{-1} \end{aligned} \tag{2.42}$$

(Benveniste, 1987). Equations (2.42) may be evaluated with any strain and stress concentration tensors $\bar{\mathbf{A}}_{\mathrm{dil}}^{(\mathrm{i})}$ and $\bar{\mathbf{B}}_{\mathrm{dil}}^{(\mathrm{i})}$ pertaining to dilute inhomogeneities embedded in a matrix. If, for example, the equivalent inclusion expressions, eqns. (2.31) and (2.32), are employed, the Mori–Tanaka matrix strain and stress concentration tensors for the non-dilute composite take the form

$$\begin{aligned} \bar{\mathbf{A}}_{\mathrm{MT}}^{(\mathrm{m})} &= \{(1-\xi)\mathbf{I} + \xi[\mathbf{I} + \mathbf{S}\mathbf{C}^{(\mathrm{m})}(\mathbf{E}^{(\mathrm{i})} - \mathbf{E}^{(\mathrm{m})})]^{-1}\}^{-1} \\ \bar{\mathbf{B}}_{\mathrm{MT}}^{(\mathrm{m})} &= \{(1-\xi)\mathbf{I} + \xi\mathbf{E}^{(\mathrm{i})}[\mathbf{I} + \mathbf{S}\mathbf{C}^{(\mathrm{m})}(\mathbf{E}^{(\mathrm{i})} - \mathbf{E}^{(\mathrm{m})})]^{-1}\mathbf{C}^{(\mathrm{m})}\}^{-1} \end{aligned} \quad , \tag{2.43}$$

compare Benveniste (1987), Benveniste and Dvorak (1990) or Benveniste et al. (1991). The Mori–Tanaka approximations to the effective elastic tensors are obtained by combining eqns. (2.42) and/or (2.43) with eqns. (2.8) and (2.9). By inserting eqns. (2.42) into eqns. (2.8) the Mori–Tanaka estimates for the effective elastic tensors are obtained as

$$\begin{aligned} \mathbf{E}_{\mathrm{MT}}^{*} &= [\xi\mathbf{E}^{(\mathrm{i})}\bar{\mathbf{A}}_{\mathrm{dil}}^{(\mathrm{i})} + (1-\xi)\mathbf{E}^{(\mathrm{m})}][\xi\bar{\mathbf{A}}_{\mathrm{dil}}^{(\mathrm{i})} + \mathbf{I}]^{-1} \\ \mathbf{C}_{\mathrm{MT}}^{*} &= [\xi\mathbf{C}^{(\mathrm{i})}\bar{\mathbf{B}}_{\mathrm{dil}}^{(\mathrm{i})} + (1-\xi)\mathbf{C}^{(\mathrm{m})}][\xi\bar{\mathbf{B}}_{\mathrm{dil}}^{(\mathrm{i})} + \mathbf{I}]^{-1} \end{aligned} \quad . \tag{2.44}$$

A number of authors gave different but essentially equivalent Mori–Tanaka-type expressions for the phase concentration tensors and effective thermoelastic tensors of inhomogeneous materials, among them Pedersen (1983), Wakashima et al. (1988), Taya et al.

[21] Equations (2.18) and (2.42) are identical because they essentially describe the same physics.

(1991), Pedersen and Withers (1992) as well as Clyne and Withers (1993). Alternatively, a Mori–Tanaka method can be formulated to directly give the macroscopic elasticity tensor as

$$\mathbf{E}_{\mathrm{T}}^{*} = \mathbf{E}^{(\mathrm{m})}\big\{\mathbf{I} - \xi[(\mathbf{E}^{(\mathrm{i})} - \mathbf{E}^{(\mathrm{m})})\big(\mathbf{S} - \xi(\mathbf{S} - \mathbf{I})\big) + \mathbf{E}^{(\mathrm{m})}]^{-1}[\mathbf{E}^{(\mathrm{i})} - \mathbf{E}^{(\mathrm{m})}]\big\}^{-1} \tag{2.45}$$

(Tandon and Weng, 1984). Because eqn. (2.45) does not explicitly use the compliance tensor of the inhomogeneities, $\mathbf{C}^{(\mathrm{i})}$, it can be modified in a straightforward way to describe the macroscopic stiffness of porous materials by setting $\mathbf{E}^{(\mathrm{i})} \to \mathbf{0}$, producing the relationship

$$\mathbf{E}_{\mathrm{MT,por}} = \mathbf{E}^{(\mathrm{m})}\big[\mathbf{I} + \frac{\xi}{1-\xi}(\mathbf{I} - \mathbf{S})^{-1}\big]^{-1} \quad . \tag{2.46}$$

which, however, should not be used for void volume fractions that are much in excess of, say, $\xi = 0.25$[22].

As is evident from their derivation, Mori–Tanaka-type theories at all volume fractions describe composites consisting of randomly positioned, aligned, ellipsoidal inhomogeneities embedded in a matrix, i.e., inhomogeneous materials with a distinct matrix–inclusion microtopology. More specifically, it was shown by Ponte Castañeda and Willis (1995) that Mori–Tanaka methods are a special case of Hashin–Shtrikman variational estimates, compare Section 2.4, in which the spatial arrangement of the inhomogeneities follows an aligned ellipsoidal distribution that is characterized by the same aspect ratio as the shape of the inhomogeneit

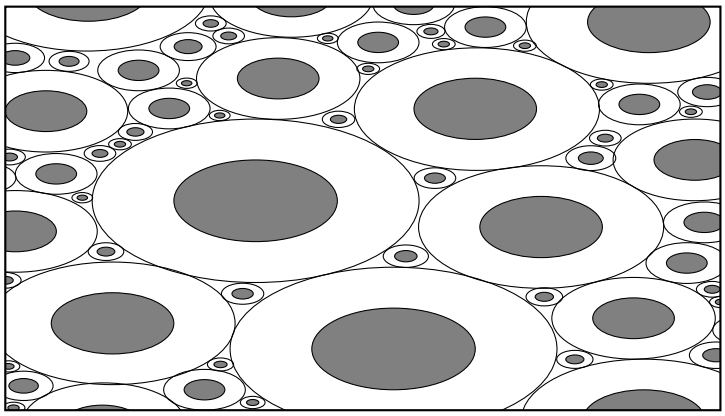

Figure 2.2: Sketch of ellipsoidal inhomogeneities in an aligned ellipsoidally distributed spatial arrangement as used implicitly in Mori–Tanaka-type models (a=2.0).

For many two-phase composites Mori–Tanaka estimates coincide with one of the Hashin–Shtrikman-type bounds as formulated in Hashin and Shtrikman (1961) and Hashin and

[22]Standard Mori–Tanaka theories use the small strain assumption, the shapes of inhomogeneities being described by ellipsoids that maintain their aspect ratios throughout the deformation history. In porous or cellular materials with high void volume fractions the linear elastic range tends to be very limited, followed by bending and buckling of cell walls or struts (Gibson and Ashby, 1988), which implies changes to the shapes of the voids. Such effects cannot be captured by Mori–Tanaka models, which consequently may markedly overestimate the effective stiffness of such materials. Within the above constraints Mori–Tanaka methods can account for some effects of fluids contained in the pores, compare, e.g., Kitazono et al. (2003). It is worth noting that the predictions of different mean field models for the the ratio $E_{\mathrm{A}}/E_{\mathrm{T}}$, and thus for the macroscopic elastic anisotropy, of porous materials tend to vary considerably.

Shtrikman (1963)[23]. For composites reinforced by spherical or aligned spheroidal reinforcements that are stiffer than the matrix, MT predictions for the overall elastic moduli are, accordingly, on the low side (see the comparisons in Section 4.1 as well as tables 6.1 to 6.3). For materials containing compliant reinforcements in a stiffer matrix, in contrast, Mori–Tanaka models provide upper estimates. In situations of high elastic contrast Mori–Tanaka approaches tend to considerably under- or overestimate the effective elastic properties. For discussions of further issues with respect to the range of validity of Mori–Tanaka theories for elastic inhomogeneous two-phase materials see Christensen et al. (1992).

Mori–Tanaka-type theories can be implemented into computer programs in a straightforward way: Because they are explicit algorithms, all that is required are matrix additions, multiplications, and inversions plus expressions for the Eshelby tensor. Despite their limitations, Mori–Tanaka models provide useful accuracy for the elastic contrasts pertaining to most practically relevant composites. This combination of features makes them important tools for evaluating the stiffness and thermal expansion properties of inhomogeneous materials that show a matrix–inclusion topology with aligned inhomogeneities. "Extended" Mori–Tanaka models for nonaligned reinforcements are discussed in Section 2.6, multi-phase Mori–Tanaka schemes in Section 2.8 and Mori–Tanaka-type approaches to describing thermoelastoplastic materials in Section 2.9,

Maxwell Schemes

The first "micromechanical" model to appear in the literature, the scheme of Maxwell (1873) for evaluating the effective conductivities of inhomogeneous materials, can be interpreted in terms of a mean-field method in elasticity, see Torquato (2002) and Sevostianov and Giraud (2013). It is based on studying a single region of inhomogeneous material that contains a sufficient number of inhomogeneities to be treated as an RVE and that is embedded in a much larger matrix region, compare fig. 2.3. This arrangement is described, on the one hand, by a sub-model incorporating the above set of inhomogeneities ("inhomogeneous region", left side of fig. 2.3), which are treated as non-interacting via eqns. (2.31) or (2.32), and, on the other hand, by a sub-model in which the region consists of an (unknown) uniform effective material ("effective inhomogeneity", right side of fig. 2.3), the overall elastic responses of the two configurations being required to be equal. Analogous approaches were used, e.g., by Giordano (2003) and, independently of Maxwell's ideas, by Shen and Yi (2001).

Using eqns. (2.8) and (2.9), summing up over the contributions of the individual inhomogeneities $^{(\mathrm{q})}$ in the arrangement on the left, and employing dilute Eshelby expressions for both configurations leads to the relations

$$\begin{aligned}
\mathbf{E}^{(\mathrm{m})} + \sum_{(\mathrm{q})\neq(\mathrm{m})} \xi^{(\mathrm{q})} (\mathbf{E}^{(\mathrm{q})} - \mathbf{E}^{(\mathrm{m})}) \bar{\mathbf{A}}^{(\mathrm{q})}_{\mathrm{dil}} &= \mathbf{E}^{(\mathrm{m})} + \xi_{\mathrm{E}} (\mathbf{E}^{*} - \mathbf{E}^{(\mathrm{m})}) \bar{\mathbf{T}}^{(*,\mathrm{m})}_{\mathrm{dil}} \\
\mathbf{C}^{(\mathrm{m})} + \sum_{(\mathrm{q})\neq(\mathrm{m})} \xi^{(\mathrm{q})} (\mathbf{C}^{(\mathrm{q})} - \mathbf{C}^{(\mathrm{m})}) \bar{\mathbf{B}}^{(\mathrm{q})}_{\mathrm{dil}} &= \mathbf{C}^{(\mathrm{m})} + \xi_{\mathrm{E}} (\mathbf{C}^{*} - \mathbf{C}^{(\mathrm{m})}) \bar{\mathbf{W}}^{(*,\mathrm{m})}_{\mathrm{dil}} \quad , \qquad (2.47)
\end{aligned}$$

[23] It should be noted, though, that Mori–Tanaka estimates correspond to Hashin–Shtrikman-type bounds only if the constituents of the composite are elastically well-ordered, compare Section 3.1.

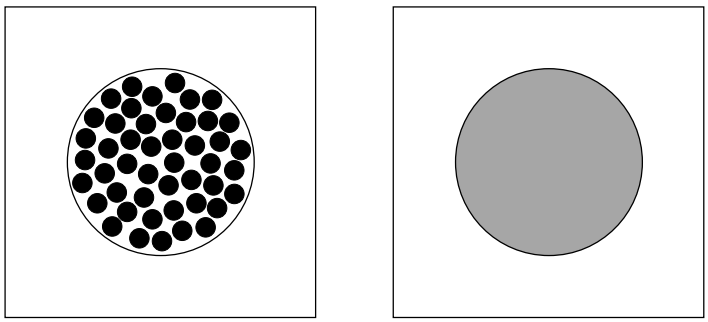

Figure 2.3: Sketch of the two configurations underlying Maxwell (1873) schemes.

where ξ_{E} and $\xi^{(\mathrm{q})}$ are the volume fractions of the inhomogeneous region and of the individual inhomogeneities, respectively. The superscript $^{(*,\mathrm{m})}$ indicates that the dilute partial concentration tensors, see eqn. (2.34), pertain to a region of effective material embedded in the matrix. If the shapes and material behaviors of all inhomogeneities $^{(\mathrm{q})}$ are identical they can be viewed as forming a reinforcement phase of volume fraction $\xi = \sum_{(\mathrm{q})\neq(\mathrm{m})} \xi^{(\mathrm{q})}/\xi_{\mathrm{E}}$. The two-phase Maxwell estimates for the effective elastic tensors, $\mathbf{E}^*_{\mathrm{MX}}$ and $\mathbf{C}^*_{\mathrm{MX}}$, can then be extracted from eqn. (2.47) as

$$\begin{aligned} \mathbf{E}^*_{\mathrm{MX}} &= \mathbf{E}^{(\mathrm{m})} + \xi\Big[(\mathbf{E}^{(\mathrm{i})} - \mathbf{E}^{(\mathrm{m})})^{-1} + (\mathbf{S}^{(\mathrm{i,m})} - \xi\mathbf{S}_{\mathrm{E}})\mathbf{C}^{(\mathrm{m})}\Big]^{-1} \\ \mathbf{C}^*_{\mathrm{MX}} &= \mathbf{C}^{(\mathrm{m})} + \xi\Big[(\mathbf{C}^{(\mathrm{i})} - \mathbf{C}^{(\mathrm{m})})^{-1} + \mathbf{E}^{(\mathrm{m})}\big((1-\xi)\mathbf{I} - \mathbf{S}^{(\mathrm{i,m})} + \xi\mathbf{S}_{\mathrm{E}}\big)\Big]^{-1} \end{aligned} \quad . \tag{2.48}$$

Here $\mathbf{S}_{\mathrm{E}}$ is an Eshelby tensor pertaining to the shape of the inhomogeneous region and $\mathbf{S}^{(\mathrm{i,m})} = \mathbf{S}$ is the "standard" Eshelby tensor depending on the shape of the inhomogeneities. Approaches in which the behavior of the inhomogeneous region is described by some interacting model rather than the dilute Eshelby one have been referred to as generalized Maxwell schemes, see, e.g., Kanaun (2016). For recent discussions of Maxwell models and their extensions see Sevostianov et al. (2019) and Buryachenko (2022b).

Equations (2.48) can be used to obtain expressions for the inhomogeneity fields that are of the same form as eqns. (2.38), making Maxwell schemes proper effective-field models. If the inhomogeneous region is chosen to have the same shape as the (aligned) inhomogeneities, so that $\mathbf{S}_{\mathrm{E}} = \mathbf{S}^{(\mathrm{i,m})}$, the two-phase Maxwell scheme, eqn. (2.48), coincides with the Mori–Tanaka expressions, eqn. (2.44).

Hashin–Shtrikman Estimates of Ponte and Willis

Ponte Castañeda and Willis (1995) developed a variationally-based effective-field scheme for inhomogeneous materials that consist of ellipsoidal arrangements of ellipsoidal inhomogeneities embedded in a matrix. In such materials the spatial correlations of the inhomogeneity arrangement can be described by an Eshelby tensor $\mathbf{S}_{\mathrm{d}}$ and the shapes of the inhomogeneities via the Eshelby tensor $\mathbf{S}^{(\mathrm{i,m})}$ (which corresponds to $\mathbf{S}$ as used in the preceding sections), both of which are evaluated using the matrix as the embedding material. The corresponding phase arrangements can be visualized by interpreting fig. 2.2 as consisting of identical, aligned, non-overlapping "safety ellipsoids" (exclusion volumes describing the ellipsoidal arrangement of reinforcements) that contain (aligned or nonaligned)

ellipsoidal inhomogeneities, the aspect ratios of the safety ellipsoids. Using the concept of Hashin–Shtrikman estimates, compare section 2.4, the inhomogeneity strain concentration tensors of such microgeometries can be expressed as

$$\begin{aligned} \bar{\mathbf{A}}_{\mathrm{PW}}^{(\mathrm{i})} &= \left[\mathbf{I} + (\mathbf{S}^{(\mathrm{i,m})} - \xi\mathbf{S}_{\mathrm{d}}\mathbf{C}^{(\mathrm{m})}(\mathbf{E}^{(\mathrm{i})} - \mathbf{E}^{(\mathrm{m})})\right]^{-1} \\ &= \bar{\mathbf{A}}_{\mathrm{dil}}^{(\mathrm{i})}\left[\mathbf{I} - \xi\mathbf{S}_{\mathrm{d}}\mathbf{C}^{(\mathrm{m})}(\mathbf{E}^{(\mathrm{i})} - \mathbf{E}^{(\mathrm{m})})\bar{\mathbf{A}}_{\mathrm{dil}}^{(\mathrm{i})}\right]^{-1} \quad , \end{aligned} \tag{2.49}$$

which fits the effective-field mold. The macroscopic elasticity tensor follows as

$$\begin{aligned} \mathbf{E}_{\mathrm{PW}}^{*} &= \mathbf{E}^{(\mathrm{m})} + \xi(\mathbf{E}^{(\mathrm{i})} - \mathbf{E}^{(\mathrm{m})})\left[\mathbf{I} + (\mathbf{S}^{(\mathrm{i,m})} - \xi\mathbf{S}_{\mathrm{d}})\mathbf{C}^{(\mathrm{m})}(\mathbf{E}^{(\mathrm{i})} - \mathbf{E}^{(\mathrm{m})})\right]^{-1} \\ &= \mathbf{E}^{(\mathrm{m})} + \left[\left(\xi(\mathbf{E}^{(\mathrm{i})} - \mathbf{E}^{(\mathrm{m})})\bar{\mathbf{A}}_{\mathrm{dil}}^{(\mathrm{i})}\right)^{-1} - \mathbf{S}_{\mathrm{d}}\mathbf{C}^{(\mathrm{m})}\right]^{-1} \end{aligned} \tag{2.50}$$

via eqn. (2.8). This model is known as the Hashin–Shtrikman estimates of Ponte Castañeda and Willis (1995). It is strictly valid as long as the inhomogeneities do not penetrate their respective safety ellipsoids. When the safety ellipsoids and the inhomogeneities are aligned and identical, $\mathbf{S}_{\mathrm{d}} = \mathbf{S}^{(\mathrm{i,m})}$, eqn. (2.50) recovers Mori–Tanaka expressions, which shows that Mori–Tanaka methods are a special case of Hashin–Shtrikman estimates.

Analogous expressions to eqn. (2.50) can be obtained with two-phase Maxwell models, compare eqns. (2.48), and the Interaction Direct Derivative (IDD) approach of Du and Zheng (2002). A further related model is the double inclusion model of Hori and Nemat-Nasser (1993), the connections of which to the Ponte–Willis estimates and a number of other micromechanical schemes were discussed by Hu and Weng (2000). All these models provide more flexibility in terms of the arrangement of inhomogeneities than do Mori–Tanaka methods.

Advanced Effective-Field Methods

Equations (2.38) obviously allow incorporating more complex approximations to the effective fields than covered up to this point, see, e.g., Kanaun and Levin (1994), Rodin and Weng (2014) or Saadat et al. (2015). For composites showing a matrix–inclusion topology, in the most general case the effective fields may be evaluated from regions containing a number of interacting inhomogeneities (a "cloud of inhomogeneities"), which gives rise to the Multi-Particle Effective-Field Method (MEFM) discussed in depth by Buryachenko (2007). Such models are formulated in terms of integral equations, are very powerful and subject to few restrictions, but are rather complex. They subsume the simpler effective-field models such as Mori–Tanaka methods as special cases.

2.3.2 Effective-Medium Approaches

The second group of mean-field estimates for the overall thermomechanical moduli of inhomogeneous materials are effective-medium approaches, in which an inhomogeneity or some phase arrangement (often referred to as a kernel) is embedded in the effective material, the properties of which are not known a priori. Figure 2.1 sketches two models of this type, the classical self-consistent and generalized self-consistent schemes[24].

[24] Within the classification of micromechanical methods given in Section 1.5, self-consistent mean-field schemes may also be viewed as analytical embedding approaches.

Classical Self-Consistent Estimates

If the kernel consists of just an inhomogeneity, classical (or two-phase) self-consistent schemes (CSCS) are obtained, see, e.g., Hill (1965b). They are based on treating both phases, $^{(\mathrm{p})}$ and $^{(\mathrm{q})}$ with volume fractions $\xi^{(\mathrm{p})}$ and $\xi^{(\mathrm{q})}$, as inhomogeneities embedded in an a priori unknown, homogeneous reference medium ^{0} and requiring the mean-field approximations to the stress and strain perturbations to vanish, which translates into the conditions

$$\begin{aligned} \xi^{(\mathrm{p})}(\mathbf{E}^{(\mathrm{p})}-\mathbf{E}^{0})\bar{\mathbf{T}}_{\mathrm{dil}}^{(\mathrm{p},0)}+\xi^{(\mathrm{q})}(\mathbf{E}^{(\mathrm{q})}-\mathbf{E}^{0})\bar{\mathbf{T}}_{\mathrm{dil}}^{(\mathrm{q},0)} &= \mathbf{0} \\ \xi^{(\mathrm{p})}(\mathbf{C}^{(\mathrm{p})}-\mathbf{C}^{0})\bar{\mathbf{W}}_{\mathrm{dil}}^{(\mathrm{p},0)}+\xi^{(\mathrm{q})}(\mathbf{C}^{(\mathrm{q})}-\mathbf{C}^{0})\bar{\mathbf{W}}_{\mathrm{dil}}^{(\mathrm{q},0)} &= \mathbf{0} \quad , \end{aligned} \tag{2.51}$$

Accordingly — in contrast to effective-field approximations — no distinction is made between contiguous (matrix) and non-contiguous (inhomogeneity) phases. Identifying the reference medium with the effective material and applying eqns. (2.8) the relationships

$$\begin{aligned} \mathbf{E}_{\mathrm{SC}}^{*} &= \mathbf{E}^{(\mathrm{q})}+\xi^{(\mathrm{p})}[\mathbf{E}^{(\mathrm{p})}-\mathbf{E}^{(\mathrm{q})}]\,\bar{\mathbf{T}}_{\mathrm{dil}}^{(\mathrm{p},*)} \\ &= \mathbf{E}^{(\mathrm{q})}+\xi^{(\mathrm{p})}[\mathbf{E}^{(\mathrm{p})}-\mathbf{E}^{(\mathrm{q})}]\,[\mathbf{I}+\mathbf{S}^{(\mathrm{p},*)}\mathbf{C}_{\mathrm{SC}}^{*}(\mathbf{E}^{(\mathrm{p})}-\mathbf{E}_{\mathrm{SC}}^{*})]^{-1} \\ \mathbf{C}_{\mathrm{SC}}^{*} &= \mathbf{C}^{(\mathrm{q})}+\xi^{(\mathrm{p})}[\mathbf{C}^{(\mathrm{p})}-\mathbf{C}^{(\mathrm{q})}]\,\bar{\mathbf{W}}_{\mathrm{dil}}^{(\mathrm{p},*)} \\ &= \mathbf{C}^{(\mathrm{q})}+\xi^{(\mathrm{p})}[\mathbf{C}^{(\mathrm{p})}-\mathbf{C}^{(\mathrm{q})}]\,[\mathbf{I}+\mathbf{E}_{\mathrm{SC}}^{*}(\mathbf{I}-\mathbf{S}^{(\mathrm{p},*)})(\mathbf{C}^{(\mathrm{p})}-\mathbf{C}_{\mathrm{SC}}^{*})]^{-1} \end{aligned} \tag{2.52}$$

are obtained, which do not obviously show the symmetry in terms of the phases evident in eqns. (2.51). In eqns. (2.52) $\mathbf{S}^{(\mathrm{p},*)}$, $\bar{\mathbf{T}}_{\mathrm{dil}}^{(\mathrm{p},*)}$ and $\bar{\mathbf{W}}_{\mathrm{dil}}^{(\mathrm{p},*)}$ stand for the Eshelby tensor and dilute partial concentration tensors, compare eqn. (2.34), of an inhomogeneity $^{(\mathrm{p})}$ embedded in the (unknown) effective material. Equations (2.52) provide systems of implicit nonlinear equations for the unknown elastic tensors, $\mathbf{E}_{\mathrm{SC}}^{*}$ and $\mathbf{C}_{\mathrm{SC}}^{*}$, describing the behavior of the effective medium. These systems can be solved by self-consistent iterative schemes of the type

$$\begin{aligned} \mathbf{E}_{\mathrm{SC},n+1} &= \mathbf{E}^{(\mathrm{q})}+\xi^{(\mathrm{p})}[\mathbf{E}^{(\mathrm{p})}-\mathbf{E}^{(\mathrm{q})}][\mathbf{I}+\mathbf{S}_{n}^{(\mathrm{p},*)}\mathbf{C}_{n}(\mathbf{E}^{(\mathrm{p})}-\mathbf{E}_{n})]^{-1} \\ \mathbf{C}_{\mathrm{SC},n+1} &= \left[\mathbf{E}_{\mathrm{SC},n+1}\right]^{-1} \quad . \end{aligned} \tag{2.53}$$

The Eshelby tensor $\mathbf{S}_{n}^{(\mathrm{p},*)}$ in eqn. (2.53) pertains to an inhomogeneity embedded in the n-th iteration for the effective medium; it must be recomputed for each iteration[25].

The predictions of the CSCS for two-phase materials differ clearly from the ones obtained with Mori–Tanaka methods, tending to be close to the Hashin–Shtrikman lower bounds (see Section 3) if the volume fraction of the more compliant phase is high and close to the upper bounds it it is low (compare figs. 4.1 to 4.9). Generally, two-phase self-consistent schemes are well suited to describing the overall properties of two-phase materials that do not show a matrix–inclusion microtopology for some or all of the volume fractions of interest[26] and are, accordingly, not the method of choice for describing

[25] For aligned spheroidal but non-spherical, isotropic inhomogeneities in an isotropic matrix the effective medium shows transversally isotropic behavior, which must be accounted for in evaluating the Eshelby tensor $\mathbf{S}_{n}^{(\mathrm{p},*)}$.

[26] Classical self-consistent schemes have been shown to correspond to perfectly disordered materials (Kröner, 1978) or self-similar hierarchical materials (Torquato, 2002). Because all phases in expressions such as eqn. (2.86) are treated on an equal footing, the CSCS is sometimes referred to as a "symmetric" scheme.

"standard" composite materials. The two-phase CSCS may, however, be used for studying Functionally Graded Materials (FGMs), which tend to show an interpenetrating phase topology for volume fractions around $\xi^{(p)} = \xi^{(q)} = \frac{1}{2}$, with phase $^{(q)}$ acting acting as the matrix for $\xi^{(p)} \to 0$ and $^{(p)}$ for $\xi^{(p)} \to 1$. Multi-phase versions of the CSCS, see, e.g., eqn. (2.86), are important methods for modeling materials with grain-like microstructures, such as polycrystals. For porous materials classical self-consistent schemes predict a breakdown of the stiffness due to percolation of the pores at $\xi^{(p)} = \frac{1}{2}$ for spherical voids and at $\xi^{(p)} = \frac{1}{3}$ for aligned cylindrical voids (Torquato, 2002).

Because self-consistent schemes are by definition implicit methods, their computational requirements are in general higher than those of Mori–Tanaka-type approaches. Like effective-field models, they have formed the basis for describing the behavior of nonlinear inhomogeneous materials.

Generalized Self-Consistent Estimates

Generalized self-consistent schemes (GSCS) are effective-medium theories that employ a kernel made up of an inhomogeneity surrounded by an appropriate volume of matrix material, compare fig. 2.1. When such configurations are embedded in a matrix and subjected to mechanical or thermal loads the fields in them in general are not homogeneous, even in the dilute case. However, the general relationships presented in Section 2.1 continue to hold.

In contrast to the other methods covered here, the GSCS proposed by Christensen and Lo (1979), see also Christensen and Lo (1986), provides results for individual effective moduli rather than elastic tensors. The results were obtained from the differential equations describing the elastic responses of spherical or cylindrical three-phase regions, respectively, under appropriate boundary and loading conditions, plus an energy equivalence closure. This leads to cubic equations for the effective shear modulus G^* in the case of spherical particles or the transverse shear modulus G^*_T in the case of aligned, continuous fibers. The original scheme pertains to isotropic inhomogeneities, but predictions for composites reinforced by continuous, aligned, transversally isotropic fibers can be obtained as a special case of models for composites reinforced by (multi-) coated fibers developed by Hervé and Zaoui (1995), compare Section 2.8.2. The results for the bulk modulus, the axial Young's and shear moduli, the transverse bulk modulus as well as the coefficients of thermal expansion coincide with the ones obtained from Mori–Tanaka approaches as well as composite sphere or composite cylinder assemblages.

GSCS models of the type sketched in Fig. 2.1 pertain to materials with matrix–inclusion microtopologies. Compared to Mori–Tanaka and Maxwell models the three-phase GSCS provides improved predictions for the effective shear modulus or the effective transverse shear modulus of typical composites. In three-dimensional cases it is available for spherical or aligned, continuous reinforcements; semi-analytical solutions were also proposed for randomly oriented spheroidal inhomogeneities (Riccardi and Montheillet, 1999). In 2D solutions were reported for aligned elliptical inhomogeneities (Huang and Hu, 1995).

Differential Schemes

A further important type of effective-medium mean-field approach are differential schemes (McLaughlin, 1977; Norris, 1985), which may be viewed as involving repeated cycles of adding small concentrations of inhomogeneities to a material and then homogenizing. Following Hashin (1988) the resulting estimates for the overall elastic tensors can be described by the coupled systems of differential equations

$$\begin{aligned} \frac{\mathrm{d}\mathbf{E}_{\mathrm{D}}^{*}}{\mathrm{d}\xi} &= \frac{1}{1-\xi}\,[\mathbf{E}^{(\mathrm{i})} - \mathbf{E}_{\mathrm{D}}^{*}]\,\bar{\mathbf{T}}_{\mathrm{dil}}^{(\mathrm{i},*)} \\ \frac{\mathrm{d}\mathbf{C}_{\mathrm{D}}^{*}}{\mathrm{d}\xi} &= \frac{1}{1-\xi}\,[\mathbf{C}^{(\mathrm{i})} - \mathbf{C}_{\mathrm{D}}^{*}]\,\bar{\mathbf{W}}_{\mathrm{dil}}^{(\mathrm{i},*)} \end{aligned} \tag{2.54}$$

with the initial conditions $\mathbf{E}_{\mathrm{D}}^{*}{=}\mathbf{E}^{(\mathrm{m})}$ and $\mathbf{C}_{\mathrm{D}}^{*}{=}\mathbf{C}^{(\mathrm{m})}$, respectively, at $\xi{=}0$. By analogy to eqn. (2.52) $\bar{\mathbf{W}}_{\mathrm{dil}}^{(\mathrm{i},*)}$ and $\bar{\mathbf{T}}_{\mathrm{dil}}^{(\mathrm{i},*)}$ depend on the current approximations to the effective response, $\mathbf{E}_{\mathrm{D}}^{*}$ and $\mathbf{C}_{\mathrm{D}}^{*}$. Equations (2.54) can be conveniently integrated with standard numerical algorithms for initial value problems, e.g., Runge–Kutta methods.

Differential schemes clearly pertain to matrix–inclusion microtopologies and have been argued to describe polydisperse distributions of the sizes of the inhomogeneities[27]. Models of this group tend to show excellent agreement with numerical models at elevated inhomogeneity volume fractions. Nevertheless, probably due to their potential association with specific microgeometries that are not necessarily typical of "classical composites" (in which reinforcement size distributions usually are rather sharp[28]) and their higher mathematical complexity (as compared, e.g., to Mori–Tanaka models), Differential Schemes have seen surprisingly limited use in modeling the thermo-mechanical behavior of actual composite materials.

2.4 General Considerations

An important concept in analytical micromechanics is that of the homogeneous reference material (or comparison medium) $^{(0)}$, which may be a constituent of a given composite or some suitable fictitious material. It allows the stress field in an inhomogeneous material to be expressed as

$$\boldsymbol{\sigma}(\mathbf{x}) = \mathbf{E}(\mathbf{x})\,\boldsymbol{\varepsilon}(\mathbf{x}) = \mathbf{E}^{0}\,\boldsymbol{\varepsilon}(\mathbf{x}) + \boldsymbol{\tau}^{0}(\mathbf{x}) \qquad , \tag{2.55}$$

where $\mathbf{E}^{0}$ is the elasticity tensor of the comparison medium and $\boldsymbol{\tau}^{0}(\mathbf{x}) = (\mathbf{E}(\mathbf{x}) - \mathbf{E}^{0})\,\boldsymbol{\varepsilon}(\mathbf{x})$ is known as the stress polarization, phase averaging of which leads to

$$\langle\boldsymbol{\tau}^{0}\rangle^{(\mathrm{p})} = (\mathbf{E}^{(\mathrm{p})} - \mathbf{E}^{0})\langle\boldsymbol{\varepsilon}\rangle^{(\mathrm{p})} = \langle\boldsymbol{\sigma}\rangle^{(\mathrm{p})} - \mathbf{E}^{0}\langle\boldsymbol{\varepsilon}\rangle^{(\mathrm{p})} \qquad , \tag{2.56}$$

[27] The interpretation of differential schemes of involving the repeated addition of infinitesimal volume fractions of inhomogeneities of increasingly larger size, followed each time by homogenization, is due to Roscoe (1973). However, Hashin (1988) pointed out that the requirements of infinitesimal volume fraction and growing size of the inhomogeneities may lead to contradictions. Avellaneda (1987) showed that differential schemes can be realized by hierarchical laminates.

[28] It is worth noting that, with the exception of very specific inhomogeneity shapes in two-dimensional conduction (Torquato and Hyun, 2001), none of the mean-field methods discussed in Section 2.3 corresponds to a realization in the form of a monodisperse matrix–inclusion microgeometry.

the phase averaged stress polarizations. Equations (2.55) can be used to develop integral representations of micromechanics, and eqns. (2.56) form the basis of generalized mean-field approaches and of many of the bounding methods discussed in Chapter 3.

Hashin–Shtrikman Tensor and Hashin–Shtrikman Estimates

Bornert (2001) pointed out that the use of phase-wise constant stress polarizations in micromechanical models may be interpreted as emphasizing the effects of inter-phase heterogeneity rather than intra-phase fluctuations. This closely corresponds to the concepts underlying mean-field models as used in the present chapter.

Equation (2.56) can be used as the starting point of variational procedures that provide strain concentration tensors in dependence on the elasticity tensor of a homogeneous reference material as

$$\begin{aligned} \bar{\mathbf{A}}_{\mathrm{HS}}^{(\mathrm{m})} &= [\mathbf{L}^{(\mathrm{i},0)} + \mathbf{E}^{(\mathrm{m})}]^{-1} \left[\xi (\mathbf{L}^{(\mathrm{i},0)} + \mathbf{E}^{(\mathrm{i})})^{-1} + (1-\xi)(\mathbf{L}^{(\mathrm{i},0)} + \mathbf{E}^{(\mathrm{m})})^{-1}\right]^{-1} \\ \bar{\mathbf{A}}_{\mathrm{HS}}^{(\mathrm{i})} &= [\mathbf{L}^{(\mathrm{i},0)} + \mathbf{E}^{(\mathrm{i})}]^{-1} \left[\xi (\mathbf{L}^{(\mathrm{i},0)} + \mathbf{E}^{(\mathrm{i})})^{-1} + (1-\xi)(\mathbf{L}^{(\mathrm{i},0)} + \mathbf{E}^{(\mathrm{m})})^{-1}\right]^{-1} \end{aligned} \quad . \tag{2.57}$$

The tensor $\mathbf{L}^{(\mathrm{i},0)}$ is referred to as the overall constraint tensor (Hill, 1965b) or Hill's influence tensor and is defined as

$$\mathbf{L}^{(\mathrm{i},0)} = \mathbf{E}^{(0)}[(\mathbf{S}^{(\mathrm{i},0)})^{-1} - \mathbf{I}] = [\mathbf{P}^{(\mathrm{i},0)}]^{-1} - \mathbf{E}^{(0)} \quad . \tag{2.58}$$

Equations (2.57) lead to estimates for the overall elasticity tensors of two-phase materials of the form

$$\begin{aligned} \mathbf{E}_{\mathrm{HS}}^{*} &= \mathbf{E}^{(\mathrm{m})} + \xi(\mathbf{E}^{(\mathrm{i})} - \mathbf{E}^{(\mathrm{m})}) \left[\mathbf{I} + (1-\xi)(\mathbf{L}^{(\mathrm{i},0)} + \mathbf{E}^{(\mathrm{m})})^{-1}(\mathbf{E}^{(\mathrm{i})} - \mathbf{E}^{(\mathrm{m})})\right]^{-1} \\ &= \left[\xi (\mathbf{L}^{(\mathrm{i},0)} + \mathbf{E}^{(\mathrm{i})})^{-1} + (1-\xi)(\mathbf{L}^{(\mathrm{i},0)} + \mathbf{E}^{(\mathrm{m})})^{-1}\right]^{-1} - \mathbf{L}^{(\mathrm{i},0)} \quad , \end{aligned} \tag{2.59}$$

Alternative expressions involving Hill tensors can be given as

$$\begin{aligned} \mathbf{E}_{\mathrm{HS}}^{*} &= \left[(1-\xi)\mathbf{E}^{(\mathrm{m})}[\mathbf{I} + \mathbf{P}^{(\mathrm{m},0)}(\mathbf{E}^{(\mathrm{m})} - \mathbf{E}^{(0)})]^{-1} + \xi \mathbf{E}^{(\mathrm{i})}[\mathbf{I} + \mathbf{P}^{(\mathrm{i},0)}(\mathbf{E}^{(\mathrm{i})} - \mathbf{E}^{(0)})]^{-1}\right] \times \\ &\quad \left[(1-\xi)[\mathbf{I} + \mathbf{P}^{(\mathrm{m},0)}(\mathbf{E}^{(\mathrm{m})} - \mathbf{E}^{(0)})]^{-1} + \xi[\mathbf{I} + \mathbf{P}^{(\mathrm{i},0)}(\mathbf{E}^{(\mathrm{i})} - \mathbf{E}^{(0)})]^{-1}\right]^{-1} \\ &= \left[(1-\xi)\mathbf{E}^{(\mathrm{m})}\bar{\mathbf{T}}_{\mathrm{dil}}^{(\mathrm{m},0)} + \xi \mathbf{E}^{(\mathrm{i})}\bar{\mathbf{T}}_{\mathrm{dil}}^{(\mathrm{i},0)}\right] \left[(1-\xi)\bar{\mathbf{T}}_{\mathrm{dil}}^{(\mathrm{m},0)} + \xi \bar{\mathbf{T}}_{\mathrm{dil}}^{(\mathrm{i},0)}\right]^{-1} \quad , \end{aligned} \tag{2.60}$$

compare, e.g., Walpole (1966) or Willis (1977). Relations like eqns. (2.59) and (2.60), which provide approximations of effective elastic tensors in terms of a reference medium, have been called Hashin–Shtrikman tensors by Bornert (2001).

If this homogeneous reference material is chosen such that $\mathbf{E}^{(0)} - \mathbf{E}^{(\mathrm{p})}$ is negative or positive semi-definite for all phases $^{(\mathrm{p})}$, Hashin–Shtrikman tensors give rise to lower and upper Hashin–Shtrikman-type bounds, respectively, compare Section 3.1. Reference media falling outside this range lead to estimates rather than bounds, which are often referred to as Hashin–Shtrikman estimates for the special case of $\mathbf{E}^{(0)} = \mathbf{E}^{(\mathrm{m})}$. These encompass Mori–Tanaka methods and, if ellipsoidal arrangements of inhomogeneities are explicitly accounted for, the Ponte–Willis estimates, see Section 2.3.1. Classical self-consistent schemes can be obtained by using the effective material as the comparison medium.

Furthermore, Hashin–Shtrikman estimates can be extended by considering geometries consisting of multi-phase "representative morphological patters" (also called "motifs") rather than uniform inhomogeneities embedded in a matrix, see the discussion by Bornert (2001). For example, if the motif takes the form of a particle or fiber surrounded by a matrix layer of appropriate thickness, the Generalized Self-Consistent scheme may be recovered. Adding further layers to such a motif leads to models for composites reinforced by coated or multi-coated particles or fibers, compare Section 2.8.2.

Integral Equations

Very general analytical models for the elastic behavior of inhomogeneous materials in terms of their microstructure and of the properties of their constituents can be given in the form of integral equations. In the case of composites having a matrix–inclusion topology the present understanding is that the most general descriptions of this type, which require the lowest number of underlying hypotheses, are "General Integral Equations", compare, e.g., Buryachenko (2015). All mean-field models discussed in Sections 2.3 and 2.8, including the MEFM, can be obtained as approximations to the General Integral Equations, which are discussed in detail in Buryachenko (2022a).

2.5 Other Analytical Estimates for Elastic Composites with Aligned Reinforcements

For convenience, in this section some analytical methods are discussed that are of practical importance but are not or only partly based on the mean-field assumptions. Nevertheless, the relations between effective elastic tensors and phase averaged fields given in Section 2.1 apply to them, which allows, e.g., concentration tensors to be extracted.

Interpolative Schemes

Interpolative schemes obtain estimates for the effective elastic tensors by interpolating between lower and upper estimates or lower and upper bounds. The simplest model of this type are the Voigt–Reuss-Hill (VRH) estimates (Hill, 1952), which are given by the arithmetic mean of the lower and upper Hill bounds, $\mathbf{E}^{*}_{\mathrm{H}-}$ and $\mathbf{E}^{*}_{\mathrm{H}+}$, defined by eqn. (3.1). A more complex interpolative scheme was proposed by Lielens et al. (1998), in which the (non-dilute) partial strain concentration tensor $\bar{\mathbf{T}}^{(\mathrm{i,m})}_{\mathrm{L}}$ is obtained by interpolating between dilute partial strain concentration tensors related to the Hashin–Shtrikman bounds as

$$\bar{\mathbf{T}}^{(\mathrm{i,m})}_{\mathrm{L}} = \Big[(1-f(\xi))\big(\mathbf{I}+\mathbf{S}^{(\mathrm{i,m})}(\mathbf{C}^{(\mathrm{m})}\mathbf{E}^{(\mathrm{i})}-\mathbf{I})\big) + f(\xi)\big(\mathbf{I}+\mathbf{S}^{(\mathrm{m,i})}(\mathbf{C}^{(\mathrm{i})}\mathbf{E}^{(\mathrm{m})}-\mathbf{I})\big)^{-1}\Big]^{-1} \tag{2.61}$$

From $\bar{\mathbf{T}}^{(\mathrm{i,m})}_{\mathrm{L}}$ the strain concentration tensors can be evaluated via eqns. (2.18) and the effective elasticity tensors via eqns. (2.85). The interpolation factors $f(\xi)$ are chosen as

$$f(\xi) = \frac{\xi+\xi^2}{2} \quad . \tag{2.62}$$

This approach is capable of providing useful estimates for some composites, see, e.g., Ghossein and Lévesque (2012), but has a weaker physical background than "standard" mean-field methods. A related scheme based on the Hill bounds, eqns. (3.1) was proposed by Perdahcıoğlu and Geijselaers (2011).

Three-Point Estimates

The analytical estimates discussed in Section 2.3 are essentially based on two-point statistics of the phase geometry, compare fig. 3.1, making them sensitive to reinforcement volume fraction and aspect ratio. Models making use of 3-point (or higher) statistical descriptors can resolve further details of the microgeometry, e.g., the relative sizes of reinforcements.

Torquato (1997, 1998a) developed third-order estimates for the effective elastic moduli of two-phase composites on the basis of weak-contrast expansions that incorporate three-point statistics via a pair of three-point microstructural parameters, $\eta(\xi)$ and $\zeta(\xi)$, which are also used in the three-point bounds discussed in Section 3.2. For convenience, these models are referred to as "three-point estimates" in the following. The three-point parameters are functions of the inhomogeneity volume fraction and are available as as fits or in tabulated form for a number of configurations involving spherical particles or aligned, continuous, cylindrical fibers; for additional information see Section 3.2. Like Generalized Self-Consistent schemes, three-point estimates provide results in terms of effective elastic moduli rather than elasticity tensors.

The three-point estimates lie between the corresponding three-point bounds, and tend to give excellent agreement with with numerical results obtained with periodic homogenization using multi-inhomogeneity volume elements, especially at moderate elastic contrasts and inhomogeneity volume fractions; differential schemes may do slightly better at elevated volume fractions. In assessing the results of these models it should be borne in mind, though, that they do not account for the effects of flaws, which are typically present in actual materials.

2.6 Mean-Field Methods for Composites with Non-aligned Reinforcements

The macroscopic symmetry of composites reinforced by nonaligned short fibers in many important cases is isotropic (e.g., for random fiber orientations) or transversally isotropic (for fiber arrangements with axisymmetric orientation distributions, e.g., fibers with planar random orientation). However, processing conditions can give rise to a wide range of fiber orientation distributions and thus to lower overall symmetries, compare, e.g., Allen and Lee (1990).

Reinforcements with General Orientation Distributions

Descriptions of the microgeometries of nonaligned and hybrid matrix–inclusion composites typically make use of the orientation distribution functions (ODFs) and/or aspect ratio or length distribution functions (LDFs) of the reinforcements, both of which can be determined experimentally. Beyond this, additional, qualitative information may be required on the phase geometry to be modeled, as is the case for materials reinforced by short fibers: At elevated fiber volume fractions local domains of (nearly) aligned fibers are typically observed in short fiber-reinforced composites, which give rise to a "grain-type" mesostructure, referred to as "aggregate systems" by Eduljee and McCullough (1993). For modeling composites of this type two-step homogenization schemes that involve meso-level

averages at the "grain" level, see, e.g., Camacho et al. (1990) or Pierard et al. (2004), may be appropriate. At low to moderate fiber volume fractions, in contrast, the orientations of neighboring fibers are essentially independent within the geometrical constraints of non-penetration. Such "dispersed systems" (Eduljee and McCullough, 1993) can be modeled via single-step mean-field schemes involving configurational averaging procedures, which may encompass aspect ratio averaging in addition to orientational averaging.

Studying the responses of nonaligned composites with dispersed geometries typically involves orientational averaging of tensor valued variables, which, in general, can be done by direct numerical integration, see, e.g., Pettermann et al. (1997), or on the basis of expansions of the ODF in terms of generalized spherical harmonics (Viglin (1961) expansions), compare, e.g., Advani and Tucker (1987). The latter approach can be formulated in a number of ways, e.g., via texture coefficients or texture matrices, compare Siegmund et al. (2004) or Hessman et al. (2021). For a discussion of a number of issues relevant to configurational averaging see Eduljee and McCullough (1993).

In order to obtain mean-field methods for composites reinforced by nonaligned inhomogeneities one may consider tensors $\mathbf{X}^{(\mathrm{i})}$ in suitably oriented local coordinate systems described by the Euler angles φ, ψ, θ. By transforming the $\mathbf{X}^{(\mathrm{i})}$ into the global coordinate system the tensors $\mathbf{X}^{(\mathrm{i})\angle}(\varphi, \psi, \theta)$ are obtained, which form the basis for generating orientational averages

$$\langle\langle \mathbf{X}^{(\mathrm{i})} \rangle\rangle = \int_0^{2\pi} \int_0^{2\pi} \int_0^{\pi} \mathbf{X}^{(\mathrm{i})\angle}(\varphi, \psi, \theta)\, \rho(\varphi, \psi, \theta)\, \mathrm{d}\varphi\, \mathrm{d}\psi\, \mathrm{d}\theta \quad . \tag{2.63}$$

Here $\rho(\varphi, \psi, \theta)$ denotes the orientation distribution function of the reinforcements, which is assumed to be normalized such that

$$\langle\langle 1 \rangle\rangle = \int_0^{2\pi} \int_0^{2\pi} \int_0^{\pi} \rho(\varphi, \psi, \theta)\, \mathrm{d}\varphi\, \mathrm{d}\psi\, \mathrm{d}\theta = 1 \quad .$$

Appropriately transforming the dilute inhomogeneity concentration tensors, $\bar{\mathbf{A}}_{\mathrm{dil}}^{(\mathrm{i})}$ and $\bar{\mathbf{B}}_{\mathrm{dil}}^{(\mathrm{i})}$, which are discussed in Section 2.2, provides rotated dilute concentration tensors, denoted as $\bar{\mathbf{A}}_{\mathrm{dil}}^{(\mathrm{i})\angle}$ and $\bar{\mathbf{B}}_{\mathrm{dil}}^{(\mathrm{i})\angle}$, to which the orientational averaging procedure can be applied in order to arrive at orientation averaged dilute concentration tensors, $\langle\langle \bar{\mathbf{A}}_{\mathrm{dil}}^{(\mathrm{i})} \rangle\rangle$ and $\langle\langle \bar{\mathbf{B}}_{\mathrm{dil}}^{(\mathrm{i})} \rangle\rangle$, respectively. The latter concentration tensors can be interpreted as describing an "equivalent phase of nonaligned, non-interacting inhomogeneities". The core statement of the Mori–Tanaka approach, eqn. (2.39), can then be written in the form

$$\langle \boldsymbol{\sigma} \rangle^{(\mathrm{i})} = \langle\langle \bar{\mathbf{B}}_{\mathrm{dil}}^{(\mathrm{i})} \rangle\rangle \langle \boldsymbol{\sigma} \rangle^{(\mathrm{m})} = \langle\langle \bar{\mathbf{B}}_{\mathrm{dil}}^{(\mathrm{i})} \rangle\rangle\, \overline{\mathbf{B}}_{\mathrm{MT}}^{(\mathrm{m})} \langle \boldsymbol{\sigma} \rangle = \overline{\mathbf{B}}_{\mathrm{MT}}^{(\mathrm{i})} \langle \boldsymbol{\sigma} \rangle \quad , \tag{2.64}$$

which allows evaluating the stress concentration tensors for the orientation averaged case, $\overline{\mathbf{B}}_{\mathrm{MT}}^{(\mathrm{m})}$ and $\overline{\mathbf{B}}_{\mathrm{MT}}^{(\mathrm{i})}$, as

$$\begin{aligned} \overline{\mathbf{B}}_{\mathrm{MT}}^{(\mathrm{m})} &= [(1-\xi)\mathbf{I} + \xi \langle\langle \bar{\mathbf{B}}_{\mathrm{dil}}^{(\mathrm{i})} \rangle\rangle]^{-1} \\ \overline{\mathbf{B}}_{\mathrm{MT}}^{(\mathrm{i})} &= \langle\langle \bar{\mathbf{B}}_{\mathrm{dil}}^{(\mathrm{i})} \rangle\rangle\, [(1-\xi)\mathbf{I} + \xi \langle\langle \bar{\mathbf{B}}_{\mathrm{dil}}^{(\mathrm{i})} \rangle\rangle]^{-1} \end{aligned} \tag{2.65}$$

by analogy to eqns. (2.42) and (2.43). Equivalent expressions can be given for the strain concentration tensors. On the basis of eqns. (2.83), (2.8) and (2.9) the effective macroscopic elasticity tensors take the form (Benveniste, 1987)

$$\begin{aligned} \mathbf{E}^*_{\mathrm{MT}} &= \mathbf{E}^{(\mathrm{m})} + \xi \langle\!\langle (\mathbf{E}^{(\mathrm{i})} - \mathbf{E}^{(\mathrm{m})}) \bar{\mathbf{A}}^{(\mathrm{i})}_{\mathrm{dil}} \rangle\!\rangle \left[(1-\xi)\mathbf{I} + \xi \langle\!\langle \bar{\mathbf{A}}^{(\mathrm{i})}_{\mathrm{dil}} \rangle\!\rangle \right]^{-1} \\ \mathbf{C}^*_{\mathrm{MT}} &= \mathbf{C}^{(\mathrm{m})} + \xi \langle\!\langle (\mathbf{C}^{(\mathrm{i})} - \mathbf{C}^{(\mathrm{m})}) \bar{\mathbf{B}}^{(\mathrm{i})}_{\mathrm{dil}} \rangle\!\rangle \left[(1-\xi)\mathbf{I} + \xi \langle\!\langle \bar{\mathbf{B}}^{(\mathrm{i})}_{\mathrm{dil}} \rangle\!\rangle \right]^{-1} \quad . \end{aligned} \tag{2.66}$$

If both phases are isotropic, eqns. (2.66) can be simplified to give

$$\begin{aligned} \mathbf{E}^*_{\mathrm{MT}} &= \mathbf{E}^{(\mathrm{m})} + \xi (\mathbf{E}^{(\mathrm{i})} - \mathbf{E}^{(\mathrm{m})}) \langle\!\langle \bar{\mathbf{A}}^{(\mathrm{i})}_{\mathrm{dil}} \rangle\!\rangle \left[(1-\xi)\mathbf{I} + \xi \langle\!\langle \bar{\mathbf{A}}^{(\mathrm{i})}_{\mathrm{dil}} \rangle\!\rangle \right]^{-1} \\ \mathbf{C}^*_{\mathrm{MT}} &= \mathbf{C}^{(\mathrm{m})} + \xi (\mathbf{C}^{(\mathrm{i})} - \mathbf{C}^{(\mathrm{m})}) \langle\!\langle \bar{\mathbf{B}}^{(\mathrm{i})}_{\mathrm{dil}} \rangle\!\rangle \left[(1-\xi)\mathbf{I} + \xi \langle\!\langle \bar{\mathbf{B}}^{(\mathrm{i})}_{\mathrm{dil}} \rangle\!\rangle \right]^{-1} \quad . \end{aligned} \tag{2.67}$$

For this case analytical expressions for $\mathbf{E}^*_{\mathrm{MT}}$ in terms of two order parameters were given by Giordano (2005).

Orientational averaging can also be used with the effective-medium approaches discussed in Section 2.3.2. For the classical self-consistent scheme, the equivalent of eqn. (2.53) takes the form

$$\begin{aligned} \mathbf{E}_{\mathrm{SC},n+1} &= \mathbf{E}^{(\mathrm{m})} + \xi^{(\mathrm{p})} \langle\!\langle (\mathbf{E}^{(\mathrm{p})} - \mathbf{E}^{(\mathrm{q})}) \, \bar{\mathbf{T}}^{(\mathrm{p},*)}_{\mathrm{dil},n} \rangle\!\rangle \\ \mathbf{C}_{\mathrm{SC},n+1} &= \left[\mathbf{E}_{\mathrm{SC},n+1} \right]^{-1} \end{aligned} \tag{2.68}$$

and for the differential scheme the expression

$$\frac{\mathrm{d}\mathbf{E}^*_{\mathrm{D}}}{\mathrm{d}\xi} = \frac{1}{1-\xi} \langle\!\langle (\mathbf{E}^{(\mathrm{i})} - \mathbf{E}^*_{\mathrm{D}}) \, \bar{\mathbf{T}}^{(\mathrm{i},*)}_{\mathrm{dil}} \rangle\!\rangle \tag{2.69}$$

can be obtained from eqn. (2.54). In contrast to the Mori–Tanaka model, which is explicit, multiple evaluations of orientation averages of the type $\langle\!\langle (\mathbf{E}^{(\mathrm{i})} - \mathbf{E}^*) \, \bar{\mathbf{T}}^{(\mathrm{i},*)}_{\mathrm{dil}} \rangle\!\rangle$ are required for both of the above methods, making them more expensive. It is worth noting that the analytical evaluation of the Eshelby tensors is only supported if the effective medium is isotropic, which implies spatially random fiber orientations, or transversally isotropic at all steps[29].

The stress $\langle \boldsymbol{\sigma} \rangle^{(\mathrm{i})}$ evaluated from eqn. (2.64) is an average over all inhomogeneities, irrespective of their orientations, and, accordingly, provides rather limited information. The average stresses in inhomogeneities of a given orientation (φ, ψ, θ), which may be of higher practical interest, can be obtained as

$$\langle \boldsymbol{\sigma} \rangle^{(\mathrm{i})\angle} = \bar{\mathbf{B}}^{(\mathrm{i})\angle}_{\mathrm{dil}} \, \overline{\mathbf{B}}^{(\mathrm{m})}_{\mathrm{MT}} \langle \boldsymbol{\sigma} \rangle \quad , \tag{2.70}$$

compare (Duschlbauer et al., 2003b). Results obtained with the above relation are in good agreement with numerical predictions for moderate reinforcement volume fractions and elastic contrasts as well as spheroidal fibers of moderate aspect ratios, compare fig. 2.4.

[29] The expressions of Clyne and Withers (1993) for Eshelby tensors of spheroids embedded in transversally isotropic matrices hold only for the case that the major axis of the former is aligned with the axis of symmetry of the latter, a condition that is not necessarily fulfilled for nontrivial ODFs. The same restriction also holds for Mori–Tanaka-type methods, such as eqns. (2.65) and (2.66). It can, of course, be circumvented by numerical evaluation of the Eshelby or Hill tensors.

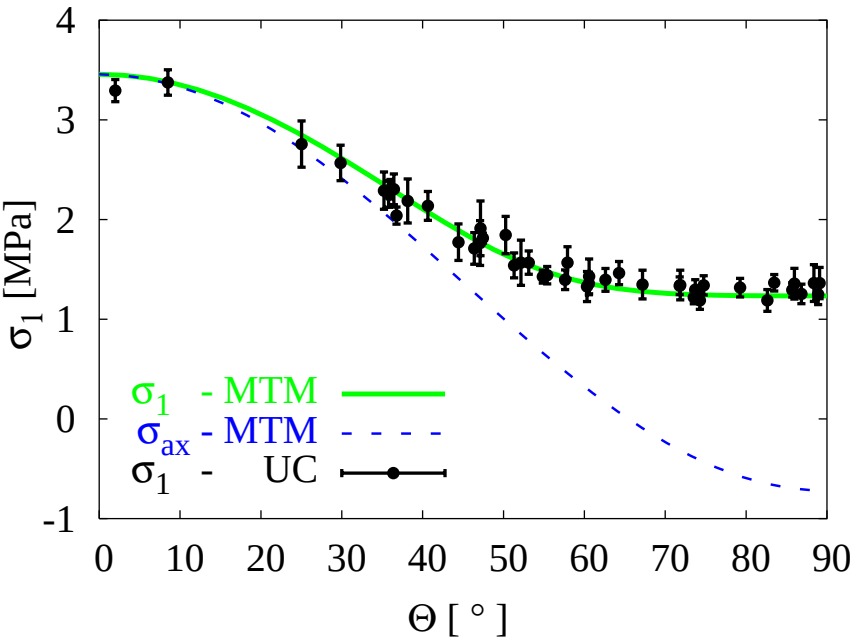

Figure 2.4: Dependence of the averaged stresses in individual fibers on the fiber orientation angle Θ predicted for a uniaxially loaded SiC/Al MMC reinforced by randomly oriented spheroidal fibers of aspect ratio $a = 5$ (Duschlbauer et al., 2003b). Results for the maximum principal stress σ_1 and the axial stress σ_{ax} obtained with an "extended" Mori–Tanaka scheme are shown as solid and dashed lines, respectively. Unit cell results are presented in terms of the mean values (solid circles) and standard deviations (error bars) of the maximum principal stress within individual fibers. Θ describes the angle between a given fiber and the loading (axial) direction.

"Extended" Mori–Tanaka methods for modeling the elastic behavior of microstructures that contain nonaligned inhomogeneities were developed by a number of authors (Benveniste, 1990; Dunn and Ledbetter, 1997; Pettermann et al., 1997; Mlekusch, 1999). These models differ mainly in the algorithms employed for orientational or configurational averaging[30]. In addition to modeling composites reinforced by nonaligned fibers or particles, methods of this type have also been used for studying fabric-reinforced composites, the orientation of the fiber tows being described by appropriate "equivalent orientations" (Gommers et al., 1998) and for approximating the behavior of composites reinforced by helicoidally twisted fibers (Shi et al., 2004). In cases involving finite numbers of fibers of known orientations, the integrals in eqn. (2.63) degenerate into sums and the model becomes a multi-phase Mori–Tanaka method analogous to eqn. (2.83), compare, e.g., Duschlbauer et al. (2011). Extended Mori–Tanaka methods are subject to similar limitations as other multi-phase Mori–Tanaka approaches, and may lead to non-symmetric "effective stiffness tensors" as mentioned in Section 2.8.

Mean-field approaches based on orientational averaging and Mori–Tanaka methods have also been employed in studies of the nonlinear behavior of nonaligned composites. Secant plasticity schemes of the above type were used for describing ductile matrix materials (Bhattacharyya and Weng, 1994; Dunn and Ledbetter, 1997) and incremental approaches

[30] Alternative modified Mori–Tanaka models for nonaligned composites that use spatial averaging of the Eshelby tensors, see, e.g., Johannesson and Pedersen (1998), have a weaker mechanical basis.

to modeling composites consisting of an elastoplastic matrix reinforced by nonaligned or random short fibers were proposed, e.g., by Lee and Simunovic (2000), where debonding between reinforcements and matrix is also accounted for.

Another option for studying composites with nonaligned reinforcements is provided by the Hashin–Shtrikman estimates of Ponte Castañeda and Willis (1995). As discussed in Section 2.3.1 this method is based on "ellipsoid-in-ellipsoid" phase arrangements, with different Eshelby tensors pertaining to the ellipsoids describing the two-point correlations of the phase arrangement and to those describing the shapes of the inhomogeneities. Equation (2.85) can be directly extended to nonaligned reinforcements by converting the sum into an orientation average to give

$$\mathbf{E}^{*}_{\mathrm{PW}} = \mathbf{E}^{(\mathrm{m})} + \xi^{(\mathrm{i})} \Big[\big\langle\!\big\langle (\mathbf{E}^{(\mathrm{i})} - \mathbf{E}^{(\mathrm{m})})\, \bar{\mathbf{A}}^{(\mathrm{i})\angle}_{\mathrm{dil}} \big\rangle\!\big\rangle - \mathbf{S}_{\mathrm{d}} \mathbf{C}^{(\mathrm{m})} \Big]^{-1} \tag{2.71}$$

As mentioned before, such Hashin–Shtrikman estimates are rigorous within the effective-field setting, provided none of the (aligned) "safety ellipsoids" described by $\mathbf{S}_{\mathrm{d}}$ overlap and none of the (nonaligned) inhomogeneities penetrate outside the associated safety ellipsoids. These requirements result in a limited range of strict applicability in terms of inhomogeneity volume fractions, which can be rather small for markedly prolate or oblate reinforcements that show a considerable degree of misalignment.

A number of analytical descriptions for short fiber-reinforced composites apply mean-field models within a two-step strategy (i.e., a hierarchical approach as discussed in Chapter 9). Laminate analogy approaches, see, e.g., Fu and Lauke (1998), and Pseudo-Grain models, compare, e.g., (Pierard et al., 2004), approximate nonaligned reinforcement arrangements by a stack of layers or a number of two-phase regions ("grains"), respectively, each of which pertains to one fiber orientation and/or one reinforcement aspect ratio or material. The effective elastic tensors are then obtained by a second homogenization step over the two-phase layers or grains. For laminate analogy approaches this is of the Voigt (strain coupling) type; such models can be useful especially for describing composites with planar random fiber orientations (Huang, 2001). Pseudo-Grain models are more flexible in terms of the homogenization method used for the second step and they have formed the basis for descriptions of the nonlinear and damage behavior of composites reinforced by nonaligned short fibers (Doghri and Tinel, 2005; Kammoun et al., 2011).

In addition to the above models a number of other analytical methods have been proposed for studying composites with nonaligned reinforcements. Most of them are based on the assumption that the contribution of a given fiber to the overall stiffness and strength depends solely on its orientation with respect to the applied load and on its length, interactions between neighboring fibers being neglected. The paper physics approach (Cox, 1952) and the Fukuda–Kawata theory (Fukuda and Kawata, 1974) are based on summing up stiffness contributions of fibers crossing an arbitrary normal section on the basis of fiber orientation and length distribution functions, compare also Jayaraman and Kortschot (1996). Such theories use shear lag models (Cox, 1952; Fukuda and Chou, 1982) or modifications thereof (Fukuda and Kawata, 1974) for describing the behavior of a single fiber embedded in matrix material, the results being typically given as modified rules of mixtures with fiber direction and fiber length corrections.

Randomly Oriented Reinforcements

For the special case of randomly oriented ("uniform random") fibers or platelets of a given aspect ratio, orientation averaged dilute partial strain concentration tensors, known as Wu tensors (Wu, 1966), may be used. Wu tensors can be inserted into Mori–Tanaka methods or classical self-consistent schemes (Berryman, 1980) to describe composites with randomly oriented phases of matrix–inclusion or certain interpenetrating topologies; in the former case eqn. (2.67) is recovered. Tandon and Weng (1986) proposed an alternative Mori–Tanaka based model for composites reinforced by randomly oriented inhomogeneities. A further mean-field method for such materials, the Kuster and Toksöz (1974) model, essentially is a dilute description applicable to matrix–inclusion topologies and tends to give non-physical results at high reinforcement volume fractions. For discussions on the relationships between some of the above approaches see, e.g., Berryman and Berge (1996) or Hu and Weng (2000). It is worth noting that, due to the overall isotropic behavior of composites reinforced by randomly oriented fibers or platelets, their elastic response must comply with the Hashin and Shtrikman (1963) bounds for macroscopically isotropic materials, compare Chapter 3 and see also table 6.2 in Section 6.5.

2.7 Mean-Field Methods for Non-Ellipsoidal Reinforcements

When non-ellipsoidal inhomogeneities are subjected to a homogeneous eigenstrain or a far-field load, the resulting stress and strain fields in them are, in general, inhomogeneous. As a consequence, the interior-point Eshelby tensors and dilute inhomogeneity concentration tensors depend on the position within such inhomogeneities. Analytical solutions (pertaining to the first Eshelby problem) are available only for certain inhomogeneity shapes, see, e.g., Mura (1987) and Onaka (2001). For some further shapes volume averaged Eshelby tensors have been reported. They have been proposed for use within approximate mean-field models for composites reinforced by non-ellipsoidal inhomogeneities, see, e.g., Zheng et al. (2006) and Hashemi et al. (2009). Depending on how they were evaluated, such tensors pertain to either the first or the second Eshelby problem, compare Section 2.2, but not to both of them.

An elegant approach to handling non-ellipsoidal inhomogeneities within a mean-field framework is provided by the contribution tensor formalism, compare eqns. (2.19) to (2.21). Using eqns. (2.19) contribution tensors pertaining to dilute inhomogeneities of general shape, $\mathbf{H}^{(\mathrm{i})}_{\mathrm{dil}}$ and $\mathbf{N}^{(\mathrm{i})}_{\mathrm{dil}}$, can be extracted from any solution for the effective compliance or elasticity tensors, $\mathbf{E}^{*}_{\mathrm{dil}}$ and $\mathbf{C}^{*}_{\mathrm{dil}}$, obtained for suitable dilute matrix–inhomogeneity configurations. In the case of non-ellipsoidal reinforcement shapes or highly anisotropic matrix behavior evaluating $\mathbf{E}^{*}_{\mathrm{dil}}$ or $\mathbf{C}^{*}_{\mathrm{dil}}$ typically involves numerical methods. For ellipsoidal inhomogeneities in isotropic or transversally isotropic matrices dilute contribution tensors can be generated with much smaller effort from solutions based on Eshelby tensors and equivalents, e.g., via eqn. (2.20). For dilute contribution tensors eqns. (2.21) simplify to

$$\mathbf{H}^{(\mathrm{i})}_{\mathrm{dil}} = -\mathbf{C}^{(\mathrm{m})}\mathbf{N}^{(\mathrm{i})}_{\mathrm{dil}}\mathbf{C}^{(\mathrm{m})} \qquad \text{and} \qquad \mathbf{N}^{(\mathrm{i})}_{\mathrm{dil}} = -\mathbf{E}^{(\mathrm{m})}\mathbf{H}^{(\mathrm{i})}_{\mathrm{dil}}\mathbf{E}^{(\mathrm{m})} \quad . \tag{2.72}$$

The dilute contribution tensors directly give rise to non-interacting solutions analogous

to the ones discussed at the end of Section 2.2. They also form the basis for effective-field and effective-medium schemes that are suitable for handling non-dilute inhomogeneity volume fractions and are fully equivalent to the models presented in Section 2.3, where descriptions employing concentration tensors are used. Within a contribution tensor-based two-phase mean-field framework, the Mori–Tanaka method takes the form

$$\begin{aligned}
\mathbf{H}^{(\mathrm{i})}_{\mathrm{MT}} &= \mathbf{H}^{(\mathrm{i})}_{\mathrm{dil}} \left[(1-\xi)\mathbf{I} + \xi(\mathbf{C}^{(\mathrm{i})} - \mathbf{C}^{(\mathrm{m})})^{-1}\mathbf{H}^{(\mathrm{i})}_{\mathrm{dil}}\right]^{-1} \\
&= \left[(1-\xi)\mathbf{H}^{(\mathrm{i})\,-1}_{\mathrm{dil}} + \xi(\mathbf{C}^{(\mathrm{i})} - \mathbf{C}^{(\mathrm{m})})^{-1}\right]^{-1} \\
\mathbf{N}^{(\mathrm{i})}_{\mathrm{MT}} &= \mathbf{N}^{(\mathrm{i})}_{\mathrm{dil}} \left[(1-\xi)\mathbf{I} + \xi(\mathbf{E}^{(\mathrm{i})} - \mathbf{E}^{(\mathrm{m})})^{-1}\mathbf{N}^{(\mathrm{i})}_{\mathrm{dil}}\right]^{-1} \\
&= \left[(1-\xi)\mathbf{N}^{(\mathrm{i})\,-1}_{\mathrm{dil}} + \xi(\mathbf{E}^{(\mathrm{i})} - \mathbf{E}^{(\mathrm{m})})^{-1}\right]^{-1} \quad ,
\end{aligned} \tag{2.73}$$

the classical self-consistent scheme becomes

$$\begin{aligned}
\mathbf{H}^{(\mathrm{p})}_{\mathrm{SC}} &= \xi^{(\mathrm{p})}(\mathbf{C}^{(\mathrm{p})} - \mathbf{C}^{(\mathrm{q})})(\mathbf{C}^{(\mathrm{p})} - \mathbf{C}^{*}_{\mathrm{SC}})^{-1}\,\mathbf{H}^{(\mathrm{p},*)}_{\mathrm{dil}} \\
\mathbf{N}^{(\mathrm{p})}_{\mathrm{SC}} &= \xi^{(\mathrm{p})}(\mathbf{E}^{(\mathrm{p})} - \mathbf{E}^{(\mathrm{q})})(\mathbf{E}^{(\mathrm{p})} - \mathbf{E}^{*}_{\mathrm{SC}})^{-1}\,\mathbf{N}^{(\mathrm{p},*)}_{\mathrm{dil}} \quad ,
\end{aligned} \tag{2.74}$$

the differential scheme is given by

$$\begin{aligned}
\frac{\mathrm{d}\mathbf{C}^{*}_{\mathrm{D}}}{\mathrm{d}\xi} &= \frac{1}{(1-\xi)}\mathbf{H}^{(\mathrm{i},*)}_{\mathrm{dil}} \\
\frac{\mathrm{d}\mathbf{E}^{*}_{\mathrm{D}}}{\mathrm{d}\xi} &= \frac{1}{(1-\xi)}\mathbf{N}^{(\mathrm{i},*)}_{\mathrm{dil}} \quad ,
\end{aligned} \tag{2.75}$$

and the Maxwell scheme results as

$$\begin{aligned}
\mathbf{H}^{(\mathrm{i})}_{\mathrm{MX}} &= \left[[\mathbf{H}^{(\mathrm{i})}_{\mathrm{dil}}]^{-1} - \xi\mathbf{E}^{(\mathrm{m})}(\mathbf{I} - \mathbf{S}_{\mathrm{E}})\right]^{-1} \\
\mathbf{N}^{(\mathrm{i})}_{\mathrm{MX}} &= \left[[\mathbf{N}^{(\mathrm{i})}_{\mathrm{dil}}]^{-1} - \xi\mathbf{S}_{\mathrm{E}}\mathbf{C}^{(\mathrm{m})}\right]^{-1} \quad ,
\end{aligned} \tag{2.76}$$

compare Eroshkin and Tsukrov (2005) and Kachanov and Sevostianov (2018). The $\mathbf{H}^{(\mathrm{i},*)}_{\mathrm{dil}}$ and $\mathbf{N}^{(\mathrm{i},*)}_{\mathrm{dil}}$ appearing in eqns. (2.74) and (2.75) are defined as

$$\mathbf{H}^{(\mathrm{i},*)}_{\mathrm{dil}} = (\mathbf{C}^{(\mathrm{i})} - \mathbf{C}^{*}_{n})\bar{\mathbf{W}}^{(\mathrm{i},*)}_{\mathrm{dil}} \qquad \text{and} \qquad \mathbf{N}^{(\mathrm{i},*)}_{\mathrm{dil}} = (\mathbf{E}^{(\mathrm{i})} - \mathbf{E}^{*}_{n})\bar{\mathbf{T}}^{(\mathrm{i},*)}_{\mathrm{dil}} \tag{2.77}$$

where $\mathbf{E}^{*}_{n}$ and $\mathbf{C}^{*}_{n}$ stand for the n-th iterates of $\mathbf{E}^{*}_{\mathrm{SC}}$ and $\mathbf{C}^{*}_{\mathrm{SC}}$ for the effective medium. For in-depth discussions of contribution-tensor based mean-field models see Sevostianov (2014) or Kachanov and Sevostianov (2018).

When expressions for $\mathbf{H}^{(\mathrm{i})}_{\mathrm{dil}}$ and $\mathbf{N}^{(\mathrm{i})}_{\mathrm{dil}}$ are evaluated from numerical models via eqn. (2.19), both ξ and terms of the type $\mathbf{E}^{*} - \mathbf{E}^{(\mathrm{m})}$ may become very small, so that considerable care is required due to the potential sensitivity of the results to roundoff and discretization errors[31], especially in the case of non-convex inhomogeneities, compare, e.g., Sevostianov et al. (2008). In such models either macrohomogeneous or periodicity boundary conditions

[31] Because extracting $\langle\boldsymbol{\varepsilon}\rangle^{(\mathrm{i})}$ or $\langle\boldsymbol{\sigma}\rangle^{(\mathrm{i})}$ is not subject to this issue, when using numerical models it may be preferable to evaluate $\mathbf{H}^{(\mathrm{i})}_{\mathrm{dil}}$ and $\mathbf{N}^{(\mathrm{i})}_{\mathrm{dil}}$ via the phase-averaged dilute concentration tensors plus eqns. (2.20) rather than directly via eqns. (2.19).

may be employed, the wide matrix region surrounding the inhomogeneity making the results rather insensitive to the boundary conditions actually used.

For non-ellipsoidal inhomogeneities the combination of numerically evaluated dilute contribution tensors with mean-field methods according to eqns. (2.73) or (2.76) gives useful approximations to the more accurate results obtained by the computationally much more expensive full field models discussed in Chapters 5 to 8, see, e.g., Trofimov et al. (2017). Such modeling strategies are, however, not very efficient when incorporating implicit micromechanical schemes, e.g., eqns. (2.74) or (2.75), which require multiple evaluations of the contribution tensors, as indicated by eqns. (2.77).

2.8 Mean-Field Methods for Multi-Phase Thermoelastic Composites

Multi-phase materials can show a wide range of microgeometries. The present section concentrates on two important groups of composites with matrix–inclusion microtopology. One of them consists of a contiguous matrix phase that is reinforced by aligned, randomly positioned, uniform inhomogeneities showing different shapes and/or material behavior. In the other group all reinforcements are identical, aligned and consist of a core surrounded by a coating, making them non-uniform. The methods discussed in this context can be extended to handling many of the more complex configurations.

2.8.1 Mean-Field Methods for Multi-Phase Thermoelastic Composites with Aligned Reinforcements

The majority of the general relations between mean-fields in thermoelastic two-phase materials given in Section 2.1 can be directly extended to multi-phase materials consisting of N phases $^{(\mathrm{p})}$. Specifically, the equivalents of eqn. (2.7) take the form

$$\begin{aligned} \sum_{(\mathrm{p})} \xi^{(\mathrm{p})} \bar{\mathbf{A}}^{(\mathrm{p})} &= \mathbf{I} & \qquad \sum_{(\mathrm{p})} \xi^{(\mathrm{p})} \bar{\boldsymbol{\beta}}^{(\mathrm{p})} &= \mathbf{o} \\ \sum_{(\mathrm{p})} \xi^{(\mathrm{p})} \bar{\mathbf{B}}^{(\mathrm{p})} &= \mathbf{I} & \qquad \sum_{(\mathrm{p})} \xi^{(\mathrm{p})} \bar{\boldsymbol{\kappa}}^{(\mathrm{p})} &= \mathbf{o} \end{aligned} \quad , \tag{2.78}$$

the effective elastic tensors can be evaluated as

$$\mathbf{E}^* = \sum_{(\mathrm{p})} \xi^{(\mathrm{p})} \mathbf{E}^{(\mathrm{p})} \bar{\mathbf{A}}^{(\mathrm{p})} \qquad \mathbf{C}^* = \sum_{(\mathrm{p})} \xi^{(\mathrm{p})} \mathbf{C}^{(\mathrm{p})} \bar{\mathbf{B}}^{(\mathrm{p})} \tag{2.79}$$

by analogy to eqns. (2.8) and (2.9), and eqns. (2.14) become

$$\bar{\mathbf{A}}^{(\mathrm{p})} = \mathbf{C}^{(\mathrm{p})}\bar{\mathbf{B}}^{(\mathrm{p})}\Big[\sum_{(\mathrm{q})} \xi^{(\mathrm{q})}\mathbf{C}^{(\mathrm{q})}\bar{\mathbf{B}}^{(\mathrm{q})}\Big]^{-1} \qquad \text{and} \qquad \bar{\mathbf{B}}^{(\mathrm{p})} = \mathbf{E}^{(\mathrm{p})}\bar{\mathbf{A}}^{(\mathrm{p})}\Big[\sum_{(\mathrm{q})} \xi^{(\mathrm{q})}\mathbf{E}^{(\mathrm{q})}\bar{\mathbf{A}}^{(\mathrm{q})}\Big]^{-1} \quad , \tag{2.80}$$

respectively. Equations (2.12), (2.14) and (2.17) hold irrespective of the number or topology of the phases. There seem to be no multi-phase equivalents of eqns. (2.15), however, which imposes considerable restrictions on doing localization or evaluating effective CTEs with multi-phase mean-field methods.

The effective properties of multi-phase composites with matrix–inclusion topology can be obtained by summing up the contribution tensors, $\mathbf{H}^{(\mathrm{i})}$ or $\mathbf{N}^{(\mathrm{i})}$, pertaining to the dilute or non-dilute micromechanical model to be used,

$$\mathbf{C}^{*} = \mathbf{C}^{(\mathrm{m})} + \sum_{(\mathrm{i})\neq(\mathrm{m})} \xi^{(\mathrm{i})}\mathbf{H}^{(\mathrm{i})} \qquad \text{and} \qquad \mathbf{E}^{*} = \mathbf{E}^{(\mathrm{m})} + \sum_{(\mathrm{i})\neq(\mathrm{m})} \xi^{(\mathrm{i})}\mathbf{N}^{(\mathrm{i})} \quad . \tag{2.81}$$

Approaches based on these relations often lead to compact expressions for the elastic tensors of multi-phase composites, compare Kachanov and Sevostianov (2018).

Formally, multi-phase versions of the methods discussed in Sections 2.3.1 and 2.3.2 can be obtained in a straightforward way. However, for the "simpler" effective-field methods the range of application of the resulting expressions tends to be rather limited. No major issues have been reported, in contrast, for more general effective-field approaches such as the multi-particle effective-field method or for effective-medium models like eqns. (2.86) and (2.87).

Multi-Phase Mori–Tanaka Estimates

For multi-phase materials consisting of a matrix $^{(\mathrm{m})}$ into which a number of aligned inhomogeneity phases $^{(\mathrm{i})}$ (understood to consist of inhomogeneities of identical material behavior and shape) are embedded, Mori–Tanaka phase concentration tensors may be obtained as

$$\begin{aligned}
\bar{\mathbf{A}}^{(\mathrm{m})}_{\mathrm{MT}} &= \big[\xi^{(\mathrm{m})}\mathbf{I} + \sum_{(\mathrm{i})\neq(\mathrm{m})} \xi^{(\mathrm{i})}\bar{\mathbf{A}}^{(\mathrm{i})}_{\mathrm{dil}}\big]^{-1} & \bar{\mathbf{A}}^{(\mathrm{i})}_{\mathrm{MT}} &= \bar{\mathbf{A}}^{(\mathrm{i})}_{\mathrm{dil}}\big[\xi^{(\mathrm{m})}\mathbf{I} + \sum_{(\mathrm{i})\neq(\mathrm{m})} \xi^{(\mathrm{i})}\bar{\mathbf{A}}^{(\mathrm{i})}_{\mathrm{dil}}\big]^{-1} \\
\bar{\mathbf{B}}^{(\mathrm{m})}_{\mathrm{MT}} &= \big[\xi^{(\mathrm{m})}\mathbf{I} + \sum_{(\mathrm{i})\neq(\mathrm{m})} \xi^{(\mathrm{i})}\bar{\mathbf{B}}^{(\mathrm{i})}_{\mathrm{dil}}\big]^{-1} & \bar{\mathbf{B}}^{(\mathrm{i})}_{\mathrm{MT}} &= \bar{\mathbf{A}}^{(\mathrm{i})}_{\mathrm{dil}}\big[\xi^{(\mathrm{m})}\mathbf{I} + \sum_{(\mathrm{j})\neq(\mathrm{m})} \xi^{(\mathrm{i})}\bar{\mathbf{B}}^{(\mathrm{i})}_{\mathrm{dil}}\big]^{-1}
\end{aligned} \tag{2.82}$$

and the corresponding effective elastic tensors become

$$\begin{aligned}
\mathbf{E}^{*}_{\mathrm{MT}} &= \Big[\sum_{(\mathrm{p})} \xi^{(\mathrm{p})}\mathbf{E}^{(\mathrm{p})}\bar{\mathbf{A}}^{(\mathrm{p})}_{\mathrm{dil}}\Big]\Big[\sum_{(\mathrm{p})} \xi^{(\mathrm{p})}\bar{\mathbf{A}}^{(\mathrm{p})}_{\mathrm{dil}}\Big]^{-1} \\
&= \mathbf{E}^{(\mathrm{m})} + \Big[\sum_{(\mathrm{i})\neq(\mathrm{m})} \xi^{(\mathrm{i})}(\mathbf{E}^{(\mathrm{i})} - \mathbf{E}^{(\mathrm{m})})\bar{\mathbf{A}}^{(\mathrm{i})}_{\mathrm{dil}}\Big]\Big[\xi^{(\mathrm{m})}\mathbf{I} + \sum_{(\mathrm{i})\neq(\mathrm{m})} \xi^{(\mathrm{i})}\bar{\mathbf{A}}^{(\mathrm{i})}_{\mathrm{dil}}\Big]^{-1} \\
\mathbf{C}^{*}_{\mathrm{MT}} &= \Big[\sum_{(\mathrm{p})} \xi^{(\mathrm{p})}\mathbf{C}^{(\mathrm{p})}\bar{\mathbf{B}}^{(\mathrm{p})}_{\mathrm{dil}}\Big]\Big[\sum_{(\mathrm{p})} \xi^{(\mathrm{p})}\bar{\mathbf{B}}^{(\mathrm{p})}_{\mathrm{dil}}\Big]^{-1} \\
&= \mathbf{C}^{(\mathrm{m})} + \Big[\sum_{(\mathrm{i})\neq(\mathrm{m})} \xi^{(\mathrm{i})}(\mathbf{C}^{(\mathrm{i})} - \mathbf{C}^{(\mathrm{m})})\bar{\mathbf{B}}^{(\mathrm{i})}_{\mathrm{dil}}\Big]\Big[\xi^{(\mathrm{m})}\mathbf{I} + \sum_{(\mathrm{i})\neq(\mathrm{m})} \xi^{(\mathrm{i})}\bar{\mathbf{B}}^{(\mathrm{i})}_{\mathrm{dil}}\Big]^{-1}
\end{aligned} \tag{2.83}$$

in direct equivalence to the two-phase expressions, eqns. (2.44); here $^{(\mathrm{p})}$ is understood to encompass all phases.

The multi-phase Mori–Tanaka methods defined by eqns. (2.82) and/or (2.83) are known to give rise to non-symmetric effective "elastic tensors" (and thus to unphysical results) in many practically relevant situations, compare Benveniste et al. (1991) or Ferrari (1991). Such behavior crops up, e.g., when studying microstructures involving aligned spheroidal inhomogeneities that show both different material behaviors and different aspect ratios; it may also appear for composites reinforced by nonaligned inhomogeneities. It is a consequence of assumptions on the linkage between phase arrangement and inhomogeneity shape implicitly incorporated into Mori–Tanaka methods, compare fig. 2.2 and the remarks on Ponte–Willis estimates in Section 2.3.1. Recent discussions of these issues were provided by, e.g., Sevostianov and Kachanov (2014), Rodin and Weng (2014) and Jiménez Segura et al. (2023).

The above limitations may be dealt with by directly symmetrizing the Mori–Tanaka elasticity tensors, eqns. (2.83), or by symmetrizing the tensors $\mathbf{A}^{(\mathrm{i})}_{\mathrm{cic}}$ or $\mathbf{B}^{(\mathrm{i})}_{\mathrm{cic}}$ defined by eqns. (2.38). The latter approach was followed by Sevostianov and Kachanov (2014) and by Jiménez Segura et al. (2023) within the contribution tensor and the concentration tensor frameworks, respectively. It is interesting to note that when using such fixes the original Mori–Tanaka assumption of equating the effective fields with the matrix fields, viz., $\boldsymbol{\varepsilon}_{\mathrm{E}} = \langle\boldsymbol{\varepsilon}\rangle^{(\mathrm{m})}$ and $\boldsymbol{\sigma}_{\mathrm{E}} = \langle\boldsymbol{\sigma}\rangle^{(\mathrm{m})}$, compare eqns. (2.38) and (2.39), is no longer fulfilled once symmetrization cuts in[32].

Multi-Phase Maxwell Schemes

A Maxwell estimate for the macroscopic elasticity tensor of a multi-phase composite of matrix–inhomogeneity topology can be given in the form

$$\mathbf{E}^{*}_{\mathrm{MX}} = \mathbf{E}^{(\mathrm{m})} + \left[\Big(\sum_{(\mathrm{i})\neq(\mathrm{m})} \xi^{(\mathrm{i})} [(\mathbf{E}^{(\mathrm{i})} - \mathbf{E}^{(\mathrm{m})})^{-1} + \mathbf{S}^{(\mathrm{i,m})}\mathbf{C}^{(\mathrm{m})}]^{-1} \Big)^{-1} - \mathbf{S}_{\mathrm{E}}\mathbf{C}^{(\mathrm{m})} \right]^{-1} \quad , \tag{2.84}$$

which is a generalization of eqns. (2.48). For the special case that all inhomogeneity phases are aligned and have identical shapes (but different material properties), their aspect ratio is a natural choice for the effective region, so that $\mathbf{S}_{\mathrm{E}} = \mathbf{S}^{(\mathrm{i,m})}$. Under these conditions the predictions of Mori–Tanaka methods and Maxwell schemes coincide.

For general cases, i.e., when the inhomogeneity phases are either not aligned or show different aspect ratios, the proper choice of the shape of the inhomogeneous region, compare fig. 2.3, and thus of $\mathbf{S}_{\mathrm{E}}$, tends to be a nontrivial issue. Sevostianov and Kachanov (2014) conjectured that the pertinent Hill tensor $\mathbf{P}_{\mathrm{E}} = \mathbf{S}_{\mathrm{E}}\mathbf{C}^{(\mathrm{m})}$ can be approximated as a weighted sum of the Hill tensors of the inhomogeneity phases, $\mathbf{P}_{\mathrm{E}} \approx \sum \xi^{(\mathrm{i})}\mathbf{P}^{(\mathrm{i,m})}$, but Buryachenko (2022b) gave counter-examples and concluded that the Maxwell scheme tends to break down for complex microgeometries.

[32] Even seemingly minor deviations from symmetry in $\mathbf{E}^{*}$ and $\mathbf{C}^{*}$ tend to compromise the validity of concentration tensors evaluated via eqns. (2.82). This issue, which is most marked for hybrid composites containing reinforcements of widely different shape, is not resolved by symmetrization.

Multi-Phase Ponte–Willis Estimates

The effective elasticity tensor of the Hashin–Shtrikman scheme of (Ponte Castañeda and Willis, 1995) for composites reinforced by multiple aligned inhomogeneity phases can be written as

$$\mathbf{E}^*_{\mathrm{PW}} = \mathbf{E}^{(\mathrm{m})} + \left(\mathbf{I} - \sum_{(\mathrm{i})\neq(\mathrm{m})} \xi^{(\mathrm{i})} \mathbf{N}^{(\mathrm{i,m})}_{\mathrm{dil}} \mathbf{S}_{\mathrm{d}} \mathbf{C}^{(\mathrm{m})} \right)^{-1} \left(\sum_{(\mathrm{i})\neq(\mathrm{m})} \xi^{(\mathrm{i})} \mathbf{N}^{(\mathrm{i,m})}_{\mathrm{dil}} \right) \quad , \tag{2.85}$$

where $\mathbf{N}^{(\mathrm{i,m})}_{\mathrm{dil}}$ stands for the dilute elasticity contribution tensor defined in eqn. (2.35). In eqn. (2.85) all phases follow the same ellipsoidal arrangement statistics described by $\mathbf{P}_{\mathrm{d}} = \mathbf{S}_{\mathrm{d}} \mathbf{C}^{(\mathrm{m})}$.

Multi-Phase Classical Self-Consistent Scheme

The multi-phase version of the classical self-consistent estimates for the effective elasticity tensor takes the form

$$\begin{aligned} \mathbf{E}^*_{\mathrm{SC},n+1} &= \sum_{(\mathrm{p})} \mathbf{E}^{(\mathrm{p})} \left\{ \mathbf{I} + \mathbf{S}^{(\mathrm{p},*)}_n \mathbf{C}_{\mathrm{SC},n} [\mathbf{E}^{(\mathrm{p})} - \mathbf{E}_{\mathrm{SC},n}] \right\}^{-1} \\ \mathbf{C}^*_{\mathrm{SC},n+1} &= (\mathbf{E}^*_{\mathrm{SC},n+1})^{-1} \end{aligned} \tag{2.86}$$

in analogy to the two-phase case, eqn. (2.53). The Eshelby tensor $\mathbf{S}^{(\mathrm{p},*)}_n$ pertains to an ellipsoidal inhomogeneity with a shape characteristic of phase $^{(\mathrm{p})}$ that is embedded in the effective medium. This model is not primarily aimed at classical composites with matrix–inclusion topology, but rather at materials with grain-like microgeometries. It may require under-relaxation to achieve convergence.

Multi-Phase Differential Scheme

The two-phase Differential Scheme, eqns. (2.54), can be extended to composites containing multiple inhomogeneity phases to give

$$\frac{\mathrm{d}\mathbf{E}^*_{\mathrm{D}}}{\mathrm{d}\xi^{\mathrm{I}}} = \frac{1}{1-\xi^{\mathrm{I}}} \sum_{(\mathrm{i})\neq(\mathrm{m})} \eta^{(\mathrm{i})} [\mathbf{E}^{(\mathrm{i})} - \mathbf{E}^*_{\mathrm{D}}] \, \bar{\mathbf{T}}^{(\mathrm{i},*)}_{\mathrm{dil}} \tag{2.87}$$

where $\xi^{\mathrm{I}} = \sum_{(\mathrm{i})\neq(\mathrm{m})} \xi^{(\mathrm{i})}$ and the partial volume fractions $\eta^{(\mathrm{i})}$ are defined in analogy to eqn. (2.92). Like its two-phase counterpart, eqn. (2.87) can be integrated up numerically, e.g., with Runge–Kutta algorithms. In eqn. (2.87) the $\eta^{(\mathrm{i})}$ are implicitly assumed to be increased proportionally, but different integration paths in phase volume space can be enforced by introducing suitable parameterizations; in general, these lead to different results for identical target volume fractions, compare Norris (1985).

Multi-Phase Hashin–Shtrikman Tensors

Multi-phase versions of eqns. (2.59) and (2.60) take the forms

$$\mathbf{E}^*_{\mathrm{HS}} = \left(\sum_{(\mathrm{p})} \xi^{(\mathrm{p})} (\mathbf{L}^{(\mathrm{i},0)} + \mathbf{E}^{(\mathrm{p})})^{-1} \right)^{-1} - \mathbf{L}^{(\mathrm{i},0)} \quad , \tag{2.88}$$

compare Bornert (2001), and

$$\mathbf{E}^{*}_{\mathrm{HS}} = \Big(\sum_{(\mathrm{p})} \xi^{(\mathrm{p})} \mathbf{E}^{(\mathrm{p})} \bar{\mathbf{T}}^{(\mathrm{p},0)}_{\mathrm{dil}}\Big) \Big(\sum_{(\mathrm{p})} \xi^{(\mathrm{p})} \bar{\mathbf{T}}^{(\mathrm{p},0)}_{\mathrm{dil}}\Big)^{-1} \quad , \tag{2.89}$$

see, e.g., Walpole (1966), respectively. When composites of matrix–inclusion topology are to be studied, both of the above expressions are limited to inhomogeneity phases of identical shape, which is described by $\mathbf{L}^{(\mathrm{i},0)}$ in eqn. (2.88).

Two-Step and Multi-Step Models for Multi-Phase Composites

Two-step and multi-step mean-field models have been devised with the main aim of circumventing the limitations of the "direct" mean-field models discussed above.

In two-step methods, an N-phase composite with matrix–inclusion topology is treated as consisting of $N-1$ two-phase regions, each of which consists of a single inhomogeneity phase embedded in the matrix. In the first step, each of these "pseudo-grains" is homogenized by a standard two-phase model. An $N-1$-phase homogenization method is then applied in the second step to estimate the effective tensors. For example, the first step of such a pseudo-grain model may be consist of two-phase Mori–Tanaka models such as eqns. (2.44), all of which use an inhomogeneity volume fraction of ξ^{I}, compare eqn. (2.92), and the second one of a multi-phase classical self-consistent scheme, eqn. (2.86), with grain volume fractions of $\eta^{(\mathrm{i})} = \xi^{(\mathrm{i})}/\xi^{\mathrm{I}}$. Results obtained with such a PGR/MT–SC model are presented in section 4.3. Conceptually similar pseudo-grain approaches have been widely used for homogenizing composites with nonaligned reinforcements, compare section 2.6.

Multi-step models (also referred to as iterative or sequential approaches) handle N-phase composites via a sequence of $N-1$ two-phase homogenization procedures such that the elasticity tensors resulting from step $n-1$ serve as the embedding material ("matrix") of step n, the actual matrix being used for this purpose in step 1. In order to recover the prescribed phase volume fractions of the inhomogeneity phases, $\xi^{(\mathrm{i})}$, the inhomogeneity volume fraction for step n, $\xi^{(\mathrm{i})}_{n}$, must be chosen as

$$\xi^{(\mathrm{i})}_{n} = \frac{\xi^{(\mathrm{n})}}{\sum_{(\mathrm{q})=(\mathrm{n})}^{(\mathrm{N}-1)} \xi^{(\mathrm{q})}} \quad . \tag{2.90}$$

Most applications of such multi-step methods have employed the Mori–Tanaka method for all steps, resulting in Sequential Mori–Tanaka or Multi-Step Mori–Tanaka models, see, e.g., Yang et al. (2007). In order to fulfill the homogenization conditions, the size of inhomogeneities should be increasing with growing number $^{(\mathrm{n})}$ of the phases. The predictions of such multi-step models for the effective tensors in general depend on the chosen sequence of the phases in the homogenization scheme.

Other Analytical Estimates for Multi-Phase Composites

The most general analytical models for multi-phase composites, such as Multi-Particle Effective-Field Methods, see, e.g., (Buryachenko, 2022b), are based on integral equation formulations, compare (Buryachenko, 2022b), and tend to be too complex to be described by the notation used in the present report.

2.8.2 Analytical Models for Composites Reinforced by Coated Inhomogeneities

Composites reinforced by coated particles or fibers (sometimes called "core–shell" inhomogeneities) show a special type of three-phase, or, in the case of multiple coatings, multi-phase microgeometry. The modeling of such materials has been the focus of considerable research interest, especially due to its relevance to nanocomposites. The most widely used analytical approaches have been versions of the Double Inclusion Method (Hori and Nemat-Nasser, 1993) and self-consistent schemes based on exact solutions for dilute, coated or multi-coated spherical inhomogeneities, see Hervé and Zaoui (1990), Hervé and Zaoui (1993) and Bonfoh et al. (2012), as well as cylindrical continuous fibers, see Hervé and Zaoui (1995). The following discussion will concentrate on the case of single, uniform interphases, i.e., three-phase configurations.

Arguably, the most flexible models for handling composites reinforced by coated inhomogeneities are two-step schemes, which describe the coated particles or fibers via equivalent uniform inhomogeneities and were referred to as the "replacement method" by (Hashin, 1972). Models of this type can also be applied to composites with imperfect interfaces[33], compare, e.g., Duan et al. (2022), and graded interphases (Sevostianov and Kachanov, 2007a). Within the two-step framework eqns. (2.78) and (2.79) give rise to the relations

$$\begin{aligned} \mathbf{E}^{*} &= \xi^{(\mathrm{m})}\mathbf{E}^{(\mathrm{m})}\bar{\mathbf{A}}^{(\mathrm{m})} + \xi^{(\mathrm{c})}\mathbf{E}^{(\mathrm{c})}\bar{\mathbf{A}}^{(\mathrm{c})}_{\mathrm{dil}} + \xi^{(\mathrm{l})}\mathbf{E}^{(\mathrm{l})}\bar{\mathbf{A}}^{(\mathrm{l})}_{\mathrm{dil}} \\ &= \xi^{(\mathrm{m})}\mathbf{E}^{(\mathrm{m})}\bar{\mathbf{A}}^{(\mathrm{m})} + \xi^{\mathrm{I}}\mathbf{E}^{\mathrm{I}}_{\mathrm{eqv}}\bar{\mathbf{A}}^{\mathrm{I}}_{\mathrm{eqv}} \\ \bar{\mathbf{A}}^{\mathrm{I}}_{\mathrm{eqv}} &= \eta^{(\mathrm{c})}\bar{\mathbf{A}}^{(\mathrm{c})} + \eta^{(\mathrm{l})}\bar{\mathbf{A}}^{(\mathrm{l})} \quad , \end{aligned} \tag{2.91}$$

at the level of the composite. Here the definitions

$$\xi^{\mathrm{I}} = \xi^{(\mathrm{c})} + \xi^{(\mathrm{l})} \qquad \eta^{(\mathrm{c})} = \frac{\xi^{(\mathrm{c})}}{\xi^{\mathrm{I}}} \qquad \eta^{(\mathrm{l})} = \frac{\xi^{(\mathrm{l})}}{\xi^{\mathrm{I}}} \tag{2.92}$$

are used, with $^{(\mathrm{c})}$ denoting the inhomogeneity core, $^{(\mathrm{l})}$ the coating layer and $^{\mathrm{I}}$ the equivalent inhomogeneity. At the level of the coated inhomogeneity the expressions

$$\begin{aligned} \bar{\mathbf{A}}^{\mathrm{I}}_{\mathrm{dil,eqv}} &= \eta^{(\mathrm{c})}\bar{\mathbf{A}}^{(\mathrm{c})}_{\mathrm{dil}} + \eta^{(\mathrm{l})}\bar{\mathbf{A}}^{(\mathrm{l})}_{\mathrm{dil}} \\ \mathbf{E}^{\mathrm{I}}_{\mathrm{eqv}} &= \left(\eta^{(\mathrm{c})}\mathbf{E}^{(\mathrm{c})}\bar{\mathbf{A}}^{(\mathrm{c})}_{\mathrm{dil}} + \eta^{(\mathrm{l})}\mathbf{E}^{(\mathrm{l})}\bar{\mathbf{A}}^{(\mathrm{l})}_{\mathrm{dil}}\right)\left(\bar{\mathbf{A}}^{\mathrm{I}}_{\mathrm{dil,eqv}}\right)^{-1} \end{aligned} \tag{2.93}$$

allow evaluating $\bar{\mathbf{A}}^{\mathrm{I}}_{\mathrm{dil,eqv}}$ as well as $\mathbf{E}^{\mathrm{I}}_{\mathrm{eqv}}$ whenever $\bar{\mathbf{A}}^{(\mathrm{l})}_{\mathrm{dil}}$ and $\bar{\mathbf{A}}^{(\mathrm{c})}_{\mathrm{dil}}$ are known, whereas the relations

$$\begin{aligned} \bar{\mathbf{A}}^{\mathrm{I}}_{\mathrm{dil,eqv}} &= [\mathbf{I} + \mathbf{S}^{\mathrm{I}}\mathbf{C}^{(\mathrm{m})}(\mathbf{E}^{\mathrm{I}}_{\mathrm{eqv}} - \mathbf{E}^{(\mathrm{m})}]^{-1} \\ \bar{\mathbf{A}}^{(\mathrm{c})} &= \frac{1}{\eta^{(\mathrm{c})}}(\mathbf{E}^{(\mathrm{c})} - \mathbf{E}^{(\mathrm{l})})^{-1}(\mathbf{E}^{\mathrm{I}}_{\mathrm{eqv}} - \mathbf{E}^{(\mathrm{l})})^{-1} \\ \bar{\mathbf{A}}^{(\mathrm{l})} &= \frac{1}{\eta^{(\mathrm{c})}}(\mathbf{E}^{(\mathrm{l})} - \mathbf{E}^{(\mathrm{c})})^{-1}(\mathbf{E}^{\mathrm{I}}_{\mathrm{eqv}} - \mathbf{E}^{(\mathrm{c})})^{-1} \end{aligned} \tag{2.94}$$

[33] In the present context a coating of finite thickness is referred to as an interphase, contrasting with a zero-thickness interface between two constituents where fields may be discontinuous.

may be used to extract the dilute concentration tensors if $\mathbf{E}^{\mathrm{I}}_{\mathrm{eqv}}$ is available. Together, eqns. (2.91) to (2.94) split up the three-phase problem into two independent two-phase ones: the "equivalent homogeneous fiber sub-model" provides expressions for $\bar{\mathbf{A}}^{\mathrm{I}}_{\mathrm{dil,eqv}}$ and $\mathbf{E}^{\mathrm{I}}_{\mathrm{eqv}}$, whereas the "composite level-level sub-model" leverages this data into obtaining results on $\bar{\mathbf{A}}^{\mathrm{I}}$ and $\mathbf{E}^{*}$ for non-dilute volume fractions ξ^{I}. For the latter step essentially any two-phase mean-field model can be used, and the two-step model as a whole supports mean-field localization for all constituents, stress concentration tensors being extracted via eqn. (2.14). For further details see Böhm (2019) and Böhm (2023). Multiple coatings can be handled by analogy and result in a sequence of two-phase micromechanical problems.

The equivalent homogeneous fiber sub-model can be tackled, on the hand, by obtaining dilute phase-averaged concentration tensors $\bar{\mathbf{A}}^{(\mathrm{c})}_{\mathrm{dil}}$ and $\bar{\mathbf{A}}^{(\mathrm{l})}_{\mathrm{dil}}$ from the non-uniform local fields predicted by the exact solutions for coated spherical particles, see Hervé and Zaoui (1990), and for continuous, coated cylinders, see Wang and Huang (2016), Wang et al. (2016) and Chatzigeorgiou and Meraghni (2019). On the other hand, the elasticity tensor of the equivalent uniform inhomogeneity can be approximated via a number of mean-field methods, among them Mori–Tanaka-type schemes of the form

$$\mathbf{E}^{(\mathrm{i})}_{\mathrm{eqv}} = \mathbf{E}^{(\mathrm{l})} + \eta^{(\mathrm{c})} \Big[(\mathbf{E}^{(\mathrm{c})} - \mathbf{E}^{(\mathrm{l})})^{-1} + \eta^{(\mathrm{l})} \mathbf{S}^{(\mathrm{c,l})} \mathbf{C}^{(\mathrm{l})} \Big]^{-1} \quad , \tag{2.95}$$

where the Eshelby tensor $\mathbf{S}^{(\mathrm{c,l})}$ describes the inhomogeneity core embedded in the interphase material[34].

The results of a number of analytical models for composites reinforced by simply coated spheres or cylinders were compared to numerical predictions for some material combinations by Böhm (2019) and Böhm (2023), respectively. The combination of the dilute concentration tensors from the exact solutions with the three-point estimates of Torquato (1997, 1998a) or the Differential Scheme at the composite level was consistently found to give excellent agreement. Interestingly, two-step schemes that combine eqn. (2.95) with the Mori–Tanaka method at the composite level, so called MTMT-models (Friebel et al., 2006), also tracked the numerical predictions well, making them (as well as the more complicated Generalized Self-Consistent Scheme based on a Reformulated Double Inclusion Model proposed by Dinzart et al. (2016), which yields identical results) good candidates for handling more general ellipsoidal reinforcement shapes.

2.9 Mean-Field Models for Nonlinear and Inelastic Composites

Since the late 1970s considerable effort has been directed at modeling the mechanical behavior of inhomogeneous materials in which one or more constituents show nonlinear elastic, viscoelastic, elastoplastic or viscoelastoplastic responses. The main motivation of such studies has been the need to describe the time dependent, creep and relaxation behavior of polymer matrix composites and the responses of composites with metallic phases.

[34] Equation (2.95) corresponds to a single, simplified step of the General Explicit Eshelby-Based Estimator (GEEE) of Ghazavizadeh et al. (2019). The GEEE uses Ponte–Willis estimates for modeling non-homothetic, multi-coated inhomogeneities.

Mean-field methods have been developed for and successfully adapted to studying many aspects of the above problems.

For nonlinear composites the instantaneous stiffness operators are not phase-wise uniform even if each constituent is homogeneous, so that Eshelby's results and mean-field models cannot be extended directly from linear elasticity to nonlinear behavior. To deal with this problem, "linear comparison composites" may be defined, which approximate the actual, nonlinear materials' responses for a given state. Accordingly, the nonlinear problem is reduced to a sequence of linear ones by suitable linearization schemes. In continuum micromechanics, the most important approaches of this type are secant (Tandon and Weng, 1988) and incremental (Hill, 1965a) methods. In addition, tangent concepts (Molinari et al., 1987), affine formulations (Masson et al., 2000; Brenner et al., 2001) and incremental secant algorithms (Wu et al., 2013) have been reported.

2.9.1 Viscoelastic Composites

Viscoelastic materials show hereditary behavior, i.e., their response at a given time depends on their previous load history. Important issues in the mechanical behavior of viscoelastic composites are, on the one hand, quasi-static responses such as relaxation and creep, which can be described via relaxation function and creep compliance tensors. The dynamic behavior under periodic excitations, on the other hand, can be studied via complex modulus tensors.

Correspondence principles are available (Hashin, 1965, 1970) that directly relate the analysis of linear viscoelastic composites to that of linear elastic composites of identical phase geometry for both of the above sets of problems, see also Schapery (1974) and Hashin (1983).

For the quasi-static case the correspondence principle requires formulating the viscoelastic problem in the Laplace–Carson transformed domain, where the transformed relaxation function and creep compliance tensors are equivalent to the elasticity and compliance tensors, respectively, in elastic micromechanics. On this basis replacement schemes can be defined (Hashin, 1972) that allow to obtain Laplace–Carson transformed macroscopic moduli, modulus tensors and phase averaged microfields of viscoelastic materials from mean-field results, such as the ones discussed in Sections 2.3 to 2.5. The back transformation from the Laplace–Carson to the time domain, however, typically is not straightforward, and closed form solutions are not available in most cases. Accordingly, approximations must be introduced or numerical methods must be used, compare, e.g., Schapery (1962) or Lévesque et al. (2007). The correspondence principle for periodic excitations uses transforms to Fourier space and the resulting replacement scheme (Hashin, 1972) directly generates effective complex modulus tensors from the effective elastic tensors obtained for a given microgeometry[35].

[35]The correspondence principles can be applied, on the one hand, to analytical expressions, such as the CSA and CCA models (Hashin, 1972) or Mori–Tanaka and self-consistent schemes (Pichler and Lackner, 2009). On the other hand, numerical discrete microfield approaches of the type discussed in Chapters 6 to 7 can be adapted to incorporate them, see, e.g., Yi et al. (1998) or Brinson and Lin (1998).

For in-depth discussions of and alternative concepts for mean-field models of linear and nonlinear viscoelastic composites see, e.g., Paquin et al. (1999), Brenner and Masson (2005), Lévesque et al. (2007), as well as Lahellec and Suquet (2007).

2.9.2 (Thermo-)Elastoplastic Composites

The following discussion is restricted to mean-field models based on continuum plasticity[36]. Nearly all work reported on such models for elastoplastic or viscoelastoplastic inhomogeneous materials has relied on secant, incremental, tangent, or affine linearization strategies; for an overview see, e.g., Ponte Castañeda and Suquet (1998).

The main difficulties in applying mean-field methods to composites with elastoplastic constituents lie in the path dependence of plastic behavior and in the often strong intra-phase fluctuations of the microstress and microstrain fields in elastoplastic inhomogeneous materials. Accordingly, each material point in an elastoplastic phase tends to follow a different trajectory in stress space, so that even a two-phase elastoplastic composite effectively behaves as a multi-phase material and phase averages over reinforcements and matrix are less useful descriptors than in the linear elastic regime. As a consequence, in mean-field models of elastoplastic composites choices have to be made with respect to the linearization procedure, the linear homogenization model, and the phase-wise equivalent stresses and equivalent strains to be used in evaluating the elastoplastic constituent material behavior (Zaoui, 2001).

Secant Methods for Elastoplastic Composites

Secant plasticity concepts in continuum micromechanics, see, e.g., Tandon and Weng (1988) or Dunn and Ledbetter (1997), are based on the deformation theory of plasticity, in which the elastoplastic behavior under radial, monotonic loading is approximated by nonlinear elastic models.

In the simplest case of an isotropic elastoplastic phase that is described by J_2 plasticity, the secant "elasticity" and "compliance" tensors, $\mathbf{E}^{(\mathrm{p})}_{\mathrm{sec}}$ and $\mathbf{C}^{(\mathrm{p})}_{\mathrm{sec}}$, take the form

$$\mathbf{E}^{(\mathrm{p})}_{\mathrm{sec}} = 3K^{(\mathrm{p})}\mathbf{O}^{\mathrm{E}}_{\mathrm{vol}} + 2G^{(\mathrm{p})}_{\mathrm{sec}}\mathbf{O}^{\mathrm{E}}_{\mathrm{dev}} \qquad \text{and} \qquad \mathbf{C}^{(\mathrm{p})}_{\mathrm{sec}} = \frac{1}{3K^{(\mathrm{p})}}\mathbf{O}^{\mathrm{C}}_{\mathrm{vol}} + \frac{1}{2G^{(\mathrm{p})}_{\mathrm{sec}}}\mathbf{O}^{\mathrm{C}}_{\mathrm{dev}} \quad , \tag{2.96}$$

respectively. Here $\mathbf{O}^{\mathrm{E}}$ and $\mathbf{O}^{\mathrm{C}}$ are the volumetric and deviatoric "partitioning tensors" for elasticities and compliances[37], respectively. The secant shear modulus $G^{(\mathrm{p})}_{\mathrm{sec}}$ is equal to the elastic shear modulus of the matrix, $G^{(\mathrm{p})}$, in the elastic range. In the post-yield regime it can be obtained from the current phase averages of the equivalent stress $\langle\sigma_{\mathrm{eqv}}\rangle^{(\mathrm{p})}$ and the equivalent plastic strain $\langle\varepsilon_{\mathrm{eqv,pl}}\rangle^{(\mathrm{p})}$ as

$$G^{(\mathrm{p})}_{\mathrm{sec}} = \frac{G^{(\mathrm{p})}\,\langle\sigma_{\mathrm{eqv}}\rangle^{(\mathrm{p})}}{\langle\sigma_{\mathrm{eqv}}\rangle^{(\mathrm{p})} + 3G^{(\mathrm{p})}\langle\varepsilon_{\mathrm{eqv,pl}}\rangle^{(\mathrm{p})}} \tag{2.97}$$

[36] In a separate type of model phase averaged stress fields obtained by mean-field methods have been used in dislocation-based descriptions of elastoplastic matrix behavior, see, e.g., Taya and Mori (1987).

[37] In index notation the $\mathbf{O}^{\mathrm{E}}$ and $\mathbf{O}^{\mathrm{C}}$ are identical and correspond to the volumetric and deviatoric projection tensors $\mathbf{O}$ defined in eqn. (2.2). If an engineering notation based on shear angles is used, however, there are differences in the "shear terms" of $\mathbf{O}^{\mathrm{E}}_{\mathrm{dev}}$, $\mathbf{O}^{\mathrm{C}}_{\mathrm{dev}}$ and $\mathbf{O}_{\mathrm{dev}}$.

on the basis of an additive strain decomposition, compare eqn. (2.1). The equivalent plastic strain $\langle \varepsilon_{\mathrm{eqv,pl}} \rangle^{(\mathrm{p})}$ must be evaluated from $\langle \sigma_{\mathrm{eqv}} \rangle^{(\mathrm{p})}$ via an appropriate hardening law. The bulk moduli $K^{(\mathrm{p})}$ are not affected by yielding due to the J_2 assumption.

Expressions for the macroscopic secant tensors $\mathbf{E}^*_{\mathrm{sec}}$ and $\mathbf{C}^*_{\mathrm{sec}}$ can be obtained from the phase secant tensors, eqn. (2.96), by mean-field relationships equivalent to eqns. (2.8) and (2.9). For the case of elastic inhomogeneities embedded in an elastoplastic matrix they can be given as

$$\begin{aligned} \mathbf{E}^*_{\mathrm{sec}} &= \mathbf{E}^{(\mathrm{m})}_{\mathrm{sec}} + \xi(\mathbf{E}^{(\mathrm{i})} - \mathbf{E}^{(\mathrm{m})}_{\mathrm{sec}})\bar{\mathbf{A}}^{(\mathrm{m})}_{\mathrm{sec}} \\ \mathbf{C}^*_{\mathrm{sec}} &= \mathbf{C}^{(\mathrm{m})}_{\mathrm{sec}} + \xi(\mathbf{C}^{(\mathrm{i})} - \mathbf{C}^{(\mathrm{m})}_{\mathrm{sec}})\bar{\mathbf{B}}^{(\mathrm{m})}_{\mathrm{sec}} \end{aligned} \quad . \tag{2.98}$$

The non-dilute secant strain and stress concentration tensors, $\bar{\mathbf{A}}^{(\mathrm{m})}_{\mathrm{sec}}$ and $\bar{\mathbf{B}}^{(\mathrm{m})}_{\mathrm{sec}}$, can be generated from dilute secant concentration tensors, $\bar{\mathbf{A}}^{(\mathrm{m})}_{\mathrm{dil,sec}}$ and $\bar{\mathbf{B}}^{(\mathrm{m})}_{\mathrm{dil,sec}}$, via a suitable mean-field theory, e.g., a Mori–Tanaka method or a self-consistent scheme, compare Section 2.3. The dilute secant concentration tensors and the Eshelby tensors used in them must be evaluated using the current secant tensors of the constituents. Iterative procedures are required for obtaining solutions corresponding to prescribed macroscopic strain or stress states.

In first order ("classical") methods, the phase average of the equivalent stress required in eqn. (2.97) is approximated from the phase averaged stress tensor,

$$\langle \sigma_{\mathrm{eqv}} \rangle^{(\mathrm{p})} \approx \left[\frac{3}{2} \langle \boldsymbol{\sigma} \rangle^T_{\mathrm{dev}} \langle \boldsymbol{\sigma} \rangle_{\mathrm{dev}} \right]^{\frac{1}{2}} \quad . \tag{2.99}$$

This neglects contributions due to the local stress fluctuations and, accordingly, tends to underestimate $\langle \sigma_{\mathrm{eqv}} \rangle^{(\mathrm{p})}$, leading to errors in the estimates for the macroscopic elastoplastic response[38]. Clear improvements in this respect can be obtained by second order approximations that evaluate the phase averaged equivalent stress in terms of approximations to the second order moments of stress, $\langle \boldsymbol{\sigma} \otimes \boldsymbol{\sigma} \rangle^{(\mathrm{p})}$, (Suquet, 1995; Buryachenko, 1996; Hu, 1997; Pierard et al., 2007), on the basis of energy considerations (Qiu and Weng, 1992), or from a "current stress norm" (Ju and Sun, 2001).

Alternatively, secant theories for composites with nonlinear constituents can be obtained from variational principles (Ponte Castañeda, 1991) or they can be formulated in terms of potentials (Bornert and Suquet, 2001), which allows for a concise mathematical presentation. Because secant models treat elastoplastic composites as nonlinearly elastic materials they are limited to strictly monotonic loading and to radial (or approximately radial) trajectories of the phase averaged stresses of the constituents in stress space[39],

[38] Because the square of the deviatoric stresses is required for evaluating $\langle \sigma_{\mathrm{eqv}} \rangle^{(\mathrm{p})}$, the fluctuations give rise to non-vanishing contributions.
As an extreme case, using eqn. (2.99) for evaluating the equivalent stress leads to predictions that materials with spherical reinforcements will not yield under macroscopically hydrostatic loads or unconstrained thermal expansion. This is in contradiction to other results.

[39] The condition of radial loading paths in stress space at the constituent level is generally violated, at least to some extent, in the phases of elastoplastic inhomogeneous materials, even for macroscopic loading paths that are perfectly radial (Pettermann, 1997). This behavior is due to changes in the accommodation of the phase stresses and strains in inhomogeneous materials upon yielding of a constituent and (to a much lesser extent) in the strain hardening regime.

which precludes their use as micromechanically based constitutive models or as lower scale models in multi-scale analysis.

"Modified secant models" (Ponte Castañeda and Suquet, 1998) that use second order approximations for $\langle\sigma_{\mathrm{eqv}}\rangle^{(\mathrm{p})}$ have been found to be highly suitable for materials characterization of elastoplastic composites, where they have shown excellent agreement with predictions from multi-particle unit cell models (Segurado et al., 2002a) and experiments. Modified secant models have also proved quite flexible. For example, a method of this type was adapted to incorporate a nonlocal plasticity model for the matrix (Hu et al., 2005) in order to study particle size effects on the macroscopic yield behavior of MMCs.

Incremental Methods for Elastoplastic Composites

Incremental mean-field methods can be formulated on the basis of strain and stress rate tensors for elastoplastic phases $^{(\mathrm{p})}$, $\mathrm{d}\langle\boldsymbol{\varepsilon}\rangle^{(\mathrm{p})}$ and $\mathrm{d}\langle\boldsymbol{\sigma}\rangle^{(\mathrm{p})}$, which can be expressed as

$$\begin{aligned} \mathrm{d}\langle\boldsymbol{\varepsilon}\rangle^{(\mathrm{p})} &= \bar{\mathbf{A}}_{\mathrm{t}}^{(\mathrm{p})}\mathrm{d}\langle\boldsymbol{\varepsilon}\rangle + \bar{\boldsymbol{\beta}}_{\mathrm{t}}^{(\mathrm{p})}\mathrm{d}T \\ \mathrm{d}\langle\boldsymbol{\sigma}\rangle^{(\mathrm{p})} &= \bar{\mathbf{B}}_{\mathrm{t}}^{(\mathrm{p})}\mathrm{d}\langle\boldsymbol{\sigma}\rangle + \bar{\boldsymbol{\kappa}}_{\mathrm{t}}^{(\mathrm{p})}\mathrm{d}T \quad . \end{aligned} \tag{2.100}$$

by analogy to eqn. (2.6). Here $\mathrm{d}\langle\boldsymbol{\varepsilon}\rangle$ stands for the macroscopic strain rate tensor, $\mathrm{d}\langle\boldsymbol{\sigma}\rangle$ for the macroscopic stress rate tensor, and $\mathrm{d}T$ for a homogeneous temperature rate. $\bar{\mathbf{A}}_{\mathrm{t}}^{(\mathrm{p})}$, $\bar{\boldsymbol{\beta}}_{\mathrm{t}}^{(\mathrm{p})}$, $\bar{\mathbf{B}}_{\mathrm{t}}^{(\mathrm{p})}$, and $\bar{\boldsymbol{\kappa}}_{\mathrm{t}}^{(\mathrm{p})}$ are instantaneous phase averaged strain and stress concentration tensors, respectively. For elastic inhomogeneities embedded in an elastoplastic matrix[40], the overall instantaneous "tangent stiffness" tensor of the elastoplastic two-phase composite can be written in terms of the phase properties and the instantaneous concentration tensors as

$$\begin{aligned} \mathbf{E}_{\mathrm{t}}^{*} &= \mathbf{E}^{(\mathrm{i})} + (1-\xi)[\mathbf{E}_{\mathrm{t}}^{(\mathrm{m})} - \mathbf{E}^{(\mathrm{i})}]\bar{\mathbf{A}}_{\mathrm{t}}^{(\mathrm{m})} \\ &= [\mathbf{C}^{(\mathrm{i})} + (1-\xi)[\mathbf{C}_{\mathrm{t}}^{(\mathrm{m})} - \mathbf{C}^{(\mathrm{i})}]\bar{\mathbf{B}}_{\mathrm{t}}^{(\mathrm{m})}]^{-1} \quad . \end{aligned} \tag{2.101}$$

Expressions of this type are closely related to eqns. (2.8) and (2.9); many of the general relations given in Section 2.1 have equivalents in the incremental mean-field framework.

Using the Mori–Tanaka formalism of Benveniste (1987), the instantaneous matrix concentration tensors can be written as

$$\begin{aligned} \bar{\mathbf{A}}_{\mathrm{t}}^{(\mathrm{m})} &= \{(1-\xi)\mathbf{I} + \xi[\mathbf{I} + \mathbf{S}_{\mathrm{t}}\mathbf{C}_{\mathrm{t}}^{(\mathrm{m})}(\mathbf{E}^{(\mathrm{i})} - \mathbf{E}_{\mathrm{t}}^{(\mathrm{m})})]^{-1}\}^{-1} \\ \bar{\mathbf{B}}_{\mathrm{t}}^{(\mathrm{m})} &= \{(1-\xi)\mathbf{I} + \xi\mathbf{E}^{(\mathrm{i})}[\mathbf{I} + \mathbf{S}_{\mathrm{t}}\mathbf{C}_{\mathrm{t}}^{(\mathrm{m})}(\mathbf{E}^{(\mathrm{i})} - \mathbf{E}_{\mathrm{t}}^{(\mathrm{m})})]^{-1}\mathbf{C}_{\mathrm{t}}^{(\mathrm{m})}\}^{-1} \quad , \end{aligned} \tag{2.102}$$

in direct analogy to eqn. (2.43). Expressions for the instantaneous thermal concentration tensors and instantaneous coefficients of thermal expansion can also be derived by analogy to the corresponding thermoelastic relations, e.g., eqns. (2.11) and (2.16). Equations (2.102) employ the instantaneous Eshelby tensor $\mathbf{S}_{\mathrm{t}}$, which depends on the current state of the (elastoplastic) matrix material, $\mathbf{E}_{\mathrm{t}}^{(\mathrm{m})}$. Because the latter tensor typically shows a low symmetry, $\mathbf{S}_{\mathrm{t}}$ must in general be evaluated numerically.

[40] Analogous expressions can be derived for elastoplastic inhomogeneities in an elastic matrix or, in general, for composites containing any required number of elastoplastic phases.

By replacing rates such as $\mathrm{d}\langle\boldsymbol{\varepsilon}\rangle^{(\mathrm{p})}$ and $\mathrm{d}\langle\boldsymbol{\sigma}\rangle^{(\mathrm{p})}$ with the corresponding finite increments, $\Delta\langle\boldsymbol{\varepsilon}\rangle^{(\mathrm{p})}$ and $\Delta\langle\boldsymbol{\sigma}\rangle^{(\mathrm{p})}$, respectively, formulations of eqns. (2.100) to (2.102) can be obtained that are suitable for implementation as micromechanically based constitutive models at the integration point level within Finite Element codes. The resulting incremental Mori–Tanaka (IMT) methods make no assumptions on the overall yield surface and the overall flow potential, the effective material behavior being entirely determined by the incremental mean-field equations and the constitutive behavior of the phases. As a consequence, mapping of the stresses onto the yield surface cannot be handled at the level of the homogenized material and radial return mapping must be applied to the matrix at the microscale instead. This, in turn, implies that the constitutive equations describing the overall behavior cannot be integrated directly (as is the case for homogeneous elastoplastic materials), and iterative algorithms are required. For example, Pettermann (1997) used an implicit Euler scheme in an implementation of an incremental Mori–Tanaka method as a user supplied material routine (UMAT) for the Finite Element code ABAQUS (Simulia, Pawtucket, RI). Extended versions of such algorithms can also handle thermal expansion effects[41] and temperature dependent material parameters.

Incremental mean-field models of the type discussed above tend to overestimate the macroscopic strain hardening in the post-yield regime to such an extent that their practical applicability is rather limited, especially for matrix dominated deformation modes, compare, e.g., the discussions by Gilormini (1995) and Suquet (1997). Later developments have involved the use of tangent operators that reflect the symmetry of the elastoplastic phase, e.g., "isotropized" operators[42] for statistically isotropic materials such as particle-reinforced composites (Bornert, 2001) together with algorithmic modifications (Doghri and Ouaar, 2003; Doghri and Friebel, 2005). These improvements have succeeded in markedly reducing the overprediction of the strain hardening behavior by incremental mean-field models such as IMTs for particle-reinforced composites, making them attractive candidates for use at the lower length scale in hierarchical and multi-scale models of ductile matrix composites. A pragmatic extension of spectral isotropization schemes to fiber-reinforced materials was introduced by Selmi et al. (2011) and further developments aimed at circumventing isotropization were proposed by Brassart et al. (2012), Lahellec and Suquet (2013) and Wu et al. (2013). Modified IMTs were also successfully extended to the large strain regime (Huber et al., 2007). An alternative approach to handling the above problems, based on transforming the elastic Eshelby tensor, was proposed by Peng et al. (2016).

Incremental mean-field models have typically used eqn. (2.99) for evaluating the phase averaged equivalent stresses, which, accordingly, tend to be underestimated. The improved estimators for $\langle\sigma_{\mathrm{eqv}}\rangle^{(\mathrm{p})}$ used in modified secant models are not suitable for incremental methods, for which an empirical correction was proposed by Delannay et al. (2007). Furthermore, because they assume elastoplastic phases to yield as a whole once the phase averaged equivalent stress exceeds the yield stress of the elastoplastic constituent, mean-

[41] Elastoplastic inhomogeneous materials such as metal matrix composites typically show a hysteretic thermal expansion response, i.e., the "coefficients of thermal expansion" are not material properties in the strict sense. This dependence of the thermal expansion behavior on the instantaneous mechanical response requires special treatment within the IMT framework, compare Pettermann (1997).

[42] For a discussion of a number of issues pertaining to the use of "isotropic" versus "anisotropic" tangent operators for macroscopically isotropic, elastoplastic materials see, e.g., Chaboche and Kanouté (2003).

field approaches predict sharp transitions from elastic to plastic states instead of the actual, gradual progress of yielded regions at the microscale.

Other mean-field schemes can also be combined with secant or incremental approaches to obtain descriptions for elastoplastic inhomogeneous materials, the most important application having been the use of classical self-consistent schemes for describing the elastoplastic behavior of polycrystalline materials, see, e.g., Hill (1965a), Hutchinson (1970) and Berveiller and Zaoui (1981). In the case of incremental methods what has to be done is replacing elastic, Eshelby and concentration tensors with the corresponding instantaneous tensors for each elastoplastic phase in expressions such as eqns. (2.52), (2.86), (2.50) or (2.85). The weaknesses and strengths of such procedures are closely related to those discussed above for Mori–Tanaka-based methods. In addition, mean-field approaches have been employed for obtaining estimates of the nonlinear response of inhomogeneous materials due to microscopic damage or to combinations of damage and plasticity, see, e.g., Tohgo and Chou (1996) and Guo et al. (1997).

As an alternative to directly extending mean-field theories into secant or incremental plasticity, they can also be combined with the Transformation Field Analysis of Dvorak (1992) in order to obtain descriptions of the overall behavior of inhomogeneous materials in the plastic range, see, e.g., Plankensteiner (2000). Such approaches may markedly overestimate the strain hardening of elastoplastic composites because they use elastic accommodation of microstresses and strains throughout the loading history. Chaboche et al. (2001) gave a discussion of modifications aimed at improving this behavior of the Transformation Field Analysis see Chaboche et al. (2001).

For a comparison of the predictions of a number of analytical modeling approaches for elastoplastic fiber-reinforced composites see, e.g., Wang and Huang (2018).

2.10 Mean-Field Methods for Conduction and Diffusion Problems

The mathematical descriptions of, on the one hand, steady-state thermoelasticity and, on the other hand, thermal conduction as well as other diffusion-type problems for heterogeneous materials are based on Poisson equations, share many common features, and can be attacked using similar techniques. Table 2.1 lists the principal variables of these two sets of problems, emphasizing the analogies between them. A number of other steady-state diffusion phenomena are mathematically equivalent to heat conduction (Hashin, 1983), among them electrical conduction and the diffusion of moisture. The differential equations describing antiplane shear in elastic solids, Darcy creep flow in porous media, and equilibrium properties such as overall dielectric constants and magnetic permeabilities are also of the Poisson type and thus equivalent to diffusive transport problems. For further discussions see Torquato (2002).

An important difference between elasticity and conduction or diffusion problems concerns the orders of the tensors involved, which is lower in the latter case. The displacements $\mathbf{u}$ are vectors whereas the temperatures T are scalars, stresses $\boldsymbol{\sigma}$ and strains $\boldsymbol{\varepsilon}$ are tensors

Table 2.1: Principal variables in steady state elasticity and heat conduction problems.

physical problem	elasticity	thermal conduction
field variable (potential)	displacement field $\mathbf{u}$ [m]	temperature field T [K]
generalized gradient tensor (intensity)	strain field $\boldsymbol{\varepsilon}$ [ ]	temperature gradient field $\mathbf{d}$ [Km^{-1}]
generalized flux tensor	stress field $\boldsymbol{\sigma}$ [Pa]	heat flux field $\mathbf{q}$ [Wm^{-2}]
generalized property tensor	elasticity $\mathbf{E}$ [Pa] compliance $\mathbf{C}$ [Pa^{-1}]	thermal conductivity $\mathcal{K}$ [$\mathrm{Wm}^{-1}\mathrm{K}^{-1}$] thermal resistivity $\mathcal{R}$ [mKW^{-1}]

of order 2, whereas the heat fluxes $\mathbf{q}$ and thermal gradients $\mathbf{d}$ are (physical) vectors, and the elasticity tensor $\mathbf{E}$ as well as its inverse, the compliance tensor $\mathbf{C} = \mathbf{E}^{-1}$, are of order 4, whereas the conductivity tensor $\mathcal{K}$ and its inverse, the resistivity tensor $\mathcal{R} = \mathcal{K}^{-1}$, are of order 2. The differences in the orders of the tensors directly affect the number of parameters required for describing the pertinent material property tensors as well as their symmetry properties (Nye, 1957). For example, cubic geometrical symmetry gives rise to macroscopic cubic symmetry in elasticity (with three independent elastic moduli) but isotropic behavior in thermal conduction.

The phase averages of the temperature gradient $\mathbf{d}$ and the heat flux $\mathbf{q}$ mentioned in table 2.1 are defined as

$$\begin{aligned} \langle \mathbf{d} \rangle &= \frac{1}{\Omega^{(\mathrm{p})}} \int_{\Omega^{(\mathrm{p})}} \mathbf{d}(\mathbf{x}) \, \mathrm{d}\Omega = \frac{1}{\Omega^{(\mathrm{p})}} \int_{\Gamma_\mathrm{s}} T(\mathbf{x}) \, \mathbf{n}(\mathbf{x}) \, \mathrm{d}\Gamma \\ \langle \mathbf{q} \rangle &= \frac{1}{\Omega^{(\mathrm{p})}} \int_{\Omega^{(\mathrm{p})}} \mathbf{q}(\mathbf{x}) \, \mathrm{d}\Omega = \frac{1}{\Omega^{(\mathrm{p})}} \int_{\Gamma_\mathrm{s}} \mathbf{x} \, \mathbf{q}(\mathbf{x}) \, \mathrm{d}\Gamma \end{aligned} \tag{2.103}$$

in analogy to eqns. (1.4) and (1.16). The Hill–Mandel condition in thermal conduction becomes

$$\langle \mathbf{q}^\mathrm{T} \, \mathbf{d} \rangle = \int_\Omega \mathbf{q}^\mathrm{T}(\mathbf{x}) \; \mathbf{d}(\mathbf{x}) \, \mathrm{d}\Omega = \langle \mathbf{q} \rangle^\mathrm{T} \, \langle \mathbf{d} \rangle \quad , \tag{2.104}$$

in direct analogy to eqn. (1.7).

Dilute Inhomogeneities

In conduction and diffusion-type problems the effects of dilute inclusions can be described via the rank 2 depolarization tensor (also referred to as "shape tensor" or "diffusion Eshelby tensor"), $\mathcal{S}$. This tensor, introduced by Fricke (1924), is directly analogous to the "mechanical" Eshelby tensor, $\mathbf{S}$, discussed in Section 2.2. In the case of spheroidal inhomogeneities embedded in an isotropic matrix the depolarization tensor depends only on the formers' aspect ratio, see, e.g., Hatta and Taya (1986) and Torquato (2002), whereas for matrices of lower symmetry their material behavior also comes into play, see, e.g., Giraud et al. (2007) for transversally isotropic matrices. For diffusion problems the Eshelby

property takes the form of constant fluxes and constant gradients within dilute ellipsoidal inhomogeneities subjected to uniform far-field thermal loads. Dilute gradient and flux concentration tensors, $\mathcal{A}^{(\mathrm{i})}_{\mathrm{dil}}$ and $\mathcal{B}^{(\mathrm{i})}_{\mathrm{dil}}$, can be obtained by analogy to eqns. (2.31) and (2.32) as

$$\begin{aligned} \mathcal{A}^{(\mathrm{i})}_{\mathrm{dil}} &= [\mathcal{I} + \mathcal{S}\mathcal{R}^{(\mathrm{m})}(\mathcal{K}^{(\mathrm{i})} - \mathcal{K}^{(\mathrm{m})})]^{-1} \\ \mathcal{B}^{(\mathrm{i})}_{\mathrm{dil}} &= [\mathcal{I} + \mathcal{K}^{(\mathrm{m})}(\mathcal{I} - \mathcal{S})(\mathcal{R}^{(\mathrm{i})} - \mathcal{R}^{(\mathrm{m})})]^{-1} \end{aligned} \quad , \tag{2.105}$$

providing the basis for non-interacting approximations applicable to dilute inhomogeneity volume fractions. $\mathcal{I}$ stands for the rank 2 identity tensor.

Equivalents to many of the general relations for elasticity problems discussed in Section 2.1 hold for diffusion-type problems, typical examples being the expressions for the effective conductivity and resistivity tensors in terms of the gradient and flux concentration tensors,

$$\begin{aligned} \mathcal{K}^{*} &= \xi\mathcal{K}^{(\mathrm{i})}\bar{\mathcal{A}}^{(\mathrm{i})} + (1-\xi)\mathcal{K}^{(\mathrm{m})}\bar{\mathcal{A}}^{(\mathrm{m})} \\ \mathcal{R}^{*} &= \xi\mathcal{R}^{(\mathrm{i})}\bar{\mathcal{B}}^{(\mathrm{i})} + (1-\xi)\mathcal{R}^{(\mathrm{m})}\bar{\mathcal{B}}^{(\mathrm{m})} \end{aligned} \quad , \tag{2.106}$$

which are directly related to eqns. (2.8) and (2.9), and the linkages between different concentration tensors,

$$\bar{\mathcal{A}}^{(\mathrm{p})} = \mathcal{R}^{(\mathrm{p})}\bar{\mathcal{B}}^{(\mathrm{p})}\mathcal{K}^{*} \qquad \text{and} \qquad \bar{\mathcal{B}}^{(\mathrm{p})} = \mathcal{K}^{(\mathrm{p})}\bar{\mathcal{A}}^{(\mathrm{p})}\mathcal{R}^{*} \quad , \tag{2.107}$$

which correspond to eqns. (2.14).

Effective-Field Approaches

Analogous methods to the effective-field and effective-medium approaches introduced in Sections 2.3, 2.5 and 2.6 have been developed for the conduction and/or diffusion behavior of non-dilute inhomogeneous materials, see, e.g., Hatta and Taya (1986), Miloh and Benveniste (1988), Dunn and Taya (1993), Chen (1997) as well as Torquato (2002). In the case of Mori–Tanaka methods the phase concentration tensors can be evaluated from their dilute equivalents, eqns. (2.105), as

$$\begin{aligned} \bar{\mathcal{A}}^{(\mathrm{m})}_{\mathrm{MT}} &= [(1-\xi)\mathcal{I} + \xi\mathcal{A}^{(\mathrm{i})}_{\mathrm{dil}}]^{-1} & \bar{\mathcal{A}}^{(\mathrm{i})}_{\mathrm{MT}} &= \mathcal{A}^{(\mathrm{i})}_{\mathrm{dil}}[(1-\xi)\mathcal{I} + \xi\mathcal{A}^{(\mathrm{i})}_{\mathrm{dil}}]^{-1} \\ \bar{\mathcal{B}}^{(\mathrm{m})}_{\mathrm{MT}} &= [(1-\xi)\mathcal{I} + \xi\mathcal{B}^{(\mathrm{i})}_{\mathrm{dil}}]^{-1} & \bar{\mathcal{B}}^{(\mathrm{i})}_{\mathrm{MT}} &= \mathcal{B}^{(\mathrm{i})}_{\mathrm{dil}}[(1-\xi)\mathcal{I} + \xi\mathcal{B}^{(\mathrm{i})}_{\mathrm{dil}}]^{-1} \end{aligned} \tag{2.108}$$

in direct analogy to eqns. (2.41) and (2.42).

The mean-field interpretation of the Maxwell scheme in thermal conduction leads to the relations

$$\mathcal{K}^{*}_{\mathrm{MX}} = \mathcal{K}^{(\mathrm{m})} + \xi(\mathcal{K}^{(\mathrm{i})} - \mathcal{K}^{(\mathrm{m})})\Big[\mathcal{I} + (\mathcal{S}_{\mathrm{i}} - \xi\mathcal{S}_{\mathrm{E}})\mathcal{R}^{(\mathrm{m})}(\mathcal{K}^{(\mathrm{i})} - \mathcal{K}^{(\mathrm{m})})\Big]^{-1} \quad , \tag{2.109}$$

with the shape tensor $\mathcal{S}_{\mathrm{E}}$ accounting for the shape of the inhomogeneous region according to fig. 2.3 and $\mathcal{S}_{\mathrm{i}}$ for the shape of the inhomogeneities, compare eqn. (2.48). The Hashin–Shtrikman estimates of Ponte Castañeda and Willis (1995) can be written as

$$\mathcal{K}^{*}_{\mathrm{PW}} = \mathcal{K}^{(\mathrm{m})} + \big[\big(\xi(\mathcal{K}^{(\mathrm{i})} - \mathcal{K}^{(\mathrm{m})})\mathcal{A}^{(\mathrm{i})}_{\mathrm{dil}}\big)^{-1} - \mathcal{S}_{\mathrm{d}}\mathcal{R}^{(\mathrm{m})}\big]^{-1} \quad , \tag{2.110}$$

where $\mathcal{S}_{\mathrm{d}}$ serves for describing the ellipsoidal arrangement of inhomogeneities by analogy to eqn. (2.50). This scheme was extended to nonaligned inhomogeneities by Duan et al. (2006).

Effective-Medium Approaches

The classical self-consistent scheme for thermal conduction, which is often referred to as the symmetrical Bruggemann (1935) method, can be denoted in the form

$$\begin{aligned} \mathcal{K}_{n+1} &= \mathcal{K}^{(\mathrm{m})} + \xi[\mathcal{K}^{(\mathrm{i})} - \mathcal{K}^{(\mathrm{m})}][\mathcal{I} + \mathcal{S}_n^{(\mathrm{p},*)}\mathcal{R}_n(\mathcal{K}^{(\mathrm{i})} - \mathcal{K}_n)]^{-1} \\ \mathcal{R}_{n+1} &= \left[\mathcal{K}_{n+1}\right]^{-1} \quad , \end{aligned} \tag{2.111}$$

which is clearly equivalent to eqn. (2.53). The differential scheme for the effective conductivity tensor can be written as

$$\frac{\mathrm{d}\mathcal{K}_{\mathrm{D}}^*}{\mathrm{d}\xi} = \frac{1}{1-\xi}\left[\mathcal{K}^{(\mathrm{i})} - \mathcal{K}_{\mathrm{D}}^*\right]\mathcal{A}_{\mathrm{dil}}^{(\mathrm{i},*)} \quad . \tag{2.112}$$

For a number of cases analytical solutions are available, see, e.g., Phan-Thien and Pham (2000). Otherwise, the above initial value problem can be solved numerically in analogy to eqn. (2.54).

Nonaligned Reinforcements

For conduction problems the equivalents of "extended" Mori–Tanaka models for nonaligned reinforcements, compare, e.g., eqns. (2.66), take the form

$$\begin{aligned} \mathcal{K}_{\mathrm{MT}}^* &= \mathcal{K}^{(\mathrm{m})} + \xi\left\langle\!\left\langle(\mathcal{K}^{(\mathrm{i})} - \mathcal{K}^{(\mathrm{m})})\mathcal{A}_{\mathrm{dil}}^{(\mathrm{i})}\right\rangle\!\right\rangle\left[(1-\xi)\mathcal{I} + \xi\left\langle\!\left\langle\mathcal{A}_{\mathrm{dil}}^{(\mathrm{i})}\right\rangle\!\right\rangle\right]^{-1} \\ \mathcal{R}_{\mathrm{MT}}^* &= \mathcal{R}^{(\mathrm{m})} + \xi\left\langle\!\left\langle(\mathcal{R}^{(\mathrm{i})} - \mathcal{R}^{(\mathrm{m})})\mathcal{B}_{\mathrm{dil}}^{(\mathrm{i})}\right\rangle\!\right\rangle\left[(1-\xi)\mathcal{I} + \xi\left\langle\!\left\langle\mathcal{B}_{\mathrm{dil}}^{(\mathrm{i})}\right\rangle\!\right\rangle\right]^{-1} \quad . \end{aligned} \tag{2.113}$$

The corresponding non-dilute phase flux concentration tensors are

$$\begin{aligned} \left\langle\!\left\langle\bar{\mathcal{B}}^{(\mathrm{m})}\right\rangle\!\right\rangle_{\mathrm{MT}} &= \left[\xi^{(\mathrm{m})}\mathcal{I} + \xi^{(\mathrm{i})}\langle\langle\mathcal{B}_{\mathrm{dil}}^{(\mathrm{i})\angle}\rangle\rangle\right]^{-1} \\ \bar{\mathcal{B}}_{\mathrm{MT}}^{(\mathrm{i})\angle}(\varphi,\psi,\theta) &= \mathcal{B}_{\mathrm{dil}}^{(\mathrm{i})\angle}\left\langle\!\left\langle\bar{\mathcal{B}}^{(\mathrm{m})}\right\rangle\!\right\rangle_{\mathrm{MT}} \quad , \end{aligned} \tag{2.114}$$

compare eqns. (2.63) to (2.70), the gradient concentration tensors being obtained by analogy.

Similarly, the other methods and relationships discussed in Section 2.6 have analogies in modeling conduction or diffusion in inhomogeneous materials.

It is worth noting that, due to the lower ranks of the tensors involved in diffusion-type problems, the latter tend to be easier to handle than mechanical ones (for materials that show orthotropic or higher symmetry the tensors $\mathcal{K}$, $\mathcal{R}$, $\bar{\mathcal{A}}$, $\bar{\mathcal{B}}$, $\mathcal{S}$, $\mathcal{H}$ and $\mathcal{N}$ are diagonal tensors). Extensive discussions of diffusion-type problems in inhomogeneous media can be found, e.g., in Markov (2000), Torquato (2002) and Milton (2002). Analogous mean-field descriptions can also be devised for a number of coupled problems, such as the electromechanical behavior of inhomogeneous materials with at least one piezoelectric constituent, see, e.g., Huang and Yu (1994).

Non-Ellipsoidal Inhomogeneities

Diffusive transport in composites containing inhomogeneities of general shape can be described in terms of resistivity and conductivity contribution tensors,

$$\mathcal{H} = \frac{1}{\xi}(\mathcal{R}^* - \mathcal{R}^{(\mathrm{m})}) \qquad \text{and} \qquad \mathcal{N} = \frac{1}{\xi}(\mathcal{K}^* - \mathcal{K}^{(\mathrm{m})}) \qquad , \tag{2.115}$$

by direct analogy to the contribution tensor formalism in elasticity, eqns. (2.19) to (2.76). Dilute contribution tensors can again be obtained from standard mean-field expressions in the case of ellipsoidal inhomogeneities and from numerical models for other reinforcement shapes; in the latter case the linearly independent thermal load cases are required. Links between, on the one hand, resistivity and conductivity contribution tensors and, on the other hand, flux and gradient concentration tensors are provided by direct equivalents to eqns. (2.20).

Multi-Phase Composites

The diffusion and conduction behavior of composites reinforced by multiple inhomogeneity phases can be handled in direct analogy their elastic responses, compare section 2.8. Since the tensors involved in the models are of rank 2 rather than rank 4, however, difficulties such as the prediction of non-symmetric effective tensors by Mori–Tanaka methods in elasticity, do not occur in conduction.

Interphases and Interfacial Conductances

The effects of finite interfacial conductances or of interphases, i.e., coatings of finite thickness, on the effective conduction behavior of materials reinforced by ellipsoidal fibers or particles can be studied by approaches based on equivalent uniform inhomogeneities in analogy to Section 2.8.2. Exact expressions for the dilute phase concentration tensors in the core inhomogeneity and the coating were given by Kerner (1956) for spheres and by Hervé-Luanco and Joannès (2016) for infinitely long cylinders. These allow a two-step treatment in analogy to Section 2.8.2.

If position-dependent interfacial properties or non-ellipsoidal inhomogeneities combined with interfacial effects are involved, dilute inhomogeneity concentration tensors that are averaged over the inhomogeneities can be employed (Duschlbauer, 2004). Appropriate averaged "replacement" dilute inhomogeneity concentration tensors, $\bar{\mathcal{A}}_{\mathrm{dil}}^{(\mathrm{i,r})}$ and $\bar{\mathcal{B}}_{\mathrm{dil}}^{(\mathrm{i,r})}$, can be evaluated from high-resolution numerical models involving a single inhomogeneity. In conductivity, three linearly independent load cases must be evaluated for a given dilute configuration, e.g., via the Finite Element method. Using eqn. (5.8), the corresponding average gradients and fluxes in the phases can then be extracted, and the replacement concentration tensors evaluated.

In order to achieve a workable formulation, in addition to evaluating $\bar{\mathcal{A}}_{\mathrm{dil}}^{(\mathrm{i,r})}$ and/or $\bar{\mathcal{B}}_{\mathrm{dil}}^{(\mathrm{i,r})}$, the "physical" conductivity and resistivity tensors of the inhomogeneities, $\mathcal{K}^{(\mathrm{i})}$ and $\mathcal{R}^{(\mathrm{i})}$, must be substituted by suitable "replacement" conductivity and resistivity tensors that account for the presence of the interface and are defined as

$$\begin{aligned} \mathcal{K}^{(\mathrm{i,r})} &= \mathcal{K}^{(\mathrm{m})} + \frac{1}{\xi_{\mathrm{dil}}}(\mathcal{K}^{*}_{\mathrm{dil}} - \mathcal{K}^{(\mathrm{m})})[\bar{\mathcal{A}}^{(\mathrm{i,r})}_{\mathrm{dil}}]^{-1} \\ \mathcal{R}^{(\mathrm{i,r})} &= \mathcal{R}^{(\mathrm{m})} + \frac{1}{\xi_{\mathrm{dil}}}(\mathcal{R}^{*}_{\mathrm{dil}} - \mathcal{R}^{(\mathrm{m})})[\bar{\mathcal{B}}^{(\mathrm{i,r})}_{\mathrm{dil}}]^{-1} \end{aligned} \quad , \tag{2.116}$$

where $\mathcal{K}^{*}_{\mathrm{dil}}$ and $\mathcal{R}^{*}_{\mathrm{dil}}$ are the (numerically evaluated) effective conductivity and resistivity tensors of the dilute single-inhomogeneity configurations and ξ_{dil} is the corresponding reinforcement volume fraction. These replacement conduction tensors ensure consistency within the mean-field framework by enforcing the equivalents of eqns. (2.9) to be fulfilled. The replacement tensors can then be inserted in lieu of the "standard" concentration and conduction tensors into the mean-field expressions given above in order to obtain estimates for composites reinforced by non-ellipsoidal inhomogeneities (Duschlbauer, 2004; Nogales and Böhm, 2008). Analogous replacement tensor schemes can also be set up for the elastic behavior.

Mean-field models employing replacement tensors following eqn. (2.116), are not suitable for studying non-ellipsoidal inhomogeneities with volume fractions closely approaching unity because in such configurations interfaces between inhomogeneities and matrix cease to make physical sense.

In the case of finite interfacial conductances the "equivalent inhomogeneity" or "replacement inhomogeneity" must account for the effects of interfacial temperature jumps, see the discussion by Duschlbauer (2004). Replacement inhomogeneity formalisms can evaluate the effects of such interfacial barrier resistances on the macroscopic conductivity of composites for more complex geometries than "standard methods", such as the well-known model of Hasselman and Johnson (1987), an example being polyhedral reinforcements having inhomogeneously distributed interfacial conductances (Nogales and Böhm, 2008).

The above groups of methods — in agreement with numerical models for composites with imperfect interfaces (compare Section 6.9) and the pertinent bounds (Torquato and Rintoul, 1995) — predict that finite interfacial conductances can give rise to marked size effects in the macroscopic conductivities. Since interfacial resistivities can hardly be avoided, below some critical size even highly conductive reinforcements accordingly fail to improve the overall conductivity of matrix–inclusion composites of given matrix behavior.

Cross-Property Relationships

Finally, it is worth mentioning that a number of authors have studied cross-property relations, compare, e.g., Gibiansky and Torquato (1996), and cross-property bounds, see, e.g., Sevostianov and Kachanov (2002), that link the elastic and conduction behaviors of given microgeometries.

Chapter 3

Bounding Methods

Whereas mean-field methods, unit cell approaches and embedding strategies can typically be used for both homogenization and localization tasks, bounding methods are limited to homogenization. The emphasis in this chapter again is put on materials consisting of two perfectly bonded constituents.

Rigorous bounds on the overall elastic properties of inhomogeneous materials are typically obtained from appropriate variational (minimum energy) principles. Only outlines of bounding methods are given here; formal treatments were provided, e.g., by Nemat-Nasser and Hori (1993), Ponte Castañeda and Suquet (1998), Markov (2000), Bornert (2001), Gross and Seelig (2001), Torquato (2002), Milton (2002) and Parnell and Calvo-Jurado (2015).

3.1 Classical Bounds

Hill Bounds

Classical expressions for the minimum potential energy and the minimum complementary energy in combination with uniform stress and strain trial functions lead to the simplest variational bounding expressions, the upper bounds of Voigt (1889) and the lower bounds of Reuss (1929). In their tensorial form (Hill, 1952) they are known as the Hill bounds (or Voigt–Reuss–Hill bounds) and can be written as

$$\mathbf{E}^*_{\mathrm{H}-} = \left[\sum\nolimits_{(\mathrm{p})} V^{(\mathrm{p})}\mathbf{C}^{(\mathrm{p})}\right]^{-1} \leq \mathbf{E} \leq \sum\nolimits_{(\mathrm{p})} V^{(\mathrm{p})}\mathbf{E}^{(\mathrm{p})} = \mathbf{E}^*_{\mathrm{H}+} \quad . \tag{3.1}$$

These bounds, while universal and very simple, do not contain any information on the microgeometry of an inhomogeneous material beyond the phase volume fractions, so that the macroscopic elastic symmetry of the bounding expressions, eqns. (3.1), depends solely on the elastic symmetries of the constituents. Hill bounds are too slack for most practical purposes[43]. but, in contrast to the Hashin–Shtrikman and higher-order bounds, they also hold for volume elements that are too small to be proper RVEs.

[43]The bounds on the Young's moduli obtained from eqn. (3.1) are equivalent to Voigt and Reuss expressions in terms of the corresponding phase moduli only if the constituents have Poisson's ratios that give rise to equal Poisson contractions. Due to the homogeneous stress and strain assumptions used for obtaining the Hill bounds, the phase strain and stress concentration tensors corresponding to them are $\bar{\mathbf{A}}^{(\mathrm{p})}_{\mathrm{V}} = \mathbf{I}$ and $\bar{\mathbf{B}}^{(\mathrm{p})}_{\mathrm{R}} = \mathbf{I}$, respectively.

Hashin–Shtrikman-Type Bounds

Considerably tighter bounds on the macroscopic elastic responses of inhomogeneous materials can be obtained from a variational formulation due to Hashin and Shtrikman (1961) which is based on phase-wise uniform stress polarization tensors, eqn. (2.56). For macroscopically isotropic composites containing spherical inhomogeneities these bounds were originally stated in terms of the effective bulk modulus K^* and the effective shear modulus[44] G^*. Analogous expressions for (macroscopically transversally isotropic) composites reinforced by aligned continuous fibers were given by Hashin (1972) and an extension to composites containing transversally isotropic aligned continuous fibers can be found in Hashin (1983). For the original Hashin–Shtrikman bounds the isotropic constituents were assumed to be elastically "well-ordered", with $(K^{(\mathrm{i})} - K^{(\mathrm{m})})(G^{(\mathrm{i})} - G^{(\mathrm{m})}) > 0$.

Walpole (1966), on the one hand, removed the restriction to well-ordered constituent properties by proposing generalized reference materials and, on the other hand, provided tensorial expressions for Hashin–Shtrikman-type bounds in the form

$$\begin{aligned} \mathbf{E}^*_{\mathrm{HSW}-} &= \Big[\sum_{(\mathrm{p})} \xi^{(\mathrm{p})} \mathbf{E}^{(\mathrm{p})} \bar{\mathbf{T}}^{(\mathrm{p},-)}_{\mathrm{dil}}\Big] \Big[\sum_{(\mathrm{p})} \xi^{(\mathrm{p})} \bar{\mathbf{T}}^{(\mathrm{p},-)}_{\mathrm{dil}}\Big]^{-1} \\ \mathbf{E}^*_{\mathrm{HSW}+} &= \Big[\sum_{(\mathrm{p})} \xi^{(\mathrm{p})} \mathbf{E}^{(\mathrm{p})} \bar{\mathbf{T}}^{(\mathrm{p},+)}_{\mathrm{dil}}\Big] \Big[\sum_{(\mathrm{p})} \xi^{(\mathrm{p})} \bar{\mathbf{T}}^{(\mathrm{p},+)}_{\mathrm{dil}}\Big]^{-1} \quad . \end{aligned} \tag{3.2}$$

Equations (3.2) are closely related to the Hashin–Shtrikman tensor, eqn. (2.89). The partial strain concentration tensors, $\bar{\mathbf{T}}^{(\mathrm{p},-)}_{\mathrm{dil}}$ and $\bar{\mathbf{T}}^{(\mathrm{p},+)}_{\mathrm{dil}}$, which pertain to a phase $^{(\mathrm{p})}$ embedded in the lower or the upper reference material, described by elasticity tensors $\mathbf{E}^-$ and $\mathbf{E}^+$, respectively, can be evaluated from eqn. (2.31) or an equivalent. Willis (1977) extended the Hashin–Shtrikman-type bounds to elastically anisotropic macroscopic behavior due to anisotropic constituent behavior and/or aligned ellipsoidal reinforcements.

In order to obtain proper bounds, the lower and upper comparison media must be at least as compliant or as stiff, respectively, as any of the constituents, which may be written as $\mathbf{E}^- \leq \mathbf{E}^{(\mathrm{p})}$ and $\mathbf{E}^+ \geq \mathbf{E}^{(\mathrm{p})}$, compare Bornert (2001). For "typical" two phase-composites, which consist of stiff reinforcements in a compliant matrix, well-orderedness implies $\mathbf{E}^- = \mathbf{E}^{(\mathrm{m})}$ and $\mathbf{E}^+ = \mathbf{E}^{(\mathrm{i})}$. The two-phase version of eqns. (3.2),

$$\begin{aligned} \mathbf{E}^*_{\mathrm{HS}-} &= \big[(1-\xi)\mathbf{E}^{(\mathrm{m})} \bar{\mathbf{T}}^{(\mathrm{m},-)}_{\mathrm{dil}} + \xi \mathbf{E}^{(\mathrm{i})} \bar{\mathbf{T}}^{(\mathrm{i},-)}_{\mathrm{dil}}\big] \big[(1-\xi)\bar{\mathbf{T}}^{(\mathrm{m},-)}_{\mathrm{dil}} + \xi \bar{\mathbf{T}}^{(\mathrm{i},-)}_{\mathrm{dil}}\big]^{-1} \\ \mathbf{E}^*_{\mathrm{HS}+} &= \big[(1-\xi)\mathbf{E}^{(\mathrm{m})} \bar{\mathbf{T}}^{(\mathrm{m},+)}_{\mathrm{dil}} + \xi \mathbf{E}^{(\mathrm{i})} \bar{\mathbf{T}}^{(\mathrm{i},+)}_{\mathrm{dil}}\big] \big[(1-\xi)\bar{\mathbf{T}}^{(\mathrm{m},+)}_{\mathrm{dil}} + \xi \bar{\mathbf{T}}^{(\mathrm{i},+)}_{\mathrm{dil}}\big]^{-1} \quad , \end{aligned} \tag{3.3}$$

[44] Whereas engineers tend to describe elastically isotropic material behavior by Young's moduli and Poisson's ratios (which can be measured from uniaxial tensile experiments in a relatively straightforward way), many homogenization expressions are best formulated in the bulk and shear moduli, which are directly linked to the hydrostatic and deviatoric responses, compare eqn. (2.96). For obtaining bounds on the effective Young's modulus E^* from the results on K^* and G^* see Hashin (1983), and for bounding expressions on the Poisson's ratios ν^* see Zimmerman (1992). The latter procedure can be extended to macroscopically transversely isotropic materials, where, however, it tends to give rise to rather slack bounds on some of the engineering moduli, especially on the transverse Poisson's ratios.

can be transformed for this case into

$$\begin{aligned}
\mathbf{E}^{*}_{\mathrm{HS}-} &= \Big[(1-\xi)\mathbf{E}^{(\mathrm{m})} + \xi\mathbf{E}^{(\mathrm{i})}\bar{\mathbf{T}}^{(\mathrm{i,m})}_{\mathrm{dil}}\Big]\Big[(1-\xi)\mathbf{I} + \xi\bar{\mathbf{T}}^{(\mathrm{i,m})}_{\mathrm{dil}}\Big]^{-1} \\
&= \mathbf{E}^{(\mathrm{m})} + \xi\Big[(\mathbf{E}^{(\mathrm{i})} - \mathbf{E}^{(\mathrm{m})})^{-1} + (1-\xi)\mathbf{S}^{(\mathrm{i,m})}\mathbf{C}^{(\mathrm{m})}\Big]^{-1} \\
\mathbf{E}^{*}_{\mathrm{HS}+} &= \Big[(1-\xi)\mathbf{E}^{(\mathrm{m})}\bar{\mathbf{T}}^{(\mathrm{m,i})}_{\mathrm{dil}} + \xi\mathbf{E}^{(\mathrm{i})}\Big]\Big[(1-\xi)\bar{\mathbf{T}}^{(\mathrm{m,i})}_{\mathrm{dil}} + \xi\mathbf{I}\Big]^{-1} \\
&= \mathbf{E}^{(\mathrm{i})} + (1-\xi)\Big[(\mathbf{E}^{(\mathrm{m})} - \mathbf{E}^{(\mathrm{i})})^{-1} + \xi\mathbf{S}^{(\mathrm{m,i})}\mathbf{C}^{(\mathrm{i})}\Big]^{-1} \quad . \qquad (3.4)
\end{aligned}$$

The first of the above equations is equivalent to the Mori–Tanaka expression, eqn. (2.44), and the second one is a "color inverted" version of it, i.e., it corresponds to a microstructure of inhomogeneity volume fraction ξ in which the materials of matrix and inhomogeneity have been interchanged. Thus, for two-phase materials with well-ordered constituent elasticities the Hashin–Shtrikman bounds can be evaluated via Mori–Tanaka estimates, compare Weng (1990) or Gross and Seelig (2001). In the case of multi-phase composites Mori–Tanaka models correspond to the upper or lower Hashin–Shtrikman-type bound if the matrix is the most compliant or the stiffest constituent. However, in general the above "shortcut" cannot be used for multi-phase materials.

For composites with matrix–inclusion topology eqns. (3.2) can only be used if all inhomogeneity phases have identical shapes, so that all pertinent $\bar{\mathbf{T}}^{(\mathrm{p},-)}_{\mathrm{dil}} = \bar{\mathbf{T}}^{(\mathrm{i},-)}_{\mathrm{dil}}$ and all $\bar{\mathbf{T}}^{(\mathrm{p},+)}_{\mathrm{dil}} = \bar{\mathbf{T}}^{(\mathrm{i},+)}_{\mathrm{dil}}$ are identical; the $\bar{\mathbf{T}}^{(\mathrm{m},-)}_{\mathrm{dil}}$ and $\bar{\mathbf{T}}^{(\mathrm{m},+)}_{\mathrm{dil}}$ are then also evaluated for the same aspect ratio, as is the case for eqns. (3.3) and (3.4). Equations (3.2) to (3.4) deliver valid bounds whenever the comparison media fulfill the conditions $\mathbf{E}^{-} \leq \mathbf{E}^{(\mathrm{p})}$ and $\mathbf{E}^{+} \geq \mathbf{E}^{(\mathrm{p})}$ for all constituents $^{(\mathrm{p})}$. Choosing the largest possible $\mathbf{E}^{-}$ and the smallest possible $\mathbf{E}^{+}$ leads to the tightest, optimal bounds. Using reference media of vanishing or infinite stiffness recovers the lower and upper Hill bounds, respectively.

Explicit constructions for optimal comparison media pertinent to the two-phase case were given by Walpole (1966) for materials in which constituents and macroscopic behavior are isotropic. Parnell and Calvo-Jurado (2015) provide an in-depth discussion of the evaluation of Hashin–Shtrikman-type bounds for composites consisting of aligned, transversally isotropic reinforcements in a transversally isotropic matrix.

For multi-phase materials in which one of the phases is the most compliant and another the stiffest one, the choice of $\mathbf{E}^{-}$ and $\mathbf{E}^{+}$ is obvious. In all other situations generalized, "synthetic" reference media must be provided. Useful tensors $\mathbf{E}^{-}$ and $\mathbf{E}^{+}$ for general multi-phase materials can typically be constructed from the minima and maxima of the eigenvalues of the phase elasticity tensors[45] $\mathbf{E}^{(\mathrm{p})}$ (Parnell and Calvo-Jurado, 2015). However, reference media generated this way may be non-optimal.

If at least one inhomogeneity phase shows vanishing stiffness, i.e., for porous materials, the above considerations lead to a trivial lower bound. Similarly, an infinite upper bound

[45] If all phases are isotropic this implies constructing the comparison material from the minima and maxima of the shear and bulk moduli $G^{(\mathrm{p})}$ and $K^{(\mathrm{p})}$. If some or all of the phases are transversally isotropic, $\mathbf{E}^{-}$ and $\mathbf{E}^{+}$ can be generated from the minima and maxima of the five phase-level Hill moduli $k^{(\mathrm{p})} = K^{(\mathrm{p})}_{\mathrm{T}}$, $l^{(\mathrm{p})} = 2K^{(\mathrm{p})}_{\mathrm{T}}\nu^{(\mathrm{p})}_{\mathrm{A}}$, $m^{(\mathrm{p})} = G^{(\mathrm{p})}_{\mathrm{T}}$, $n^{(\mathrm{p})} = E^{(\mathrm{p})}_{\mathrm{A}} + 4K^{(\mathrm{p})}_{\mathrm{T}}(\nu^{(\mathrm{p})}_{\mathrm{A}})^2$ and $p^{(\mathrm{p})} = G^{(\mathrm{p})}_{\mathrm{A}}$.

results if at least one of the constituents is rigid. Composites reinforced by randomly oriented, isotropic fibers or platelets follow the Hashin–Shtrikman bounds for macroscopically isotropic materials. A discussion of Hashin–Shtrikman-type bounds on the elastic responses of composites with more general fiber orientation distributions can be found in Eduljee and McCullough (1993).

Hashin–Shtrikman-type variational formulations can also be employed for generating bounds for more general phase arrangements. Evaluating the stress polarizations for "composite regions" consisting of inhomogeneities embedded in a matrix gives rise to Hervé–Stolz–Zaoui bounds (Hervé et al., 1991). When complex phase patterns are considered (Bornert, 1996; Bornert et al., 1996) numerical methods must be used for evaluating the polarization fields. If exact solutions are available for the concentration tensors of non-uniform inhomogeneities, as is the case for coated spherical and cylindrical reinforcements, compare Section 2.8.2, they can be directly inserted into eqns. (3.3) or (3.4) to provide bounds.

Hashin–Shtrikman-type bounds can also be derived for simple periodic phase arrangements, see, e.g., Nemat-Nasser and Hori (1993). Among the bounding methods for such phase arrangements are those of Bisegna and Luciano (1996), which uses approximate variational principles evaluated from periodic unit cells via Finite Element models, and of Teply and Dvorak (1988), which evaluates bounds for the elastoplastic behavior of fiber-reinforced composites with periodic hexagonal phase arrangements.

Hashin–Shtrikman-type bounds are sharp, i.e., they are the tightest bounds that can be given for the geometrical information used, viz., volume fraction and overall symmetry, corresponding to two-point correlations. Bounds of this group tend to be rather slack, however, i.e., the lower and upper bounds are relatively far apart, especially for elevated phase contrasts.

3.2 Improved Bounds

A considerable number of statistical descriptors have been used for characterizing the phase arrangements of inhomogeneous materials, see, e.g., Torquato (2002). An important group of them are n-point probability functions, which are obtained by randomly placing sets on n points into the microstructure and recording which phases they end up in. For one-point correlations this procedure provides the phase volume fractions. When two-point probabilities are evaluated for two-phase composites, on the one hand, the probabilities of finding both points in the matrix or in the inhomogeneities, $S_{\mathrm{mm}}(\mathbf{r})$ and $S_{\mathrm{ii}}(\mathbf{r})$, respectively, or in different phases, $S_{\mathrm{mi}}(\mathbf{r})$, can be obtained, compare fig. 3.1. On the other hand, the vector $\mathbf{r}$ between the two points provides information on the anisotropy of the arrangement and on the dependence of the S_{pq} on the distance between the points. The Hill bounds are closely related to one-point and Hashin–Shtrikman bounds to two-point probabilities.

Three-point probability functions $S_{\mathrm{pqr}}(\mathbf{r}_1, \mathbf{r}_2)$ can provide additional information, e.g., on inhomogeneity shapes, sizes and clustering. Most work on three-point correlations has involved isotropic configurations in two or three dimensions, giving rise to three-point

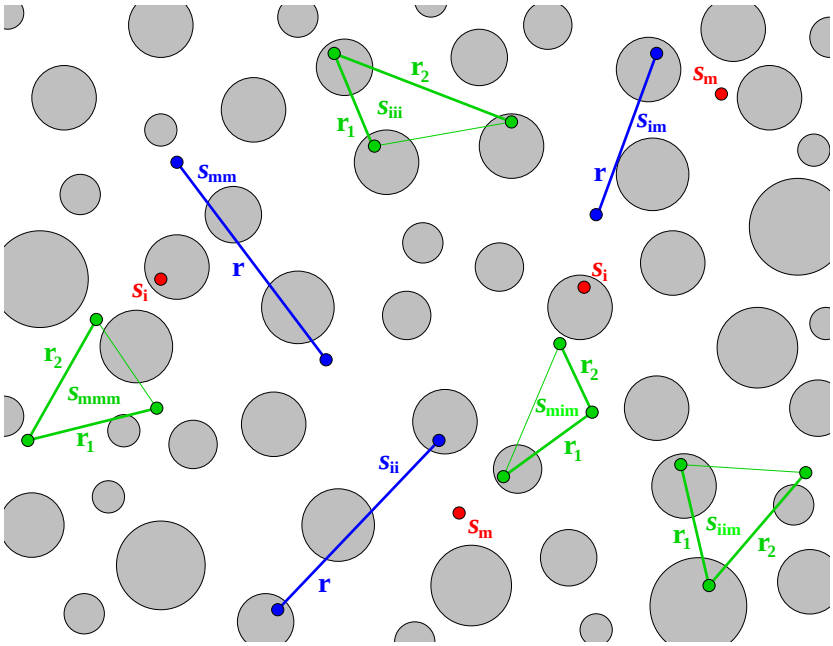

Figure 3.1: Sketch of sampling for one-point (red), two-point (blue) and three-point (green) probability functions in a two-dimensional matrix–inclusion composite; adapted from Gillman et al. (2015).

probabilities such as $S_{\mathrm{iii}}(r_1, r_2)$, where r_i stands for the length of the vector $\mathbf{r}_i$. They form the basis of three-point bounds, which use more complex trial functions than Hashin–Shtrikman bounds and, accordingly, require additional statistical information on the phase arrangement. The resulting "improved bounds" are significantly tighter than the two-point Hashin–Shtrikman-type expressions.

Three-point bounds for statistically isotropic two-phase materials were developed by Beran and Molyneux (1966), Milton (1981) as well as Phan-Thien and Milton (1983) and can be formulated in such a way that the information on the phase arrangement statistics is contained in two three-point microstructural parameters, $\eta(\xi)$ and $\zeta(\xi)$, which take the form of multiple integrals over the three-point correlation functions, see, e.g., Torquato (2002). These correlation functions and the resulting parameters $\zeta(\xi)$ and $\eta(\xi)$ can in principle be obtained for any given two- or three-dimensional microstructure that is statistically homogeneous, but in practice their evaluation may be demanding and require sophisticated numerical algorithms, see Gillman et al. (2015). Analytical expressions or tabulated data for $\zeta(\xi)$ and $\eta(\xi)$ in terms of the reinforcement volume fraction ξ are available for a number of generic microgeometries of practical importance, among them statistically homogeneous isotropic materials containing identical, bidisperse and polydisperse impenetrable ("hard") spheres (that describe matrix–inclusion composites) as well as monodisperse overlapping spheres ("Boolean models" that can describe many interwoven phase arrangements), and statistically homogeneous transversally isotropic materials reinforced by impenetrable or overlapping aligned cylinders. References to a number of expressions for η and ζ applicable to some two-phase composites can be found in Section 4.1, where results from mean-field and bounding approaches are compared. Recently, three-point parameters were published

for randomly positioned particles having the shapes of Platonic polyhedra (Gillman et al., 2015). Three-point bounds for multi-phase composites were discussed by Genin and Birman (2009). For reviews of higher-order bounds for elastic (as well as other) properties of inhomogeneous materials see, e.g., Quintanilla (1999), Torquato (1991) and Torquato (2002).

Improved bounds can provide highly useful information for low and moderate phase contrasts (as typically found in technical composites), but even they become rather slack for elevated phase contrasts and inhomogeneity volume fractions exceeding, say, $\xi^{(i)} = 0.3$. It is worth noting that, due to the additional geometrical information available, n-point bounds are always nested within $(n-1)$-point bounds. This implies that, for a given inhomogeneous material, the three-point bounds are tighter than Hashin–Shtrikman-type bounds which, in turn, are nested within the Hill bounds.

3.3 Bounds on Nonlinear Mechanical Behavior

Equivalents to the Hill bounds in elasticity, eqn. (3.1), were introduced for nonlinear inhomogeneous materials by Bishop and Hill (1951). For polycrystals the nonlinear equivalents to Voigt and Reuss expressions are usually referred to as Taylor (1938) and Sachs (1928) bounds, respectively.

In analogy to mean-field estimates for nonlinear material behavior, nonlinear bounds are typically obtained by evaluating sequences of linear bounds. Such bounds typically describe responses to loads that are radial in stress space and usually pertain to uniaxial tensile tests. Talbot and Willis (1985) extended the Hashin–Shtrikman variational principles to obtain one-sided bounds (i.e., upper or lower bounds, depending on the combination of constituents) on the nonlinear mechanical behavior of inhomogeneous materials.

An important development took place with the derivation of a variational principle by Ponte Castañeda (1992), which allows upper bounds on specific stress-strain responses of elastoplastic inhomogeneous materials to be generated on the basis of upper bounds on the elastic tensors[46]. It uses a sequence of inhomogeneous reference materials, the properties of which have to be obtained by optimization procedures for each strain level. Essentially, the variational principle guarantees the best choice for the comparison material at a given load. The Ponte Castañeda bounds are closely related to mean-field approaches using improved secant plasticity methods, compare Section 2.9. For higher-order bounds on the nonlinear response of inhomogeneous materials see, e.g., Talbot and Willis (1998).

The study of bounds — like the development of improved estimates — for the overall nonlinear mechanical behavior of inhomogeneous materials has been an active field of research during the past decades, see the reviews by Suquet (1997), Ponte Castañeda and Suquet (1998) and Willis (2000).

[46]The Ponte Castañeda bounds are rigorous for nonlinear elastic inhomogeneous materials and, on the basis of deformation theory, are excellent approximations for materials with at least one elastoplastic constituent. Applying the Ponte Castañeda variational procedure to elastic lower bounds does not necessarily lead to a lower bound for the inelastic behavior.

3.4 Bounds on Conduction and Diffusion-Like Properties

Because many bounding approaches are closely related to mean-field models it is not surprising that all of the bounding methods for the macroscopic elastic responses of inhomogeneous materials discussed in Sections 3.1 and 3.2 have direct equivalents in terms of diffusion properties by analogy to Section 2.10. The equivalents in thermal and electrical conduction to the elastic Hill bounds, eqn. (3.1), are known as the Wiener (1912) bounds and take the form

$$\left[\sum\nolimits_{(\mathrm{p})} V^{(\mathrm{p})}\mathcal{R}^{(\mathrm{p})}\right]^{-1} \leq \mathcal{K} \leq \sum\nolimits_{(\mathrm{p})} V^{(\mathrm{p})}\mathcal{K}^{(\mathrm{p})} \quad . \tag{3.5}$$

Hashin–Shtrikman bounds for diffusive transport were developed concurrently with the bounds for elasticity (Hashin and Shtrikman, 1962) and can be expressed in analogy to eqns. (3.3) as

$$\begin{aligned} \mathcal{K}^{*}_{\mathrm{HS}-} &= \mathcal{K}^{(\mathrm{m})} + \xi\left[(\mathcal{K}^{(\mathrm{i})} - \mathcal{K}^{(\mathrm{m})})^{-1} + (1-\xi)\mathcal{S}^{(\mathrm{i,m})}\mathcal{R}^{(\mathrm{m})}\right]^{-1} \\ \mathcal{K}^{*}_{\mathrm{HS}+} &= \mathcal{K}^{(\mathrm{i})} + (1-\xi)\left[(\mathcal{K}^{(\mathrm{m})} - \mathcal{K}^{(\mathrm{i})})^{-1} + \xi\mathcal{S}^{(\mathrm{m,i})}\mathcal{R}^{(\mathrm{i})}\right]^{-1} \end{aligned} \tag{3.6}$$

for the case that the inclusions are more conductive than the matrix. Willis bounds on effective conductivities can be given in direct equivalence to eqn. (3.2), compare, e.g., Calvo-Jurado and Parnell (2017).

Three-point bounds for diffusion properties were proposed, e.g., by Milton (1981). They require only one of the two statistical parameters used in bounding the elastic behavior, viz., $\zeta(\xi)$.

Chapter 4

Some Comparisons of Mean-Field Estimates and Bounds

4.1 Comparisons of Mean-Field and Bounding Predictions for Effective Thermoelastic Moduli of Two-Phase Composites

In order to show some of the basic features of the predictions that can be obtained by different mean-field (and related) approaches and by bounding methods for the thermomechanical responses of inhomogeneous thermoelastic materials, in this section selected results on the overall elastic moduli and coefficients of thermal expansion are presented as functions of the reinforcement volume fraction ξ. The comparisons are based on E-glass particles or fibers embedded in an epoxy matrix, the pertinent material parameters being listed in table 4.1. The elastic contrast of this pair of constituents is $c_{\mathrm{el}} \approx 21$ and the thermal expansion contrast takes a value of approximately 0.14.

Table 4.1: Constituent material parameters of the epoxy matrix and the E-glass reinforcements used for generating figs. 4.1 to 4.9.

	E[GPa]	ν[ ]	α[1/K]
matrix	3.5	0.35	3.6×10^{-5}
reinforcements	74.0	0.2	4.9×10^{-6}

Figures 4.1 and 4.2 show predictions for the overall Young's and shear moduli of a particle-reinforced two-phase composite using the above constituent parameters. The Hill bounds can be seen to be very slack. A macroscopically isotropic two-phase composite being studied, the Mori–Tanaka estimates (MTM) coincide with the lower Hashin–Shtrikman bounds (H/S LB), compare Section 3.1. The classical self-consistent scheme (CSCS) shows a typical behavior in that it is close to one Hashin–Shtrikman bound at low volume fractions, approaches the other at high volume fractions, and displays a transitional behavior in the form of a sigmoid curve in-between.

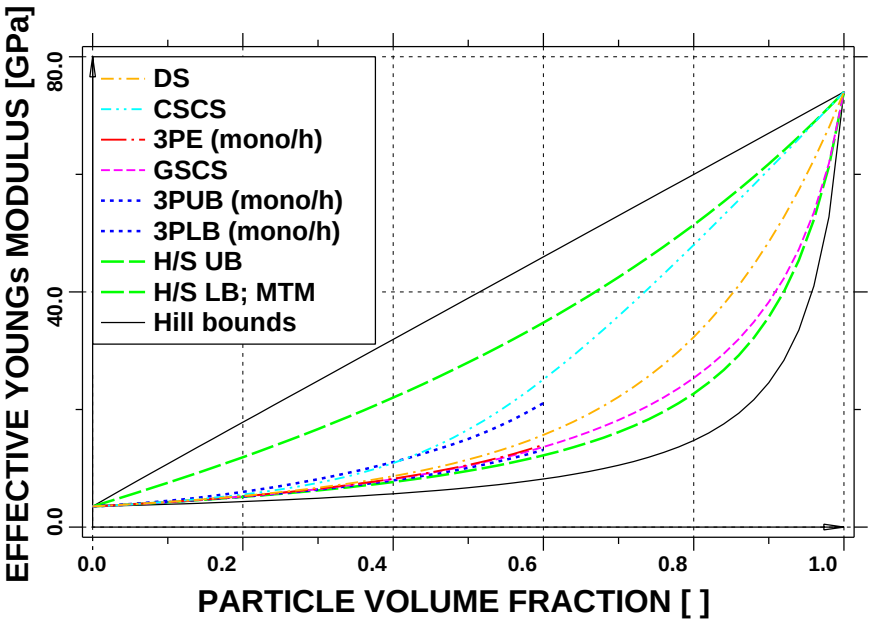

Figure 4.1: Bounds and estimates for the effective Young's moduli of glass/epoxy particle-reinforced composites as functions of the particle volume fraction.

The three-point bounds (3PLB and 3PUB) shown in figs. 4.1 pertain to impenetrable spherical particles of equal size and use expressions for the statistical parameters η and ζ listed by Torquato (2002), which are available for reinforcement volume fractions up to $\xi = 0.6$[47]. As expected, these improved bounds are significantly tighter than the Hashin–Shtrikman bounds. The three-point estimates (3PE) of Torquato (1998a), which were

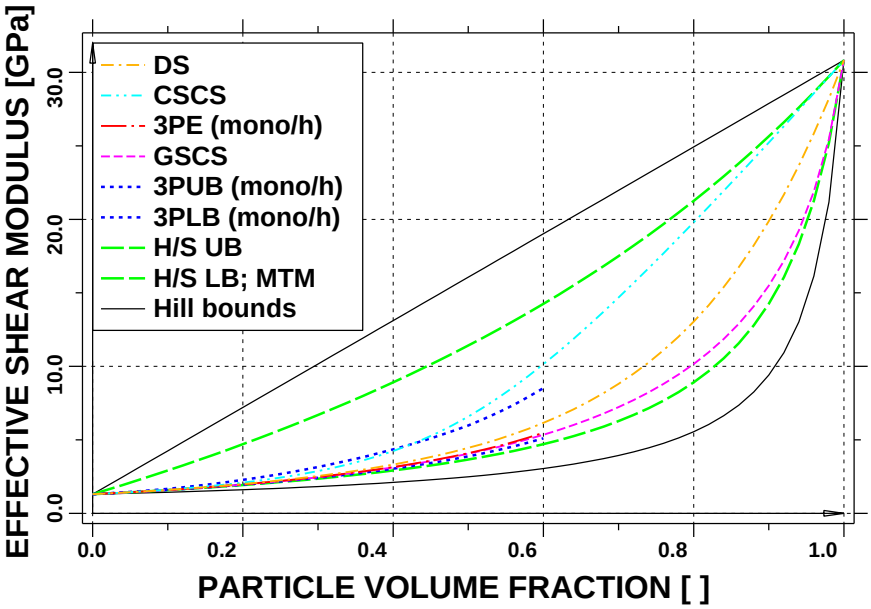

Figure 4.2: Bounds and estimates for the effective shear moduli of glass/epoxy particle-reinforced composites as functions of the particle volume fraction.

[47]This value approaches the maximum volume fraction achievable in random packings of identical spheres, which is $\xi \approx 0.64$ (Weisstein, 2000).

evaluated with the same choice of η and ζ, fall between the three-point bounds. For the composite considered here the results from the generalized self-consistent scheme (GSCS), which predicts a slightly stiffer behavior than the Mori–Tanaka method, are very close to the lower three-point bounds even though the GSCS is not associated with monodisperse particle microgeometries. The predictions of the differential scheme (DS) pertain to composites with polydisperse reinforcements and can be seen to be stiffer than either the three-point estimates for identical spheres or the GSCS results.

Alternatively, the elastic moduli of macroscopically isotropic composites can be visualized by plotting the shear modulus over the bulk modulus following Berryman and Milton (1988). In fig. 4.3 this format is used to compare the Hashin–Shtrikman (outermost, solid box) and three-point bounds for impenetrable, identical spheres (inner, dashed box) with a number of estimates for a glass–epoxy composite having a particle volume fraction of $\xi^{(\mathrm{p})} = 0.4$. The typical behavior of composites consisting of a compliant matrix reinforced by stiff particles is shown: the three-point bounds and all estimates pertinent to matrix–inclusion materials cluster in the corner corresponding to low bulk and shear moduli, whereas the classical self-consistent scheme predicts clearly different responses appropriate for materials having other phase-level topologies.

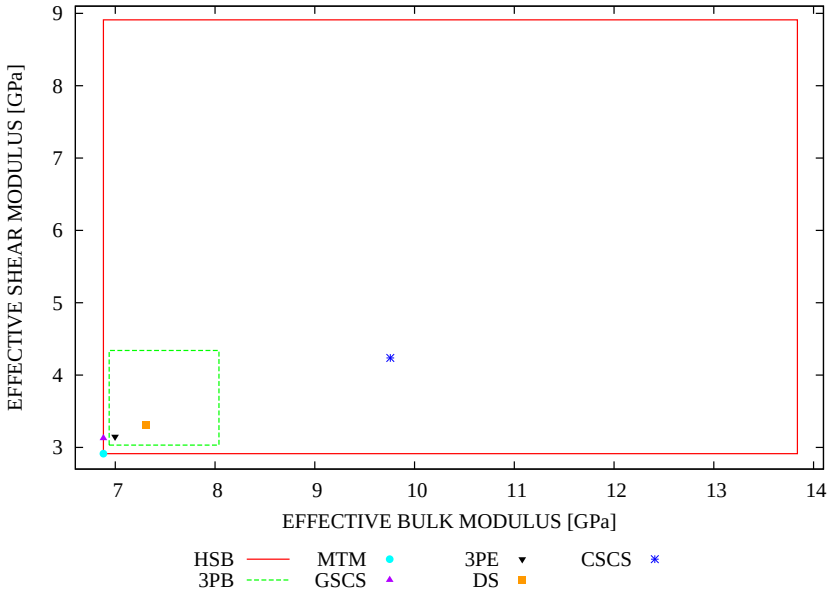

Figure 4.3: Bounds and estimates for the effective bulk and shear moduli of a glass/epoxy particle-reinforced composite of particle volume fraction $\xi^{(\mathrm{p})} = 0.4$.

Predictions for the macroscopic coefficients of thermal expansion of this macroscopically isotropic inhomogeneous material are presented in fig. 4.4. Levin's formula, eqn.(2.12), was combined with the Hashin–Shtrikman bounds, the three-point bounds, the generalized self-consistent estimates and the three-point estimates for the effective bulk modulus to obtain the corresponding bounds and estimates for the CTE. In the case of the classical self-consistent and differential schemes eqns. (2.10) and (2.16) were used. Being based on the same estimates for the effective bulk modulus, the results presented for the GSCS and the Mori–Tanaka-scheme coincide with the upper Levin/Hashin–Shtrikman bounds.

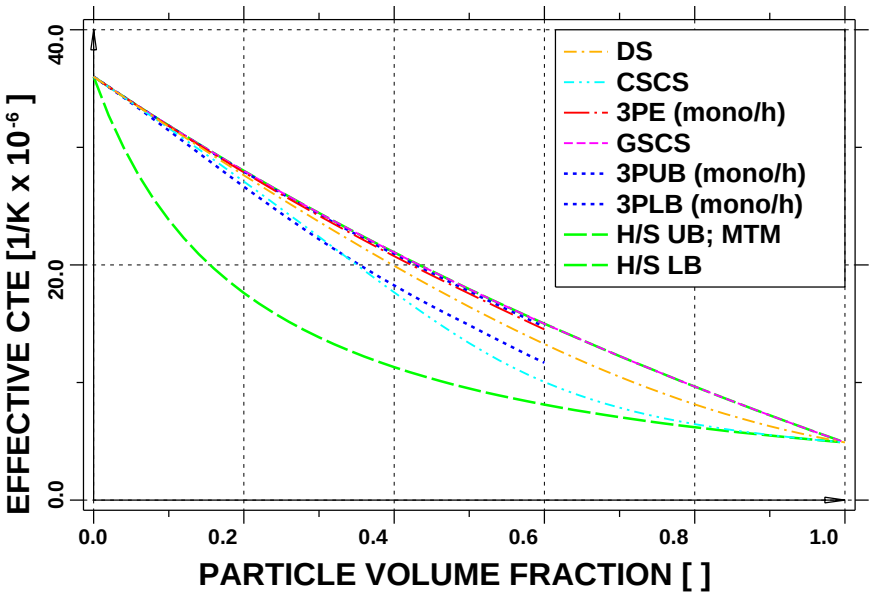

Figure 4.4: Bounds and estimates for the effective CTEs of glass/epoxy particle-reinforced composites as functions of the particle volume fraction.

Applying the constituent data given in table table 4.1 to an epoxy matrix reinforced by continuous aligned glass fibers gives rise to transversally isotropic macroscopic behavior. Pertinent results are presented in figs. 4.5 to 4.9 for the overall transverse Young's moduli[48],

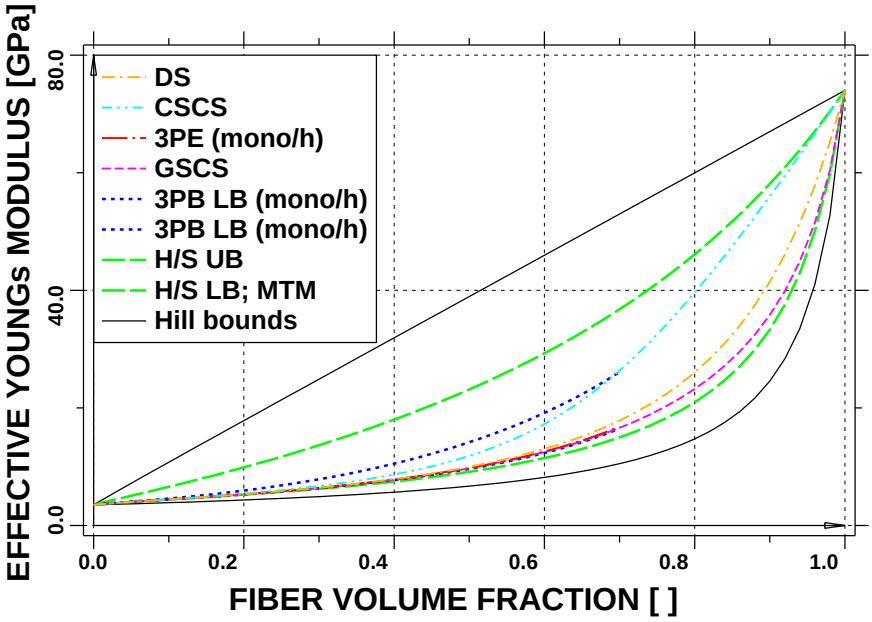

Figure 4.5: Bounds and estimates for the effective transverse Young's moduli of glass/epoxy fiber-reinforced composites as functions of the fiber volume fraction.

[48]The estimates and bounds for the axial Young's moduli are indistinguishable from each other (and from the rule-of-mixture result, $E_{\mathrm{A}}^{*} = \xi E_{\mathrm{A}}^{(\mathrm{i})} + (1-\xi)E^{(\mathrm{m})}$, as well as the Hill upper bound given in fig. 4.5) for the scaling used in fig. 4.5 and are, accordingly, not shown.

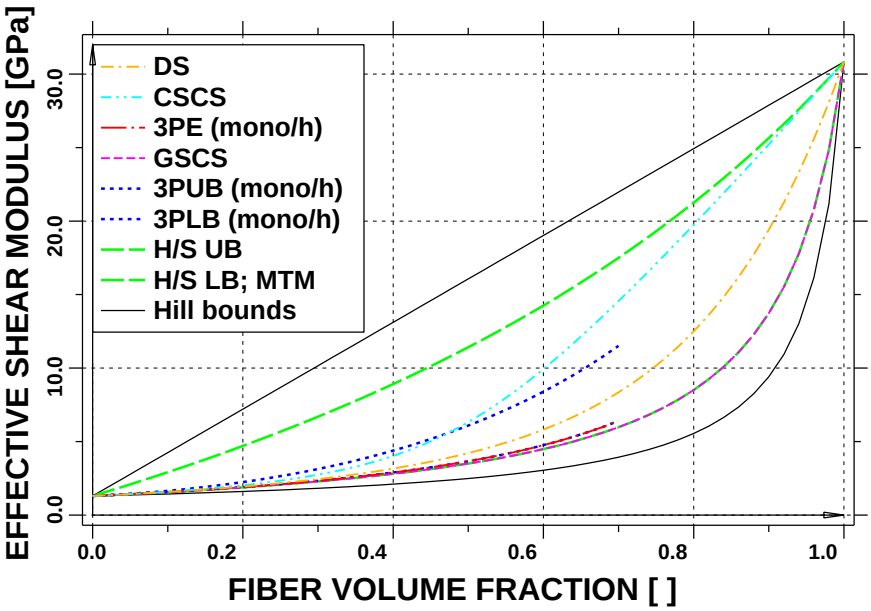

Figure 4.6: Bounds and estimates for the effective axial shear moduli of glass/epoxy fiber-reinforced composites as functions of the fiber volume fraction.

the overall axial and transverse shear moduli, as well as the overall axial and transverse coefficients of thermal expansion. The results for the three-point bounds shown are based on the formalisms of Silnutzer (1972) and Milton (1981), correspond to a microgeometry of aligned impenetrable circular cylindrical fibers of equal diameter, and use statistical parameters evaluated by Torquato and Lado (1992) for fiber volume fractions $\xi \lessapprox 0.7$. The coefficients of thermal expansion were evaluated on the basis of the relations of Rosen and Hashin (1970).

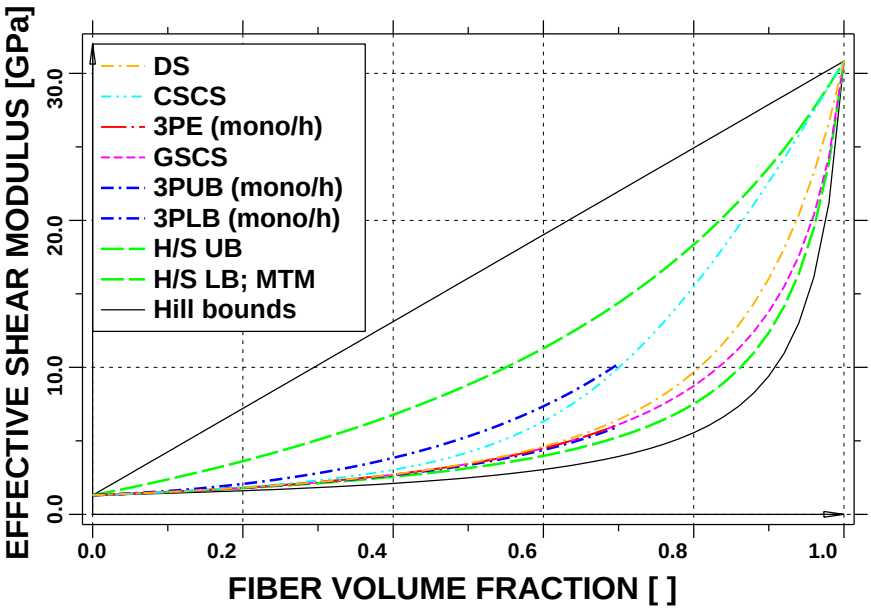

Figure 4.7: Bounds and estimates for the effective transverse shear moduli of glass/epoxy fiber-reinforced composites as functions of the fiber volume fraction.

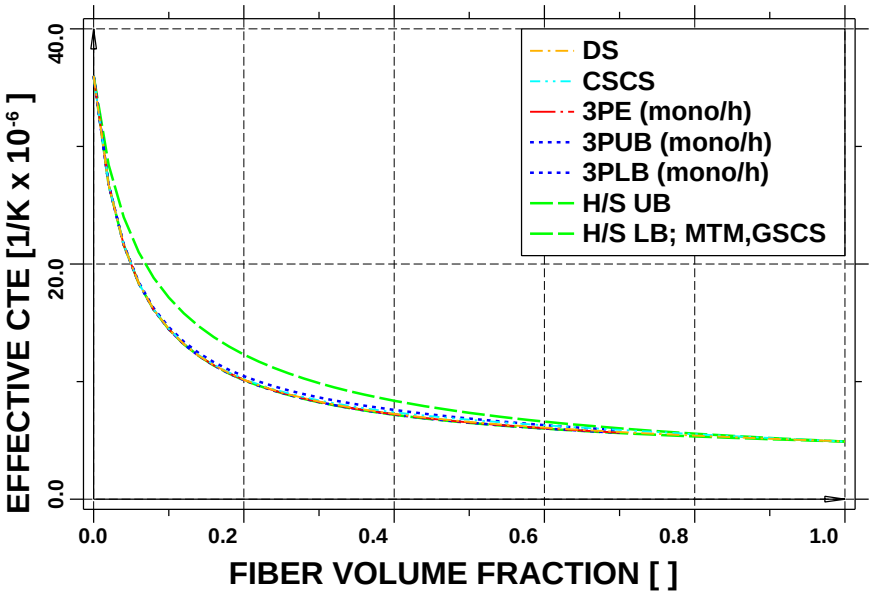

Figure 4.8: Estimates and bounds for the effective axial CTEs of glass/epoxy fiber-reinforced composites as functions of the fiber volume fraction.

Generally, a qualitatively similar behavior to the particle-reinforced case can be observed. It is noteworthy that the overall transverse CTEs in fig. 4.9 at low fiber volume fractions exceeds the CTEs of both constituents. Such behavior is typical for continuously reinforced composites and is caused by the marked axial constraint enforced by the fibers. As expected for continuously reinforced materials, there is little variation between the pre-

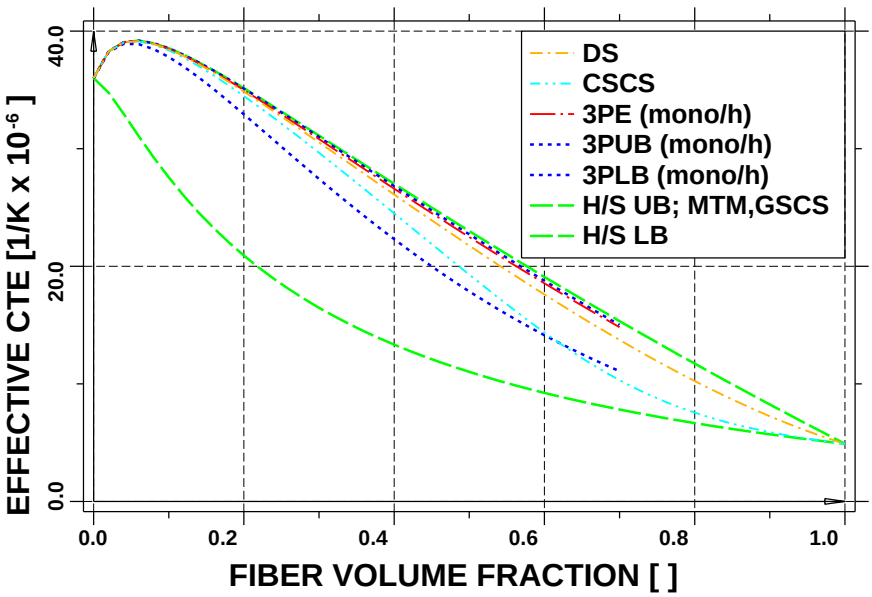

Figure 4.9: Estimates and bounds for the effective transverse CTEs of glass/epoxy fiber-reinforced composites as functions of the fiber volume fraction.

dictions of the different models for the axial thermal expansion behavior, fig. 4.8. The Mori–Tanaka estimates correspond to the upper bound for the transverse CTE in analogy to the macroscopically homogeneous case. For the axial CTE, however, the Mori–Tanaka results agree with the lower bound, which is a consequence of the axial constraint introduced by the fibers.

In figs. 4.1 to 4.7 the classical self-consistent scheme is not in good agreement with the three-point bounds shown, because the latter explicitly correspond to matrix–inclusion topologies. Considerably better agreement with the CSCS can be obtained by using three-point parameters of the overlapping sphere or cylinder type (which can also describe cases where both phases percolate, but are not as symmetrical with respect to the constituents as the CSCS). From a practical point of view it is worth noting that despite their sophistication higher order estimates (and improved bounds) may give overly optimistic predictions for the overall moduli because they describe ideal composites, whereas in actual "two-phase" materials it is practically impossible to avoid flaws such as porosity.

Before closing this section it is worth mentioning that more complex responses may be obtained when at least one of the constituents is transversally isotropic and one of the elastic or conductivity contrasts exceeds unity whereas the other is smaller (such situations can occur, e.g., in metals reinforced by carbon fibers). Also, the differences between the predictions of different mean-field models typically tend to be more pronounced when these algorithms are used to describe nonlinear responses, e.g., elastoplastic behavior. Furthermore, the angular dependences of stiffnesses and CTEs in fiber-reinforced materials can be quite rich, compare, e.g., Pettermann et al. (1997).

4.2 Comparisons of Mean-Field and Bounding Predictions for Effective Conductivities

Predictions for the effective conductivities of composites as functions of the phase volume fractions are qualitatively similar to the corresponding data for the elastic moduli, as can be seen in figs. 4.10 and 4.11, which pertain to a polyetherimide matrix reinforced by aligned short graphite fibers of aspect ratio $a = 10$. The plots use material parameters given by Harte and Mc Namara (2006), which are listed in table 4.2. The fibers show transversally isotropic conductivity, the axial conductivity contrast taking a value of approximately 37, whereas the transverse conductivity contrast is an order of magnitude smaller.

Table 4.2: Constituent material parameters of polyetherimide matrix and the T-300 graphite fibers used for generating figs. 4.10 to 4.11.

	$k_\mathrm{A}[\mathrm{Wm^{-1}K^{-1}}]$	$k_\mathrm{T}[\mathrm{Wm^{-1}K^{-1}}]$
matrix	0.22	0.22
reinforcements	8.40	0.84

Because for the composite described by figs. 4.10 and 4.11 the matrix conductivity is smaller than either the axial or the transverse fiber conductivities, the Mori–Tanaka es-

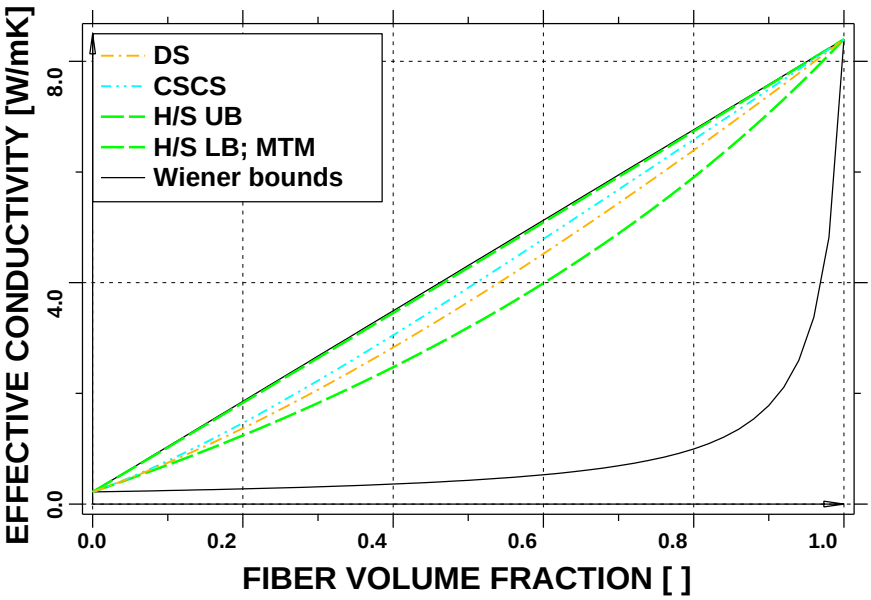

Figure 4.10: Bounds and estimates for the effective axial conductivity of composites consisting of aligned short graphite fibers ($a = 10$) in a polyetherimide matrix as functions of the fiber volume fraction.

timates for the effective conductivity coincide with the lower Hashin–Shtrikman bounds. Even though the selected fiber aspect ratio is rather moderate, the macroscopic conduction behavior approaches that of a continuously reinforced composite, with the upper Wiener and Hashin–Shtrikman bounds being nearly identical. As in the elastic case the classical self-consistent scheme, which does not describe matrix–inclusion topologies for all volume

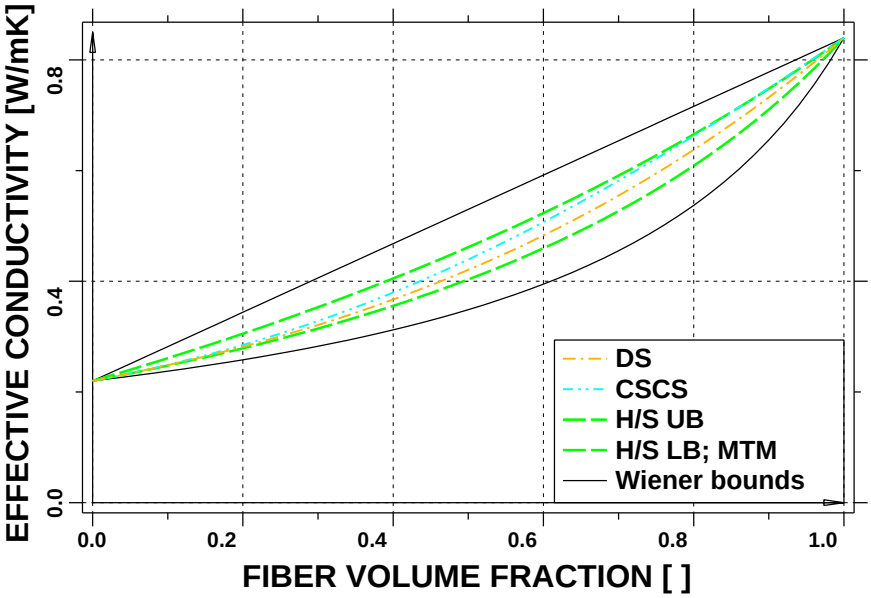

Figure 4.11: Bounds and estimates for the effective transverse conductivity of composites consisting of aligned short graphite fibers ($a = 10$) in a polyetherimide matrix as functions of the fiber volume fraction.

fractions, is close to one Hashin–Shtrikman bound at low fiber volume fractions and close to the other at high ones. The predictions of the differential scheme differ rather strongly from the lower Hashin–Shtrikman bounds, a behavior that tends to be especially marked in materials with elevated conductivity contrasts (which may reach very high values, indeed, in the case of electrical conduction).

4.3 Comparisons of Mean-Field and Bounding Predictions for Effective Elastic Moduli of Multi-Phase Composites

For the sake of brevity only three-phase composites with matrix–inclusion microtopology are considered here. The first four figures explore fictitious composites made up of a set of three isotropic phases, the normalized elastic parameters of which are listed in table 4.3. One of the inhomogeneity phases, denoted as $^{(i1)}$, is stiffer than the matrix, whereas inhomogeneity phase $^{(i2)}$ is more compliant. The elastic contrast between phases $^{(i1)}$ and $^{(i2)}$ takes a value of 25.

Table 4.3: Constituent material parameters of fictitious three-phase composites used in generating figs. 4.12 to 4.15.

	$E[\,]$	$\nu[\,]$
matrix $^{(m)}$	1.0	0.30
reinforcements $^{(i1)}$	5.0	0.10
reinforcements $^{(i2)}$	0.2	0.40

Whereas for plots of the effective responses of two-phase composites one of the phase volume fractions tends to be a natural choice for the independent variable, things may be less clear-cut for multi-phase composites. Most of the following diagrams show the behavior of an effective modulus with respect to the total inhomogeneity volume fraction, $\xi^{\mathrm{I}} = \sum_{(\mathrm{i})\neq(\mathrm{m})} \xi^{(\mathrm{i})} = 1 - \xi^{(\mathrm{m})}$, compare also eqns. (2.92).

Figure 4.12 presents the normalized, effective elastic moduli of composites reinforced by randomly positioned spherical particles of phases $^{(i1)}$ and $^{(i2)}$ embedded in the matrix $^{(m)}$, the volume fraction $\xi^{(i1)}$ being chosen as $9\,\xi^{(i2)}$. Such materials show macroscopically isotropic elastic behavior. Bounding results are provided by the Hill bounds, eqn. (3.1) and the Hashin–Sthrikman–Walpole bounds (HSW), eqns. (3.2), for which the lower and upper comparison media correspond to the two inhomogeneity phases. In addition, estimates obtained with the Mori–Tanaka Method (MTM), the classical Self-Consistent Scheme (CSCS), the Differential Scheme (DS) and a pseudo-grain model (PGR/MT-SC) are given. For the DS the inhomogeneity volume fractions of the inhomogeneity phases are increased proportionally. The PGR/MT-SC scheme describes individual pseudo-grains by a Mori–Tanaka method and homogenizes the grain-level elastic tensors by a Classical Self-Consistent Scheme, compare section 2.8.1. For particle volume fractions $\xi^{\mathrm{I}} \gtrapprox 0.5$ the

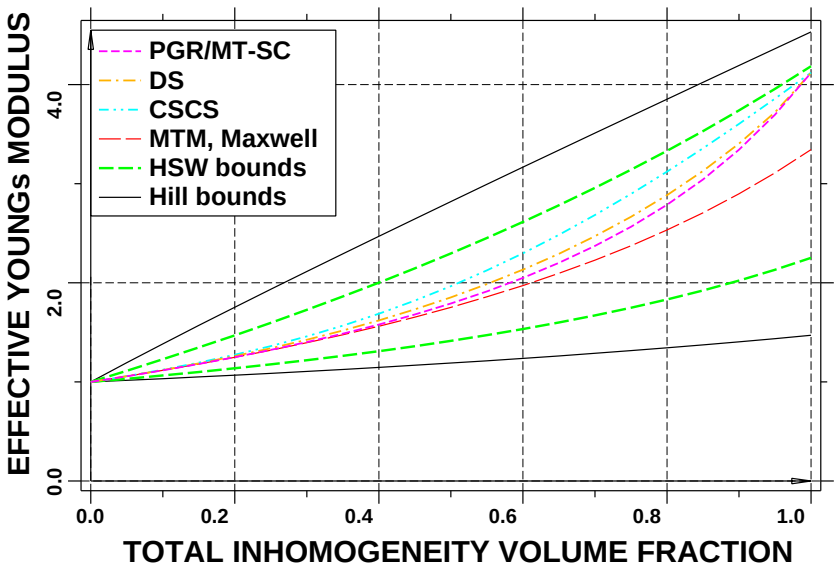

Figure 4.12: Bounds and estimates for the normalized effective Young's modulus of a fictitious three-phase particle reinforced composite with constituent properties following table 4.3, evaluated as functions of the total particle volume fraction $\xi^{\mathrm{I}} = \xi^{(\mathrm{i1})} + \xi^{(\mathrm{i2})}$, where $\xi^{(\mathrm{i1})} = 9\,\xi^{(\mathrm{i2})}$.

various predictions differ considerably. Since since $\xi^{\mathrm{I}} = 1$ refers to a two-phase inhomogeneous material, the plots are qualitatively different from two-phase results such as fig. 4.1. The MTM elasticity tensors remain symmetric and, because the matrix is not one of the comparison media, the MTM results do not coincide with one of the HSW bounds.

Figure 4.13 shows the effective normalized Young's moduli of composites reinforced by spherical particles consisting of a core of material $^{(\mathrm{i1})}$ concentrically coated by a homoge-

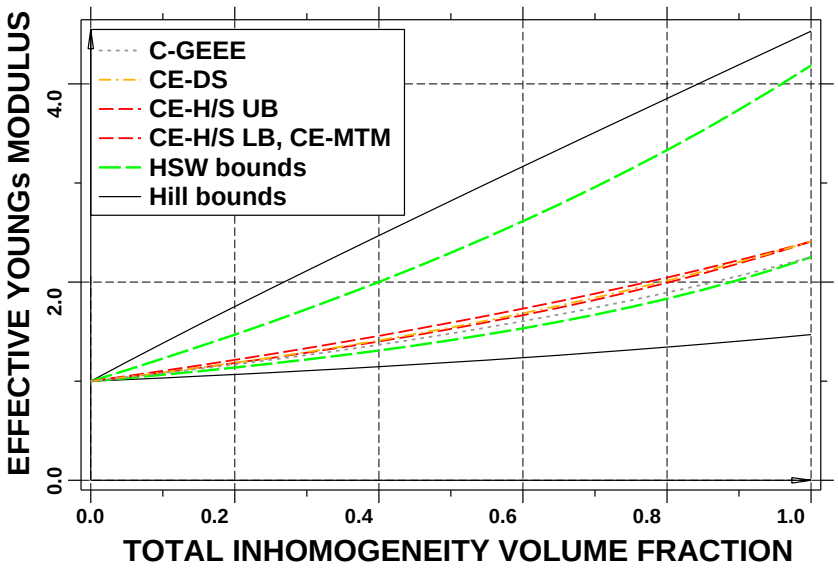

Figure 4.13: Bounds and estimates for the normalized effective Young's modulus of a fictitious composite reinforced by particles made up of a core of phase $^{(\mathrm{i1})}$ coated by phase $^{(\mathrm{i2})}$, evaluated as functions of the total inhomogeneity volume fraction $\xi^{\mathrm{I}} = \xi^{(\mathrm{i1})} + \xi^{(\mathrm{i2})}$, where $\xi^{(\mathrm{i1})} = 9\,\xi^{(\mathrm{i2})}$. Constituent properties are given in table 4.3.

neous layer of phase $^{(i2)}$, i.e., to the case of stiff core particles surrounded by a compliant interphase. Predictions obtained by combining the exact results for the equivalent homogeneous particles proposed by Hervé and Zaoui (1990) with the two-phase Hashin–Shtrikman bounds (CE-H/S), the two phase Mori–Tanaka method (CE-MTM) and the two-phase Differential Scheme (CE-DS) are given. The results marked as GEEE were obtained with the General Explicit Eshelby-Based Estimator of Ghazavizadeh et al. (2019); they also pertain to the MTMT-approaches mentioned in section 2.8.2. The CE-H/S bounds, which account for the fact that phase $^{(i2)}$ acts as a coating for spherical cores of phase $^{(i1)}$, making the geometry "more deterministic", can be seen to be markedly tighter than the HSW bounds, which pertain to the case where spheres of the two inhomogeneity phases are randomly distributed in the matrix. The GEEE predictions, which make use of an approximate rather than exact model for the effective inhomogeneities, can be seen to fall slightly outside the the CE-H/S bounds. Interchanging the roles of phases $^{(i1)}$ and $^{(i2)}$ in the coated inhomogeneities leads to considerably different results.

Predictions for the normalized axial shear modulus of three-phase composites reinforced by aligned, continuous, randomly arranged fibers consisting of materials $^{(i1)}$ and $^{(i2)}$ are presented in fig. 4.14. The resulting composite shows transversally isotropic macroscopic elastic symmetry. All parameters except the shapes of the reinforcements are kept as in the previous two figures. Most aspects of the behavior predicted for individual macroscopic moduli are similar to fig. 4.12, with the various estimates differing considerably for $\xi^{\mathrm{I}} \gtrapprox 0.5$. The Hashin–Shtrikman-type bounds can be seen to be clearly tighter than the Hill bounds. As in the particle reinforced case the Mori–Tanaka predictions coincide with Maxwell results obtained when setting $\mathbf{S}_{\mathrm{E}} = \mathbf{S}^{(\mathrm{i,m})}$ in eqn. (2.84). As in the analyses underlying Fig. 4.12 no difficulties were encountered in the application of any of the methods considered.

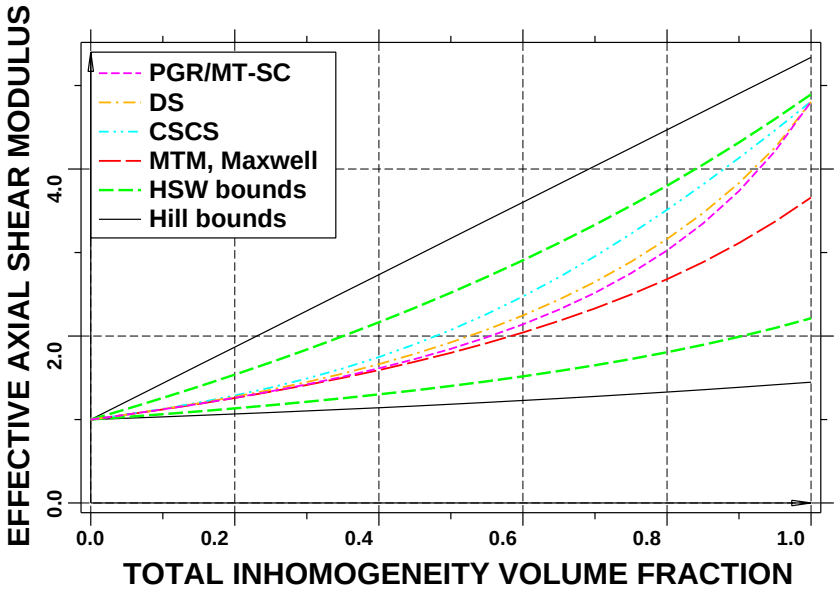

Figure 4.14: Bounds and estimates for the normalized effective axial shear modulus of a fictitious three-phase composite reinforced by aligned, continuous fibers with properties as given in table 4.3, evaluated as functions of the total fiber volume fraction $\xi^{\mathrm{I}} = \xi^{(i1)} + \xi^{(i2)}$, where $\xi^{(i1)} = 9\,\xi^{(i2)}$.

The micromechanical models cannot be used in such a carefree way for the configuration covered by Fig. 4.15, which shows bounds and estimates for the normalized effective transverse shear modulus of a fictitious three-phase hybrid composite in which the inhomogeneities of phase $^{(i1)}$ are aligned, prolate spheroids of aspect ratio $a^{(i1)} = 10$, whereas phase $^{(i2)}$ consists of aligned, oblate spheroids of aspect ratio $a^{(i2)} = 0.1$. The elastic properties of the constituents again follow table 4.3 and the volume fractions of the fiber phases vary proportionally with $\xi^{(i1)} = 9\,\xi^{(i2)}$. For these configurations Hashin–Shtrikman–Willis bounds as described by eqns. (3.2) cannot be evaluated and the Mori–Tanaka method gives rise to non-symmetrical elasticity tensors, so that a symmetrized Mori–Tanaka scheme (MTM/S) as proposed by Sevostianov and Kachanov (2014) is used instead. Nevertheless, the predictions obtained with the different estimates agree fairly well and the Maxwell method using the conjecture of Sevostianov and Kachanov (2014) for the shape of the inhomogeneous region gives reasonable predictions for this problem.

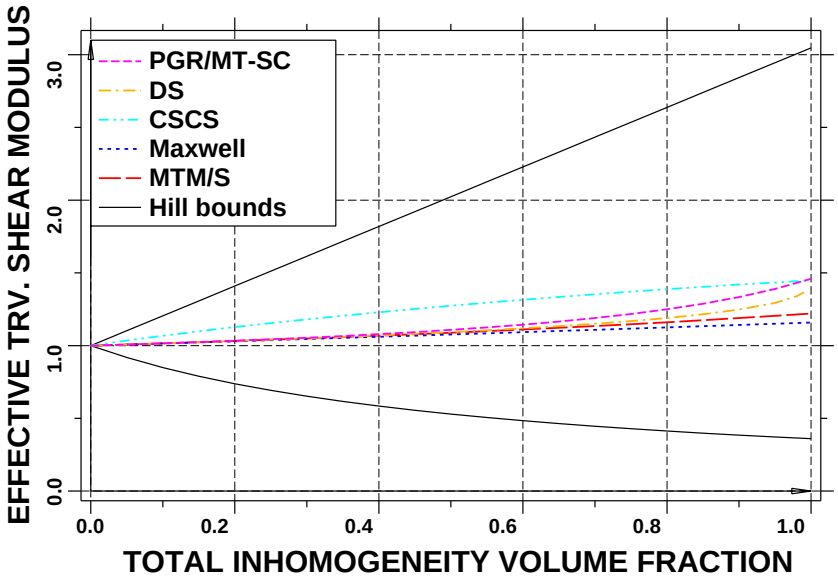

Figure 4.15: Bounds and estimates for the normalized effective transverse shear modulus of a fictitious three-phase hybrid composite reinforced by aligned spheroidal inhomogeneities of aspect ratios $a^{(i1)} = 10$ and $a^{(i2)} = 0.1$, evaluated as functions of the total fiber volume fraction $\xi^{I} = \xi^{(i1)} + \xi^{(i2)}$, where $\xi^{(i1)} = 9\,\xi^{(i2)}$. Constituent properties are given in table 4.3.

Table 4.4 introduces a further set of constituent properties which describe two transversally isotropic fiber phases embedded in a matrix. The material data are chosen such that the matrix becomes the lower comparison medium required for the Hashin–Shtrikman–

Table 4.4: Constituent material parameters of fictitious three-phase composite used in generating fig. 4.16.

	$E_A[\,]$	$E_T[\,]$	$G_A[\,]$	$\nu_A[\,]$	$\nu_T[\,]$
matrix $^{(m)}$	1.0	1.0	3.846	0.30	0.30
reinforcements $^{(i1)}$	10.0	3.0	2.5	0.10	0.40
reinforcements $^{(i2)}$	2.0	5.0	2.0	0.35	0.15

Willis bounds, whereas a synthetic upper comparison medium must be constructed, e.g., from the maxima of the Hill moduli of the phases. Figure 4.16 presents predictions for the normalized, macroscopic transverse bulk modulus of a composite reinforced by aligned, short fibers of aspect ratio $a^{(i1)} = a^{(i2)} = 5$ with this phase behavior. The volume fractions of both fiber phases are assumed to be identical. Because the lower comparison medium corresponds to the matrix, the lower Hashin–Sthrikman–Willis bounds coincide with the Mori–Tanaka predictions, which are slightly more compliant than the Maxwell results (not shown). For this case the Hashin–Sthrikman–Willis bounds are markedly tighter than the Hill ones and the different estimates agree reasonably well.

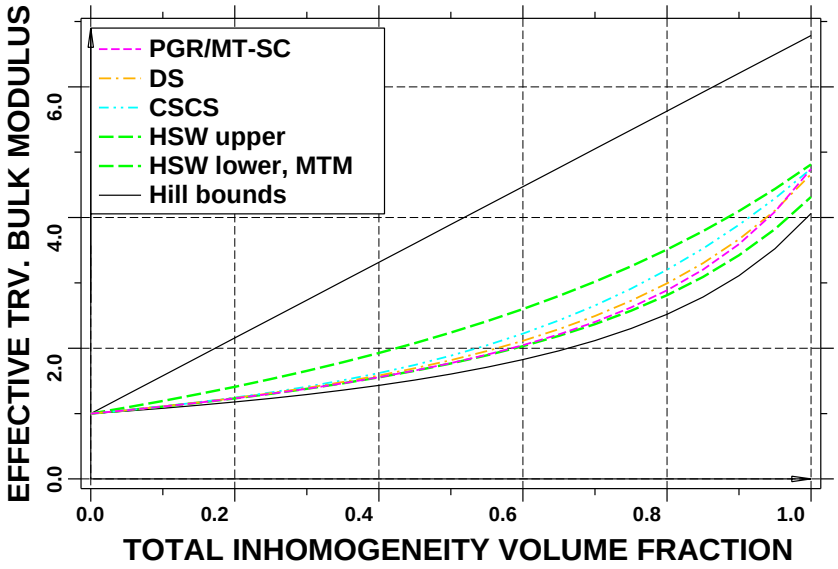

Figure 4.16: Bounds and estimates for the normalized effective transverse bulk modulus of a fictitious three-phase composite reinforced by aligned short fibers of aspect ratios $a^{(i1)} = a^{(i2)} = 5$, evaluated as functions of the total fiber volume fraction $\xi^{I} = \xi^{(i1)} + \xi^{(i2)}$, where $\xi^{(i1)} = \xi^{(i2)}$. The material properties of matrix and fibers follow Table 4.4.

The final example, Fig. 4.17, targets the transverse Young's moduli of composites consisting of unidirectional, continuous glass fibers embedded in an epoxy matrix with 5% of porosity, i.e., $\xi^{(m)} = 19\,\xi^{(i2)}$, where the spherical pores form phase $^{(i2)}$. The material properties of matrix and fibers follow Table 4.1 and the same scaling is used as for Fig. 4.5, which pertains to the same fibers embedded in a pore-free matrix, in order to allow direct comparisons.

As in the case of Fig. 4.15 for this composite the Hashin–Shtrikman–Willis bounds cannot be evaluated and the standard Mori–Tanaka approach results in non-symmetrical elasticity tensors, so that a symmetrized Mori–Tanaka scheme (MT/S) must be used; its results differ slightly from those of a Maxwell scheme using the conjecture of Sevostianov and Kachanov (2014) (not shown). Furthermore, the presence of a pore phase of vanishing stiffness implies that lower bounds become trivially zero, so that only the upper Hill bounds are given. No solutions from a Differential Scheme are shown because at $\xi^{(i)} = \xi^{(i1)} = 0$ a porosity of 5% is present in the matrix, so that no suitable starting configuration is available for a DS with proportionally increasing inhomogeneity volume fractions (this

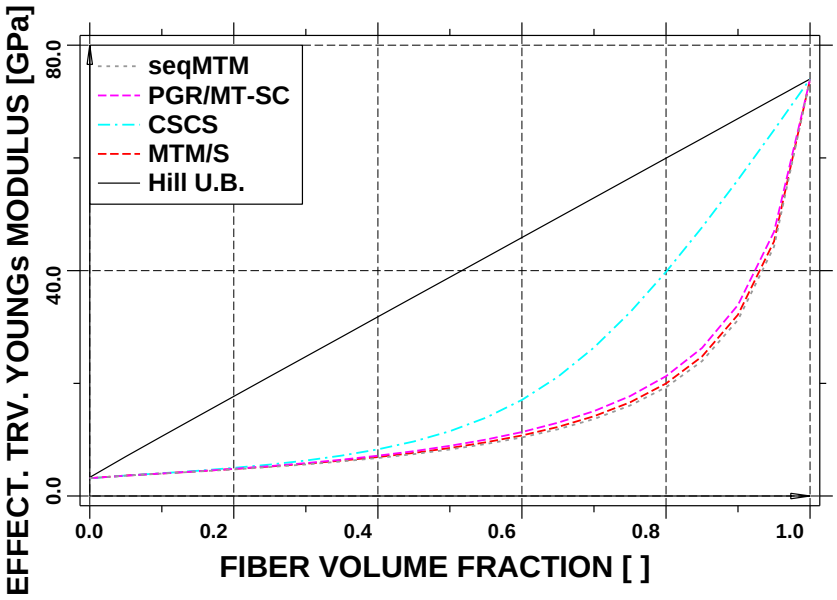

Figure 4.17: Bounds and estimates for the normalized effective transverse Young's modulus of unidirectionally, continuously reinforced glass/epoxy composites, evaluated as functions of the fiber volume fraction $\xi^{(\mathrm{i})} = \xi^{(\mathrm{i}1)}$. The material properties of matrix and fibers follow Table 4.1 and the pore volume fraction is proportional to the matrix volume fraction with $\xi^{(\mathrm{v})} = \xi^{(\mathrm{i}2)} = 0.05\,\xi^{(\mathrm{m})}$.

issue can be resolved, however, by suitably modifying the model). Figure 4.17, however, shows results from a sequential Mori–Tanaka model (seqMTM), compare section 2.8.1, in which the porous matrix is homogenized in a first step and the fibers are embedded in the resulting medium in a second step; this procedure is compatible with the assumption that the voids have a much smaller diameter than the fibers. As in Fig. 4.5 the estimates — with the exception of the classical self-consistent scheme — give rather similar predictions, the influence of the matrix porosity on the overall behavior being rather limited.

Chapter 5

General Remarks on Modeling Approaches Based on Discrete Microstructures

In the following, micromechanical approaches based on discrete microstructures are understood to encompass the periodic homogenization, embedding and windowing methods discussed in Chapters 6 to 8 and sketched in fig. 1.1. Broadly speaking, these "full field models" trade off potential restrictions to the generality of the phase arrangements against the capability of using fine-grained geometrical descriptions and of resolving details of the stress and strain fields at the length scale of the inhomogeneities[49]. The most important applications of such methods are homogenizing the behavior of inhomogeneous materials and evaluating the microscopic stress and strain fields in relevant microgeometries at high resolution. The latter information, on the one hand, is important when the local fields fluctuate strongly and, consequently, much information is lost by volume averaging. On the other hand, it is important for understanding the damage and failure behavior of inhomogeneous materials, which in many cases depends on details of their microgeometry.

The most common work flow in models involving discrete microstructures consists of first obtaining appropriate phase arrangements, see Section 5.1, discretizing the resulting volume elements and preparing them for application of a numerical engineering method, see Sections 5.2 and 5.3, solving for the microfields, and, finally, postprocessing, see Section 5.4.

5.1 Microgeometries and Volume Elements

The heterogeneous volume elements ("microgeometries") used in full field models range from highly idealized periodic geometries ("simple periodic arrays"), such as cubic arrays of spheres in a matrix, to large phase arrangements that aim at closely approximating the geometrical complexity and/or arrangement statistics of actual inhomogeneous materials ("microstructural volume elements"). There are two main strategies for generating heterogeneous volume elements for modeling, viz., using synthetic microstructures, usu-

[49]Such methods by construction aim at resolving inter-particle and intra-particle interactions at the maximum level attainable within continuum mechanics.

ally obtained from computer-based simulations, or employing phase arrangements that are directly based on microgeometries obtained by experimental methods. The following considerations concentrate on microgeometries with matrix–inclusion topology.

Synthetic Phase Arrangements

Synthetically generated volume elements that go beyond simple periodic arrays may be classified into two groups, the first of which makes use of generic arrangements of a number of randomly positioned and, where appropriate, randomly oriented, sized, or shaped reinforcements. The second group aims at constructing phase arrangements that have phase distribution statistics identical to those of the target material. A further possible approach to synthesizing realistic volume elements by computer algorithms, which consists of modeling relevant production processes, has seen little use to date for composites due to the complexity of the task. Synthetic volume elements have found wide use for studying composites with matrix–inclusion and interpenetrating phase arrangements, polycrystals as well as cellular materials and a considerable amount of relevant work has been done in the context of modeling the behavior of concrete-like materials. For a recent review on generating three-dimensional inhomogeneous volume elements see Bargmann et al. (2018).

Synthesizing generic "multi-inhomogeneity" model geometries with random arrangements of reinforcements in many cases has involved random sequential addition methods[50]. The reinforcement volume fractions that can be reached by RSA methods tend to be moderate due to jamming ("geometrical frustration"), however, their representativeness for actual phase arrangements generated by mixing processes is open to question (Stroeven et al., 2004), and they may give rise to biased phase arrangements (Pontefisso et al., 2016). Major improvements can be obtained by using RSA geometries as "starting configurations" for random perturbation, "hard core shaking" or "migration models", compare, e.g., Buryachenko et al. (2003) or Schneider (2017). Such algorithms apply small random displacements to each inhomogeneity to obtain improved and, if the size of the volume element is reduced in the process, more tightly packed arrangements of reinforcements. Alternatively, simply periodic arrays or arrangements generated with sophisticated packing algorithms, see, e.g., Maggi et al. (2008), were used as starting configurations, whereas RSA methods were combined with stirring models (Zangenberg and Brøndsted, 2013) or with optimization procedures (Pathan et al., 2017) to reach elevated inhomogeneity volume fractions. RSA based approaches have been used to generate (approximately) statistically homogeneous distributions of particulate or fibrous reinforcements, see, e.g., Gusev (1997), Böhm and Han (2001), Lusti et al. (2002), Duschlbauer et al. (2006) or Rasool and Böhm (2012), as well as idealized clustered microgeometries (Segurado et al.,

[50] In random sequential addition (RSA) algorithms (also known as random sequential insertion or random sequential adsorption models, and sometimes referred to as "static simulations"), positions and, where applicable, orientations for new reinforcements are created by random processes, a candidate inhomogeneity being accepted if it does not "collide" with any of the existing ones and rejected otherwise. In contrast to random packing, in generating microgeometrical models a "collision" often involves the violation of some minimum distance rather than actual touching of (or overlapping with) neighboring inhomogeneities. Whereas collision checking is straightforward with circular or spherical inhomogeneities, algorithms such as the separating axis method (Schneider and Eberly, 2003) may be required for polyhedral shapes.
If periodic phase arrangements are generated, up to 8 periodic copies must be maintained for any inhomogeneity that is intersected by one or more faces of the volume element.

2003), and they can be adapted for obtaining volume elements that follow prescribed fiber orientation distributions, see, e.g., Schneider (2017).

Matrix–inclusion configurations of elevated inhomogeneity volume fraction can also be obtained by "random particle dropping" (Chiaia et al., 1997) or gravitational methods (Khalevitsky and Konovalov, 2019), discrete-element-based models (Ismail et al., 2016), particle expansion methods (Zhang et al., 2019), or molecular-dynamics-like algorithms (Lubachevsky et al., 1991), also known as collective rearrangement models, see, e.g., Ghossein and Lévesque (2013), as well as Discrete Element-based models, compare Majewski et al. (2017). Furthermore, arrangements of particles may be generated via hydrodynamic interactions in a pseudo-fluid (Elliott and Windle, 2000). For a discussion of methods for generating geometrically complex volume elements containing fibrous inhomogeneities that are compliant in bending, see, e.g., Altendorf and Jeulin (2011).

Additional approaches to generating multi-inhomogeneity synthetic volume elements with matrix–inclusion topology have been based on "eroding" (or shrinking) the individual cells of suitable Voronoi tesselations (Fritzen and Böhlke, 2011) of the whole volume or on first filling the unit cell with tetrahedra which are then assigned to the required phases by a suitable algorithm (Galli et al., 2008), randomness being introduced via the underlying tesselation in both cases. Both methods result in arrangements of randomly positioned and oriented inhomogeneities of irregular polygonal or polyhedral shape, the first mentioned one being applicable to a wide range of inhomogeneity volume fractions.

The most important alternative strategy for generating volume elements by simulation aims at obtaining "statistically reconstructed" phase arrangements, which are not identical to any given sample, but rather are statistically equivalent to the material to be modeled; the resulting phase arrangements have been called "statistically equivalent virtual microstructures". Statistical reconstruction typically gives rise to optimization problems in which some starting configuration (e.g., a periodic phase arrangement of appropriate volume fraction) is modified such that suitable statistical and/or stereological descriptors of the phase distributions approach the chosen target descriptor(s) as closely as possible. Procedures for reconstructing matrix–inclusion and more general microgeometries have been reported that employ simulated annealing procedures (Rintoul and Torquato, 1997; Torquato, 1998b; Bochenek and Pyrz, 2004), genetic algorithms (Zeman and Šejnoha, 2001), and other minimization methods (Roberts and Garboczi, 1999). For in-depth discussions of the underlying issues, such as statistical descriptors for the phase arrangements of inhomogeneous materials, see, e.g., Torquato (2002) or Zeman (2003); questions of the uniqueness of reconstructed two-phase microgeometries were discussed by Jiao et al. (2007). Alternative approaches to statistical reconstruction were reported, e.g., by Vaughan and McCarthy (2010) or de Francqueville et al. (2019). Most studies on statistical reconstruction have been based on a number of statistical descriptors of phase arrangements, among them n-point, nearest neighbor and radial distribution functions as well as correlation functions, i.e., they follow the concept of geometrical RVEs discussed in Section 1.3. Reconstructed microstructures considering both statistical geometrical descriptors and model responses (and thus combine both flavors of RVEs) have been termed "statistically equivalent representative volume elements" (SERVE); for in-depth discussions see the overview of Ghosh et al. (2023).

Microstructures generated by statistical reconstruction are especially attractive because the phase arrangements in at least some actual composites were found to be not completely spatially random (Trias, 2005). For volume elements that contain considerable numbers of inhomogeneities or other microstructural features, statistically reconstructed phase arrangements are more specific to a given target material than are generic random microgeometries. Because at present computational requirements limit the sizes of volume elements that can be handled routinely by numerical engineering methods, this advantage has been of limited practical impact in the context of continuum micromechanics. This issue can be addressed by the concept of "statistically similar volume elements", in which volume elements of smaller size than RVEs are optimized to approach statistical descriptors of the target material as closely as possible, see, e.g., Balzani et al. (2010) and Scheunemann et al. (2015). A recent development is the generation of volume elements via Neural Networks trained on actual microstructures, see, e.g., Henkes and Wessels (2022).

Synthetically generated matrix–inhomogeneity microgeometries have tended to employ idealized reinforcement shapes, equiaxed particles embedded in a matrix, for example, being often represented by spheres, and fibers by cylinders or prolate spheroids[51] of appropriate aspect ratio. However, recent work has also targeted polyhedral inhomogeneities, see, e.g., Nogales and Böhm (2008), Rasool and Böhm (2012), Zhang et al. (2014), Sheng et al. (2016) or Böhm and Rasool (2016), as well as reinforcements of other, non-ellipsoidal shapes, see, e.g., Peng et al. (2020) or Majewski et al. (2022).

Real Structure Phase Arrangements

Instead of generating phase arrangements by computer algorithms, volume elements may be chosen to follow as closely as possible the actual microgeometry in some appropriate subvolume of the material to be modeled, obtained from metallographic sections (Fischmeister and Karlsson, 1977), serial sections (Terada and Kikuchi, 1996; Li et al., 1999), tomographic data (Hollister et al., 1994; Kenesei et al., 2004; Chawla and Chawla, 2006; Buffière et al., 2008), etc. The resulting volume elements are often called "real microstructure" models.

The generation of real-structure models from pixel (digital images) or voxel (tomographic) data describing the geometries of inhomogeneous materials has been the focus of considerable research efforts. Such work involves the steps of selecting from experimental data sets appropriate volume elements for analysis ("registration") and of identifying the regions occupied by the different constituents by thresholding of the grey values of the pixels or voxels ("segmentation"). At this stage pixel or voxel models (compare Section 5.3) can be generated directly from the segmented data set or contouring procedures may be used for obtaining "smooth" phase domains, the latter operation typically being more man-

[51] For uniform boundary conditions it can be shown that the overall elastic behavior of matrix–inclusion type composites can be bounded by approximating the actual shape of particles by inner and outer envelopes of "smooth" shape, e.g., inscribed and circumscribed ellipsoids. This is known as the Hill modification theorem (Hill's comparison theorem, auxiliary theorem or strengthening theorem), compare Hill (1963) and Huet et al. (1990). Approximations of actual inhomogeneity shapes by ellipsoids typically work considerably better for convex than for non-convex particle shapes (Kachanov and Sevostianov, 2005).

power intensive[52]. Alternatively, irregular particle shapes in real-structure arrangements have been approximated by ellipsoids of appropriate size, shape and orientation, compare Li et al. (1999). Computed tomography has proven especially useful for determining the microgeometries of inhomogeneous materials with constituents that differ considerably in X-ray absorption, e.g., porous and cellular materials.

Real microstructure models provide accurate descriptions of actual phase arrangements, which, however, may depend to a considerable extent on details of the underlying experiments, e.g., the resolution of the digital images, as well as of the registration, segmentation and, where applicable, smoothing procedures. In general, the resulting volume elements obviously are non-periodic, which restricts their use with the periodic homogenization techniques discussed in Chapter 6, but makes them well suited to windowing and embedding approaches, compare Chapters 7 and 8. For a discussion of three-dimensional sampling of general microstructures and the categorization of a variety of types of resulting volume elements see Echlin et al. (2014).

Sizes of Volume Elements

When small volume elements are used in full field simulations, the predicted macroscopic responses tend to show a marked dependence on the size of the volume elements, see, e.g., Iorga et al. (2008). Such behavior may be due, on the one hand, to the boundary conditions used (e.g., in the case of multi-inhomogeneity, simple periodic arrays using non-periodicity BCs) or, on the other hand, to the "insufficient geometrical information" contained in the volume elements. The latter issue immediately raises the question of the size of volume element required for adequately capturing the macroscopic physical behavior of the material to be studied[53] and thus for evaluating effective rather than apparent responses. On the one hand, considerations of computational cost obviously put a premium on using the smallest viable volume element but, on the other hand, suitably resolving microgeometry effects militates for using microgeometries that are or approach representative volume elements (compare Section 1.3). These conflicting demands led to the concepts of "minimum RVEs" by Ren and Zheng (2004), of "statistical RVEs" by Trias et al. (2006), of P-SERVEs by Swaminathan et al. (2006) and of statistical volume elements (SVEs) by Ostoja-Starzewski (2006), which are less stringent than that of "proper RVEs".

When the philosophy of geometrical RVEs is followed, estimates for suitable sizes of volume elements can be obtained on the basis of descriptors of the microgeometry alone, the physical property to be modeled playing no role. In such a context the adequacy of the size of a volume element may be assessed, e.g., on the basis of experimentally obtained correlation lengths (Bulsara et al., 1999) or covariances (Jeulin, 2001) of the phase arrangement or by posing requirements such as having at least two statistically independent inhomogeneities in the volume element (Zeman and Šejnoha, 2001). Such approaches can

[52]For a review of work directed at automatically generating high quality structured meshes from voxel data sets, see, e.g., Young et al. (2008).

[53]Traditionally, RVEs have been defined in terms of macroscopic responses. Assessing higher statistical moments of phase-level microstresses in addition to the first one (which underlies modulus-based considerations) appears feasible but may lead to a further tightening of requirements on RVEs. However, no pertinent, systematic studies seem to be available.

be extended to anisotropic microgeometries (Wang et al., 2019) and they have proven successful for micromechanical models of the elastic behavior of inhomogeneous materials.

The concept of physical RVEs as stated in Section 1.3, in contrast, implies that the suitability of a given size of volume element for micromechanical modeling depends on the physical property to be studied. Assessing the representativeness of a volume element in this sense can, in principle, be carried out by windowing analysis, compare Chapter 7, with identical predictions of the macroscopic behavior under macroscopically homogeneous stress and strain boundary conditions, respectively, being indicative of physical RVEs in the strict sense. In practice, this criterion has proved difficult to fulfill in a rigorous way, and, consequently, the suitability of volume elements for a given task is typically assessed by specifying suitable thresholds or by checking other criteria for representativeness. The most important pertinent approach is based on studying the convergence of estimates for the macroscopic behavior with growing size of the volume elements, compare, e.g., Savvas et al. (2016). Furthermore, the compliance of the predicted effective responses with tight bounds (e.g., three-point bounds, see Section 3.2) and/or the appropriate macroscopic material symmetry may be checked for. It must be kept in mind, though, that fulfilling the latter criteria — while going a considerable way towards ensuring useful modeling results — is not sufficient for establishing proper RVEs. For comparisons of different geometry and microfield based criteria for choosing the size of model geometries see, e.g., Trias et al. (2006) and Moussaddy et al. (2013).

Assessments based solely on the geometry or on the overall elastic behavior predict that relatively small volume elements can give fairly accurate results. Zeman (2003) reported that the transversally elastic behavior of composites reinforced by continuous fibers can be satisfactorily described by unit cells containing reconstructed arrangements of 10 to 20 fibers. "Pragmatic" definitions, in which a given volume element must fulfill some given criterion to a specified accuracy to be accepted as a physical RVE, have been used to a considerable extent. Using a nonlocal Hashin–Shtrikman model Drugan and Willis (1996) found that, for statistically isotropic composites consisting of a matrix reinforced by spherical particles, volume elements with sizes of some two and five particle diameters are sufficient for obtaining errors of less than 5% and less than 1%, respectively, in terms of the macroscopic elastic stiffness. Interestingly, these sizes of volume elements come out as being independent of the particle volume fraction[54], a prediction that is not shared by alternative models for assessing RVE sizes (Pensée and He, 2007; Xu and Chen, 2009). Considerably larger volume elements are required for obtaining a given level of accuracy for aligned ellipsoidal inhomogeneities, where the RVE size depends on the reinforcement volume fraction (Monetto and Drugan, 2009), and different estimates for the RVE size result when modeling elastic and thermal conduction behavior (Kanit et al., 2003).

For cases involving nonlinear or inelastic constituent behavior, a number of numerical studies (Zohdi and Wriggers, 2001; Jiang et al., 2001; Böhm and Han, 2001) have indicated that larger volume elements than in the linear case tend to be required for satisfactorily approximating the overall symmetries and for obtaining good agreement between the responses of different phase arrangements designed to be statistically equivalent. Later stud-

[54]For a given level of uncertainty, this corresponds to the number of identical inhomogeneities within the volume element scaling with their volume fraction, ξ.

ies (Cugnoni and Galli, 2010; Galli et al., 2012; Zhang et al., 2014) have confirmed the need for relatively large volume elements in order to approach representativeness in elastoplastic composites, especially at elevated strains. They report a clear dependence of the RVE size on the inhomogeneity volume fraction and on the macroscopic strain for particle-reinforced ductile matrix composites. The main reason for this behavior lies in the marked inhomogeneity of the microscopic strain fields that is typically present in nonlinear composites. For example, there tend to be contiguous zones of concentrated plastic strain, which evolve to become considerably larger than individual reinforcements, thus effectively introducing a new length scale into the problem[55]. In the case of path dependent material behaviors assessments of the suitability of a given volume element, strictly speaking, pertain only to the load paths actually considered. Eliminating the dependence of the homogenized response on the size of the volume element can be argued, in fact, to become impossible in the presence of strain localization (Gitman et al., 2007), the statistical homogeneity of the whole sample or component being lost. Large volume elements are also required if material behavior depends strongly on "rare features" of the microgeometry, see, e.g., Przybyla and McDowell (2010), and for configurations that contain markedly non-equiaxed phase regions, e.g., randomly oriented fibers of elevated aspect ratio. Comparisons between equivalent volume element sizes for various macroscopic behaviors of two-dimensional inhomogeneous materials were reported by Ostoja-Starzewski et al. (2007).

Modeling work in most cases has been based on volume elements that are known to be of insufficient size to be proper RVEs, the main reasons for using them being limits in the size of models that can be handled and difficulties in providing suitable RVEs for actual materials. Such "sub-RVE" volume elements, which may be periodic or non-periodic, are best referred to as statistical volume elements (SVEs, Ostoja-Starzewski (2006)), testing volume elements (TVEs, Diebels et al. (2005)) or windows, compare Chapter 7 — simply calling them RVEs is not good practice. When a number of SVEs of comparable volume and pertaining to a given inhomogeneous material are available, they may be viewed as being different realizations of the phase arrangement statistics describing that material. In such cases ensemble averaging over the results obtained from sets of volume elements can be used to obtain improved estimates for the effective material properties, compare, e.g., Kanit et al. (2003) and Stroeven et al. (2004). The number of different volume elements required for a given level of accuracy of the ensemble averages decreases as their size increases (Khisaeva and Ostoja-Starzewski, 2006). As to using a lower number of larger vs. a higher number of smaller volume elements, Harper et al. (2012b) reported that the former option is more efficient[56]. For macroscopically isotropic materials the anisotropic contributions to the ensemble averaged results were reported to be markedly reduced compared

[55]For elastoplastic matrices, weaker strain hardening tends to cause more inhomogeneous microstrains, which leads to a requirement for volume elements with higher numbers of inhomogeneities. Also, in the hardening regime phase arrangements of high reinforcement volume fraction may be associated with smaller RVEs than configurations of lower V.F., the inhomogeneities interfering with the formation of zones of concentrated plastic strain (Cugnoni and Galli, 2010). Extremely large volumes were reported to be necessary when one of the phases shows softening, e.g., due to damage (Zohdi and Wriggers, 2001; Swaminathan and Ghosh, 2006; Gitman, 2006). For elastic polycrystals, the anisotropy and shape of the grains may also influence the required size of volume elements (Ren and Zheng, 2004).

[56]This result is subject to the caveat that in practice volume elements exceeding a certain size, determined by limitations of the available hardware and the spatial resolution of the discretization used, cannot be handled with comparable efficiency as a larger number of smaller ones.

to the predictions of the individual SVEs (El Houdaigui et al., 2007). However, Galli et al. (2012) found that ensemble averaging over non-periodic statistical volume elements in the elastoplastic range may be compromised by boundary layer effects.

For linear properties Kanit et al. (2003) proposed confidence intervals for assessing the quality of the ensemble averaged results obtained from sets of SVEs. In this context an error measure can be defined in terms of the standard deviation $S(Y)$ of some given modulus or tensor element, Y, as

$$\mathrm{err}(Y) = \frac{1.96\, S(Y)}{\sqrt{n_{\mathrm{SVE}}}} \quad , \tag{5.1}$$

where n_{SVE} is the number of statistically equivalent SVEs used in ensemble averaging. A related approach for nonlinear behavior was proposed by Pelissou et al. (2009). A further refinement consists in weighting the contributions of the SVEs according to statistical parameters (Qidwai et al., 2012). The statistical evaluation of very large ensembles of SVEs and the corresponding sizes of RVEs are discussed in Dirrenberger et al. (2014).

The size of the volume element(s) used in modeling affects not only the macroscopic responses, but also the predicted microfields. Accordingly, some authors have explored the question of what size of volume element is required for studying the local fields at some specific location. This may be done by studying series of volume elements of different size that pertain to a given microstructure, see, e.g., Ozturk et al. (2016).

As to the dimensionality of volume elements, for composites reinforced by aligned, continuous fibers two-dimensional VEs can be used for studying many (but not all) load cases in linear and nonlinear regimes, compare Section 6.4. For composites containing particles, platelets and/or short fibers, however, three-dimensional volume elements are in general necessary, see, e.g., Iung and Grange (1995), Böhm and Han (2001) and Weidt and Figiel (2014) as well as Sections 6.5 and 6.6.

The above considerations pertain to synthetic as well as real-structure phase arrangements and to two-phase as well as multi-phase materials. Rather large volume elements may be necessary if one or more of the inhomogeneity phases have low volume fractions or if different inhomogeneity phases differ markedly in their volume fractions.

5.2 Boundary Conditions

As the size of volume elements describing inhomogeneous materials is increased, the resulting predictions for the apparent overall behavior approach that of the bulk behavior more and more closely until representativeness is achieved; from then on further increases in model size do not lead to further changes in the results and the effective behavior is obtained. The rate of convergence towards proper effective behavior depends on the boundary conditions applied to the volume element.

Fulfilling the surface integral version of the Hill–Mandel condition, eqn. (1.7), which can be written in the form[57]

$$\int_\Gamma \big[\mathbf{t}(\mathbf{x}) - \langle\boldsymbol{\sigma}\rangle * \mathbf{n}_\Gamma(\mathbf{x})\big]^{\mathrm{T}} \big[\mathbf{u}(\mathbf{x}) - \langle\boldsymbol{\varepsilon}\rangle * \mathbf{x}\big]\, \mathrm{d}\Gamma = 0 \quad , \tag{5.2}$$

see Hill (1967) and Hazanov (1998), for inhomogeneous volume elements of finite size, can be achieved by four types of boundary conditions, three of which are based on uniform B.C.s (Hazanov and Amieur, 1995; Ostoja-Starzewski, 2006).

First, the traction term in eqn. (5.2) can be made to vanish over the whole boundary by specifying appropriate Neumann ("natural") boundary conditions for the tractions $\mathbf{t}(\mathbf{x})$. These are obtained by prescribing a macroscopically homogeneous stress tensor $\boldsymbol{\sigma}^{\mathrm{a}}$ on all faces of the volume element,

$$\mathbf{t}(\mathbf{x}) = \boldsymbol{\sigma}^{\mathrm{a}} * \mathbf{n}_\Gamma(\mathbf{x}) \qquad \forall \mathbf{x} \in \Gamma \quad , \tag{5.3}$$

leading to statically uniform boundary conditions (SUBC, or uniform Neumann BC, UNBC).

Second, the right hand term in eqn. (5.2) can be enforced to be zero by imposing a given macroscopically homogeneous strain tensor $\boldsymbol{\varepsilon}^{\mathrm{a}}$ on all boundary surfaces,

$$\mathbf{u}(\mathbf{x}) = \boldsymbol{\varepsilon}^{\mathrm{a}} * \mathbf{x} \qquad \forall \mathbf{x} \in \Gamma \quad , \tag{5.4}$$

resulting in kinematically uniform boundary conditions (KUBC, uniform Dirichlet BC, UDBC, or linear displacement BC, LDBC), which, in FE parlance, are a type of essential BC. Because eqns. (5.3) and (5.4) impose homogeneous stress or strain fields on the boundary of the volume element, they are known as macrohomogeneous boundary conditions. Some authors also refer to them as Hashin boundary conditions.

Third, mixed uniform boundary conditions (MUBC) may be specified, in which the scalar product under the integral is made to vanish separately for each face Γ_k that is part of the surface of the volume element,

$$\big[\mathbf{t}(\mathbf{x}) - \langle\boldsymbol{\sigma}\rangle * \mathbf{n}_\Gamma(\mathbf{x})\big]^{\mathrm{T}} \big[\mathbf{u}(\mathbf{x}) - \langle\boldsymbol{\varepsilon}\rangle * \mathbf{x}\big]\, \mathrm{d}\Gamma = 0 \qquad \forall \mathbf{x} \in \Gamma_k \quad . \tag{5.5}$$

This involves appropriate combinations of traction and strain components that are uniform over a given face of the volume element rather than specifying a macroscopically homogeneous field. Mixed uniform boundary conditions that fulfill eqns. (5.2) and (5.5) must be orthogonal in their fluctuating contributions (Hazanov and Amieur, 1995). The symmetry boundary conditions discussed in Section 6.2 are a type of MUBC and specific sets of MUBC useful for window-type microgeometries are presented in Chapter 7.

Finally, the displacement and traction fields may be decomposed into slow and fast contributions in analogy to eqn. (1.2),

$$\mathbf{u}(\mathbf{x}) = \langle\boldsymbol{\varepsilon}\rangle * \mathbf{x} + \mathbf{u}'(\mathbf{x}) \qquad \text{and} \qquad \mathbf{t}(\mathbf{x}) = \langle\boldsymbol{\sigma}\rangle * \mathbf{n}_\Gamma(\mathbf{x}) + \mathbf{t}'(\mathbf{x}) \quad . \tag{5.6}$$

[57] Equation (5.2) essentially states that energy equivalence is achieved when local fluctuations do not contribute to the elastic strain energy density.

Inserting these expressions into the Hill–Mandel criterion, eqn. (5.2), directly leads to the condition

$$\int_{\Gamma} \mathbf{t}'(\mathbf{x})^{\mathrm{T}}\ \mathbf{u}'(\mathbf{x})\ \mathrm{d}\Gamma = 0 \tag{5.7}$$

on the boundary fluctuations of displacements and tractions, which is fulfilled by periodic phase arrangements. By definition, such geometries can be fully described by a single periodic volume element, often called a unit cell, the surface of which must consist of pairs of parallel surface elements, compare Section 6.2. For homologous points on such pairs of faces the stress and strain tensors must be identical, which implies that the displacement fluctuation vectors $\mathbf{u}'(\mathbf{x})$ at the two faces are identical, too, whereas the traction fluctuation vectors $\mathbf{t}'(\mathbf{x})$ have equal absolute values but opposite orientations, compare fig. 5.1. As a consequence, contributions to eqn. (5.7) from each pair of homologous faces cancel out and the Hill condition is fulfilled for the periodic unit cell itself as well as for larger periodic assemblages of unit cells. A more detailed discussion of periodic unit cells and the associated periodicity B.C. is given in Section 6.2. Incidentally, if the shape of a volume element is such that for each surface point there exists an "antipodic" point having the opposite normal vector (as is the case, e.g., for spheres), eqn. (5.7) can be formally enforced in a point-wise way even for non-periodic volume elements (Glüge et al., 2012), giving rise to so-called "antipodic periodicity" boundary conditions. For a further discussion of microscopic boundary conditions see, e.g., Nguyen et al. (2017).

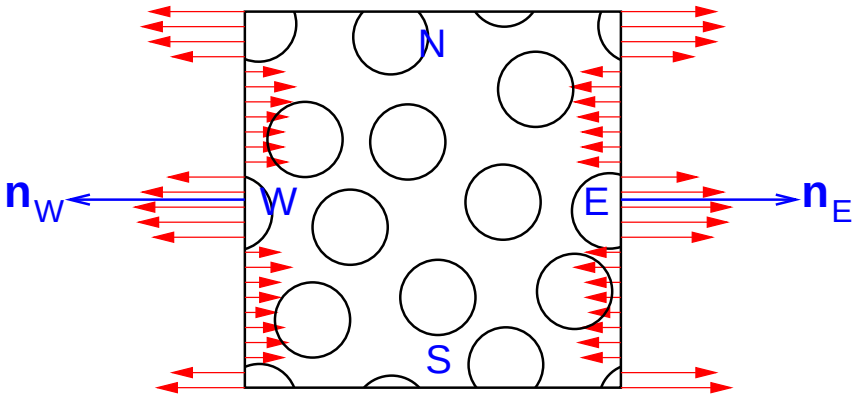

Figure 5.1: Symbolic sketch of antiperiodic traction fluctuations at faces of a periodic VE under macroscopic uniaxial tensile loading.

Macrohomogeneous boundary conditions following eqns. (5.3) and (5.4) can be shown to give rise to lower and upper estimates, respectively, for the overall elastic tensor of a given mesoscopic volume element (Nemat-Nasser and Hori, 1993). Results obtained with mixed uniform and periodicity boundary conditions must lie between the corresponding lower and upper estimates (Hazanov and Huet, 1994) and show a faster convergence towards the effective response with increasing size of volume elements. There is, however, no guarantee that periodic boundary conditions give the best estimates among the above four types of boundary conditions (Terada et al., 2000).

KUBC-based predictions for the elastic macroscopic behavior of fiber-reinforced composites can be improved via an approach developed by Ghosh and Kubair (2016). It

modifies $\mathbf{u}(\mathbf{x})$ in eqn. (5.4) by an additional, position dependent displacement contribution that is evaluated by a modified Eshelby formalism incorporating two-point statistical information on the microstructure outside the volume element.

SUBC and KUBC do not pose restrictions on the phase geometry or on the shape of volume elements, but some MUBC are subject to certain restrictions on the latter count, compare Section 6.2. Periodic homogenization is best suited to volume elements describing periodic phase geometries (which restricts admissible shapes), to which periodicity boundary conditions or, in special cases, symmetry and antisymmetry boundary conditions can be directly applied, see Chapter 6. Antipodic boundary conditions require volume elements of specific shapes, but are not restricted to periodic geometries.

In addition to the above four types of boundary condition, the Hill–Mandel criterion can also be fulfilled by configurations in which the volume element proper is surrounded by a layer of homogeneous material that is given the effective behavior of the core. Elastic tensors obtained by applying macrohomogeneous or periodicity boundary conditions, eqns. (5.3) to (5.7), to the outer surface of the embedding layer can be shown to fall within the upper and lower estimates generated by applying the macrohomogeneous B.C. directly to the volume element, see Temizer et al. (2013). Such configurations form the basis of self-consistent embedding schemes, compare Chapter 8. Furthermore, weak formulations of periodicity and macrohomogeneous boundary conditions have been developed, see, e.g., Mesarovic and Padbidri (2005) or Larsson et al. (2011).

Among the above types of models and boundary conditions only fully implemented periodicity B.C. do not lead to boundary layers in the predicted microscopic stress and strain fields[58], which is a clear advantage since boundary perturbations may lead to spurious behavior when nonlinear constitutive response of the constituents is considered. Periodic homogenization also is unique in that volume elements consisting of multiple copies of a given unit cell give rise to the same prediction as the unit cell itself (unless wave phenomena or buckling are involved).

5.3 Numerical Engineering Methods

The majority of continuum micromechanical studies of discrete microstructures have employed standard numerical engineering methods for resolving the microfields. Work reported in the literature has involved Finite Difference and Finite Volume algorithms, compare Adams and Doner (1967), Bansal and Pindera (2006), Cavalcante et al. (2012) or Chen et al. (2016), spring lattice models, compare Ostoja-Starzewski (2002), the Boundary Element Method (BEM), compare Achenbach and Zhu (1989), Liu et al. (2005b) or Bai et al. (2015), as well as the Finite Element Method (FEM) and its derivatives such as Extended Finite Element Methods, mesh-free, particle and isogeometric methods, compare Sukumar et al. (2001), Dang and Sankar (2007) and Missoum-Benziane et al. (2007), or

[58] Perturbations caused by the application of uniform boundary conditions to inhomogeneous surfaces or by the local incompatibility between homogenized and inhomogeneous regions depend on the local material contrasts and do not necessarily become smaller with increasing volume element size. For a discussion of correcting such effects see Fergoug et al. (2022).

FE-based discrete dislocation models (Cleveringa et al., 1997). In general, spring lattice models tend to show some advantages in handling traction boundary conditions and in modeling the progress of microcracks due to local brittle failure. Boundary element methods typically are at their best in studying geometrically complex linear elastic problems.

In addition to the above methods, techniques using Fast Fourier Transforms (FFT), compare Moulinec and Suquet (1994), and Discrete Fourier Transforms (DFT), compare Müller (1996), have found considerable use in continuum micromechanics, especially in periodic homogenization. Typically, the starting point for such iterative algorithms is a Lippmann–Schwinger equation, compare eqn. (2.36). The convolution integral in this equation is solved in Fourier space (where it reduces to a tensor contraction) and the strains are updated in physical space within each iteration, transforms and back transforms between the two spaces being handled by fast numerical algorithms. Such spectral methods are directly applicable to analyzing periodic volume elements, where they tend to be highly efficient, compare, e.g., Michel et al. (1999) or Ghossein and Lévesque (2012), for both linear and nonlinear phase behavior. Further developments of these approaches have allowed the handling of infinite phase contrasts (Brisard and Dormieux, 2010) and nonlinear problems (Schneider, 2021). Homogenization via FFT at present is a highly active research field and FFT-based schemes are becoming the methods of choice for handling very large, periodic, voxel-type models. DFT methods have found use in studying the evolution of microstructures (Dreyer et al., 1999).

A further approach, the Transformation Field Analysis of Dvorak (1992), allows the prediction of the nonlinear responses of inhomogeneous materials based on either mean-field descriptions (compare the remarks in Section 2.9) or on full field approximations. High computational efficiency is claimed for "classical" TFA models employing piecewise uniform transformation fields (Dvorak et al., 1994), and the extension to FE^2-type models has been reported (Marfia and Sacco, 2018). A development of the TFA, the Nonuniform Transformation Field Analysis (Michel and Suquet, 2004), expands the inelastic strains into a number of non-uniform, incompressible and orthogonal "plastic flow modes" to achieve efficient descriptions of the elastoplastic behavior of inhomogeneous materials.

Furthermore, integral equations describing the displacement, stress and strain fields in inhomogeneous materials may be solved by numerical integration schemes, compare, e.g., Lee et al. (2011a) or Tashkinov (2021). For a number of additional numerical approaches that have been mainly used for periodic homogenization see Section 6.1.

Obviously, when numerical engineering methods are used in continuum micromechanics, the characteristic length of the discretization ("mesh size") must be chosen considerably smaller than the microscale of the considered problem in order to obtain spatially well resolved results.

At present, due to its flexibility in handling complex geometries, the FEM is the most popular numerical scheme for evaluating full field models. In nonlinear regimes its capability of supporting a wide range of constitutive descriptions for the constituents and the

interfaces between them are especially appreciated[59]. A further asset of the FEM in the context of continuum micromechanics is its ability to handle discontinuities in the stress and strain components (which typically occur at interfaces between different constituents) in a natural way via appropriately placed element boundaries. Finally, Finite Element codes are widely available and many of them provide for linear constraint equations for coupling multiple degrees of freedom, which are required for periodic homogenization, compare Section 6.2.

Applications of (more or less) standard Finite Element methods to micromechanical studies may be classed into five main groups, compare fig. 5.2, all of which involve specific trade-offs in terms of complexity of the models, required meshing effort, computational efficiency and aspects of accuracy.

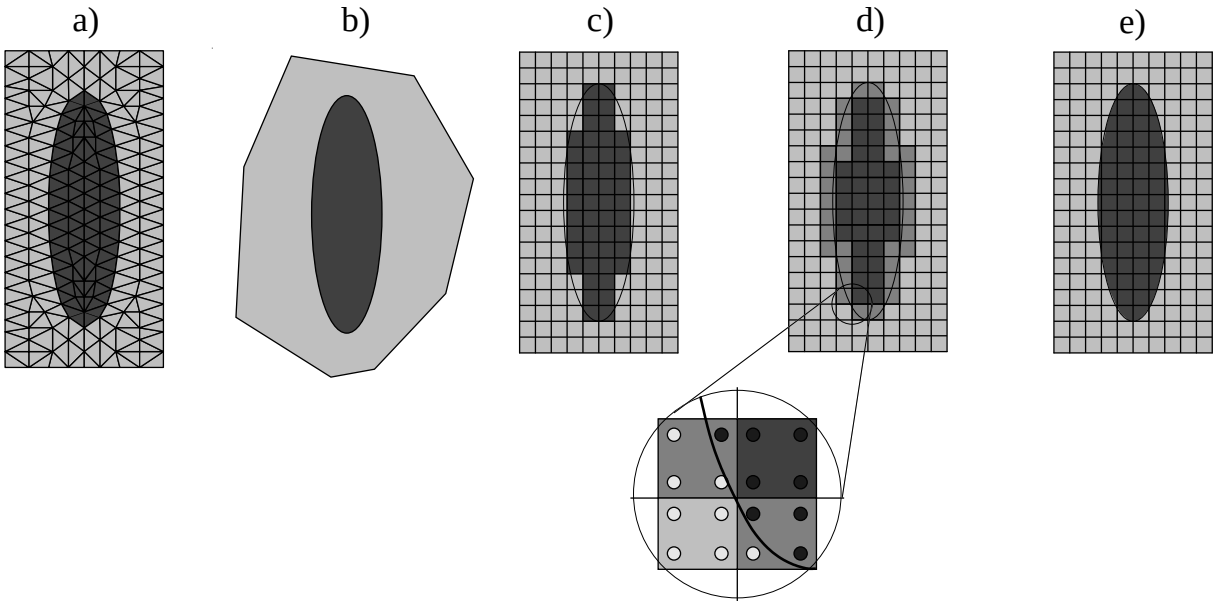

Figure 5.2: Sketch of FEM approaches used in micromechanics: a) discretization by standard elements, b) specialized hybrid elements, c) pixel/voxel discretization, d) "multi-phase elements", e) use of XFEM

In most published work in FE-based micromechanics the phase arrangements are discretized by an often high number of "standard" continuum elements, the mesh being designed in such a way that element boundaries (and, where appropriate, special interface elements) are positioned at all interfaces between constituents. Such "classical meshing approaches" typically use unstructured meshes and have the advantage that in principle any microgeometry can be discretized at the required level of accuracy, making them the most flexible way of using the FEM in continuum micromechanics. The resulting meshes are suitable for analysis with many readily available FE packages. However, the actual modeling of complex phase configurations in many cases requires sophisticated and/or specialized

[59]Constitutive models for constituents used in FEM-based micromechanics have included a wide range of elastoplastic, viscoelastic, viscoelastoplastic and continuum damage mechanics descriptions as well as crystal plasticity models, see, e.g., McHugh et al. (1993), and nonlocal models, see, e.g., Bassani et al. (2001). In addition, the FEM has supported a range of modeling options for interfaces between phases.

preprocessors for generating the mesh, a task that may be work intensive and has been found to be difficult to automatize[60], especially in the case of periodic phase arrangements. In addition, the resulting stiffness matrices may show unfavorable conditioning due to sub-optimal element shapes. Classical meshing approaches are capable of highly resolving the microfields at local "hot spots" (e.g., between closely neighboring reinforcements), but the resulting mesh refinements can lead to very large models, indeed. Nevertheless, its built-in capabilities for providing mesh refinement where it is needed and for using standard mesh refinement procedures are major strengths of this discretization strategy.

Alternatively, finite elements that are less restricted in their shapes may be employed for meshing of multi-phase arrangements. On the one hand, the application of the Virtual Element Method, which provides general-purpose elements of general polygonal or polyhedral shapes, to computational micromechanics has been reported (Lo Cascio et al., 2020). On the other hand, special-purpose hybrid finite elements have been developed, which are formulated to model the deformation, stress, and strain fields in inhomogeneous regions consisting of a single inhomogeneity or void together with the surrounding matrix on the basis of some appropriate analytical theory (Accorsi, 1988). The most highly developed approach of the latter type at present is the Voronoi Finite Element Method (Ghosh et al., 1996), in which the mesh for the hybrid elements is obtained from Voronoi tessellations based on the positions of the reinforcements. This way the meshing effort can be kept rather low and large planar multi-inhomogeneity arrangements can be analyzed using a limited number of (albeit rather complex) elements. Numerous phase-level constitutive and damage models have been implemented into the method and extensions to coated inhomogeneities (Zhang and Guo, 2021) as well as to three dimensional problems (Ghosh and Moorthy, 2004) were reported. Such approaches elements are specifically tailored (and limited) to inhomogeneous materials with matrix–inclusion topologies, and good accuracy as well as significant gains in efficiency have been claimed for them.

Especially when the phase arrangements to be studied are based on digital images of actual microgeometries, a third approach to discretizing microgeometries is of interest. It involves using a mesh consisting of regular, rectangular or hexahedral, elements of fixed size having the same resolution as the digital data, each element being assigned to one of the constituents by operations such as thresholding of the grey values of the corresponding pixel or voxel. The use of structured meshes in such "digital image based" (DIB) models has the advantage of allowing an automatic, relatively straightforward model generation from appropriate experimental data (metallographic sections, tomographic scans) and of avoiding ambiguities in smoothing the digital data (which are generally present if "standard", unstructured FE meshes are employed for discretizing pixel- or voxel-based data of this type). However, modeling approaches that directly discretize pixel or voxel geometries obviously lead to ragged phase boundaries, which may give rise to some oscillatory

[60]Most preprocessors for Finite Element analysis are not geared towards discretizing matrix–inclusion topologies with thin matrix bridges between closely neighboring inhomogeneities (finely resolving the microfields in such regions has limited influence on the elastic and small-strain plastic macroscopic responses, but tends to be important in evaluating the microfields and may be critical for modeling damage initiation). Other major sources of practical difficulties are intersections between phase and cell boundaries at very acute or obtuse angles and the generation of the periodic meshes at the surfaces of volume elements required for PMAs.

behavior of the solutions (Niebur et al., 1999), can cause high local stress maxima (Terada et al., 1997), may degrade accuracy, and negate detailed modeling of interfacial effects. Because the resolution of the microgeometry is determined by the chosen voxel size, mesh size control tends to be a difficult issue with DIB models, with global mesh refinement by supersampling tending to be an inefficient approach. Some of these limitations can, however, be addressed by local smoothing algorithms, compare Boyd and Müller (2006). Despite the above concerns, pixel- or voxel-based models have been claimed not to cause unacceptably large errors in the predicted macroscopic behavior even for relatively coarse discretizations, at least in the linear elastic range (Guldberg et al., 1998), where they have found wide use. In nonlinear regimes, however, local stress concentrations at ragged interfaces may give rise to considerable errors which can be attenuated by averaging procedures, compare Fang et al. (2016).

When volume elements with matrix–inclusion topology are studied by voxel-based methods, care may be required to ensure that the "matrix bridges" between closely neighboring inhomogeneities are properly resolved. This issue may also apply to FFT-based micromechanical methods.

A fourth, related approach also uses structured FE meshes, but assigns phase properties at the integration point level of standard elements ("multi-phase elements"), see, e.g., Schmauder et al. (1996) or Quilici and Cailletaud (1999). Essentially, this amounts to trading off the ragged boundaries caused by the voxel mesh against smeared-out (and typically degraded) microfields within any element that contains a phase boundary, standard FE shape functions being of limited suitability for handling stress or strain discontinuities within elements. With respect to the element stiffnesses the latter concern can be countered by overintegrating elements containing phase boundaries, which leads to improved approximations of integrals involving non-smooth displacements by numerical quadrature, see Zohdi and Wriggers (2001). The resulting stress and strain distributions, however, remain smeared-out approximations in elements that contain phase boundaries. Multi-phase element models are, accordingly, also limited in their capabilities for detailed modeling of interfaces. An alternative technique giving rise to a similar pattern of strengths and limitations consists in prescribing suitably modified material properties to all elements containing a phase boundary (Toulemonde et al., 2008). In a recent development, "composite voxel" techniques (Kabel et al., 2017; Mareau and Robert, 2017) have been introduced within the framework of FFT-based homogenization, stiffnesses in both linear and nonlinear regimes being approximated in a consistent way, e.g., via laminate models.

A further computational strategy uses static condensation to remove the degrees of freedom of the interior nodes of the inhomogeneities (or, in the case of coated reinforcements, of inhomogeneities plus interphases) from the stiffness matrix pertaining to a heterogeneous volume (Liu et al., 2005a), whereas standard meshing is applied to the matrix. This may considerably reduce the computational requirements of linear multi-inhomogeneity models.

In addition, there are some FE-based micromechanical methods that do not fall within the groups shown in fig. 5.2. Among them are "embedded element" ("embedded mesh", "embedded reinforcement") or "domain superposition" techniques, which aim at reducing modeling and computational costs by avoiding conformal meshing of individual reinforce-

ments. Such approaches typically use a structured and often relatively coarse mesh of continuum elements ("host mesh") for the matrix. This is combined with truss or beam elements, see, e.g., Harper et al. (2012a), solid elements, compare, e.g., Jiang et al. (2008), or shell elements, see, e.g., Matveeva et al. (2014), that represent the inhomogeneities; the nodal points used in discretizing the reinforcements in general do not coincide with those of the host mesh. The elements describing the reinforcement are superposed over the host mesh, the different parts of the model being tied together, e.g., via appropriate extended FE formulations (Radtke et al., 2011) or by constraint equations [61]. Embedded reinforcement modeling strategies imply the presence of excess volume in the models ("volume redundancy"), giving rise to a tendency towards overestimating the overall stiffness, especially at non-dilute volume fractions, which, however, can be compensated for in many cases, compare Hoffmann (2012). Such approaches can markedly reduce the meshing and computational effort in FE-based micromechanical analysis, allowing very complex fiber–matrix configurations to be handled[62]. The resolution in terms of local displacement, strain and stress fields is closely tied to the pertinent capabilities of the host mesh, tending to limit the local accuracy achievable with such models; this can be counteracted by enriching the shape functions of appropriate matrix elements and/or by adaptive mesh refinement, compare Goudarzi and Simone (2019). A different FE-based approach to studying composites reinforced by long fibers that are neither straight nor aligned can be based on modeling the latter by "strings" of volume elements and filling the matrix space in-between by a suitable volume mesh (Fliegener et al., 2014). Again, local resolution of the microfields is traded off against the capability of handling complex fiber reinforcement geometries.

The idea of reducing the considerable effort implied in classical meshing approaches has also led to applying a number additional of Finite Element modeling techniques to continuum micromechanics that make use of structured "base meshes" which are suitably modified for handling inhomogeneous phase arrangements[63]. Strategies of this type have been based on the Extended Finite Element method (XFEM) or the Generalized Finite Element Method (GFEM), phase boundaries that pass through individual elements being handled via appropriately enriched, non-smooth shape functions, see, e.g., Moës et al. (2003), Legrain et al. (2011), Soghrati et al. (2012) and Dunant et al. (2013). The resulting models can closely follow the shapes of phase boundaries, compare the sketch in fig. 5.2e, and are subject to few restrictions in terms of microgeometries that can be handled. Alternatively, automated mesh refinement techniques may be applied to regular, voxel-type, base meshes (Fangye et al., 2020).

A relatively recent development for studying microgeometries involving large numbers of inhomogeneities (hundreds to thousands) by Finite Element methods involves finite element programs specially geared towards solving micromechanical problems. Such codes may make use, e.g., of matrix-free iterative solvers such as Conjugate Gradient (CG) methods, analytical solutions for the microfields (such as constant strain approximations

[61] Embedded element techniques were originally developed for modeling rebars in reinforced concrete structures.

[62] Reinforcements approximated by rigid, one-dimensional objects are referred to as rigid line inclusions; they show some interesting properties, compare Wang et al. (1985).

[63] It is not clear, however, if or to what extent structured and voxel-type meshes introduce a systematic bias into the orientation of regions of elevated strain in nonlinear regimes at elevated loads.

corresponding to the upper Hill bounds, eqn. (3.1)), being employed as starting solutions to speed up convergence[64]. For micromechanical studies involving such solvers see, e.g., Gusev (1997), Zohdi and Wriggers (2001) or Arbenz et al. (2008). An alternative approach in this context are multi-grid solvers, compare, e.g., Gu et al. (2016). Very fast solvers have opened the possibility of handling very large volume elements as well as inverse problems, e.g., for finding optimal particle shapes for given load cases and damage modes (Zohdi, 2003). Further increases in efficiency can be achieved for very large voxel-based linear DIB models by exploiting the fact that, in the case of linear analysis, all elements pertaining to a given phase have identical element stiffness matrices.

A further, relatively recent numerical approach that is related to FE methods are reduced basis (or reduced order) homogenization schemes, see, e.g., Fritzen and Kunc (2018), which use globally supported trial and weighting functions to obtain much smaller algebraic systems. Appropriately choosing such functions and performing efficient numerical integration on them are important issues for such reduced order methods. The Nonuniform Transformation Analysis mentioned earlier was among the first methods of this type. Another recent strategy for generating computationally less demanding models makes use of soft computing methods such as neural networks (Kim et al., 2021). Like reduced order schemes, such approaches require considerable up-front effort which typically involves "classical" numerically-based models.

Discrete microstructure approaches employing numerical engineering methods are best suited to studying phase arrangements in which the characteristic lengths of the important geometrical features do not differ excessively. If this is not the case, e.g., for randomly oriented inhomogeneities of high aspect ratio, very large volume elements may be required, meshing may become onerous, and the numerical effort for solving the models may become very high, especially for three-dimensional configurations. For methods making use of structured meshes, such as FFT algorithms and FE-based voxel models, the chosen mesh or voxel size intrinsically limits the achievable geometrical resolution. In the case of approaches that employ unstructured meshes and support local mesh refinement, such as standard FE methods in the sense of figure 5.2, practical limits on resolution tend to be imposed by the size and conditioning of the resulting systems of algebraic equations. For example, discrete microstructure models of composites reinforced by polydispersely sized particles the diameters of which differ by more than, say, an order of magnitude tend to become very unwieldy; similar difficulties arise when modeling inhomogeneities with thin coatings. Another issue requiring special precautions is the handling of extremely closely spaced or touching reinforcements numerically-based full field models[65], compare, e.g., Gusev (2016); such geometrical features may be of considerable importance to the damage behavior of composites, see, e.g., (Grufman and Ellyin, 2008).

[64] Essentially, in such a scheme the initial guess gives a reasonable estimate of "long wavelength" contributions to the solution, and the CG iterations take care of "short wavelength" variations.

[65] Strict two-phase configurations may, in fact, constitute a considerable idealization for the regions close to touching ("percolating") or nearly touching inhomogeneities. On the one hand, production processes may give rise to preferential accumulation of pores and impurities at such positions in actual materials. On the other hand, it is not clear to what extent point contact between neighboring inhomogeneities is a physically reasonable model.

Under conditions of macroscopic softening, e.g., due to damage or localization, discretizing methods are liable to producing mesh-dependent results. Such tendencies may be counteracted by appropriate regularization procedures, among them enrichment with higher-order gradients, see e.g., Geers et al. (2001a), nonlocal averaging of the rate of an appropriate internal variable, compare, e.g., Jirásek and Rolshoven (2003), the use of time dependent formulations involving rate effects, see, e.g., Needleman (1987), or local averaging, compare, e.g., Fang et al. (2016).

Special Finite Element formulations (and dedicated software) have been required in many cases for asymptotic homogenization models, compare section 6.3, and for other schemes that concurrently solve the macroscopic and microscopic problems, compare Urbański (1999).

5.4 Evaluation of Results

When linear elastic or thermoelastic inhomogeneous materials are studied, the aim of homogenization in full field approaches consists in evaluating the effective elasticity tensors, $\mathbf{E}^*$, and thermal expansion tensors, $\boldsymbol{\alpha}^*$, or (some of) the pertinent moduli. In homogenization studies involving nonlinear, path-dependent constituent behavior, e.g., elastoplasticity, thermoelastoplasticity, viscoelastoplasticity or damage no solutions of a generality comparable to that of the above tensors exist. Here, typically the evolution of appropriate macroscopic variables is followed along some specified load path, e.g., in the form of effective stress–strain relations. Most of these tasks involve evaluating the macroscopic stresses and/or strains from the responses of a given volume element to some load case. This may be done by approximate volume integration, compare eqns. (5.8), or via the approaches discussed in Section 6.3.

In linear elastic homogenization it is typically preferable to solve for the macroscopic elastic tensors, which automatically provide full information on the macroscopic elastic symmetry of the volume element, rather than reconstructing them from results on individual moduli[66]. For three-dimensional configurations, six linearly independent mechanical load cases must be applied to the volume element for evaluating macroscopic elastic tensors, and a homogeneous temperature change is required for obtaining the macroscopic thermal expansion tensor. The effective elastic tensors of inhomogeneous materials with orthotropic or higher symmetry show similar structures to those of isotropic symmetry, see eqns. (1.12) and (1.13), i.e., in Voigt/Nye notation all tensor elements are zero with the exception of the upper left submatrix and the diagonal of the lower right submatrix. In contrast, volume elements obtained from real structures or generated with stochastics-based models are typically too small to be proper RVEs and, accordingly, give rise to homogenized tensors that show small contributions from lower elastic symmetries, typically making them triclinc (Karimi et al., 2020). In addition, minor perturbations due to roundoff errors may be present. Evidently, volume elements aimed at describing statisti-

[66] Ensemble averaging over a number of SVEs also is arguably best done in terms of the elastic tensors. Furthermore, if load-controlled periodic homogenization is used, elastic tensors can be obtained at moderate cost because solutions for the required linearly independent load vectors can be found cheaply once the system matrix has been factorized.

cally isotropic, transversally isotropic or orthotropic material behavior must be expected to actually return lower macroscopic material symmetries.

Such deviations from an "elastic target symmetry", which tend to decrease with growing size (and number, if ensemble averaging is used) of SVEs used (Harper et al., 2012b), can be mitigated to some extent by finding the elastic tensor of the required symmetry that is closest to the "raw" elastic tensor obtained from homogenization and averaging. Pahr and Böhm (2008) proposed a simplified approach in which this raw elastic tensor obtained from an SVE of the type shown in fig. 6.4 (which aims at describing a statistically isotropic composite) is first projected onto an orthotropic base[67]. Closest isotropic tensors can then be obtained as the isotropic term of a generalized spherical harmonics expansion, using a procedure developed by He and Curnier (1997). Alternatively, expressions resulting from the minimization of an appropriately defined distance between an elasticity tensor of prescribed symmetry and a given anisotropic elasticity tensor, as discussed by Norris (2006), Moakher and Norris (2006) as well as Bucataru and Slawinski (2009), may be used for finding the closest isotropic, cubic or transversally isotropic elasticity tensors[68]. Such procedures have been successfully applied to evaluating effective moduli pertaining to macroscopically isotropic elastic behavior from ensemble averaged sets of SVEs by Rasool and Böhm (2012), giving excellent agreement with the three-point estimates of Torquato (1997, 1998a) for randomly positioned, non-interpenetrating, identical spherical reinforcements. Alternative ways for extracting elasticity tensors of the required macroscopic symmetry consist, on the one hand, of rotational averaging for obtaining isotropic or transversally isotropic effective elastic behavior and, on the other hand, of projection to appropriate tensor bases. For studies involving isotropic averaging in such a context see, e.g., Cook and Young (1985) or Gusev (2016), and for transversally isotropic averaging compare, e.g., Aboudi (1987). Even though such methods can be highly useful in SVE-based homogenization, they are of an inherently ad-hoc character.

In addition to studying the macroscopic responses of volume elements (i.e., homogenization), the behavior of the fluctuating displacements, stresses and strains as well as fields derived from them (and thus localization) are of considerable interest. In micromechanical applications numerical engineering methods directly evaluate the above microscopic fields at considerable spatial resolution. In the case of displacement-based FE methods using isoparametric elements, the microscopic stresses and strains are primarily evaluated at the integration point level of the individual elements, nodal values of these variables being typically obtained by extrapolation and averaging procedures. Some care, however, is necessary in using such data, because the extreme values of microscopic stresses and strains may depend markedly on details of the microgeometry, of the discretization used and, in the case of nodal data, of the evaluation procedure. Furthermore, idiosyncrasies

[67] Actually, in finding the orthotropic elasticity tensor that is closest to a raw elastic tensor the orientations of the former's principal axes should also be considered. In raw elastic tensors obtained by periodic homogenization from reasonably large volume elements typically only relatively small deviations from the target symmetry are present, whereas results from windowing methods, compare Chapter 7, using small volume elements may lead to more pronounced deviations from the expected macroscopic elastic symmetry.

[68] Applying such procedures to transversally isotropic elastic tensors obtained from micromechanical modeling may, however, run into difficulties because the algorithms are not informed about microgeometrical parameters such as the aspect ratios of the inhomogeneities, which may effectively constrain physically admissible anisotropies.

of the numerical methods may come into play, one case being the reduced accuracy of stress and strain fields obtained by displacement-based FE methods at interfaces between constituents and at the models' surfaces compared to the interior of regions occupied by a given phase.

For evaluating volume averages of stress- and strain-like variables from numerical predictions for microscopic fields in a small strain setting, it is typically good practice to use direct volume integration on the basis of eqn. (1.16)[69]. Many FE codes provide the data necessary for approximating volume averaging by approximate numerical quadrature,

$$\langle f \rangle = \frac{1}{\Omega} \int_{\Omega} f(\mathbf{z}) d\Omega \approx \frac{1}{\Omega} \sum_{l=1}^{N_i} f_l \, \Omega_l \qquad . \tag{5.8}$$

Here f_l and Ω_l are the function value and the integration weight (in terms of the volume of the integration point), respectively, associated with the l-th integration point within a given integration volume Ω that contains N_i integration points. By analogy, the standard deviation of function $f(\mathbf{z})$ over volume Ω can be evaluated as[70]

$$S(f) \approx \sqrt{\frac{1}{\Omega} \sum_{l=1}^{N_i} (f_l - \langle f \rangle)^2 \, \Omega_l} \qquad . \tag{5.9}$$

The standard deviations may, however, to be less robust with respect to details of the model than are the phase averages. If the volumes associated with integration points are not available a simplified version of eqn. (5.8),

$$\langle f \rangle \approx \frac{1}{\Omega} \sum_{n=1}^{N_e} f_n \, \Omega_n \qquad , \tag{5.10}$$

may be used, where N_e is the number of pertinent elements, f_n is the averaged or the centroidal value of function $f(\mathbf{z})$ in element n, and Ω_n is the volume of the element. Equation (5.10) typically tends to be less accurate compared to eqn. (5.8).

When phase averages are to be generated of variables that are nonlinear functions of the stress and strain components (e.g., equivalent stresses, equivalent strains, stress triaxialities), only direct volume averaging of these variables may be used, because evaluating nonlinear variables from the averaged components may lead to unacceptable inaccuracies,

[69] It is of practical interest that volume averaged and phase averaged microfields obtained from full field analysis must fulfill all relations given in Section 2.1; this can be conveniently used to check the consistency of a given model by inserting appropriate results into eqns. (2.5). Note, however, that in the finite deformation regime appropriate stress and strain measures must be used for this purpose. Whereas the volume averaged nominal stress can generally be obtained via eqns. (1.3) and (5.8), this does not hold for the Cauchy stress (Hill, 1972; Nemat-Nasser, 1999). In fact, volume averaging of stress and strain tensors in the finite strain regime is not necessarily possible, compare, e.g., Kouznetsova et al. (2002). If eqn. (5.8) or equivalents are to be used for such a purpose, special care as well as knowledge of the stress and strain measures actually used by the FE code are required.

[70] Procedures analogous to eqns. (5.8) and (5.9) may also be used for evaluating other volume integrals, e.g., in computing Weibull-type fracture probabilities for reinforcement particles or fibers (Antretter, 1998; Böhm et al., 2002).

compare Section 2.9. Provided sufficiently fine meshes are employed, eqn. (5.8) typically returns fairly accurate results on phase averages in the small strain regime and useful approximations in other cases. For most types of finite element eqn. (5.10) is less accurate than eqn. (5.8).

Besides generating overall and phase averages, microscopic variables can also be evaluated in terms of averages and standard deviations in individual inhomogeneities, which supports assessing inter- and intra-inhomogeneity fluctuations of the stress and strain fields, compare the fiber level averages and standard deviations of the maximum principal stress displayed in fig. 2.4.

In addition, distribution functions of the microscopic variables, see, e.g., Bornert et al. (1994), Böhm and Rammerstorfer (1995) or Böhm and Han (2001)), can be extracted from full field models for the whole composite, for a given phase or for individual inhomogeneities. Such "stress spectra" can help in visualizing the local loading environments the constitutive models of the phases are subjected to. The predictions for the tail regions of the distributions, however, tend to show at least some dependence on the mesh and discretization used, so that care is typically required in interpreting them.

Chapter 6

Periodic Microfield Approaches

Periodic Microfield Approaches (PMAs) aim at approximating the macroscopic and microscopic behavior of inhomogeneous materials by studying model materials that have periodic microstructures.

6.1 Basic Concepts of Periodic Homogenization

Periodic microfield approaches analyze the behavior of infinite (one, two- or three-dimensional) periodic phase arrangements under the action of far-field mechanical loads or uniform temperature fields[71], for which the Hill–Mandel criterion can be fulfilled as discussed in Section 5.2. The most common approach to studying the stress and strain fields in such periodic configurations is based on describing the microgeometry by a periodically repeating unit cell[72] (RUC), to which the investigations may be limited without loss of information or generality, at least for static analysis[73].

[71] Standard PMAs cannot handle macroscopic gradients in mechanical loads, temperature or composition in any direction in which periodicity of the fields is prescribed. Such gradients or boundaries can be studied, however, in directions where periodicity is not prescribed, a typical case being layer-type models that are non-periodic in one direction and periodic in the other(s), see, e.g., Wittig and Allen (1994), Reiter et al. (1997) and Weissenbek et al. (1997).

[72] In the present report the designation "unit cell" is used for any volume element that can generate a periodic microgeometry. Accordingly, a unit cell may comprise a simple periodic base unit (or part of it), a collective of simple periodic base units, or a phase arrangement of arbitrary geometrical complexity (multi-fiber or multi-particle unit cell) that shows translational periodicity; in the limiting case a unit cell may thus be a proper representative volume element. Accordingly, the discussion of volume element sizes in Section 5.1 is fully pertinent to unit cell models.

[73] Periodic phase arrangements are not very well suited to modeling the transient behaviors of structural composite materials. In dynamic settings, RUC act as phononic crystals, i.e., as metamaterials exhibiting phononic band structures and dispersion relations. Studying such behavior, however, is a research field in its own right, compare, e.g., Hussein et al. (2014), in which periodic volume elements play an important role, see, e.g., Suzuki and Yu (1998).

fill

Unit cells are typically limited to describing wavelengths smaller than or equal to their relevant dimension, which is a direct consequence of the boundary conditions required for obtaining periodicity. By analogy, in stability analysis of inhomogeneous materials RUCs can directly resolve only buckling modes of specific wavelengths, so that considerable care is required in using them, compare Vonach (2001) or Pahr and Rammerstorfer (2006). However, bifurcation modes with wavelengths exceeding the size of the unit cell can be handled via periodic linear models by using the Bloch theorem (Gong et al., 2005).

The literature on periodic homogenization of inhomogeneous materials is fairly extensive, and well developed mathematical theories are available on scale transitions in periodic structures and materials, compare Michel et al. (2001). A wide variety of unit cells have been employed in such studies, ranging from geometries that describe simple periodic arrays ("lattices") of inhomogeneities to complex periodic phase arrangements, such as volume elements containing considerable numbers of statistically arranged inhomogeneities. For some simple periodic phase arrangements and for linear material behavior it has proven possible to find analytical solutions based on series expansions making direct use of the periodicity (Sangani and Lu, 1987; Wang et al., 2000; Cohen, 2004; Drago and Pindera, 2008).

Even though most PMA studies in the literature have used standard numerical engineering methods as discussed in Section 5.3, some other numerical schemes have been proposed that are specialized to periodic phase arrangements. One of them, known as the Method of Cells (Aboudi, 1989, 1991), in its basic form discretizes unit cells that correspond to square arrangements of square fibers into four subcells, within each of which displacements are approximated by low-order polynomials. Traction and displacement continuity conditions at the faces of the subcells are imposed in an average sense and analytical and/or semi-analytical approximations to the deformation fields are obtained in the elastic and inelastic ranges. Because they use highly idealized microgeometries, provide only limited information on the microscopic stress and strain fields, and have limited capabilities for handling axial shear, the resulting models pose relatively low computational requirements and can provide constitutive descriptions for analyzing structures made of continuously reinforced composites, see, e.g., Arenburg and Reddy (1991). Developments of the algorithm led to the Generalized Method of Cells (Aboudi, 1996), which is more flexible geometrically and allows finer discretizations of unit cells for fiber and particle-reinforced composites, reinforcement and matrix being essentially split into a number of "subregions" of rectangular or hexahedral shape. For some comparisons with microfields obtained by Finite Element based unit cells see, e.g., Iyer et al. (2000) or Pahr and Arnold (2002). Later, higher order displacement interpolants were brought in to obtain the High-Fidelity Generalized Method of Cells (Aboudi, 2004), which provides an alternative to Finite Element algorithms for "pixel element" micromechanical models (compare Section 5.3). This method was also extended to general quadrilateral cell shapes (Haj-Ali and Aboudi, 2010).

A further group of solution strategies for PMAs reported in the literature (Axelsen and Pyrz, 1995; Fond et al., 2001; Schjødt-Thomsen and Pyrz, 2004) use numerically evaluated equivalent inclusion approaches that account for interacting inhomogeneities as provided, e.g., by the work of Moschovidis and Mura (1975). Alternatively, multipole expansion methods can handle complex periodic matrix–inclusion microgeometries (Sangani and Mo, 1997; Kushch et al., 2008; Kushch, 2013). Furthermore, the elastic fields in periodic inhomogeneous materials can be evaluated numerically via variational methods for determining stress-free strain fields (Wang et al., 2002).

As mentioned in Section 1.5, periodic homogenization cannot be freely used for modeling damage in and failure of inhomogeneous materials, all relevant geometrical features, among them crack patterns, being per definition periodic. Consequently, PMAs cannot describe behavior involving macroscopic localization of damage, failure in periodic models rather being akin to some kind of fragmentation. This, however, does not rule out the use

of PMAs for modeling smeared-out damage in parts of larger models, e.g., within domain-splitting schemes as used by Raghavan and Ghosh (2004).

For developing periodic microfield approaches the strain and stress fields are typically decomposed into constant macroscopic strain and stress contributions ("slow variables"), $\langle\boldsymbol{\varepsilon}\rangle$ and $\langle\boldsymbol{\sigma}\rangle$, plus periodically varying microscopic fluctuations ("fast variables"), $\boldsymbol{\varepsilon}'(\mathbf{z})$ and $\boldsymbol{\sigma}'(\mathbf{z})$, compare Section 5.2. Furthermore, it is convenient to introduce a "microscopic coordinate" $\mathbf{z}$ that is scaled such that it can resolve the local features of the unit cell.

An idealized depiction of periodic microfields is presented in fig. 6.1, which shows the variations of the strains $\varepsilon_s(z) = \langle\varepsilon_s\rangle + \varepsilon'_s(z)$ and of the corresponding displacements $u_s(z) = \langle\varepsilon_s\rangle\, z + u'_s(z)$ along some line z in a hypothetical one-dimensional periodic two-phase material consisting of constituents A and B, the length of the unit cell ("unit of periodicity") being c_z. The volume averaged strain, $\langle\varepsilon_s\rangle$, is linked to the displacement increment per unit cell, Δu_s, by the relations

$$\langle\varepsilon_s\rangle = \Delta u_s / c_z \quad \text{and} \quad u_s(z + c_z) = u_s(z) + \langle\varepsilon_s\rangle\, c_z \qquad . \tag{6.1}$$

The periodicity of the strains and the quasi-periodic, cumulative nature of the displacements are evident.

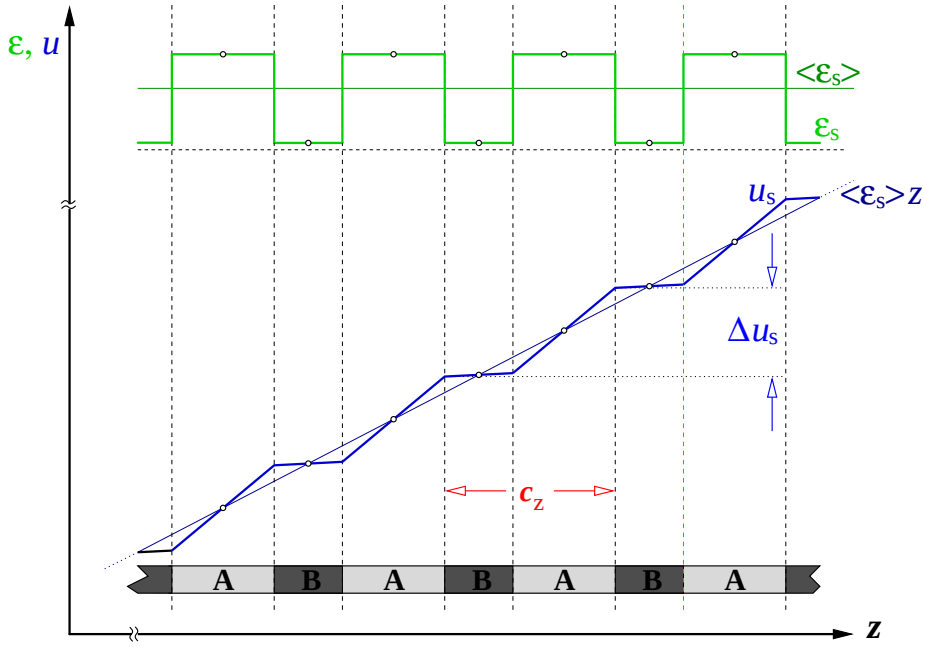

Figure 6.1: Schematic depiction of the variation of the strains $\varepsilon_s(z)$ and the displacements $u_s(z)$ along a generic "one-dimensional periodic composite" of constituents A and B with unit of periodicity c_z. Symmetry points of $\varepsilon_s(z)$ and $u_s(z)$ are indicated by small circles.

6.2 Boundary Conditions

Unit cells together with the boundary conditions (B.C.s) prescribed on them must generate valid tilings of the undeformed geometry as well as for all deformed states pertinent to a

given micromechanical problem. Accordingly, gaps and overlaps between neighboring volume elements as well as unphysical constraints on their deformations must not be allowed, i.e., the cells must be geometrically compatible. In order to achieve this, the boundary conditions for the unit cells must be specified in such a way that all deformation modes appropriate for the load cases to be studied can be attained. The major types of boundary conditions used in periodic microfield analysis are periodicity, symmetry, and antisymmetry B.C.s[74]. In PMA models one of these three types of boundary conditions must be used for any subset of any exterior boundary (unless it is a free boundary) of the volume element, irrespective of the numerical method employed for solving the equilibrium equations.

Generally, for any given periodic phase arrangement unit cells are non-unique, the range of possible shapes being especially wide when point or mirror symmetries are present in the microgeometry (as tends to be the case for regular lattices). As an example, fig. 6.2 depicts a (two-dimensional) periodic hexagonal array of circular inhomogeneities (e.g., fibers oriented normally to the plane) and some of the unit cells that can be used to study aspects of the behavior of this phase arrangement. There are considerable differences in the sizes and capabilities of the unit cells shown.

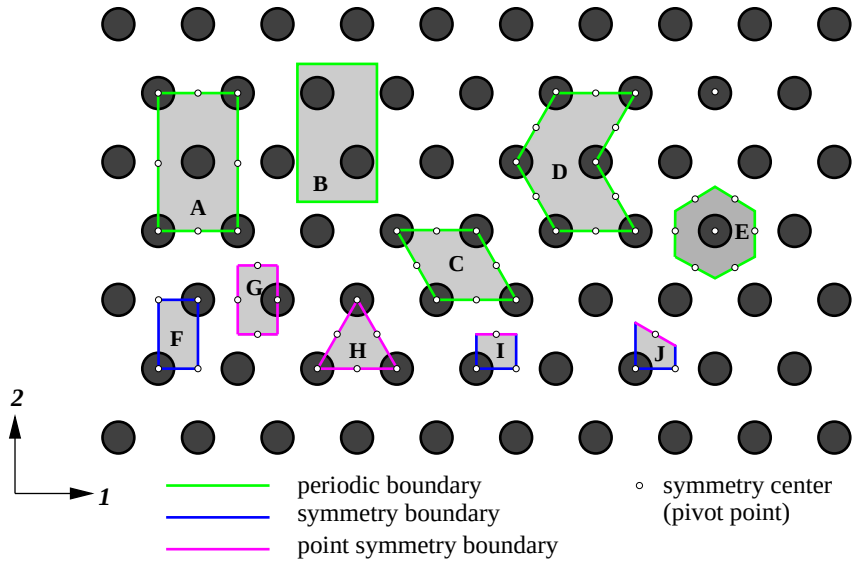

Figure 6.2: Periodic hexagonal array of circular inhomogeneities in a matrix and 10 unit cells or "reduced cells" that can be used to describe the mechanical responses of this arrangement under loads acting parallel to the coordinate axes.

Periodicity Boundary Conditions

The most general boundary conditions for volume elements in periodic homogenization are periodicity (periodic fluctuation, "toroidal", "cyclic") B.C.s, which can handle any physically valid deformation state of the unit cell and, consequently, of the inhomogeneous

[74]For more formal treatments of boundary conditions for unit cells than given here see, e.g., Anthoine (1995) or Michel et al. (1999).

material to be modeled. Periodicity boundary conditions make use of translatoric symmetries of a given geometry; in fig. 6.2 cells A to E belong to this group.

In order to describe an N-dimensional phase arrangement with translatoric periodicity, a suitable unit cell and a set of N linearly independent periodicity vectors $\mathbf{p}_n$ are required. These periodicity vectors are neither unique nor do they have to be orthogonal. For any given periodic microgeometry the minimum volume of pertinent unit cells is well defined, but such "minimum unit cells" can take a wide range of shapes, some examples being shown for a simple two-dimensional case in fig. 6.3. The surface of any unit cell to be used with periodicity boundary conditions must consist of at least N pairs of faces (or pairs of parts of faces) Γ_k, and the surface elements making up a given pair, k^- and k^+, must be identical but shifted relative to each other by "shift vectors" $\mathbf{c}_k$. Each shift vector, in turn, must be a linear combination of the periodicity vectors, i.e., $\mathbf{c}_k = \sum_l m_l^k \mathbf{p}_l$, where the m_l^k are integer numbers. In fig. 6.3 matching pairs of faces (or, in the case of some cells, parts of faces) Γ_k are marked by being drawn in identical color and line style. Obviously, faces of unit cells may be curved, compare, e.g., Garnich and Karami (2004).

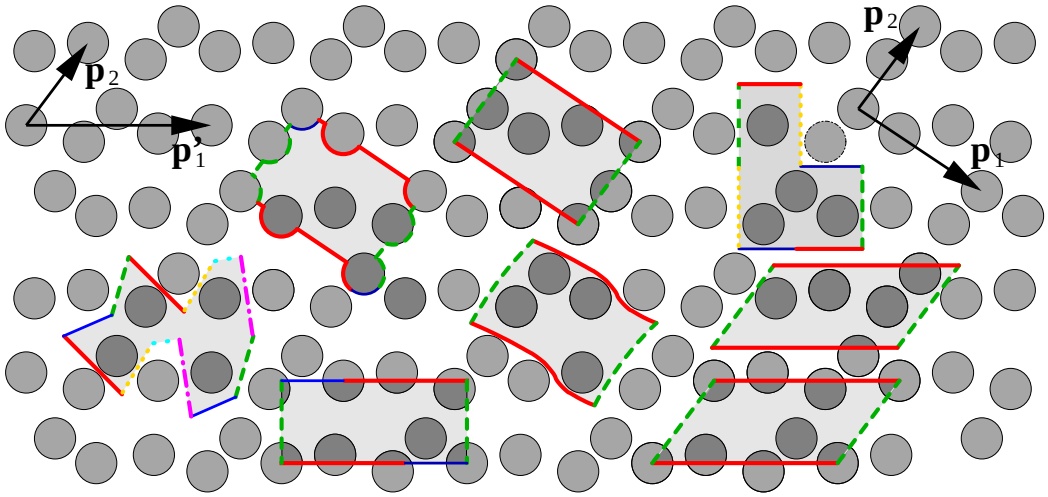

Figure 6.3: Eight different but equivalent periodic minimum-size unit cells for a two-dimensional periodic matrix–inclusion medium with two (slightly) non-orthogonal periodicity vectors $\mathbf{p}_1$ and $\mathbf{p}_2$ ($\mathbf{p}'_1$ and $\mathbf{p}_2$ form an alternative pair of periodicity vectors). Paired faces (or parts of faces) Γ_k are marked by identical line styles as well as colors.

The selection of the shape of unit cells involves trade-offs: On the one hand, unit cells of simple shape facilitate the application of periodicity boundary conditions at least to some extent. On the other hand, low-angle intersections between phase boundaries and cell faces as well as phase boundaries that closely approach cell faces often make such cells difficult to mesh for FE analysis. The latter issue can be alleviated or avoided by choosing suitably shaped and positioned unit cells. The process of defining such cells can be automated, e.g., by using modified Voronoi-type algorithms, which, however, leads to volume elements of irregular shape such as the leftmost unit cell in fig. 6.3. In practice, computer generated periodic volume elements have typically been set up such that the periodicity vectors are orthogonal, which facilitates generating unit cells that are rectangles or right hexahedra and supports straightforward naming schemes of faces, edges, and vertices.

In the following a nomenclature is used in which the faces of two-dimensional quadrilateral unit cells are denoted as N, S, E and W (for North, South, East, and West which are used as in topographical maps), vertices being named according to the adjoining cell faces, compare figs. 6.5 to 6.7. The faces of three-dimensional cells of hexahedral shape are, by analogy, referred to as N, S, E, W, B and T (the latter standing for bottom and top), and edges as well as vertices are referred to via the adjoining faces (e.g., SE or SWB), see fig. 6.4.

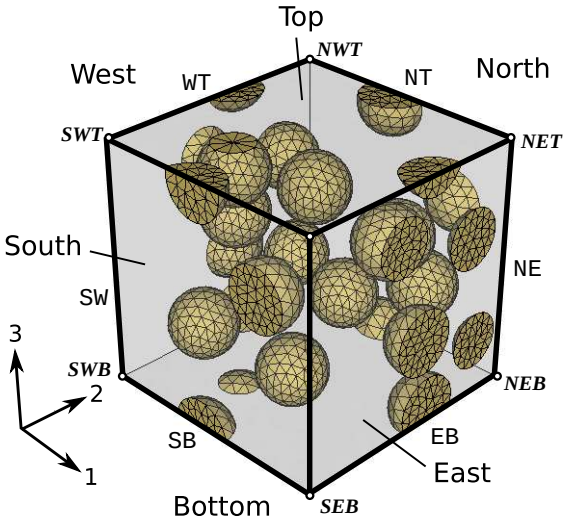

Figure 6.4: Cube-shaped periodic unit cell containing 15 randomly positioned spherical particles of equal size at a volume fraction of $\xi^{(i)}$=0.15. Designators of the six faces (East, West, North, South, Top, Bottom) and of the vertices are given (Pahr and Böhm, 2008).

On the basis of the above discussion of unit cell geometries, eqn. (6.1) can be expanded into the expression

$$\mathbf{u}(\mathbf{z} + \mathbf{c}_k) = \mathbf{u}(\mathbf{z}) + \langle \boldsymbol{\varepsilon} \rangle * \mathbf{c}_k \tag{6.2}$$

for multi-dimensional cases, $\mathbf{c}_k$ being an appropriate shift vector and $\mathbf{z}$ a local coordinate. The unit cells tile the computational space by translation, so that neighboring cells (and, consequently, the "opposite" faces of a given cell) must fit into each other like the pieces of a jigsaw puzzle in both undeformed and deformed states. For each pair of surface elements, Γ_k, eqn. (6.2) allows expressing periodicity boundary conditions for the mechanical problem in the small strain regime as

$$\Delta\mathbf{u}_k = \mathbf{u}_{k^+} - \mathbf{u}_{k^-} = \mathbf{u}(\mathbf{s}_k + \mathbf{c}_k) - \mathbf{u}(\mathbf{s}_k) = \langle \boldsymbol{\varepsilon} \rangle * \mathbf{c}_k \qquad , \tag{6.3}$$

where $\mathbf{u}_{k^-}$ and $\mathbf{u}_{k^+}$ are the displacements at pairs of homologous nodes positioned at $\mathbf{s}_k$ and $\mathbf{s}_k + \mathbf{c}_k$, respectively, on the surface elements Γ_{k^-} and Γ_{k^+} (which may, e.g., correspond to faces N and S in figs. 6.4 and 6.5). The vector linking such pairs of nodes in a deformed state is $\hat{\mathbf{c}}_k = \mathbf{c}_k + \Delta\mathbf{u}_k$. The macroscopic strain $\langle \boldsymbol{\varepsilon} \rangle$ in eqn. (6.3) is prescribed in displacement controlled analysis and is a macroscopic response in load controlled analysis. Equation (6.3) allows expressing the displacement vector $\mathbf{u}_{k^+}$ as

$$\mathbf{u}_{k^+} = \mathbf{u}_{k^-} + \mathbf{u}_{M^+} - \mathbf{u}_{M^-} \qquad , \tag{6.4}$$

where $\mathbf{u}_{M+}$ and $\mathbf{u}_{M-}$ are the displacements of an appropriate pair of homologous "master nodes", which may (but do not have to) be chosen among the vertices of the periodic volume element. These control nodes carry the information on $\hat{\mathbf{c}}_k$. Such constraint conditions enforce a seamless fit between neighboring unit cells for all possible deformed states.

For the special case of initially rectangular two-dimensional unit cells, such as the one shown in fig. 6.5, eqns. (6.4) lead to the expressions

$$\mathbf{u}_{\mathrm{N}}(\tilde{s}_1) = \mathbf{u}_{\mathrm{S}}(\tilde{s}_1) + \mathbf{u}_{\mathrm{NW}} \quad \text{and} \quad \mathbf{u}_{\mathrm{E}}(\tilde{s}_2) = \mathbf{u}_{\mathrm{W}}(\tilde{s}_2) + \mathbf{u}_{\mathrm{SE}} \qquad , \tag{6.5}$$

where the vertex SW ("M^-" in the above scheme) is chosen to be fixed and $\tilde{s}_k$ are local "face coordinates" that are used to identify homologous nodes on pairs of faces. Note that eqns. (6.5) directly imply that

$$\mathbf{u}_{\mathrm{NE}} = \mathbf{u}_{\mathrm{NW}} + \mathbf{u}_{\mathrm{SE}} \qquad .$$

For numerical analysis the two faces making up a homologous pair Γ_k are best discretized in a compatible way, so that the nodal points on them are positioned at identical values of the "face coordinates" $\tilde{s}_k$, ensuring that they are separated by a shift vector $\mathbf{c}_k$. Equations (6.3) then become sets of linear constraints each of which links three nodal displacement DOFs[75]. Comparing eqns. (6.3) and (6.5) shows that the displacements of the "master nodes", SE and NW, contain the information on the macroscopic strain tensor $\langle\boldsymbol{\varepsilon}\rangle$. In addition, the displacements of the master nodes and of faces S and W fully control the displacements of the "slave faces" N and E.

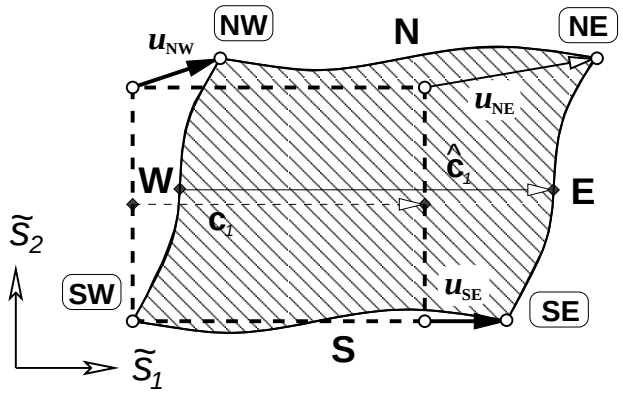

Figure 6.5: Sketch of periodicity boundary conditions as used with an initially rectangular two-dimensional unit cell.

Conditions analogous to eqn. (6.5) can be specified for any periodic, space-filling and regular two-dimensional cell that has an even number of sides (e.g., squares, rectangles, or

[75] In principle, all variables (i.e., for mechanical analysis the displacements, strains and stresses) must be linked by appropriate periodicity conditions (note that, in contrast to stresses, boundary traction vectors are antiperiodic). When a displacement based FE code is used such conditions can be specified explicitly only for the displacement components (including, where appropriate, rotational DOFs), the implied natural traction B.C. giving rise to antiperiodic tractions in such a setting (Li, 2012). Usually, however, the periodicity of nodal tractions is fulfilled only approximately. It is also worth noting that the averaging procedures typically employed for evaluating nodal stresses do not account for a periodicity linkage in typical FE implementations.

hexagons) or three-dimensional cell that has an even number of faces (e.g., cubes, hexahedra, rhombic dodecahedra, or regular tetrakaidecahedra) arranged such that they form homologous pairs. The scheme can also be extended to unit cells of less regular shape provided their faces can be suitably paired off, compare Cruz and Patera (1995), Estrin et al. (1999) or Xia et al. (2003) as well as figs. 6.2 and 6.3. Periodicity B.C.s may be viewed as the least restrictive option for multi-inhomogeneity unit cell models using phase arrangements generated by statistics-based algorithms (see, however, Mesarovic and Padbidri (2005)). Compared to other discrete microstructure approaches, periodic homogenization typically shows the fastest convergence in terms of sizes of volume elements, see, e.g., El Houdaigui et al. (2007). For further discussions of periodicity B.C. see, e.g., Garoz et al. (2019).

For layer-type models, which can be generated by specifying free surfaces at appropriate pairs of boundaries, macroscopic rotational degrees of freedom, i.e., macroscopic bending and twisting, can be studied by appropriately modifying the standard periodicity B.C.s, eqns. (6.2) to (6.5), for the other faces. When such "structure-type" macroscopic rotational degrees of freedom are present, out-of-plane shear loads must be accompanied by appropriate bending moments to achieve stress equilibrium, compare, e.g., Urbański (1999). Models of this type allow using periodic homogenization for evaluating homogenized "laminate stiffnesses" of inhomogeneous plates and shells for use within classical lamination theory (Jones, 1999), for details see, e.g., Pahr and Rammerstorfer (2006).

The above treatment can be carried over into the large strain regime. Periodicity boundary conditions that are conceptual developments of eqn. (6.5) can be devised for cases where standard conditions for homogenization are not met, gradient (nonlocal) theories are employed on the macroscale, and higher-order stresses as well as strain gradients figure in coupling the length scales (Geers et al., 2001b). The resulting deformation patterns of the cells, however, no longer follow geometrical compatibility as discussed above.

In practice FE-based studies of volume elements subjected to periodicity boundary conditions can be somewhat expensive and some effort may be required for providing compatible discretizations on periodic pairs of faces. Accordingly, there has been research interest in relaxing the compatibility requirements, see, e.g., Wippler et al. (2011) and in implementing periodicity B.C. for non-compatible meshes via constraint equations, compare, e.g., Nguyen et al. (2012) or Wang et al. (2017). Such approximations typically give rise to some perturbations of the microfields at the cell boundaries in analogy to the boundary layers shown by windowing and embedding models, compare Section 5.2. For reasonably large volume elements the effects of such perturbations on the predicted homogenized behavior in linear and weakly nonlinear regimes tends to be minor, however. For strongly nonlinear local behaviors, such as phase-level damage, however, spurious local fields due to boundary perturbations may markedly influence the predicted macroscopic responses, even for volume elements that closely approach representativity for linear properties.

Finally, it is worth noting that high-quality discretizations of periodic volume elements can be obtained with reasonable effort by employing preprocessors that support the automatic generation of compatible meshes on homologous periodic faces, such as Netgen (`https://ngsolve.org/`).

Symmetry Boundary Conditions

For rectangular and hexahedral volume elements in which the faces of the unit cell coincide with symmetry planes of the phase arrangement and for which this property is retained for all deformed states that are to be studied, periodicity B.C.s simplify to symmetry (or mirror) boundary conditions over a subset of the periodic volume, called a "reduced cell" in the following. Following the nomenclature of fig. 6.6 these B.C.s take the form

$$u_{\mathrm{E}}(\tilde{s}_2) = u_{\mathrm{SE}} \qquad v_{\mathrm{N}}(\tilde{s}_1) = v_{\mathrm{NW}} \qquad u_{\mathrm{W}}(\tilde{s}_2) = 0 \qquad v_{\mathrm{S}}(\tilde{s}_1) = 0 \qquad , \tag{6.6}$$

where u and v stand for the displacement components in 1- and 2-direction, respectively. Equation (6.6) places constraints on the normal displacement components at the cells' surfaces, but leaves the tangential displacements free, thus enforcing the condition that pairs of opposite faces must stay parallel throughout the deformation history. Accordingly, symmetry boundary conditions do not allow fluctuations of the local fields in directions normal to a given face of a unit cell or reduced cell[76]. Symmetry B.C.s pose no requirements with respect to compatibility of phase arrangements or meshes at different faces, but they may lead to undesirable shapes of inhomogeneities intersected by a cell face when their mirror images are taken into account.

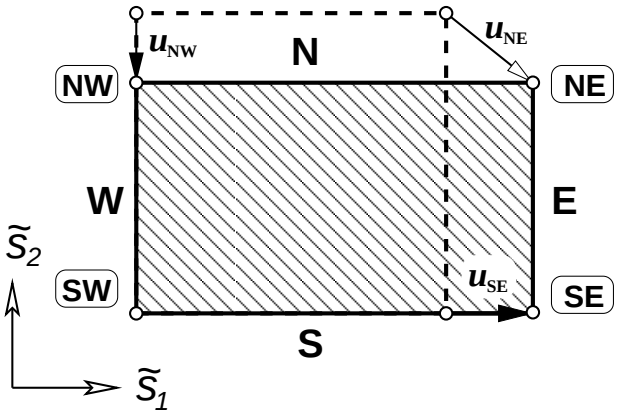

Figure 6.6: Sketch of symmetry boundary conditions as used with a rectangular two-dimensional reduced cell.

Symmetry boundary conditions are fairly easy to use and tend to give rise to small reduced cells for simply periodic phase arrangements. However, the load cases that can be handled are limited to uniform thermal loads, mechanical loads that act in directions normal to one or more pairs of faces, and combinations of the above[77]. In fig. 6.2 cell F uses boundary conditions of this type. Symmetry boundary conditions are typically highly useful for describing relatively simple microgeometries but may impose marked limitations on the geometries of complex phase arrangements.

[76] The stress and strain fluctuations $\boldsymbol{\varepsilon}'(\mathbf{z})$ and $\boldsymbol{\sigma}'(\mathbf{z})$ must obviously be symmetric with respect to symmetry planes, whereas displacements accumulate across symmetry planes, compare fig. 6.1.

[77] Symmetry boundary conditions are compatible with uniaxial stress, uniaxial strain, extensional shear (obtained, e.g., in the two-dimensional case by applying normal stresses σ_{a} to the vertical and $-\sigma_{\mathrm{a}}$ to the horizontal faces), hydrostatic and (hygro)thermal load cases. Accordingly, symmetry B.C.s are often sufficient for materials characterization. However, the normal and shear stresses evaluated as above do not pertain to the same material coordinate system, extensional shear corresponds to pure shear in a coordinate system rotated by 45°.

Antisymmetry Boundary Conditions

Antisymmetry (point symmetry, central reflection) boundary conditions require the presence of centers of point symmetry ("pivot points") and are, accordingly, even more limited in terms of the microgeometries that they can handle. In contrast to symmetry boundary conditions, however, unit cells employing antisymmetry B.C. on all faces are subject to few restrictions in terms of the load cases that can be handled. Among the volume elements shown in fig. 6.2, cells G and H use point symmetry B.C.s on all faces and can handle any in-plane deformation[78]. Alternatively, antisymmetry B.C.s can be combined with symmetry B.C.s to obtain very small reduced cells that are restricted to loads acting normal to the symmetry faces, compare cells I and J in fig. 6.2. Figure 6.7 shows such a reduced cell, the antisymmetry boundary conditions being applied on face E where a pivot point P is present. For this configuration the boundary conditions

$$\begin{aligned} \mathbf{u}_{\mathrm{U}}(\tilde{s}_{\mathrm{P}}) + \mathbf{u}_{\mathrm{L}}(-\tilde{s}_{\mathrm{P}}) &= 2\mathbf{u}_{\mathrm{P}} \\ v_{\mathrm{N}}(\tilde{s}_1) &= v_{\mathrm{NW}} = 2v_{\mathrm{P}} \qquad v_{\mathrm{S}}(\tilde{s}_1) = 0 \qquad u_{\mathrm{W}}(\tilde{s}_2) = 0 \qquad , \end{aligned} \tag{6.7}$$

must be fulfilled, where $\mathbf{u}_{\mathrm{U}}(\tilde{s}_{\mathrm{P}})$ and $\mathbf{u}_{\mathrm{L}}(-\tilde{s}_{\mathrm{P}})$ are the displacement vectors of pairs of homologous nodes U and L that are positioned symmetrically with respect to the pivot point P. As indicated in fig. 6.7 the local coordinate system $\tilde{s}$ is defined on face E and centered

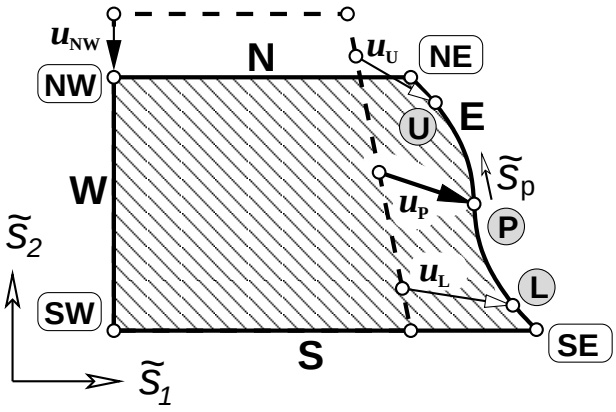

Figure 6.7: Sketch of a quadrilateral two-dimensional reduced cell that combines antisymmetry boundary conditions on face E with symmetry boundary conditions on faces N, S and W.

on P. The undeformed geometry of such a face also must be antisymmetric with respect to the pivot point P, and the phase arrangements as well as the discretizations on both halves of face E must be compatible. Three-dimensional reduced cells employing combinations of symmetry and point symmetry B.C.s can, e.g., be used to advantage for studying cubic arrays of particles, see Weissenbek et al. (1994), or woven composites, compare Li and Zou (2011).

[78] Unit cells and reduced cells using antisymmetry boundary conditions may have odd numbers of faces. Triangular volume elements similar to cell H in fig. 6.2 were used, e.g., by Teply and Dvorak (1988) to study the transverse mechanical behavior of hexagonal arrays of fibers. Rectangular cells with point symmetries on each boundary were introduced by Marketz and Fischer (1994) for perturbed square arrangements of inhomogeneities. The periodic cells D and E also show point symmetry on their faces.

For a reduced cell of the type shown in fig. 6.7, either the displacements of the master nodes SE and NW, $\mathbf{u}_{\mathrm{SE}}$ and $\mathbf{u}_{\mathrm{NW}}$, or the displacements of the pivot P, $\mathbf{u}_{\mathrm{P}}$, can be used for evaluating the macroscopic strain of the corresponding periodic model material, compare eqn. (6.17).

The favorable convergence properties of periodicity B.C., compare Section 5.2, have led to proposals to apply them to non-periodic volume elements, too, see, e.g., Schneider et al. (2017). This strategy, however, may give rise to unrealistic phase geometries in the boundary regions, leading to spurious perturbations in stresses and strains. Nevertheless, it has been argued that, for sufficiently large volume elements valid results on the macroscopic behavior may be obtained[79], see, e.g., Terada et al. (2000). These issues were discussed in depth by Schneider et al. (2022), who, for synthetic phase arrangements, come out in favor of an alternative strategy, viz., properly "periodizing" volume elements. For linear analysis of non-periodic real-structure volume elements, windowing methods using appropriate mixed boundary conditions, compare Chapter 7, are the preferable choice.

Finally, it is worth noting that all of the above boundary conditions, eqns. (6.4), (6.5), (6.6) and (6.7) as well as their three-dimensional equivalents, can be handled by any FE code that provides linear multipoint constraints between degrees of freedom and thus allows the linking of three or more DOFs by linear equations.

6.3 Application of Loads and Evaluation of Fields

Once suitable volume elements have been defined and appropriate boundary conditions applied, the appropriate loads in the form of uniform macroscopic stresses, uniform macroscopic strains and/or homogeneous temperature excursions must be applied to link the microscopic and macroscopic fields. Whereas loading by uniform temperature increments does not pose major difficulties, applying far-field stresses or strains is not necessarily straightforward. For example, the variations of the stresses along the faces of a unit cell in general are not known a priori, so that it is not possible to prescribe the boundary tractions via distributed loads. There are two major approaches to implementing the micro–macro linkage, both of which allow handling arbitrary stress or strain controlled load cases in linear and nonlinear regimes.

Asymptotic Homogenization

The most versatile and elegant strategy for linking the macroscopic and microscopic fields in periodic microfield models is based on a mathematical framework referred to as asymptotic homogenization, asymptotic expansion homogenization, or homogenization theory, see, e.g., Suquet (1987) or Auriault (2002). It is based on explicitly introducing macroscopic and microscopic coordinates, $\mathbf{y}$ and $\mathbf{z}$, respectively, into the formulation of the problem.

[79] In the same vein, non-periodic, rectangular or cube-shaped volume elements may simply be subjected to symmetry B.C. (or may be mirrored with respect to two or three of their faces and then subjected to periodicity B.C). Again, such operations may lead to undesirable reinforcement shapes, changes in the phase arrangement statistics and perturbations of the microfields.

Microscopic and physical coordinates are linked by the expression

$$z_i = x_i/\epsilon \tag{6.8}$$

where $\epsilon = \ell/L \ll 1$ is a scaling parameter. L and ℓ stand for the characteristic lengths of the macro- and microscales[80]. The displacement field in the unit cell can then be represented by an asymptotic expansion of the type

$$u_i(\mathbf{y},\mathbf{z},\epsilon) = u_i^{(0)}(\mathbf{y}) + \epsilon\, u_i^{(1)}(\mathbf{y},\mathbf{z}) + \epsilon^2\, u_i^{(2)}(\mathbf{y},\mathbf{z}) + \text{H.O.T.} \qquad , \tag{6.9}$$

where the $u_i^{(0)}$ are the effective or macroscopic displacements and $u_i^{(1)}$ stands for the periodically varying displacement fluctuations due to the microstructure[81].

Using the chain rule, i.e.,

$$\frac{\partial}{\partial \mathbf{x}} f(\mathbf{y}(\mathbf{x}),\mathbf{z}(\mathbf{x}),\epsilon) \quad \rightarrow \quad \frac{\partial}{\partial \mathbf{y}} f + \frac{1}{\epsilon}\frac{\partial}{\partial \mathbf{z}} f \qquad , \tag{6.10}$$

in the small strain regime the strains can be related to the displacements as

$$\begin{aligned} \varepsilon_{ij}(\mathbf{y},\mathbf{z},\epsilon) &= \frac{1}{2}\left\{\left(\frac{\partial}{\partial y_j}u_i^{(0)} + \frac{\partial}{\partial y_i}u_j^{(0)}\right) + \left(\frac{\partial}{\partial z_j}u_i^{(1)} + \frac{\partial}{\partial z_i}u_j^{(1)}\right)\right\} \\ &+ \frac{\epsilon}{2}\left\{\left(\frac{\partial}{\partial y_j}u_i^{(1)} + \frac{\partial}{\partial y_i}u_j^{(1)}\right) + \left(\frac{\partial}{\partial z_j}u_i^{(2)} + \frac{\partial}{\partial z_i}u_j^{(2)}\right)\right\} + \text{H.O.T.} \\ &= \varepsilon_{ij}^{(1)}(\mathbf{y},\mathbf{z}) + \epsilon\,\varepsilon_{ij}^{(2)}(\mathbf{y},\mathbf{z}) + \text{H.O.T.} \qquad , \end{aligned} \tag{6.11}$$

where terms of the type $\varepsilon_{ij}^{(0)} = \frac{1}{\epsilon}\frac{\partial}{\partial z_j}u_i^{(0)}$ are deleted due to the underlying assumption that the variations of slow variables are negligible at the microscale. By analogy the stresses can be expanded into the expression

$$\sigma_{ij}(\mathbf{y},\mathbf{z},\epsilon) = \sigma_{ij}^{(1)}(\mathbf{y},\mathbf{z}) + \epsilon\,\sigma_{ij}^{(2)}(\mathbf{y},\mathbf{z}) + \text{H.O.T.} \qquad . \tag{6.12}$$

Using the two-scale assumption and, as a consequence, eqn. (6.10), the equilibrium equations take the form

$$\left(\frac{\partial}{\partial y_j} + \frac{1}{\epsilon}\frac{\partial}{\partial z_j}\right)\sigma_{ij}(\mathbf{y},\mathbf{z},\epsilon) + f_i(\mathbf{y}) = 0 \qquad , \tag{6.13}$$

the f_i being macroscopic body forces. By inserting eqn. (6.12) into this expression and sorting the resulting terms by order of ϵ a hierarchical system of partial differential equations is obtained, the first two of which are

$$\begin{aligned} \frac{\partial}{\partial z_j}\sigma_{ij}^{(1)} &= 0 && \text{(order} \quad \epsilon^{-1}\text{)} \\ \frac{\partial}{\partial y_j}\sigma_{ij}^{(1)} + \frac{\partial}{\partial z_j}\sigma_{ij}^{(2)} + f_i &= 0 && \text{(order} \quad \epsilon^{0}\text{)} \qquad . \end{aligned} \tag{6.14}$$

[80] Equation (6.8) may be viewed as "stretching" the microscale so it becomes comparable to the macroscale, $f(\mathbf{x}) \rightarrow f(\mathbf{y},\mathbf{y}/\epsilon) = f(\mathbf{y},\mathbf{z})$.

[81] The nomenclature used in eqns. (6.8) to (6.15) follows typical usage in asymptotic homogenization. It is more general than but can be directly compared to the one used in eqns. (1.2) to (6.7), where no macroscopic coordinates $\mathbf{y}$ are employed.

The first of these equations gives rise to a boundary value problem at the unit cell level that is referred to as the "micro equation". By making a specific ansatz for the strains at the microlevel and by volume averaging over the second equation in the system (6.14), which is known as the "macro equation", for elastic problems the microscopic and macroscopic fields can be linked such that the homogenized elasticity tensor, E^*_{ijkl}, is obtained as

$$E^*_{ijkl} = \frac{1}{\Omega_{\mathrm{UC}}} \int_{\Omega_{\mathrm{UC}}} E_{ijkl}(\mathbf{z}) \left[I_{klmn} + \frac{\partial}{\partial z_l} \chi_{kmn}(\mathbf{z}) \right] \mathrm{d}\Omega \qquad . \tag{6.15}$$

Here Ω_{UC} is the volume of the unit cell, $E_{ijkl}(\mathbf{z})$ is the microscopic elasticity tensor, which depends on the constituent present at position $\mathbf{z}$, I_{ijkl} is the 4th-order unit tensor, and the "characteristic function" $\chi_{kmn}(\mathbf{z})$, a tensor of order 3, describes the deformation modes of the unit cell[82] and, accordingly, relates the micro- and macrofields. Analogous expressions can be derived for the tangent modulus tensors used in inelastic analysis, compare Ghosh et al. (1996).

The above relations can be used as the basis of Finite Element algorithms that solve for the characteristic function $\chi_{ijk}(\mathbf{z})$, a task that in most cases has required special analysis codes. For detailed discussions of asymptotic homogenization methods within the framework of FEM-based micromechanics see, e.g., Hollister et al. (1991), Ghosh et al. (1996), Hassani and Hinton (1999), Chung et al. (2001) or Kanouté et al. (2009). Asymptotic homogenization procedures for elastic composites using commercial FE packages were proposed by a number of authors, among them Banks-Sills and Leiderman (1999), Barroqueiro et al. (2016), Colera and Kim (2019) and Christoff et al. (2020).

Asymptotic homogenization supports the direct coupling of FE models on the macro- and microscales, compare, e.g., Ghosh et al. (1996) or Terada et al. (2003), an approach that has been used in a number of multi-scale studies (compare Chapter 9); concurrent coupling is sometimes referred to as the FE^2 method (Feyel, 2003). A treatment of homogenization in the vicinity of macroscopic boundaries can be found in Schrefler et al. (1997). Asymptotic homogenization schemes are suitably for handling finite strains and they have also been employed for problems combining higher-order stresses and strain gradients with nonlocal behavior on the macroscale (Kouznetsova et al., 2004)[83], an approach referred to as higher order homogenization. For recent reviews of asymptotic homogenization see, e.g., Kalamkarov et al. (2009) and Charalambakis (2010).

An alternative unit-cell based asymptotic homogenization scheme solves for a displacement-like "fluctuation function" rather than for the characteristic function appearing in eqn. (6.15). This Variational Asymptotical Method for Unit Cell Homogenization (VAMUCH) (Yu and Tang, 2007) also is suitable for implementation within a Finite Element framework. Developments of this approach are discussed, e.g., by Tang and Yu (2011).

[82] Note that, even though eqns. (6.14) and (6.15) are derived from an explicit two-scale formulation, neither of them contains the scale parameter ϵ, see the discussion by Chung et al. (2001).

[83] Such methods are especially useful for problems in which the length scales are not well separated; in them the "unit cells" do not necessarily remain periodic during the deformation process.

Method of Macroscopic Degrees of Freedom

When asymptotic homogenization is not used, it is good practice to apply far-field stresses (in the case of load controlled analysis) or strains (in the case of displacement control) to a given unit cell via concentrated nodal forces or prescribed displacements, respectively, at the master nodes and/or pivot points discussed in Section 6.2. This approach was termed the "method of macroscopic degrees of freedom" by Michel et al. (1999).

For load controlled analysis, the nodal forces to be applied to the master nodes can be evaluated from the macroscopic stress $\boldsymbol{\sigma}^{\mathrm{a}}$ via the divergence theorem, see Smit et al. (1998). For the configuration shown in fig. 6.5 the concentrated forces acting on the master nodes SE and NW of a two-dimensional volume element, $\mathbf{f}_{\mathrm{SE}}$ and $\mathbf{f}_{\mathrm{NW}}$, can be shown to be given by the surface integrals

$$\mathbf{f}_{\mathrm{SE}} = \int_{\Gamma_{\mathrm{E}}} \mathbf{t}^{\mathrm{a}}(\mathbf{s})\, \mathrm{d}\Gamma \qquad \text{and} \qquad \mathbf{f}_{\mathrm{NW}} = \int_{\Gamma_{\mathrm{N}}} \mathbf{t}^{\mathrm{a}}(\mathbf{s})\, \mathrm{d}\Gamma \qquad . \tag{6.16}$$

Here $\mathbf{t}^{\mathrm{a}}(\mathbf{s}) = \boldsymbol{\sigma}^{\mathrm{a}} * \mathbf{n}_{\Gamma}(\mathbf{s})$ stands for the surface traction vector corresponding to the homogeneous macroscopic (applied, far-field) stress field[84] at some given point $\mathbf{s}$ on the cell's surface Γ_{UC}, and $\mathbf{n}_{\Gamma}(\mathbf{s})$ is the local normal vector of the appropriate face. Equation (6.16) can be generalized to require that each master node is loaded by a force corresponding to the surface integral of the surface traction vectors over the face slaved to it via an equivalent of eqns. (6.16). Analogous procedures hold for three-dimensional cases, and symmetry as well as antisymmetry boundary conditions as described by eqns. (6.6) and (6.7), respectively, can be handled by eqn. (6.16).

For applying far-field strains to periodic volume elements in displacement controlled analysis, the displacements to be prescribed to the master nodes must be obtained from the macroscopic strains via appropriate strain–displacement relations. For example, using the notation of eqns. (6.5), the displacement vectors to be prescribed to the master nodes NW and SE of the unit cell shown in fig. 6.5 can be evaluated from eqn. (6.3) as

$$\mathbf{u}_{\mathrm{NW}} = \boldsymbol{\varepsilon}^{\mathrm{a}} * \mathbf{c}_{\mathrm{W}} \qquad \text{and} \qquad \mathbf{u}_{\mathrm{SE}} = \boldsymbol{\varepsilon}^{\mathrm{a}} * \mathbf{c}_{\mathrm{S}} \tag{6.17}$$

for an applied strain $\boldsymbol{\varepsilon}^{\mathrm{a}}$ and linear strain–displacement relations[85]. For suitably chosen unit cells, the shift vectors $\mathbf{c}_k$ are equal to the cell's side lengths in the undeformed state and they are, accordingly, referred to as $\mathbf{c}_{\mathrm{W}}$ and $\mathbf{c}_{\mathrm{S}}$ in eqn. (6.17). In many cases displacement controlled unit cell models are somewhat easier to handle than load controlled ones[86].

[84] Note that the $\mathbf{t}^{\mathrm{a}}(\mathbf{s})$ are not identical to the actual local values of the tractions at the cell boundaries, $\mathbf{t}(\mathbf{s})$, which contain contributions due to the local field fluctuations. However, the $\mathbf{t}^{\mathrm{a}}(\mathbf{s})$ are equal to the $\mathbf{t}(\mathbf{s})$ over a given cell face in an integral sense. For geometrically nonlinear analysis eqn. (6.16) must be applied to the current configuration. Because the far-field stress $\boldsymbol{\sigma}^{\mathrm{a}}$ is constant it can be factored out of the surface integrals, so that the force applied to a master node M, $\mathbf{f}_{\mathrm{M}}$, can be expressed as $\mathbf{f}_{\mathrm{M}} = \boldsymbol{\sigma}^{\mathrm{a}} * \int_{\Gamma_{\mathrm{S}}} \mathbf{n}_{\Gamma}(\mathbf{z})\, \mathrm{d}\Gamma$.

[85] Equations (6.17) can be directly extended to three-dimensional configurations. For handling finite strains and geometrical nonlinearities within such a framework see, e.g., Huber et al. (2007) or Barulich et al. (2018).

[86] Even though the loads acting on the master nodes obtained from eqn. (6.16) are equilibrated, in stress controlled analysis solid body rotations may be induced through small numerical errors. Suppressing these solid body rotations by deactivating degrees of freedom beyond the ones required for enforcing periodicity may give rise to incompatibilities between the additional DOFs, the "periodicity DOFs" and the concentrated loads acting on the master nodes.

The overall stress and strain tensors pertaining to volume element, which in many cases are required for describing the macroscopic behavior, can be evaluated by volume averaging or via the equivalent surface integrals given in eqn. (1.4). In a finite strain setting consistent macroscopic strain tensors can be extracted from the volume averages of the deformation gradients. In practice, it is often fairly straightforward to approximate volume integrals by numerical integration schemes such as eqns. (5.8) of (5.10), whereas comparably convenient approximations are not available for surface integrals within an FE framework.

In the case of rectangular or hexahedral unit cells or of reduced cells that are aligned with the coordinate axes, averaged engineering stress and strain components can, of course, be evaluated by simply dividing the applied or reaction forces at the master nodes by the appropriate surface areas and by dividing the displacements of the master nodes by the appropriate cell lengths, respectively. The displacements of and concentrated forces acting on the master nodes can also be used for evaluating the macroscopic stresses and strains from skewed unit cells having non-rectangular periodicity vectors, compare, e.g., Pahr (2003), where, in addition, some additional aspects of unit cells, master nodes, and the method of macroscopic degrees of freedom are discussed. Care is required in applying as well as evaluating macroscopic stresses and strains if the volume elements are not quadrilaterals or hexahedra.

An alternative extracting the effective elastic moduli from the volume averages of the macroscopic stress and strain tensors consists in basing their evaluation on the average of the elastic energy, which can have beneficial effects on the numerical accuracy of the predicted elastic properties (Schneider, 2022).

In order to obtain three-dimensional homogenized elastic tensors with the method of macroscopic degrees of freedom six suitable, linearly independent load cases must be solved for in the most general case.

6.4 Periodic Models for Composites Reinforced by Continuous Fibers

A wide range of periodic models have been reported for the most important groups of continuously reinforced composites, viz., unidirectionally reinforced, angle-ply and cross-ply materials, as well as fabric-reinforced composites.

Composites Reinforced by Unidirectional Continuous Fibers

Composites reinforced by continuous, aligned fibers typically show a statistically transversally isotropic overall behavior and can be studied well with periodic homogenization. Materials characterization with the exception of the overall axial shear behavior can be carried out with two-dimensional unit cell or reduced cell models employing generalized plane strain elements that use a global degree of freedom for describing the axial defor-

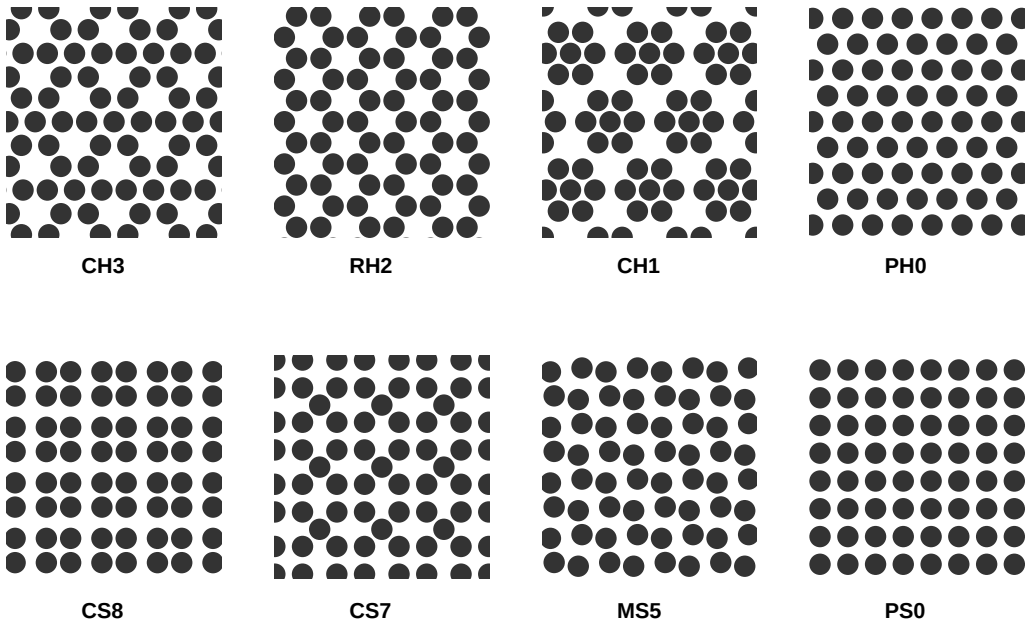

Figure 6.8: Eight simple periodic fiber arrangements of fiber volume fraction ξ=0.475 for modeling continuously fiber-reinforced composites (Böhm and Rammerstorfer, 1995).

mation of the whole model[87]. For handling the overall axial shear response (required, e.g., for establishing macroscopic elasticity tensors) special generalized plane strain elements (Adams and Crane, 1984; Sørensen, 1992) or three-dimensional models with appropriate periodicity boundary conditions, see, e.g., Pettermann and Suresh (2000), are required[88]. Three-dimensional modeling is required for materials characterization of composites reinforced by continuous aligned fibers when the effects of fiber misalignment, of fiber waviness (Garnich and Karami, 2004), of pores in the matrix, or of broken fibers[89] (Mahishi, 1986) or of local damage to matrix or interface are to be studied. Unit cell models used for general nonlinear constitutive modeling of continuously reinforced composites must be fully three-dimensional and employ periodicity boundary conditions.

The most basic generalized plane strain models of continuously reinforced composites make use of simple periodic fiber arrangements as shown in fig. 6.8, all of which can be described by rather small reduced cells using symmetry and/or antisymmetry B.Cs, compare fig. 6.2. The simplest among these phase geometries are the periodic hexagonal (PH0) and periodic square (PS0) arrays, the use of which goes back to the 1960s (Adams and Doner, 1967). Models with hexagonal symmetry (PH0,CH1,RH2,CH3) give rise to transversally

[87]Generalized plane strain elements suitable for such analysis are implemented in a number of commercial FE codes. Because the axial stiffness of composites reinforced by continuous aligned fibers can usually be satisfactorily described by Voigt-type ("rule of mixture") models, PMA studies of such materials have tended to concentrate on the transverse behavior. Note that plane strain models do not properly account for the axial constraints in such materials.

[88]For linear elastic material behavior there is the additional option of describing out-of-plane shear behavior via the formal analogy between antiplane shear and diffusion (e.g., conduction) problems.

[89]For investigating the axial failure behavior of continuously reinforced MMCs, statistical methods concentrating on fiber fragmentation within spring lattice models, see, e.g., Zhou and Curtin (1995), have been used successfully.

isotropic thermoelastic overall behavior[90], compare, e.g., Ptashnyk and Seguin (2016), whereas the other fiber arrangements shown in fig. 6.8 have tetragonal (PS0,CS7,CS8) or monoclinic (MS5) overall symmetry. In the elastoplastic and damage regimes the macroscopic symmetries of the fiber arrangements are degraded for most load cases, compare fig. 6.9, and hexagonal arrangements are not transversally isotropic with respect to ultimate strength. This behavior is due to the low symmetry of the distributions of the plastic strains in the matrix (and, as a consequence, the strain hardening state), which depend on the load history a given point has undergone. In many cases simple periodic microgeometries do not provide satisfactory descriptions of fiber-reinforced materials, most of which show at least some randomness in the fiber positions. Much improved models can be obtained by periodic multi-fiber unit cells that employ quasi-random fiber positions. Such models can either use symmetry B.C.s, compare the cell shown in fig. 6.10, which is based on the work of Nakamura and Suresh (1993), or periodicity B.C.s (Moulinec and Suquet, 1997; Gusev et al., 2000; Zeman and Šejnoha, 2007). With growing computer power multi-fiber unit cells have become a standard tool for periodic homogenization of continuously reinforced composites.

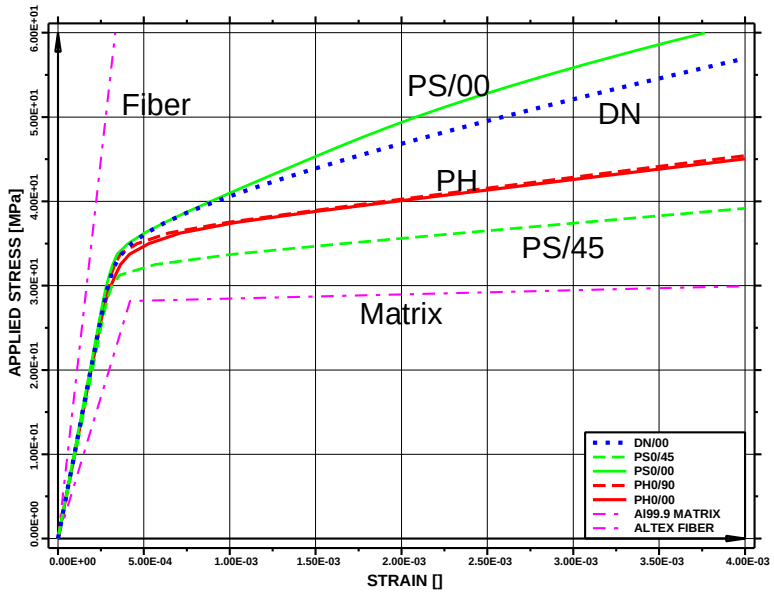

Figure 6.9: Transverse elastoplastic response of a unidirectional continuously reinforced ALTEX/Al MMC (ξ=0.453, elastic material parameters as in table 6.1, matrix with linear hardening, yield stress $\sigma_{\mathrm{y}}^{(\mathrm{m})}$=28.2 MPa and hardening modulus $E_{\mathrm{h}}^{(\mathrm{m})}$ =637.5 MPa) to transverse uniaxial loading as predicted by PMA models PH0, PS0 and DN.

In table 6.1 thermoelastic moduli of an aligned continuously reinforced ALTEX/Al MMC as predicted by bounding methods, MFAs and unit cell methods using arrangements PH0, CH1 and PS0 (compare fig. 6.8) as well as DN (see fig. 6.10) are listed.

[90]Like the macroscopic elastic responses, the phase averages of the local stress and strain fields of hexagonal arrangements of aligned fibers are independent of the orientations of transverse loads. The higher statistical moments and the distributions function of these fields at the phase level, however, may show such a dependence. Consequently, the equivalent stress varies to some extent with the loading direction, which underlies the small differences in initial yielding between the two "PH" curves in fig. 6.9.

Table 6.1: Overall thermoelastic moduli of a unidirectional continuously reinforced ALTEX/Al MMC (ξ=0.453 nominal) as predicted by the Hashin–Shtrikman (HSB) and three-point (3PB) bounds, by the Mori–Tanaka method (MTM), the generalized self-consistent scheme (GSCS), the differential scheme (DS) and Torquato's three-point estimates (3PE), as well as by PMA analysis using periodic arrangements shown in fig. 6.8 (PH0, CH1, PS0) and the multi-fiber cell displayed in fig. 6.10 (DN). For arrangement PS0 responses in the 0° and 45°, and for arrangement DN responses in the 0° and 90° directions are listed.

	E^*_A [GPa]	E^*_T [GPa]	ν^*_A []	ν^*_T []	α^*_A [$K^{-1}\times10^{-6}$]	α^*_T [$K^{-1}\times10^{-6}$]
fibers	180.0	180.0	0.20	0.20	6.0	6.0
matrix	67.2	67.2	0.35	0.35	23.0	23.0
HSB/lo	118.8	103.1	0.276	0.277	11.84	15.77
HSB/hi	119.3	107.1	0.279	0.394	12.47	16.46
3PB/lo	118.8	103.8	0.278	0.326	11.85	16.31
3PB/hi	118.9	104.5	0.279	0.347	11.98	16.45
MTM	118.8	103.1	0.279	0.342	11.84	16.46
GSCS	118.8	103.9	0.279	0.337	11.84	16.46
DS	118.8	103.9	0.278	0.339	11.94	16.35
3PE	118.8	103.9	0.279	0.338	11.89	16.40
PH0	118.8	103.7	0.279	0.340	11.84	16.46
CH1	118.7	103.9	0.279	0.338	11.90	16.42
PS0/00	118.8	107.6	0.279	0.314	11.85	16.45
PS0/45	118.8	99.9	0.279	0.363	11.85	16.45
DN/00	118.8	104.8	0.278	0.334	11.90	16.31
DN/90	118.8	104.6	0.278	0.333	11.90	16.46

For this material combination all PMA results (even for arrangement PS0, which is not transversally isotropic) fall within the Hashin–Shtrikman bounds[91], but the predictions for the square arrangement show clear in-plane anisotropy and do not follow the three-point bounds (which in this case pertain to aligned, identical, non-overlapping cylindrical fibers, compare Section 4.1). The results for the multi-fiber arrangement indicate some minor deviation from transversally isotropic macroscopic behavior.

The fiber arrangements shown in figs. 6.8 and 6.10 give nearly identical results for the overall thermoelastoplastic behavior of continuously reinforced composites under axial mechanical loading, and the predicted overall axial and transverse responses under thermal loading are also very similar. The overall behavior under transverse mechanical loading, however, depends markedly on the phase arrangement, see fig. 6.9. In addition, for fiber arrangements of tetragonal or lower symmetry (e.g., PS0, MS5, CS7 and CS8 in fig. 6.8) the predicted transverse stress-strain responses typically vary strongly with the loading direction in the transverse plane. The behavior of the hexagonal arrangements is sandwiched

[91] The constituents' material properties underlying table 6.1 show a low elastic contrast of $c_{el} \approx 3$, making them relatively insensitive to perturbations of macroscopic symmetry. In general the elastic moduli obtained from square-type arrangements may violate the Hashin–Shtrikman bounds and usually lie outside the three-point bounds.

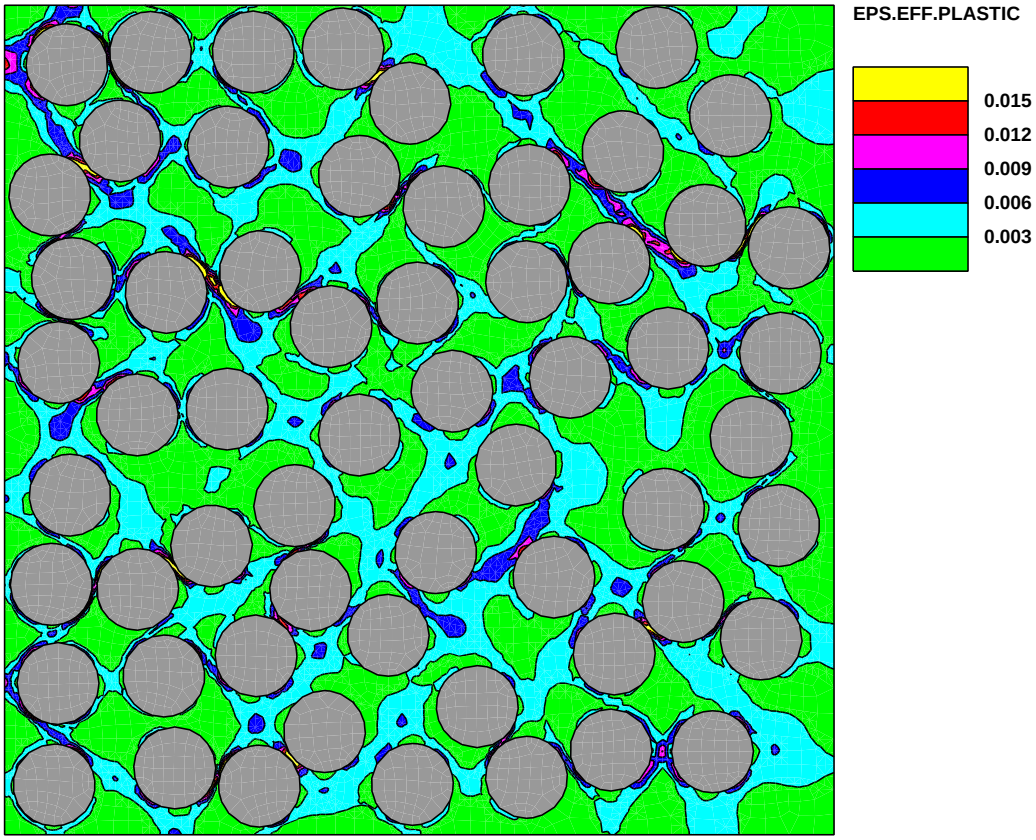

Figure 6.10: Microscopic distributions of the accumulated equivalent plastic strain in the matrix of a transversally loaded unidirectional continuously reinforced ALTEX/Al MMC (ξ=0.453) as predicted by a multi-fiber cell (arrangement DN).

between the stiff (0°) and the compliant (45°) responses of periodic square arrangements in both the elastic and elastoplastic ranges. Multi-fiber cells with statistical fiber positions (such as the one shown in fig. 6.10) tend to show noticeably stronger macroscopic strain hardening compared to periodic hexagonal arrangements of the same fiber volume fraction, compare Moulinec and Suquet (1997), and to approach transversal isotropy. It is worth noting that the macroscopic yield surfaces of uniaxially reinforced MMCs in general are not of the Hill (1948) type, but can be better described by a bimodal description (Dvorak and Bahei-el Din, 1987). Analogous macroscopic behavior has been reported for viscoelastic composites (Li et al., 2015).

The distributions of microstresses and microstrains in fibers and matrix typically depend strongly on the fiber arrangement in the transverse plane, especially under thermal and transverse mechanical loading. In the plastic regime, the microscopic distributions of equivalent and hydrostatic stresses, as expected, show large-scale patterns when simple periodic fiber arrangements are used. Such patterns tend to be absent in predictions obtained with volume elements containing randomly positioned fibers. Distributions of equivalent stresses, plastic strains and stress triaxialities typically are markedly inhomogeneous[92], see, e.g., fig. 6.10. As a consequence of the inhomogeneity of the microfields,

[92]The corresponding distribution functions, phase averages, and higher statistical moments are also significantly influenced by the fiber arrangement, compare Böhm and Rammerstorfer (1995).

there tend to be strong constrained plasticity effects in continuously reinforced MMCs and the onset of damage in the matrix, of fracture of the fibers, and of interfacial decohesion at the fiber–matrix interfaces show a clear dependence on the fiber arrangement.

In general, models based on periodic multi-fiber volume elements are clearly superior to ones making use of simple periodic arrangements of fibers, making the former the preferred option in computational periodic homogenization of continuously reinforced, unidirectional composites.

Cross-Ply and Angle-Ply Composites

Another group of composite materials reinforced by continuous fibers that can be studied to advantage by unit cell methods are laminates consisting of plies the thickness of which is not much greater than the fiber diameter. The left side of fig. 6.11 depicts a unit cell for a cross-ply laminate with double layers of fibers which is suitable for use with periodicity and symmetry boundary conditions. In the the center a minimum reduced cell for cross ply laminates with one fiber layer per ply is shown, which requires the use of symmetry boundary conditions. A unit cell for studying angle-ply laminates with a general ply angle β via periodicity boundary conditions is displayed on the right side of fig. 6.11. Extending models of the above type to multi-fiber cells with randomly arranged fiber positions appears feasible.

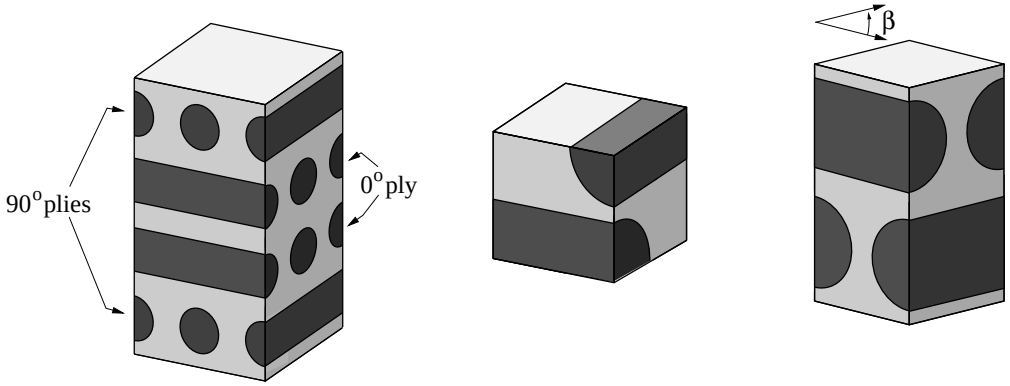

Figure 6.11: Unit cell for a double layer cross-ply laminate (left), minimum reduced cell for a cross ply-laminate (center) and unit cell for an angle-ply laminate with ply angle β (right).

Unit cells with symmetry boundary conditions were used for studying the thermomechanical behavior of cross ply laminates, e.g., by Lerch et al. (1991) as well as Ismar and Schröter (2000), and volume elements with periodicity BC, e.g., by Soni et al. (2014). For unit cell studies of angle ply laminates see, e.g., Xia et al. (2003) and Abolfathi et al. (2008).

Fabric Reinforced Composites

Periodic homogenization has played an important role in modeling the behavior of fabric-reinforced composites, i.e., materials containing woven, braided, or knitted reinforcements, see, e.g., Ivanov and Lomov (2020). In such "textile composites" the reinforcing phase

takes the form of textile-like structures consisting of interlacing bundles of continuous fibers (tows). Unit cell and reduced cell models for such materials are typically based on modeling fiber bundles as a "mesophase" with smeared-out material properties, which, in turn, are obtained from analyzing unidirectionally continuously reinforced composites[93]. Free surface boundary conditions are specified for the out-of-plane faces of the cell, and a number of cells may be stacked on top of each other in order to account for in-plane offsets and constraint effects between the layers (Byström et al., 2000). Symmetry boundary conditions can be specified for the in-plane faces, giving reasonably small unit cells as shown in fig. 6.12, and combinations of periodicity, symmetry and antisymmetry boundary conditions may be used to achieve very small volume elements, see, e.g., (Tang and Whitcomb, 2003). Such models, however, are restricted to handling in-plane normal and thermal loads. By applying extended periodicity boundary conditions to larger unit cells macroscopic rotational degrees of freedom can be introduced to allow studying all deformation modes, including the macroscopic warping and twisting of the laminae.

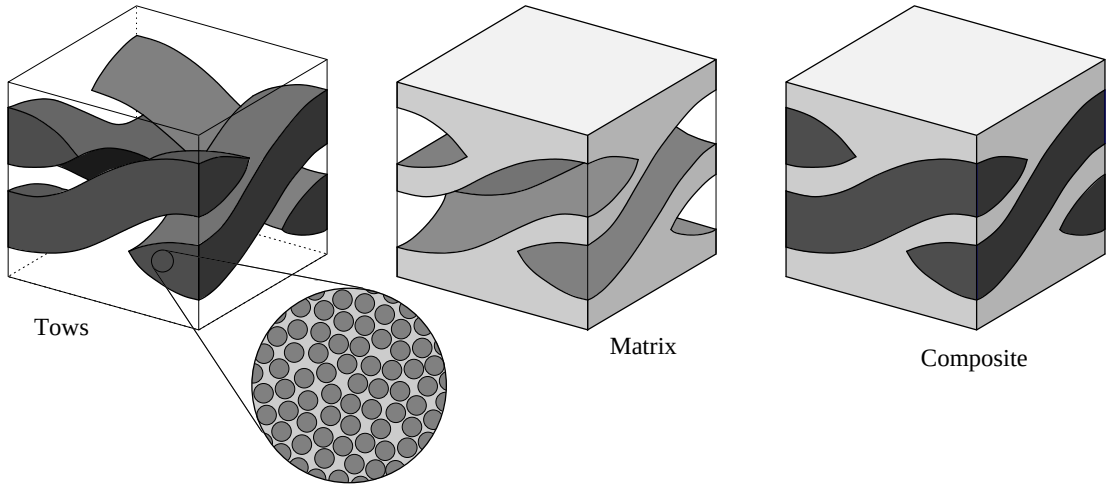

Figure 6.12: Schematic of a reduced cell using symmetry boundary conditions for modeling a plain weave lamina. The tow region (left), the matrix region (center) and the "assembled" unit cell (right) are shown.

There is a wide range of weaves as well as knitting and braiding architectures that can be modeled with PMAs. Unit cells for woven, knitted and braided composites tend to be fairly complex geometrically, may be difficult to mesh for Finite Element analysis and may pose considerable computational requirements, especially when nonlinear behavior is to be studied. Over the past 25 years a considerable number of studies have been published on unit cell modeling of fabric-reinforced composites, see, e.g., Cox and Flanagan (1997), Huang and Ramakrishna (2000), Tang and Whitcomb (2003) or Lomov et al. (2006), and on software for generating appropriate unit cells (Robitaille et al., 2003; Sherburn, 2007). Gager and Pettermann (2012) proposed shell element-based unit cells for textile composites that can significantly reduce the modeling effort.

[93]This modeling strategy obviously is a type of multiscale modeling as discussed in Chapter 9.

6.5 Periodic Models for Composites Reinforced by Short Fibers

The overall symmetry of short-fiber-reinforced composites in many cases is isotropic (for random fiber orientations) or transversally isotropic (for aligned fibers, planar random fibers and other fiber arrangements with axisymmetric orientation distributions). However, processing conditions can give rise to a wide range of fiber orientation distributions and, consequently, lower overall symmetries (Allen and Lee, 1990). The thermoelastic and thermoelastoplastic behavior of aligned short-fiber-reinforced composites has been successfully estimated by Mori–Tanaka methods[94], which can also be extended to nonaligned fibers and reinforcements showing an aspect ratio distribution, compare Section 2.6. Such mean-field approaches are, however, limited in resolving details of fiber arrangements, especially for inelastic material behavior. At present the most powerful tools for studying the influence of fiber shapes and orientations, of clustering effects, of the interaction of fibers of different sizes, and of local stress and strain fields between neighboring fibers are periodic microfield methods. Platelet-reinforced composites can be described by analogy to short-fiber-reinforced materials.

Composites Reinforced by Aligned Short Fibers

In contrast to continuously reinforced composites, the phase arrangements of discontinuously reinforced materials are inherently three-dimensional. The simplest three-dimensional PMA models of aligned short-fiber-reinforced composites have used periodic square arrangements of non-staggered or staggered aligned cylindrical fibers[95], see, e.g., Levy and Papazian (1991) and compare fig. 6.13. Such geometries are relatively simple to set up and do not pose major computational requirements, but are rather restrictive in terms of fiber arrangements and load conditions that can be handled. By using larger volume elements supporting periodicity boundary conditions the full thermomechanical behavior of the fiber arrangements can be studied. Analogous microgeometries based on periodic hexagonal arrangements of non-staggered (Järvstråt, 1992) or staggered (Tucker and Liang, 1999) fibers as well as ellipsoidal cells aimed at describing composite "ellipsoid assembly" microgeometries (Järvstråt, 1993) were also proposed.

For many materials characterization studies, a more economical alternative to the above three-dimensional unit cells takes the form of axisymmetric models describing the axial behavior of non-staggered or staggered arrays of aligned cylindrical short fibers in an approximate way. The basic idea behind these models is replacing unit cells for square or hexagonal arrangements by circular composite cylinders of equivalent cross sectional area (and volume fraction) as sketched in Fig. 6.14. The resulting axisymmetric cells are not proper unit cells, because they overlap and are not space filling. In addition, their association with three-dimensional phase arrangements is somewhat tenuous — note that they do not show the same transverse fiber spacing as the "equivalent" periodic arrangements in Fig. 6.14 — and they are severely limited in the type of loading conditions they

[94]For a comparison between unit cell and analytical predictions for the overall elastic properties of short-fiber-reinforced composites see, e.g., Tucker and Liang (1999).

[95]Such square arrangements give rise to tetragonal overall symmetry, and, consequently, the transverse overall properties are direction dependent.

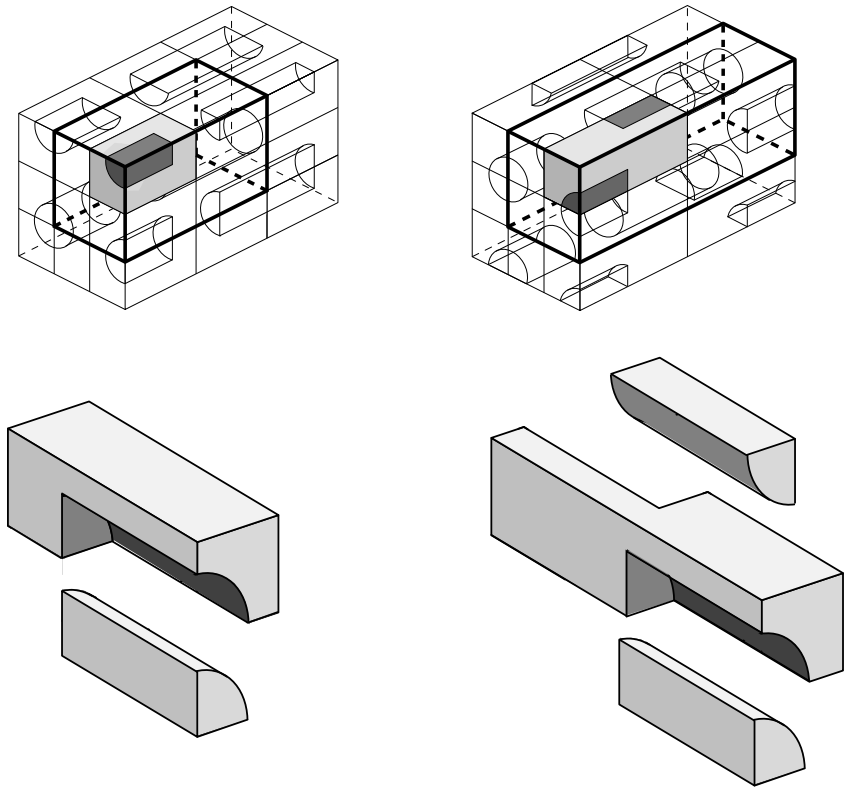

Figure 6.13: Three-dimensional cells for modeling non-staggered (left) and staggered (right) square arrangements of aligned short fibers. The shaded reduced cells, which follow Levy and Papazian (1991), require symmetry B.C., cells outlined in bold are suitable for periodicity B.C.

can handle[96]. However, they have the advantage of significantly reduced computational requirements, which has made them especially suitable for qualitative studies of highly nonlinear behavior such as damage.

Symmetry boundary conditions are used for the top and bottom faces of the cells shown in Fig. 6.14. The circumferential surfaces must be chosen to enforce identical cross sectional areas along the axial direction for any aggregate of cells. In the case of non-staggered fibers this can be easily done by specifying symmetry-type boundary conditions, eqns. (6.6), for the outer surfaces.

For staggered arrangements a pair of cells with different fiber positions is considered, the total cross sectional area of which is required to be independent of the axial coordinate[97]. By choosing the two cells making up the pair such that they are antisymmetric with respect to a pivot point P the behavior of the staggered arrangement can be described by a single cell with an antisymmetric outer (E-) face, U and L being nodes on this face that are positioned symmetrically with respect to the pivot. Using the nomenclature of fig. 6.15

[96] Axisymmetric cells are limited to load cases in which the deformed shape of the cell remains axisymmetric. These include uniaxial stress and strain, volumetric stress, "in plane hydrostatic stress" (where a homogeneous radial stress is prescribed) and isochoric strain (obtained, in the small strain regime, by applying constant normal displacements at the "upper" and "outer" faces of, $v_N = 2u_E$, respectively).

[97] As originally proposed by Tvergaard (1990) the nonlinear displacement boundary conditions in eqn. (6.18) were combined with antisymmetry traction B.C.s for use with a hybrid FE formulation.

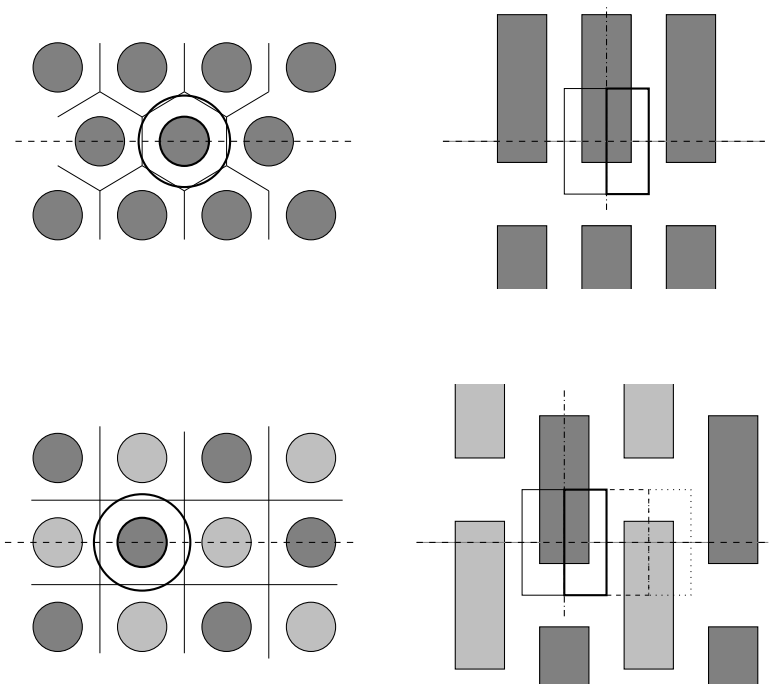

Figure 6.14: Periodic arrays of aligned non-staggered (top) and staggered (bottom) short fibers and corresponding axisymmetric cells (left: sections in transverse plane; right: sections parallel to fibers).

and the notation of eqns. (6.5) to (6.7), this leads to nonlinear relations for the radial displacements u and linear constraints for the axial displacements v at the outer surface,

$$(r_{\mathrm{U}} + u_{\mathrm{U}})^2 + (r_{\mathrm{L}} + u_{\mathrm{L}})^2 = 2(r_{\mathrm{P}} + u_{\mathrm{P}})^2 \qquad \text{and} \qquad v_{\mathrm{U}} + v_{\mathrm{L}} = 2v_{\mathrm{P}} \qquad , \tag{6.18}$$

respectively, where r is the radius of the undeformed cell. Nonlinear constraints such as eqn. (6.18), however, tend to be cumbersome to use and are not widely available in FE codes[98]. For typical small-strain problems the boundary conditions for the radial displacements at the outer surfaces of the cylinders, eqn. (6.18), can be linearized without major loss in accuracy to give sets of linear constraint equations

$$u_{\mathrm{U}} + u_{\mathrm{L}} = 2u_{\mathrm{P}} \qquad \text{and} \qquad v_{\mathrm{U}} + v_{\mathrm{L}} = 2v_{\mathrm{P}} \qquad , \tag{6.19}$$

which can be seen to be formally identical to the antisymmetry boundary conditions described by eqn. (6.7).

Axisymmetric cell models of the types shown in fig. 6.14 were the the workhorses of PMA studies of short-fiber-reinforced composites in the 1990s, see, e.g., Povirk et al. (1992) or Tvergaard (1994). Typically, descriptions using staggered arrangements allow a wider range of microgeometries to be covered, compare Böhm et al. (1993) or Tvergaard (2003), and give more realistic descriptions of actual composites. Both staggered and non-staggered axisymmetric models can be extended to studying a considerable range of arrangements

[98] For an example of the use of the nonlinear B.C.s described in eqn. (6.18) with a commercial FE code see Ishikawa et al. (2000), where cells of truncated cone shape are employed to describe bcc arrangements of particles.

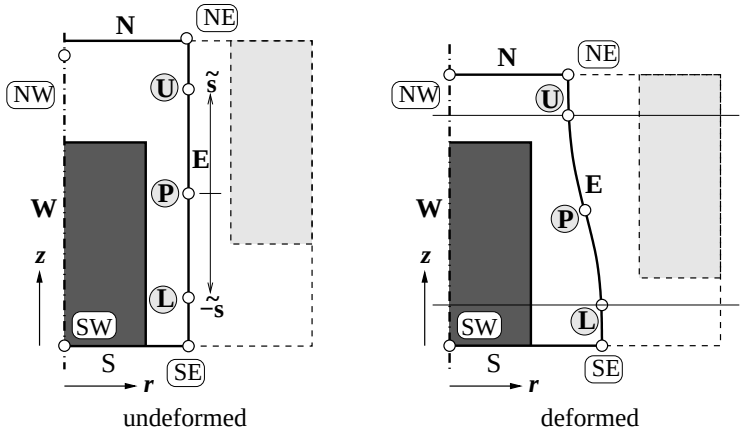

Figure 6.15: Axisymmetric cell for staggered arrangement of short fibers: undeformed and deformed shapes as used in eqn. (6.18).

incorporating aligned fibers of different size and/or aspect ratio by coupling two or more different cells via the condition of keeping the cross sectional area of the aggregate independent of the axial coordinate (Böhm et al., 1993).

Axisymmetric cells and simple three-dimensional unit cells have been used successfully for studying the nonlinear thermomechanical behavior of aligned short-fiber-reinforced MMCs, e.g., with respect to the their stress–strain responses, to the pseudo-Bauschinger effect, and to thermal residual stresses. They have provided valuable insight into causes and effects of matrix, interface and fiber damage. Over the past years, however, multi-fiber unit cells have become the standard tool for studying composites reinforced by aligned short fibers.

Composites Reinforced by Nonaligned Short Fibers

Among the first unit cell studies of materials reinforced by nonaligned discontinuous fibers were based on three-dimensional models of composites reinforced by alternatingly tilted misaligned fibers (Sørensen et al., 1995) and plane-stress models describing planar random short fibers (Courage and Schreurs, 1992). Multi-fiber unit cells of such materials have started coming into their own in the 2000s. It is worth noting that the situation with respect to mean-field models for composites reinforced by short fibers is not fully satisfactory for the elastic range, compare Section 2.6, and MFAs have found limited application for work on inelastic thermomechanical behavior.

At present the most powerful continuum modeling strategy for nonaligned short-fiber-reinforced composites consists of using three-dimensional multi-fiber volume elements in which the fibers are randomly positioned and oriented such that the required ODF is fulfilled to a suitable level of approximation. If the geometries are periodic, they are obviously suitable for periodic homogenization. Among early reports for such multi-fiber unit cells were, e.g., Lusti et al. (2002) or Böhm et al. (2002) for spatially random fiber orientations and Duschlbauer et al. (2006) or Iorga et al. (2008) for planar random fiber orientations. Models of this type can also account for the distributions of fiber sizes and/or aspect ratios. Such modeling approaches tend to pose considerable challenges in generating appropriate

fiber arrangements at non-dilute volume fractions due to geometrical frustration, relatively large volume elements being required for handling periodic microgeometries with fiber aspect ratio in excess of, say, 5. The meshing of the resulting phase arrangements for use with the FEM may also be difficult, compare Shephard et al. (1995), and analyzing the mechanical response of the resulting cells may require considerable computing power, especially for nonlinear constituent behavior. The first studies of this type were, accordingly, restricted to the linear elastic range, where the BEM has been found to answer well, see, e.g., Banerjee and Henry (1992). Commercial micromechanics codes such as Digimat (e-Xstream Engineering, Mont-Saint-Guibert, Belgium) have become available that provide capabilities for setting up and solving periodic models with considerable numbers of non-aligned short fibers.

As a simple example of a multi-fiber unit cell for a composite reinforced by nonaligned short fibers, fig. 6.16 shows a cube-shaped cell that contains 15 randomly oriented cylindrical fibers of aspect ratio $a = 5$, supports periodicity boundary conditions, was generated by random sequential addition, and is discretized by tetrahedral elements. The phase arrangement is set up in such a way that spheroidal fibers of the same aspect ratio, volume fractions, center points, and orientations can also be used in order to allow studying fiber shape effects (Böhm et al., 2002).

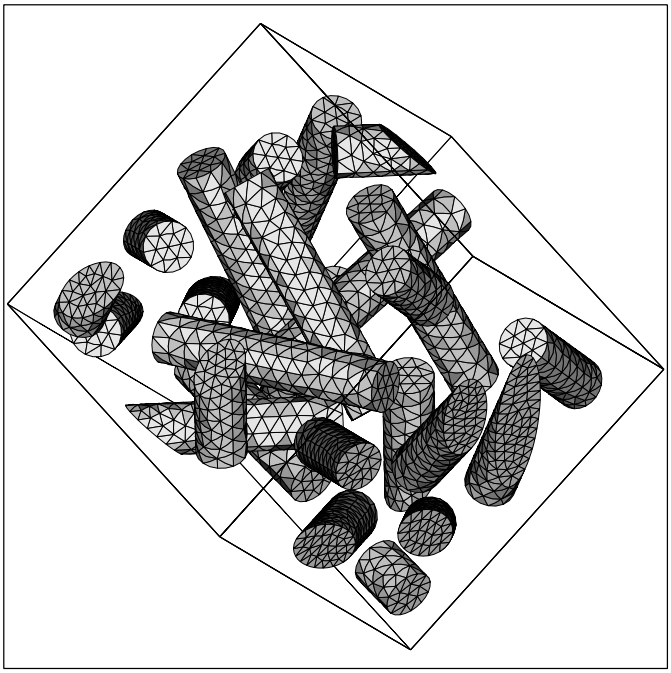

Figure 6.16: Unit cell for a composite reinforced by randomly oriented short fibers (Böhm et al., 2002). The nominal fiber volume fraction is $\xi = 0.15$ and the 15 cylindrical fibers in the cell have an aspect ratio of $a = 5$.

Table 6.2 lists predictions for the overall elastic response of a composite reinforced by randomly positioned and oriented fibers obtained by analytical estimates, the Hashin–Shtrikman bounds (Hashin and Shtrikman, 1963) and results obtained with the above type of unit cell, for which data are shown pertaining to cylindrical and spheroidal fibers. Interestingly, noticeable differences were found between the predictions for reinforcement

Table 6.2: Overall elastic properties of a SiC/Al2618 MMC reinforced by randomly oriented fibers ($a = 5$, ξ=0.15) as predicted by the Hashin–Shtrikman bounds (HSB), by the extended Mori–Tanaka method (MTM) of Wei and Edwards (1999), by the classical self-consistent scheme (CSCS) of Berryman (1980), by the Kuster and Toksöz (1974) model (KTM) and by multi-fiber unit cells of the type shown in fig. 6.16 (MFUC), which contain 15 spheroidal or cylindrical fibers (Böhm et al., 2002).

	E^* [GPa]	ν^* []
fibers	450.0	0.17
matrix	70.0	0.30
HSB/lo	87.6	0.246
HSB/hi	106.1	0.305
MTM	89.8	0.285
CSCS	91.2	0.284
KTM	90.3	0.285
MFUC/sph	89.4	0.285
MFUC/cyl	90.0	0.284

by cylindrical and spheroidal fibers that have the same fiber volume fraction and aspect ratio, occupy the same positions and show the same orientations, with the spheroidal reinforcements leading to a more compliant response, especially in the inelastic regime. Useful results were obtained despite the low number of fibers in the unit cell and excellent agreement with analytical descriptions was achieved in terms of the orientation dependence of the stresses in individual fibers, compare fig. 2.4. Whereas the phase arrangement shown in fig. 6.16 does not contain a sufficient number of fibers for approaching representativeness even in the elastic range, recent studies using much larger volume elements have markedly improved this situation, see, e.g., Tian et al. (2015).

Three-dimensional models based on volume elements that contain multiple fibers in general form the basis of the most powerful and versatile numerical models of aligned or nonaligned short-fiber-reinforced composites.

6.6 Periodic Models for Particle-Reinforced Composites

Actual particle-reinforced composite materials often show rather irregular particle shapes, and anisotropy in the microgeometry as well as in the overall responses may be introduced by processing effects such as extrusion textures. Nevertheless, for materials reinforced by statistically uniformly distributed, (approximately) equiaxed particles isotropic macroscopic behavior is a useful approximation that has been applied in many modeling studies. The thermoelastic behavior of macroscopically isotropic composites has been successfully described by mean-field methods that approximate the particles as spheres, see Section 2.3. Extensions of the mean-field solutions into the nonlinear range are available, compare Section 2.9, but they are subject to some limitations in predicting the overall thermome-

chanical response in the post-yield regime. In addition, mean-field models are limited in accounting for many particle shape, clustering, and size distribution effects and cannot resolve local fluctuations of the stress and strain fields. As a consequence, the past 30 years have witnessed marked interest in periodic homogenization models for studying the thermomechanical behavior of particle-reinforced composites.

One issue in applying periodic microfield approaches to the modeling of particle-reinforced materials with macroscopically isotropic behavior is that there exists no simple periodic three-dimensional phase arrangement that shows matrix–inclusion topology and is inherently elastically isotropic[99]. Together with the wide variation in microgeometries and particle shapes in actual materials, this gives rise to non-trivial tradeoffs between keeping computational requirements reasonably low (favoring simple particle shapes and two-dimensional or simple three-dimensional microgeometries) and obtaining sufficiently realistic models for a given purpose (best fulfilled by three-dimensional volume elements containing considerable numbers of randomly positioned particles of complex shape). In many respects periodic models of particle-reinforced composites are subject to similar constraints and use analogous approaches as work on short-fiber-reinforced composites.

Many three-dimensional unit cell studies of generic microgeometries for particle-reinforced composites have been based on simple cubic (sc), face centered cubic (fcc) or body centered cubic (bcc) arrays of spherical, cylindrical or cube-shaped particles, compare, e.g., Hom and McMeeking (1991). By invoking the symmetries of these arrays and using symmetry as well as antisymmetry boundary conditions, rather small "reduced" cells can be obtained for materials characterization[100], compare Weissenbek et al. (1994) and fig. 6.17. In addition, work employing hexagonal or tetrakaidecahedral arrays of particles (Rodin, 1993) and Voronoi cells for cubic arrays of particles (Li and Wongsto, 2004) was reported.

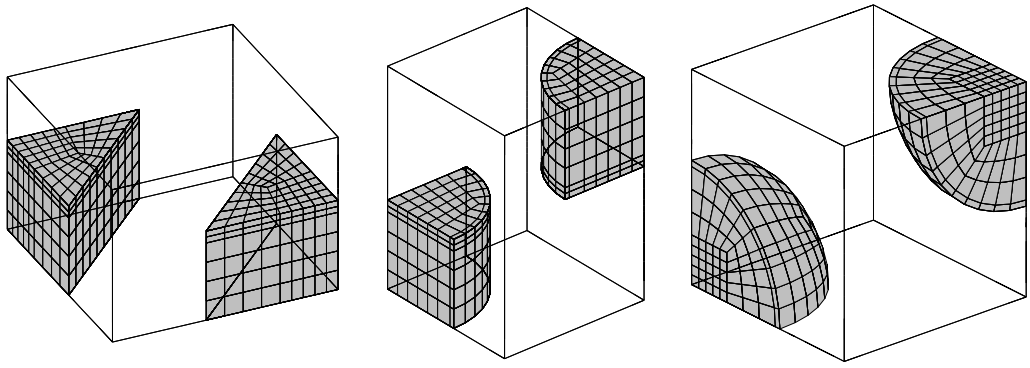

Figure 6.17: Examples of reduced cells for particle-reinforced composites using cubic arrays of inhomogeneities: s.c. arrangement of cubes, b.c.c. arrangement of cylinders and f.c.c. arrangement of spheres (Weissenbek et al., 1994).

[99] Even though volume elements in the shape of pentagonal dodecahedra and icosahedra have the appropriate symmetry properties (Christensen, 1987), they are not space filling.

[100] Among the reduced cells shown in fig. 6.17 the one on the left uses symmetry boundary conditions and is restricted in the load cases that can be handled. The other two cells employ antisymmetry B.C.s and can be used more freely. Unit cells suitable for periodicity boundary conditions are considerably larger, but allow unrestricted modeling of the full thermomechanical response of cubic phase arrangements.

The effective elastic tensors obtained from cubic arrays of particles show cubic symmetry[101]. As a consequence, the corresponding moduli do not necessarily fulfill the Hashin–Shtrikman bounds for macroscopically isotropic materials, and often lie outside the three-point bounds, compare table 6.3. Among the cubic arrays of particles, sc ones are easiest to handle by unit cell models, but their mechanical behavior shows a more pronounced anisotropy than do bcc and fcc arrangements.

Axisymmetric cells describing staggered or non-staggered arrangements of particles can be used for materials characterization of particle-reinforced composites in full analogy with short-fiber-reinforced materials, compare figs. 6.14 and 6.15. By appropriate choice of the dimensions of the axisymmetric cells sc, bcc and fcc arrays of particles can be approximated to some extent, and a range of axisymmetric particle shapes can be studied. Such models were a mainstay of PMA modeling of materials containing particulate inhomogeneities, see, e.g., Bao et al. (1991) or LLorca (1996). A related type of model are spherical cells (Guild and Kinloch, 1995).

Due to their low computational requirements and the relative ease of incorporating irregular particle shapes, planar unit cell models of particle-reinforced materials have also been used to a considerable extent. Typically, plane stress models (which actually describe thin "reinforced sheets" or the stress states at the surface of inhomogeneous bodies) show a more compliant and plane strain models (which describe reinforcing by aligned continuous fibers rather than by particles) show a stiffer overall response than three-dimensional descriptions, compare table 6.3. With respect to the overall behavior, plane stress analysis may be preferable to plane strain analysis, compare (Weissenbek, 1994), but no two-dimensional model gives satisfactory results in terms of the predicted microstress and microstrain distributions[102] (Böhm and Han, 2001). Axisymmetric cell models typically provide better results for the behavior of particle-reinforced composites than do planar ones.

During the past 20 years studies based on increasingly complex three-dimensional phase arrangements have assumed a prominent role in the literature. Gusev (1997) used Finite Element methods in combination with unit cells containing up to 64 statistically positioned particles to describe the overall behavior of elastic particle-reinforced composites. Hexahedral unit cells containing up to 10 particles in a perturbed cubic configuration (Watt et al., 1996) as well as cube shaped cells incorporating at least 15 spherical particles in quasi-

[101] Cubic elastic symmetry is a special case of orthotropy with equal responses in all principal directions. It gives rise to direction dependent moduli and requires three independent parameters for describing the elastic behavior. For a discussion of the elastic anisotropy of cubic materials see, e.g., Cazzani and Rovati (2003). The conduction and diffusion behavior of materials with cubic symmetry is isotropic.

[102] One issue giving rise to difficulties in describing macroscopically isotropic phase arrangements with two-dimensional models is the latters' lack of a proper hydrostatic load case. Its closest planar equivalent, equi-biaxial loading, is controlled by the plane strain bulk modulus, K_T, or the plane stress bulk modulus, respectively, both of which differ from the "three-dimensional" bulk modulus K.
In plastic regimes, plane stress configurations tend to give much higher equivalent plastic strains in the matrix and weaker overall hardening than do plane strain and generalized plane strain models using the same planar phase geometry. The configurations of regions of concentrated strains that underlie this behavior depend strongly on the geometrical constraints, compare, e.g., Iung and Grange (1995), Gänser et al. (1998), Böhm et al. (1999) or Shen and Lissenden (2002). For continuously reinforced composites under transverse loading the equivalent plastic strains tend to concentrate in bands oriented at 45° to the loading directions, whereas the patterns are qualitatively different in particle-reinforced materials.

random arrangements (Böhm et al., 1999; Böhm and Han, 2001), compare fig. 6.18, or clusters of particles (Segurado et al., 2003; Lee et al., 2011b) were used in Finite Element based studies of elastoplastic particle-reinforced MMCs and related materials. Three-dimensional simulations involving high numbers of particles have been reported, e.g., for investigating the elastic behavior of composites (Michel et al., 1999), for studying brittle matrix composites that develop damage (Zohdi and Wriggers, 2001), and for rubber-reinforced polymers (Fond et al., 2001).

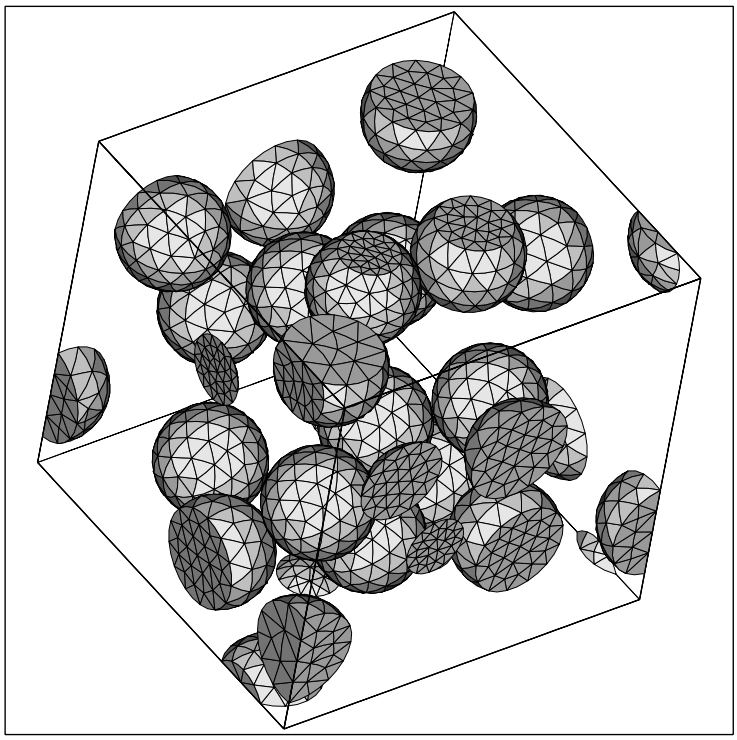

Figure 6.18: Unit cell for a particle-reinforced MMC (ξ=0.2) containing 20 spherical particles in a quasi-random arrangement that is suitable for using periodicity B.C. (Böhm and Han, 2001).

Table 6.3 provides comparisons between the predictions for the effective Young's moduli, Poisson numbers and coefficients of thermal expansion predicted by a number of bounding methods, mean-field approaches and periodic homogenization models. The data pertain to a particle-reinforced SiC/Al MMC (elastic contrast $c_{\text{el}} \approx 5.5$) that is subjected to macroscopic uniaxial stress; the particle volume fraction is chosen as $\xi = 0.2$. The loading directions for the cubic arrays are identified by Miller indices, with $<ijk>$ denoting a family of equivalent directions, results being provided for the <100> (edges), <110> (face diagonals) and <111> (space diagonals) orientations[103]. Despite the moderate elastic contrast and particle volume fraction considered, fewer than half of the predictions for the Young's moduli obtained from the cubic arrays fall within the 3-point bounds pertaining to randomly positioned spheres and some of them even violate the lower Hashin–Shtrikman bounds. The axisymmetric cells (axi/sc, axi/bcc and axi/fcc) and the planar multi-particle models (2D/PST using plane stress and 2D/PSE using plane strain kinematics) do even worse. The two results for three-dimensional multi-particle volume elements (3D/sr per-

[103]This choice covers the extremal values of the Young's moduli of the cubic arrays, which are known to be associated with loading in the <100> and <111> directions (Nye, 1957).

Table 6.3: Overall thermoelastic properties of a particle-reinforced SiC/Al MMC (spherical particles, ξ=0.2) predicted by the Hashin–Shtrikman (HSB) and three-point (3PB) bounds, by the Mori–Tanaka method (MTM), the generalized self-consistent scheme (GSCS), the differential scheme (DS), and Torquato's three-point estimates (3PE), as well as by unit cell analysis using three-dimensional cubic arrays, axisymmetric cells approximating sc, bcc and fcc geometries, two-dimensional multi-particle models based on plane stress (2D/PST) and plane strain (2D/PSE) kinematics, as well as three-dimensional models containing 20 randomly positioned spherical particles (3D/sr and 3D/eac).

	E^* [GPa]	E^*<100> [GPa]	E^*<110> [GPa]	E^*<111> [GPa]	ν^* []	α^*_A [$K^{-1}\times10^{-6}$]
particles	429.0	—	—	—	0.17	4.3
matrix	67.2	—	—	—	0.35	23.0
HSB/lo	91.2	—	—	—	0.285	16.8
HSB/hi	115.4	—	—	—	0.340	18.5
3PB/lo	91.7	—	—	—	0.323	18.4
3PB/hi	94.2	—	—	—	0.328	18.5
MTM	91.2	—	—	—	0.328	18.5
GSCS	91.9	—	—	—	0.327	18.5
DS	92.7	—	—	—	0.326	18.4
3PE	92.2	—	—	—	0.327	18.5
sc	—	96.5	90.6	89.5		18.5
bcc	—	90.1	91.8	92.2		18.5
fcc	—	90.2	91.7	92.1		18.5
axi/sc	95.4	—	—	—		18.6/18.6
axi/bcc	87.9	—	—	—	/	18.4/18.8
axi/fcc	88.1	—	—	—		18.1/19.0
2D/PST	85.5	—	—	—	0.334	
2D/PSE	98.7	—	—	—		
3D/sr	92.4	—	—	—	0.326	
3D/eac	92.2	—	—	—	0.327	18.5

tains to the arrangement shown in fig. 6.18 loaded in an edge direction and 3D/eac uses ensemble averaging over 3 arrangements of 20 particles each followed by evaluation of the closest isotropic elasticity tensor as discussed in Section 5.4), however, fall within both the Hashin–Shtrikman and the three-point bounds. The different predictions for the moduli used for obtaining result 3D/eac differed by nearly 1.5%, which is somewhat in excess of what might be expected from the nonlocal estimates of Drugan and Willis (1996). The above value also gives an idea of the elastic anisotropy of such volume elements.

The nonlinear macroscopic mechanical responses of particle-reinforced composites tend to be more sensitive to the phase arrangements than is their elastic behavior. This is demonstrated in fig. 6.19 where unit cell predictions for the macroscopic uniaxial tensile elastoplastic stress–strain responses of the same Al matrix as used in fig. 6.9 (von Mises plasticity with linear hardening), reinforced by 40 vol.% of spherical, linear elastic SiC particles (identical to the ones in table 6.3), are compared. For the sc, bcc and fcc cubic arrays the responses to tensile loads acting in the <100>, <110> and <111> each are

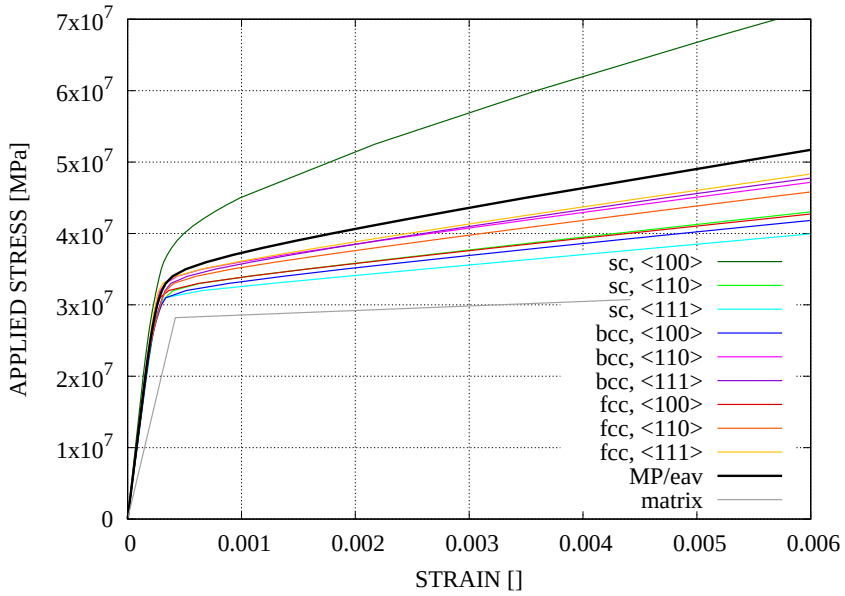

Figure 6.19: Elastoplastic response of a particle-reinforced SiC/Al MMC (ξ=0.4, matrix as in fig. 6.9, particles as in table 6.3) to uniaxial loading as predicted by PMA models using sc, bcc and fcc arrays as well as multi-particle volume elements (MP/eav).

shown together with the ensemble averaged predictions for loads in the 3 edge directions of two volume elements containing 20 randomly positioned particles each, 3D/ea. Somewhat similarly to the case of fiber-reinforced composites, fig. 6.9, the macroscopic hardening behavior of the multi-particle models is considerably more pronounced than that of the cubic arrays in most situations, then main exception being the sc array subjected to tensile uniaxial loading in <100>, which is excessively stiff.

Like fiber-reinforced MMCs, particle-reinforced composites typically display highly inhomogeneous microscopic stress and strain distributions, especially in nonlinear regimes. As an example, fig. 6.20, shows the predicted equivalent plastic strains of the elastoplastic matrix inside the multi-particle unit cell model depicted in fig. 6.18. This behavior tends to give rise to microscopic "structures" that can be considerably larger than individual particles, leading to longer ranged interactions between inhomogeneities[104]. The latter, in turn, underlie the need for larger volume elements for studying composites with nonlinear matrix behavior mentioned in Chapter 5.

Periodic volume elements are highly suitable for carrying out numerical experiments that explore the influence of different aspects of the microgeometry of particle-reinforced composites on their microscopic and macroscopic responses. For example, Rasool and Böhm (2012) and Böhm and Rasool (2016) studied model composites that contain equal volume fractions of randomly positioned and, where applicable, randomly oriented, identi-

[104]Due to the filtering effect of periodic phase arrangements mentioned in Section 6.1, the length of such features can exceed the side length of the unit cell only in certain directions, which may induce a spurious direction dependence into the predicted large-strain behavior of sub-RVE unit cells. Cubic arrays give rise to highly regular, long range patterns of the microfields that may strongly favor such structures; the maxima of microfields in cubic arrays depend on the loading direction both in their location and magnitude.

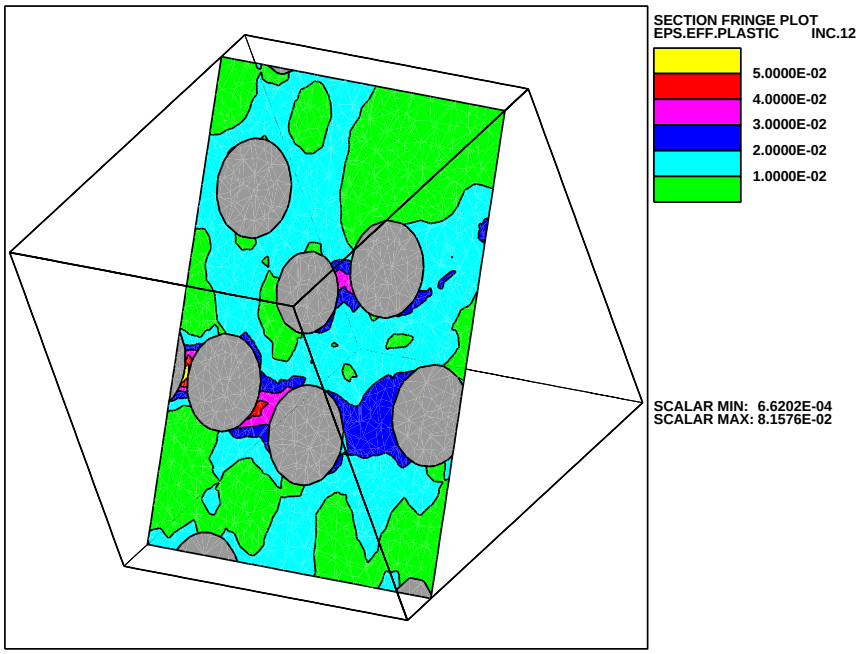

Figure 6.20: Predicted distribution of equivalent plastic strain in the matrix of a particle-reinforced MMC (ξ=0.2) subjected to uniaxial tensile loading (in left–right direction) obtained for a unit cell with 20 spherical particles in a quasi-random arrangement (Böhm and Han, 2001).

cal particles having the shapes of spheres, cubes, regular octahedra and regular tetrahedra, respectively. Figure 6.21 shows the resulting predictions for the responses to a single, non-symmetric, uniaxial stress loading cycle, clear effects of the particle shape on the hardening behavior and on the residual strains being evident.

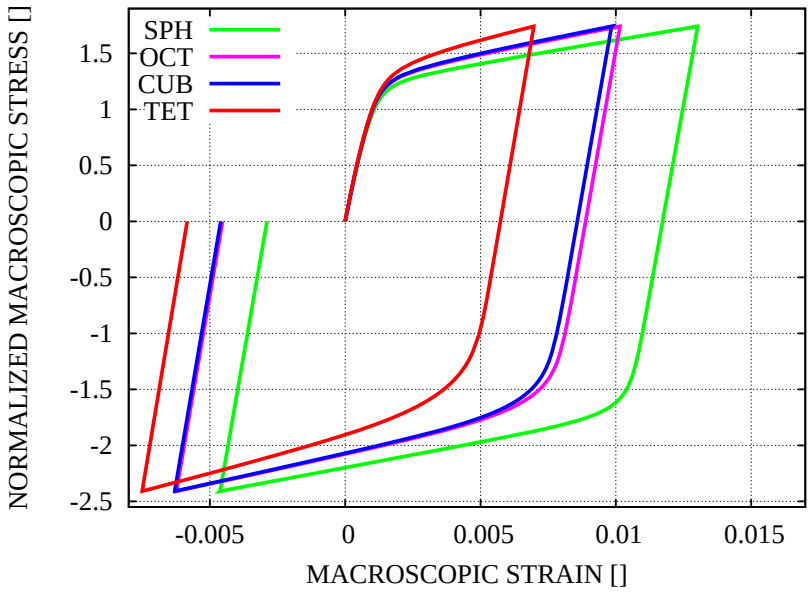

Figure 6.21: PMA predictions for the responses to a uniaxial load cycle of elastoplastic, particle-reinforced MMCs (ξ=0.2) containing identical spherical (SPH), cube-shaped (CUB), octahedral (OCT) and tetrahedral (TET) inhomogeneities, respectively.

A comparison of the modeling approaches for studying the mechanical behavior of particle-reinforced composites discussed in this section clearly brings out three-dimensional multi-particle models as being superior to the other options for evaluating both macroscopic responses and microscopic stress and strain fields. Their main drawback, however, are their computational costs, especially for nonlinear problems.

6.7 Periodic Models for Porous and Cellular Materials

Due to their relevance to the ductile damage and failure of metallic materials elastoplastic porous materials have been the subjects of a considerable number of PMA studies[105]. Generally, modeling concepts for porous materials are closely related to the ones employed for particle-reinforced composites, the main difference being that the shapes of the voids may evolve significantly through the loading history[106]. Axisymmetric cells of the types discussed in Sections 6.5 and 6.6, compare, e.g., Koplik and Needleman (1988) or Gărăjeu et al. (2000), and three-dimensional unit cells based on cubic arrangements of voids, see, e.g., McMeeking and Hom (1990) or Segurado et al. (2002b), have been used in the majority of pertinent PMA studies. In addition, studies of void growth in ductile materials based on multi-void cells and using geometry data from serial sectioning were reported (Shan and Gokhale, 2001).

In cellular materials, such as foams, wood and trabecular bone, the volume fraction of the solid phase is very low (often amounting to no more than a few percent) and the void phase may be topologically connected (open cell foams), unconnected (closed cell foams, syntactic foams), or both of the above (e.g., hollow sphere foams). The linear elastic regime of cellular materials in many cases is limited to a very small range of macroscopic strains. Furthermore, marked differences tend to be present between tensile and compressive inelastic macroscopic responses: As strains increase, gross shape changes of the cells typically take place on the microscale, with large bending deformations, the formation of plastic hinges, elastic as well as plastic buckling, and brittle failure of struts and cells walls playing major roles, especially under compressive loading. For compression-dominated load cases this regime tends to give rise to a stress plateau on the macroscale, which underlies the favorable energy absorption properties of many cellular materials. At some elevated

[105] Many models and constitutive descriptions of the ductile damage and failure of metals, among them contributions by Rice and Tracey (1969), Gurson (1977), Tvergaard and Needleman (1984), Gologanu et al. (1997) as well as Benzerga and Besson (2001), are based on micromechanics-based considerations of the growth of pre-existing voids in a ductile matrix.

[106] The evolution of the shapes of initially spheroidal voids under non-hydrostatic loads has been the subject of studies by mean-field type methods, compare Kailasam et al. (2000). Such models use the assumption that initially spherical pores will stay ellipsoids throughout the deformation history, which axisymmetric cell analysis (Gărăjeu et al., 2000) has shown to be an excellent approximation for axisymmetric tensile load cases. For compressive loading, however, initially spherical pores may evolve into markedly different shapes and contact between the walls of pores tends to play an increasing role as the voids as their volume fraction is more and more reduced (Segurado et al., 2002b). Void size effects (Tvergaard, 1996) and void coalescence (Faleskog and Shih, 1997) introduce additional complexity into studies of the ductile damage and failure of metals.

strain the effective stiffness under compression typically rises sharply, the cellular structure having collapsed to such an extent that many cell walls or struts are in contact and the void volume fraction has decreased dramatically. No comparable behavior is present under tensile or shear loading.

Periodic microfield methods are generally well suited to studying the thermomechanical behavior of cellular materials. The widely used analytical results of Gibson and Ashby (1988) were derived by analytically studying arrangements of beams (for open cell foams) or plates (for closed cell foams). They give the macroscopic moduli and other physical properties of cellular materials as power laws of the type

$$\frac{E^*}{E^{(\mathrm{m})}} \propto \left(\frac{\rho^*}{\rho^{(\mathrm{m})}}\right)^n \tag{6.20}$$

in terms of the relative density[107], $\rho^*/\rho^{(\mathrm{m})}$.

In Finite Element based models of cellular materials the solid phase may be described either by continuum or by structural elements (shells for the cell walls of closed cell foams and beams for the struts in open cell foams)[108]. The influence of the gas filling closed cells can also be accounted for within such an FE setting (Mills et al., 2009). In order to model buckling and compaction phenomena, unit cells for cellular materials require explicit provision for handling large deformations of and contact (including self-contact) between cell walls or struts. Boundary conditions must be applied to the unit cells in such a way that they do not interfere with relevant buckling modes. Specifically, models must be sufficiently large for non-trivial deformation and buckling patterns to develop, or Bloch wave theory (Gong et al., 2005) must be used to account for long wavelength buckling modes[109].

The geometrically simplest cellular materials are regular honeycombs, the in-plane behavior of which can be modeled with planar hexagonal cell models. Somewhat less ordered two-dimensional arrangements have been used for studying the crushing behavior of soft woods (Holmberg et al., 1999), and highly irregular planar arrangements, of the type shown in fig. 6.22, may be used to generically investigate aspects of the geometry dependence of the mechanical response of cellular materials.

[107] The exponent n in eqn. (6.20) allows inferring the dominant local deformation mode of a cellular microgeometry, with n=2 implying deformation by bending and n=1 by axial stretching of struts in open cell foams. The Gibson–Ashby cell for open cell foams gives n=2 and, as a consequence, tends to underestimate the stiffness of actual open-cell foams.
Stretching-dominated cellular materials tend to be more weight-efficient than bending-dominated ones (Deshpande et al., 2001).

[108] At high levels of porosity it is typically necessary to account for the overlap of shell elements at edges and of beam elements at vertices when evaluating the phase volume fractions of the discretized unit cells. When structural finite elements are used in unit cell studies periodicity conditions must obviously be enforced in terms of both translational and rotational degrees of freedom.

[109] For perfectly regular structures such as hexagonal honeycombs the minimum size of a unit cell for capturing bifurcation effects can be estimated from extended homogenization theory (Saiki et al., 2002). When symmetry boundary conditions are employed care must be taken that cell walls that may buckle do not coincide with symmetry planes at the boundaries, and periodic contact may have to be provided for if periodicity boundary conditions are used.

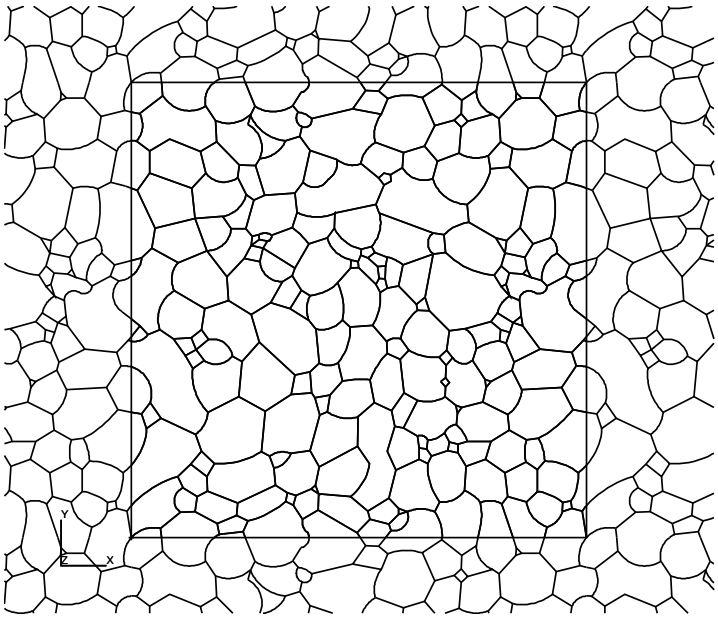

Figure 6.22: Planar periodic unit cell for studying irregular cellular materials (Daxner, 2003).

The modeling of typical closed cell foams, however, requires three-dimensional microgeometries. In the simplest cases generic phase arrangements based of cubic cells, see, e.g., Hollister et al. (1991), truncated cubes plus small cubes (Santosa and Wierzbicki, 1998), rhombic dodecahedra, regular tetrakaidecahedra (Grenestedt, 1998; Simone and Gibson, 1998), compare fig. 6.23, as well as Kelvin, Williams and Weaire–Phelan (Kraynik and Reinelt, 1996; Daxner et al., 2007) geometries[110] may be used. Analogous regular microgeometries have formed the basis for analytical and numerical "lattice models" of open cell foams, see, e.g., Zhu et al. (1997), Shulmeister et al. (1998) and Vajjhala et al. (2000) as well as fig. 6.24, the struts connecting the nodes of the cellular structures being modeled by beam or solid elements[111]. In addition, tetrahedral arrangements (Sihn and Roy, 2005) and cubic arrangements of struts with additional "reinforcements" as well as perturbed strut configurations (Luxner et al., 2005) have been covered by such studies. Voronoi tesselations have become a common tool in modeling irregular open and closed cell foams, and random Laguerre tessellations have been proposed for generating periodic multi-cell models (Redenbach, 2009).

The effects of details of the microgeometries of cellular materials (e.g., thickness distributions and geometrical imperfections or flaws of cell walls or struts or the Plateau borders formed at the intersections of cell walls), which can considerably influence the overall behavior, have been a fruitful field of research employing periodic homogenization, see, e.g.,

[110] In Kelvin, Williams and Weaire–Phelan (Weaire and Phelan, 1994) foams some of the cell walls are spatially distorted in order to minimize the total surface, whereas in polyhedral foams all cell walls are planar. At low solid volume fractions these small distortions lead to noticeable differences in the overall elastic response.

[111] Models of foams employing regular arrangements of polyhedral cells are not macroscopically isotropic, compare, e.g., Luxner et al. (2005). A specific issue of beam lattice models for open cell foams are the limitations of Timoshenko beams that typically fully account for nonlinear material behavior in the axial and bending stiffnesses only, but not in shear stiffness, see, e.g., Pettermann and Hüsing (2012).

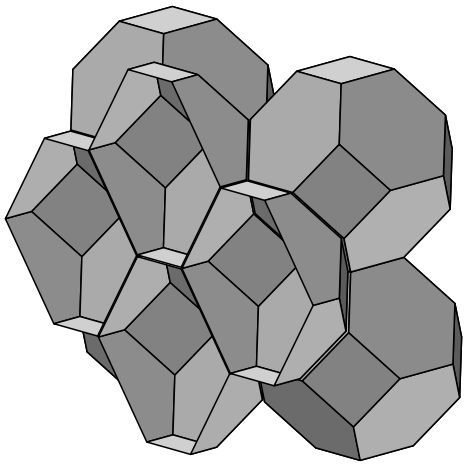

Figure 6.23: Idealized closed-cell foam microstructure modeled by regular tetrakaidecahedra (truncated octahedra).

Grenestedt (1998) and Daxner (2003). Typically, unit cell analysis of cellular materials with realistic microgeometries is rather complex and numerically demanding due to these materials' tendency to deform by local mechanisms and instabilities. Nevertheless, analytical solutions have been reported for the linear elastic behavior of some simple periodic phase arrangements, see, e.g., Warren and Kraynik (1991) or Sullivan and Ghosn (2009).

The high flexibility of FE-based periodic homogenization has allowed, on the hand, modeling a wide range of material behaviors of cellular materials, among them plasticity, viscoelasticity (Pettermann and Hüsing, 2012) and metal creep (Oppenheimer and Dunand, 2007), and, on the other hand, studying fairly complex microgeometries. An example of the latter describes hollow strut foams produced by coating a precursor cellular material and then removing this "template". Figure 6.24 shows a model for such a foam that is based on a Weaire–Phelan geometry and was meshed by a combination of solid and shell elements (Daxner et al., 2007).

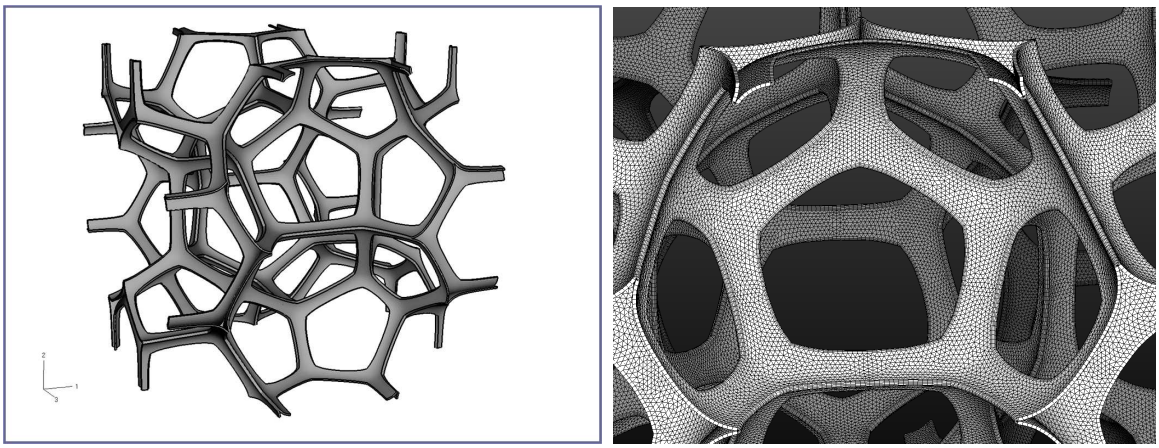

Figure 6.24: Weaire–Phelan model of an open cell foam with hollow struts (left) and detail of the FE-model (right), from Daxner et al. (2007).

Due to the inherent X-ray absorption contrast between matrix and voids, cellular materials are well suited to high-resolution computed tomography, giving access to "real-structure" microgeometries that can be directly converted into voxel models (compare Section 5.3) of open-cell or closed-cell foams[112], see, e.g., Maire et al. (2000) or Roberts and Garboczi (2001). Alternatively, image processing methods my be used to generate a surface model of the solid phase in the volume element to allow meshing with "standard" FE techniques (Youssef et al., 2005; Young et al., 2008). Because the microgeometries extracted from the experiments are, in general, not periodic, windowing approaches using homogeneous or mixed uniform boundary conditions, compare Chapter 7, tend to be the method of choice for such models, however.

A specific group of cellular materials amenable to PMA modeling are syntactic foams (i.e., hollow spheres embedded in a solid matrix) and hollow sphere foams (in which the spaces between the spheres are "empty", giving them both an open-cell and a closed cell flavor). Syntactic foams have been studied via axisymmetric or three-dimensional cell models that are based on closest packings of spheres (Rammerstorfer and Böhm, 2000; Sanders and Gibson, 2003) and by multi-void volume elements.

Recent advances in additive manufacturing have led to major interest in architected, lattice or shell micro- and nanostructures, which are periodic by design at the microscale. They are, accordingly, amenable to study by periodic homogenization, compare, e.g., Abueidda et al. (2017). However, for samples of finite size boundary effects may play a major role in their behavior, which requires modeling by full structural models (Luxner et al., 2005) or by second order homogenization (Desmoulins and Kochmann, 2017).

A further type of cellular material, trabecular (cancellous, spongy) bone, has attracted considerable modeling interest for more than thirty years[113]. Cancellous bone shows a wide range of microgeometries, which can be idealized as beam or beam–plate configurations (Gibson, 1985). In studying the mechanical behavior of trabecular bone, large three-dimensional unit cell models based on tomographic scans of actual samples and using voxel-based or smooth discretization schemes have become fairly widely used, see, e.g., Hollister et al. (1991), Hollister et al. (1994) or van Rietbergen et al. (1999).

In addition to periodic homogenization, windowing methods, compare Chapter 7, and embedding models, see Chapter 8, have been successfully employed for studying cellular materials.

[112] Roberts and Garboczi (2001) estimated the "systematic discretization error" to be of the order of 10% in terms of the overall moduli for voxel-based models of elastic open-cell and closed-cell foams.

[113] Like many materials of biological origin, bone is an inhomogeneous material at a number of length scales. The solid phase of trabecular bone is inhomogeneous and can itself be studied with micromechanical methods.

6.8 Periodic Models for Some Other Inhomogeneous Materials

At the continuum level, the thermomechanical behavior of essentially any inhomogeneous material can be studied by periodic homogenization techniques. For example, the elastic, elastoplastic, creep and damage behaviors of polycrystals, of high speed steels and dual phase steels, of intermetallics, of superalloys, and of graded materials have been the targets of unit cell models. In addition, "smart materials", such as piezoelectric composites and shape memory alloys, and solid state phase transitions in general have been studied. A comprehensive discussion of the models involved would by far exceed the present scope, so that the present section is limited to a small number of examples.

Generic PMA Models for Clustered, Graded, and Interpenetrating Microgeometries

Many commercially important steels may be viewed as matrix–inclusion-type composites. For example, high speed steels (HSS) contain carbidic inclusions in a steel matrix, with arrangements ranging from statistically homogeneous to highly clustered or layered (meso)geometries. Such materials can be modeled like particle-reinforced MMCs. A straightforward and flexible strategy for setting up generic planar model geometries for such studies consists of tiling the computational plane with regular hexagonal cells which are assigned to one of the constituents by statistical or deterministic rules. If required, the shapes of the cells can be modified or randomly distorted and their sizes can be changed to adjust phase volume fractions. Such a Hexagonal Cell Tiling (HCT) concept can be used, e.g., to generate unit cells for analyzing layer structured HSSs, compare (Plankensteiner et al., 1997) and fig. 6.25, and clustered or random arrangements of inhomogeneities in a matrix. HCT and related models of matrix–inclusion topologies are, however, restricted to low reinforcement volume fractions.

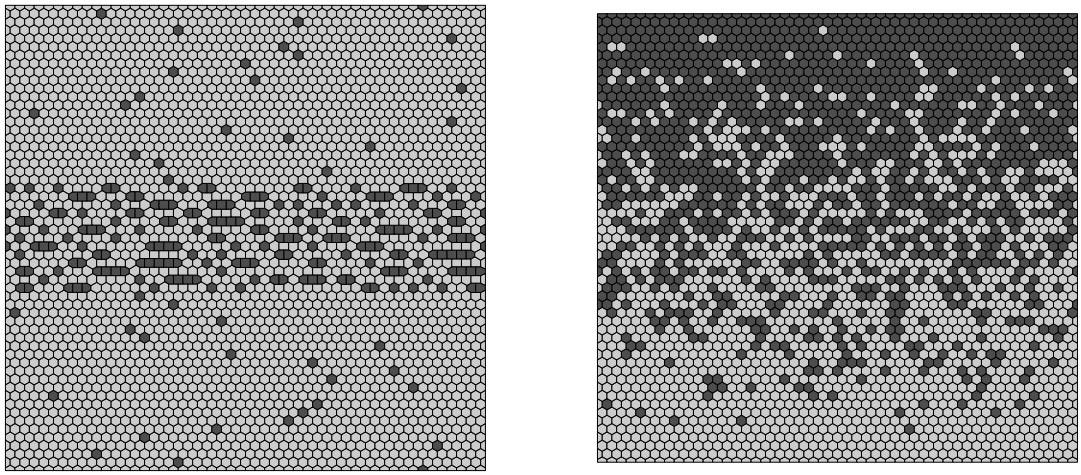

Figure 6.25: HCT cell models for a layer structured high-speed steel (left) and a functionally graded material (right).

Related concepts can be used to obtain generic geometries for planar models for studying functionally graded materials[114] (FGMs), in which the phase volume fractions run through the full physically possible range (Weissenbek et al., 1997; Reiter et al., 1997), so that there are regions that show matrix–inclusion microtopologies and others that do not, compare fig. 6.25 (right). A further application of such models have been investigations of the microstructure–property relationships in duplex steels, for which matrix–inclusion and interwoven phase arrangements were compared[115], see Siegmund et al. (1995) as well as Silberschmidt and Werner (2001). An FFT-based modeling scheme employing HCT-type geometries was developed by Michel et al. (1999) explicitly for studying interpenetrating microgeometries. There is no direct three-dimensional equivalent to HCT models, but unit cells partitioned into cube-shaped or tetrakaidecahedral subregions can be used in an analogous manner to obtain generic microgeometries (which, however, may be numerically expensive if meshes are chosen such that details of the microfields can be resolved). A distantly related, but geometrically much more flexible approach based on tetrahedral regions was reported by Galli et al. (2008).

For topological reasons most interpenetrating phase composites (IPC) must be studied with three-dimensional models. Beyond this restriction, however, fairly standard periodic homogenization approaches can be used for investigating their effective thermomechanical behavior, see, e.g., Dalaq et al. (2016) or Soyarslan et al. (2018).

PMA Models for Polycrystals

A large number of materials that are of technological interest are polycrystals and, accordingly, are inhomogeneous at some sufficiently small length scale. In the special case of metals and metallic alloys phenomena associated with plastic flow and ductile failure can be investigated at a number of length scales (McDowell, 2000), some of which are amenable to study by continuum micromechanical methods.

Micromechanical methods, especially analytical self-consistent approaches, have been applied to studying the mechanical behavior of polycrystals since the 1950s. The more recent concept of studying polycrystals by full field approaches, among them periodic homogenization, is quite straightforward in principle — a planar or three-dimensional unit cell is partitioned into suitable subregions that correspond to individual grains[116]. For these grains appropriate material models must be prescribed, and suitable material as well as orientation parameters must be assigned to them. The generation of appropriate grain geometries may be based, e.g., on Voronoi tessellations using Poisson or hardcore distributed

[114] In contrast to most other materials discussed in the present report, FGMs are statistically inhomogeneous materials, so that phase arrangements must be non-periodic in at least one direction, for which free-surface boundary conditions are used on the unit cells. Accordingly, volume averaging is of limited value in modeling such materials.

[115] In HSSs and FGMs particulate inhomogeneities are present at least in part of the volume fraction range, so that planar analysis must be viewed as a compromise between modeling accuracy and computational requirements. Duplex steels, in contrast, typically show elongated aligned grains, which can be described well by generalized plane strain analysis in the transverse plane.

[116] Usually symmetry boundaries passing through grains must be avoided in models of this type because they give rise to "twin-like" pairs of grains that are unphysical in most situations.

seed points, or on modified Voronoi tessellations[117]. Such microgeometries may be linked to uniform and isotropic grain growth that stops where neighboring grains contact each other, may be efficiently generated as well as meshed by appropriate software (Fritzen et al., 2009), and can provide periodic or non-periodic volume elements. Alternatively, the grain geometries can be based on experimental data obtained, e.g., by microscopy and serial sectioning.

Anisotropic elasticity and crystal plasticity models are best suited to describing the material behavior of the individual grains, the orientation of which can be described by stochastic models. The number of grains required for achieving a given accuracy in terms of the macroscopic elastic tensor has been shown to depend on the level of anisotropy of the individual grains (Nygårds, 2003). Analysis involving crystal plasticity tends to pose considerable demands on computational resources for three-dimensional models, compare Quilici and Cailletaud (1999). For a general discussion of the issues involved in micromechanical models in crystal plasticity and related fields see, e.g., Dawson (2000) and Roters et al. (2010).

PMA Models for Two-Phase Single Crystal Superalloys

Nickel-base single crystal superalloys, which consist of a γ matrix phase containing aligned cuboidal γ' precipitates, are of considerable importance due to their creep resistance at high temperatures, their main field of application being the hot sections of gas turbines. Because these materials show relatively regular microgeometries that change under load, due to a process known as rafting, there has been considerable interest in micromechanical modeling for elucidating their thermomechanical behavior and for better understanding their microstructural evolution. The elastic behavior of two-phase superalloys can be handled relatively easily by hexahedral unit cells with appropriately oriented anisotropic phases. In the inelastic range, however, the highly constrained plastic flow in the γ channels is difficult to describe even by crystal plasticity models, see, e.g., Nouailhas and Cailletaud (1996).

6.9 Periodic Models Models for Diffusion-Type Problems

Periodic microfield methods analogous to those discussed in Sections 6.1 to 6.8 can be used for studying linear diffusion-type problems of the types mentioned in Section 2.10. The Laplace solvers required for numerically-based homogenization in diffusion problems are widely available in FE packages, usually for modeling heat conduction. Specialized solvers are, however, required in some cases, e.g., when studying the frequency dependent dielectric properties of composites via complex potentials, see, e.g., Krakovsky and Myroshnychenko (2002).

For the most common application, thermal conduction, the equivalent to eqn. (6.2) takes the form

$$T(\mathbf{z} + \mathbf{c}_k) = T(\mathbf{z}) + \langle \mathbf{d} \rangle \, \mathbf{c}_k \qquad , \tag{6.21}$$

[117] Although Voronoi tessellations are commonly used for generating microgeometries for modeling polycrystals, the results may differ noticeably from actual microgeometries, see, e.g., Lazar et al. (2012).

where the nomenclature of table 2.1 is followed and $\langle \mathbf{d} \rangle$ is the volume averaged temperature gradient, compare also Section 2.10. Periodicity boundary conditions can then be expressed in terms of the nodal temperatures as

$$\Delta T_k = T_{k^+} - T_{k^-} = T(\mathbf{s}_k + \mathbf{c}_k) - T(\mathbf{s}_k) = \langle \mathbf{d} \rangle \mathbf{c}_k \tag{6.22}$$

in direct analogy to eqn. (6.3). Asymptotic homogenization for thermal conduction was discussed, e.g., by Auriault (1983), Matt and Cruz (2002), or Tang and Yu (2007), and the method of macroscopic degrees of freedom, compare Section 6.3, can be formulated in terms of temperatures, thermal gradients and fluxes rather than displacements, strains and stresses (Nogales, 2008). Furthermore, symmetry planes of the phase arrangement that are oriented parallel or normally to far-field gradients can be used to specify "symmetry-like" boundary conditions by not constraining temperatures at all or by setting them to a fixed value, respectively[118]. Volume and phase averages of fluxes are best evaluated according to eqn. (5.8). Finite interfacial conductances can be handled by using appropriate interface elements, compare, e.g., Matt and Cruz (2008) or Nogales and Böhm (2008).

There are, however, some intrinsic conceptual difficulties in applying periodic homogenization to transport problems where nonlinear conduction or diffusion behavior of the constituents is involved. Whereas in solid mechanics material nonlinearities are typically formulated in terms of the microscopic stresses and strains, which may be viewed as "generalized gradient" and "generalized flux" fields (compare table 2.1), respectively, nonlinear conductivities and diffusivities in transport problems typically depend on the "direct variable" (or "potential"), e.g., the temperature in heat conduction. As is evident from fig. 6.1, in PMAs the generalized gradients and fluxes are periodic (and have constant averages), whereas the direct variables consist of fluctuating and linearly varying contributions that accumulate from cell to cell. As a consequence, whereas in solid mechanics periodic homogenization involving nonlinear material behavior uses identical material properties for all unit cells, this is in general not the case for transport problems. Accordingly, even though solutions in terms of both microscopic (gradient and flux) fields and homogenized macroscopic conductivities can be obtained from unit cell analysis involving material nonlinearities of the above type, the underlying model material is inconsistent[119]. Temizer and Wriggers (2011) carried out a detailed analysis of two-scale homogenization for conduction problems and showed that there is a general thermodynamical inconsistency for finite deviations of microscopic temperatures from the macroscopic ones. Accordingly, the use of periodic homogenization for studying nonlinear transport problems in inhomogeneous media has to be viewed with some reservation and windowing or embedding methods, see Chapters 7 and 8, may be preferable for such work.

[118] As discussed by Duschlbauer et al. (2003a), symmetry planes oriented parallel to the far-field gradient act as insulating surfaces, whereas symmetry planes oriented normally to the applied gradient are isothermal planes. Gradient fields are symmetric with respect to the latter planes, temperature fields are antisymmetric and flux fields non-symmetric.

[119] The fact that periodicity implies that the direct variable can take values from $-\infty$ to $+\infty$ leads to another inconsistency in PMAs for thermal conduction, where the variable T has a thermodynamical lower bound at absolute zero. However, this issue does not appear to have any practical repercussions.

Chapter 7

Windowing Approaches

The aim of windowing methods lies in obtaining estimates for or bounds on the macroscopic properties of inhomogeneous materials on the basis of — typically non-periodic — volume elements that are referred to as mesoscopic test windows, observation windows or, in short, "windows". These volume elements typically are too small to be RVEs, so that the results of windowing analysis tend to pertain to specific samples rather than to a material and are, accordingly, referred to as apparent (rather than effective) material properties.

Windowing implicitly assumes that the material to be studied is statistically homogeneous, so that windows can be extracted from it at random positions. For convenience, windows are often chosen to be rectangles or right hexahedra, but other shapes may be used just as well. If the material is known (or at least assumed) to be macroscopically isotropic, windows are best extracted at random orientations, as shown in fig. 7.1. For anisotropic materials, however, the orientations of windows must either be taken into consideration in taking the samples or it must be accounted for explicitly in processing the results of the analysis.

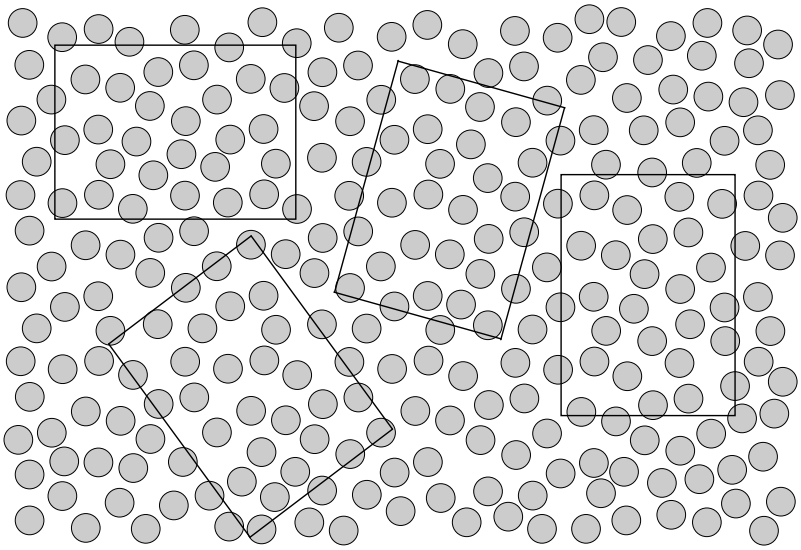

Figure 7.1: Schematic depiction of a composite that is statistically transversally isotropic and of four rectangular windows of equal size in the transverse plane.

Windowing methods subject window-type, inhomogeneous volume elements to statically uniform boundary conditions (SUBC), eqn. (5.3), kinematically uniform boundary conditions (KUBC), eqn. (5.4), or mixed uniform boundary conditions (MUBC), eqn. (5.5) for obtaining estimates on their macroscopic behavior.

Macrohomogeneous Boundary Conditions

SUBC and KUBC are collectively referred to as macrohomogeneous boundary conditions. Compliance tensors obtained with SUBC and elasticity tensors obtained with KUBC provide lower and upper estimates on the macroscopic elastic tensors of volume elements, respectively (Nemat-Nasser and Hori, 1993). For volume elements of equal size, ensemble averages of these lower and upper estimates give rise to lower and upper bounds on the overall apparent tensors (Huet, 1990); for unequally sized windows weighted averages must be used. These bounds are sometimes referred to as mesoscale bounds and provide information on the macroscopic properties pertinent to a collection of windows of given size. For further discussions of these issues see, e.g., Ostoja-Starzewski (2008).

By definition, if the windows are of sufficient size to be proper RVEs the lower and upper estimates and bounds on the overall elastic properties must coincide (Huet, 1990; Sab, 1992), defining the effective behavior. Accordingly, hierarchies of bounds that are generated from sequences of sets of sub-RVE testing volume elements of increasing volume can be used for assessing the size of proper representative volume elements. Actually achieving the coincidence of lower and upper mesoscale bounds has been found very difficult in practice, however. This is at least partly due to boundary layers, see, e.g., Pahr and Böhm (2008), that form due to the interaction of the uniform B.C. with phase boundaries intersecting the volume elements' surfaces, compare the remarks in Section 5.2. Consequently, using volumes that are shaped such that their boundaries stay within the contiguous phase of matrix–inclusion composites, which reduces boundary perturbations, has been found to improve the convergence of hierarchies of mesoscale bounds to a considerable extent (Salmi et al., 2012; Acton et al., 2019). This expedient, however, may bias phase volume fractions in the windows, which, in turn, may give rise to difficulties in identifying proper RVEs. As another consequence of boundary perturbations, it is typically not advisable to combine macrohomogeneous or mixed uniform B.C. with single-particle volume elements, compare also the discussion in Vilchevskaya et al. (2021).

The concept of generating lower and upper estimates by windowing using SUBC and KUBC can be shown to be also valid in the context of nonlinear elasticity and deformation plasticity (Jiang et al., 2001). Discussions of windowing bounds in finite strain elasticity, in viscoelasticity and in incremental plasticity settings were given by Khisaeva and Ostoja-Starzewski (2006), Zhang and Ostoja-Starzewski (2015) as well as Li and Ostoja-Starzewski (2006), respectively. Windowing methods are directly applicable to conduction problems, with macrohomogeneous flux and gradient boundary conditions giving rise to lower and upper estimates, respectively, as well as mesoscale bounds for the conductivity tensor.

Generally, if the individual windows are small, considerable variations in the phase volume fractions will typically be present in different realizations and the macroscopic material

symmetry must be expected to be subject to considerable perturbations. Furthermore, for relatively small windows, within which the phase arrangement deviates significantly from statistical homogeneity, different boundary conditions, especially SUBC and KUBC, tend to give rise to marked differences in the distributions of the microfields, especially the plastic strains in elastoplastic models. When larger windows are used, however, increasingly similar statistical distributions of the microstresses and microstrains are obtained (Shen and Brinson, 2006).

For most combinations of microgeometries and phase materials macrohomogeneous boundary conditions are fairly straightforward to implement in a Finite Element setting. However, in general homogeneous macrostrains cannot be prescribed along boundaries that intersect rigid inhomogeneities and homogeneous tangential tractions cannot be imposed along boundaries that intersect voids.

Mixed Uniform Boundary Conditions

Equations (5.5) are fulfilled by a range of different sets of MUBC, resulting in different estimates for the apparent macroscopic elastic tensors, all of which lie between the lower and upper estimates provided by the macrohomogeneous boundary conditions (Hazanov and Huet, 1994). A specific set of mixed uniform boundary conditions for volume elements that avoids prescribing non-zero boundary tractions was proposed by Pahr and Zysset (2008) for obtaining accurate apparent elastic tensors of volume elements of cellular materials. Table 7.1 lists these conditions which corresponding to six linearly independent mechanical load cases for use with three-dimensional volume elements that have the shape of right hexahedra aligned with the coordinate system. The distances l_1, l_2 and l_3 correspond to

Table 7.1: The six linearly independent uniform strain load cases making up the periodicity compatible mixed uniform boundary conditions (PMUBC) proposed by Pahr and Zysset (2008) and the pertinent boundary conditions for loading by a uniform temperature; East, West, North, South, Top, and Bottom denote the faces of a right hexahedral volume element, compare fig. 6.4, and the the distances l_i correspond to the cell's edge lengths in the 1-, 2- and 3-directions.

	East	West	North	South	Top	Bottom
Tensile 1	$u_1 = \varepsilon^a_{11} l_1/2$ $\tau^a_2 = \tau^a_3 = 0$	$u_1 = -\varepsilon^a_{11} l_1/2$ $\tau^a_2 = \tau^a_3 = 0$	$u_2 = 0$ $\tau^a_1 = \tau^a_3 = 0$	$u_2 = 0$ $\tau^a_1 = \tau^a_3 = 0$	$u_3 = 0$ $\tau^a_1 = \tau^a_2 = 0$	$u_3 = 0$ $\tau^a_1 = \tau^a_2 = 0$
Tensile 2	$u_1 = 0$ $\tau^a_2 = \tau^a_3 = 0$	$u_1 = 0$ $\tau^a_2 = \tau^a_3 = 0$	$u_2 = \varepsilon^a_{22} l_2/2$ $\tau^a_1 = \tau^a_3 = 0$	$u_2 = -\varepsilon^a_{22} l_2/2$ $\tau^a_1 = \tau^a_3 = 0$	$u_3 = 0$ $\tau^a_1 = \tau^a_2 = 0$	$u_3 = 0$ $\tau^a_1 = \tau^a_2 = 0$
Tensile 3	$u_1 = 0$ $\tau^a_2 = \tau^a_3 = 0$	$u_1 = 0$ $\tau^a_2 = \tau^a_3 = 0$	$u_2 = 0$ $\tau^a_1 = \tau^a_3 = 0$	$u_2 = 0$ $\tau^a_1 = \tau^a_3 = 0$	$u_3 = \varepsilon^a_{33} l_3/2$ $\tau^a_1 = \tau^a_2 = 0$	$u_3 = -\varepsilon^a_{33} l_3/2$ $\tau^a_1 = \tau^a_2 = 0$
Shear 12	$u_2 = \varepsilon^a_{21} l_1/2$ $u_3 = 0$, $\tau^a_1 = 0$	$u_2 = -\varepsilon^a_{21} l_1/2$ $u_3 = 0$, $\tau^a_1 = 0$	$u_1 = \varepsilon^a_{12} l_2/2$ $u_3 = 0$, $\tau^a_2 = 0$	$u_1 = -\varepsilon^a_{12} l_2/2$ $u_3 = 0$, $\tau^a_2 = 0$	$u_3 = 0$ $\tau^a_1 = \tau^a_2 = 0$	$u_3 = 0$ $\tau^a_1 = \tau^a_2 = 0$
Shear 13	$u_3 = \varepsilon^a_{31} l_1/2$ $u_2 = 0$, $\tau^a_1 = 0$	$u_3 = -\varepsilon^a_{31} l_1/2$ $u_2 = 0$, $\tau^a_1 = 0$	$u_2 = 0$ $\tau^a_1 = \tau^a_3 = 0$	$u_2 = 0$ $\tau^a_1 = \tau^a_3 = 0$	$u_1 = \varepsilon^a_{13} l_3/2$ $u_2 = 0$, $\tau^a_3 = 0$	$u_1 = -\varepsilon^a_{13} l_3/2$ $u_2 = 0$, $\tau^a_3 = 0$
Shear 23	$u_1 = 0$ $\tau^a_2 = \tau^a_3 = 0$	$u_1 = 0$ $\tau^a_2 = \tau^a_3 = 0$	$u_3 = \varepsilon^a_{32} l_2/2$ $u_1 = 0$, $\tau^a_2 = 0$	$u_3 = -\varepsilon^a_{32} l_2/2$ $u_1 = 0$, $\tau^a_2 = 0$	$u_2 = \varepsilon^a_{23} l_3/2$ $u_1 = 0$, $\tau^a_3 = 0$	$u_2 = -\varepsilon^a_{23} l_3/2$ $u_1 = 0$, $\tau^a_3 = 0$
Thermal Expansion	$u_1 = 0$ $\tau^a_2 = \tau^a_3 = 0$	$u_1 = 0$ $\tau^a_2 = \tau^a_3 = 0$	$u_2 = 0$ $\tau^a_1 = \tau^a_3 = 0$	$u_2 = 0$ $\tau^a_1 = \tau^a_3 = 0$	$u_3 = 0$ $\tau^a_1 = \tau^a_2 = 0$	$u_3 = 0$ $\tau^a_1 = \tau^a_2 = 0$

cell's edge lengths in the 1-, 2- and 3-directions, compare Fig. 6.4. The components of the prescribed strain tensor are denoted as $\varepsilon_{ij}^{\mathrm{a}}$ and those of the prescribed traction vector as τ_i^{a}. Compared to macrohomogeneous boundary conditions the PMUBC lead to much faster convergence of the predicted homogenized properties in terms of the size of the volume elements, similarly to periodicity boundary conditions, compare Section 6.2, and to certain embedding schemes, compare Chapter 8.

The use of these MUBC is not limited to cellular materials, and when applied to periodic volume elements of orthotropic effective behavior, they were found to give very similar predictions for the macroscopic elasticity tensor as does periodic homogenization (Pahr and Böhm, 2008). This led to their being named periodicity compatible mixed uniform boundary conditions (PMUBC). Their behavior with periodic microgeometries indicates that PMUBC can also be used to advantage for obtaining estimates from non-periodic volume elements, at least when the sub-orthotropic contributions to the overall symmetry are relatively small. Accordingly, these boundary conditions offer an attractive option for obtaining estimates of the macroscopic elastic behavior and of macroscopic yield surfaces (Panyasantisuk et al., 2016) on the basis of SVEs.

The concept of periodicity compatible mixed uniform boundary conditions can be extended to thermoelasticity by adding a load case that constrains all displacements normal to the faces of the volume element, sets all in-plane tractions to zero, and applies a uniform temperature increment ΔT, see table 7.1. This allows evaluating the volume averaged specific thermal stress tensor $\langle \boldsymbol{\lambda} \rangle$, from which the apparent thermal expansion tensor can be obtained as $\boldsymbol{\alpha} = -\mathbf{C}\langle \boldsymbol{\lambda} \rangle$, the apparent compliance tensor $\mathbf{C}$ being evaluated from the first six equations of table 7.1.

Mixed uniform boundary conditions for diffusion-like problems were discussed, e.g., by Jiang et al. (2001). Boundary conditions that show an analogous behavior to the PMUBC in elasticity were reported by Jiang et al. (2002a) for thermal conduction in two-dimensional orthotropic periodic media, see table 7.2. The handling of finite interfacial conductances in the context of windowing was studied by Nogales (2008).

Table 7.2: The three linearly independent uniform gradient load cases making up the periodicity compatible mixed uniform boundary conditions (PMUBC) in thermal conduction; East, West, North, South, Top, and Bottom denote the faces of a hexahedral volume element, compare fig. 6.4, the d_i^{a} are the components of the applied temperature gradient, and the the distances l_i can be obtained by scaling the cell's edge lengths, c_i, by a suitable common factor.

	East	West	North	South	Top	Bottom
Thermal 1	$T = d_1^{\mathrm{a}} l_1/2$	$T = -d_1^{\mathrm{a}} l_1/2$	$q_2^{\mathrm{a}} = 0$	$q_2^{\mathrm{a}} = 0$	$q_3^{\mathrm{a}} = 0$	$q_3^{\mathrm{a}} = 0$
Thermal 2	$q_1^{\mathrm{a}} = 0$	$q_1^{\mathrm{a}} = 0$	$T = d_2^{\mathrm{a}} l_2/2$	$T = d_2^{\mathrm{a}} l_2/2$	$q_3^{\mathrm{a}} = 0$	$q_3^{\mathrm{a}} = 0$
Thermal 3	$q_1^{\mathrm{a}} = 0$	$q_1^{\mathrm{a}} = 0$	$q_2^{\mathrm{a}} = 0$	$q_2^{\mathrm{a}} = 0$	$T = d_3^{\mathrm{a}} l_3/2$	$T = d_3^{\mathrm{a}} l_3/2$

In contrast to periodicity and macrohomogeneous boundary conditions, the PMUBC listed in table 7.1 are strictly limited to handling these seven specific load cases if nonlinear behavior is present and the superposition principle ceases to hold. This implies that general load paths in stress and strain space cannot be followed, so that in nonlinear regimes

this type of model is restricted to materials characterization, compare (Pahr and Böhm, 2008).

Certain MUBC, e.g., ones that handle macroscopic uniaxial loading by specifying normal displacements plus zero tangential tractions for one pair of faces and setting all traction components to zero for all other faces, compare, e.g., Galli et al. (2008), can be interpreted physically as describing the behavior of small, inhomogeneous samples[120] as discussed in Section 1.5. Due to the weaker boundary constraints such sample-type (or "structure-type") MUBC can be expected to predict more compliant macroscopic behavior than do the periodicity boundary conditions discussed in Section 6.2 or the PMUBC listed in table 7.1. As mentioned in Section 1.5, structure-type boundary conditions do not involve scale transitions. At this point, it is worth noting that the symmetry BC discussed in Section 6.2 may also be interpreted as a set of MUBC with good convergence properties.

Important strengths of windowing methods lie in providing an approach to studying the behavior of non-periodic volume elements and in being considerably easier to handle than PMAs for periodic volume elements. The main reasons for the latter point are that the meshing of homologous faces is not an issue in windowing and multi-point constraint equations are not required.

[120] In contrast to periodicity BC, these specific MUBC give different results for volume elements made up of a number "base units" compared to models consisting of a single unit. This is in keeping with their interpretation as "structural" rather than "material" models.
If the tangential strains rather than the tangential stresses are set to zero for the pair of faces controlling the macroscopic axial deformation, the physical interpretation is that of a sample "sticking" to the base plates, implying the presence of strain gradients at the length scale of the sample. Such models are not capable of describing a proper uniaxial stress load case.

Chapter 8

Embedding Approaches and Related Models

Embedded Cell Approaches (ECAs) aim at predicting the microfields in specific, geometrically highly resolved (sub)regions of models of inhomogeneous materials or structures. Such models consist of two parts, as is evident in figs. 8.1 and 8.2. On the one hand, there is a core (or "local heterogeneous region") consisting of a discrete microstructure ("motif"), which can range from rather simple to highly complex phase arrangements. On the other hand, there is a homogeneous outer region ("embedding region", "frame", "effective region") into which the core is embedded and which serves mainly for transmitting the applied loads. Embedding strategies tend to give rise to relatively complex models, but they avoid the main drawback of PMAs, viz., the requirement that the microgeometry and all microfields must be periodic.

An intrinsic feature of embedding models are boundary layers that occur at the "interfaces" between the core and the embedding region and perturb the local stress and strain fields[121], see, e.g., Harper et al. (2012a) and compare Section 5.2. Provision must be made to keep regions of specific interest, such as crack tips or process zones, at a sufficient distance from the boundary layers[122], which, in turn, implies that cores must exceed some minimum size in order to provide useful results.

Most of the embedding approaches reported in the literature for tasks related to continuum micromechanics fall into two groups.

[121] The interfaces between core and embedding region are a consequence of the modeling approach and do not have any physical background or significance. In elasticity such boundary layers typically have a thickness of at least the distance between the centers of neighboring inhomogeneities, but they may be longer ranged for nonlinear material behavior.

[122] Boundary layers and embedding regions may interfere with extended regions of concentrated strains, with shear bands, or with the growth of damaged regions. Such difficulties can only be avoided or mitigated by choosing a sufficiently large core region. In dynamic models the boundaries between core and embedding region may lead lead to the reflection and/or refraction of waves. Special transition layers can, however, be introduced to mitigate boundary layer effects in the latter case.

Embedding Region with Self-Consistently Determined Response

One group of embedding schemes employ the homogenized thermomechanical response of the core for determining the effective behavior of the surrounding medium via self-consistent procedures. By applying suitable uniform far-field loads to the outer boundaries of such an embedding layer, as sketched in Fig. 8.1, models of this type can be used for carrying out scale transitions in terms of homogenization and, with some precautions, localization.

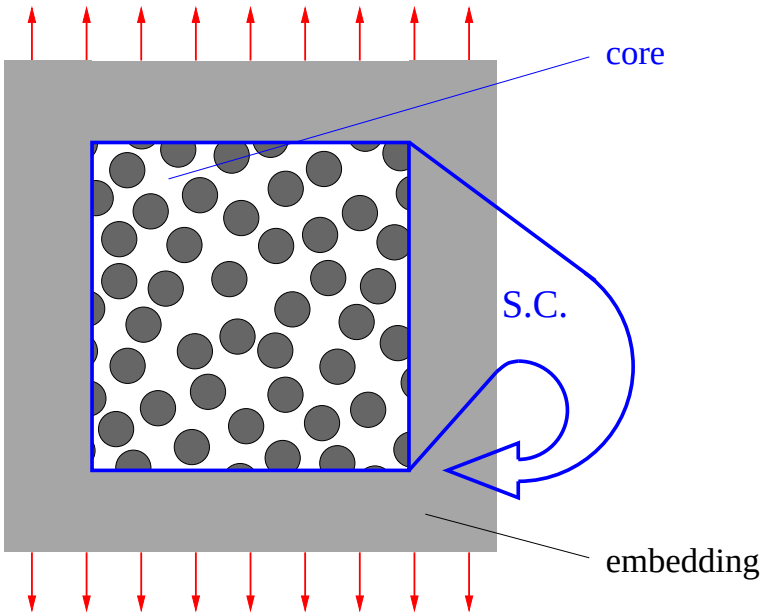

Figure 8.1: Schematic depiction of the arrangement of core and embedding region in a self-consistent embedded cell model subjected to a uniform far-field load.

As mentioned in Section 5.2 self-consistent embedding schemes employing macrohomogeneous or periodic boundary conditions[123] provide predictions for the effective elasticity tensors that lie between the lower and upper estimates on the apparent tensors and, by extension, within the mesoscale bounds discussed in Chapter 7. Such approaches, in which the embedding layer mainly serves for smoothening out fluctuations at the core's boundaries was termed the "Window Method" by some authors (Krabbenhøft et al., 2008; Temizer et al., 2013), and the smeared-out embedding region has been termed an "augmentation strip" (Babuška et al., 1999) or an "envelope surrounding the RVE" (Vazeille and Laberge Lebel, 2024). In a similar vein, the use of a self-consistent embedding "buffer layer" has been proposed for models in which periodicity boundary conditions are applied to non-periodic volume elements (Makowski et al., 2013). Methods of this type typically aim at carrying out scale transitions and, accordingly, the core should at least approach the size of a proper RVE.

[123] In such schemes either the full core (including the boundary layers) or core's interior (the regions affected by the boundary layer being discarded) may be used for evaluating the effective responses. In their analysis of such self-consistent schemes (Temizer et al., 2013) take the former approach. For elastic spherical inhomogeneities in an elastic matrix the thickness of the boundary layer may be estimated as four particle radii (Buryachenko, 2007).

Because they involve self-consistent iterations, self-consistent embedding methods tend to be more expensive numerically than are periodic homogenization and windowing analysis (in the sense of Chapter 7). In the elastic regime, however, the required number of iterations tends to be fairly low and the approach has been shown to be unconditionally stable by Salit and Gross (2014). A number of issues in choosing the width of the embedding layer for thermoelastic analysis were discussed by Temizer et al. (2013).

The use of self-consistency procedures is, of course, predicated on the availability of suitable parameterizable constitutive laws for the embedding material that can follow the core's (instantaneous) homogenized behavior with high accuracy for all load cases and loading histories considered. This requirement can typically be fulfilled easily in the linear range, see e.g., Yang et al. (1994) and Chen et al. (1994), but may lead to considerable complexity when at least one of the constituents shows elastoplastic or viscoplastic material behavior[124]. Accordingly, approximations may have to be used (the consequences of which may be difficult to assess in view of the nonlinearity and path dependence of such material behaviors) and models of this type are best termed "quasi-self-consistent schemes". Approaches of this type were discussed, e.g., by Bornert et al. (1994) and by Dong and Schmauder (1996).

Self-consistent and quasi-self-consistent embedding models are not suitable for handling "strong features", such as localized cracks of the type shown in fig. 8.2, within the core and their physical interpretation may be difficult when the core includes subregions subject to damage.

Embedding Region with Prescribed Material Response

In the other group of embedding methods the material behavior of the outer region is described via appropriate, pre-defined, "smeared-out" constitutive models. These typically take the form of semi-empirical or micromechanically based constitutive laws that are prescribed a priori for the embedding zone and are chosen to represent the appropriate (usually damage-free) material behavior[125]. This way, conceptually simple models are obtained that are very well suited to studying local phenomena such as the stress and strain

[124]Typically, the effective yielding behavior of elastoplastic composites shows some dependence on the first stress invariant, and, for low plastic strains, the homogenized response of the core tends to be strongly influenced by the fractions of the elastoplastic constituent(s) that have actually yielded. In addition, in many cases anisotropy of the yielding and hardening behavior is induced by the phase topology (e.g., aligned fibers) and/or by the phase arrangement of the core. Identifying constitutive laws that, on the one hand, can satisfactorily account for such phenomena and, on the other hand, have the capability of being easily adapted to the instantaneous homogenized responses of the core by adjusting free parameters, poses an important challenge in applying self-consistent embedding schemes to nonlinear material behavior.

[125]The constitutive model and the pertinent material parameters required for the embedding layer may be obtained, e.g., from micromechanical modeling or from experiments (Ayyar et al., 2008).
The description chosen for the embedding region must reflect the material symmetry, e.g., for metal matrices reinforced by continuous fibers the yield surface, the flow rule and the hardening behavior must account for these materials' marked anisotropy in the elastoplastic regime.
When the core is used for studying local damage and failure, special care should be exercised with respect to its boundary regions — the perturbed local stress and strain fields there may conceivably trigger unphysical behavior. However, if failure or localized damage are restricted to the core this may impact the generality of models, compare, e.g., Bao (1992).

distributions in the vicinity of crack tips (Aoki et al., 1996), around local defects (Xia et al., 2001) or at macroscopic interfaces in composites (Chimani et al., 1997), the growth of cracks in inhomogeneous materials (van der Giessen and Tvergaard, 1994; Wulf et al., 1996; Motz et al., 2001; Mishnaevsky, 2004; González and LLorca, 2007), the behavior of composites close to an indenter (Shedbale et al., 2017), or the damage due to the processing of composites (Monaghan and Brazil, 1997).

In applications of this type loads may be applied or displacement boundary conditions may be specified that impose a far-field behavior obtained from a suitable analytical or numerical solution (e.g., the displacements describing the far-field of a crack tip in elasticity or small-scale plasticity) pertinent to the problem under study. Alternatively, the embedding region may be chosen to represent the structure or sample to be considered, with the core zooming in on a detail of special interest. Such approaches, which may be viewed as a type of concurrent multiscale modeling scheme, allow complete specimens or components to be studied via "simulated experiments" as sketched in fig. 8.2.

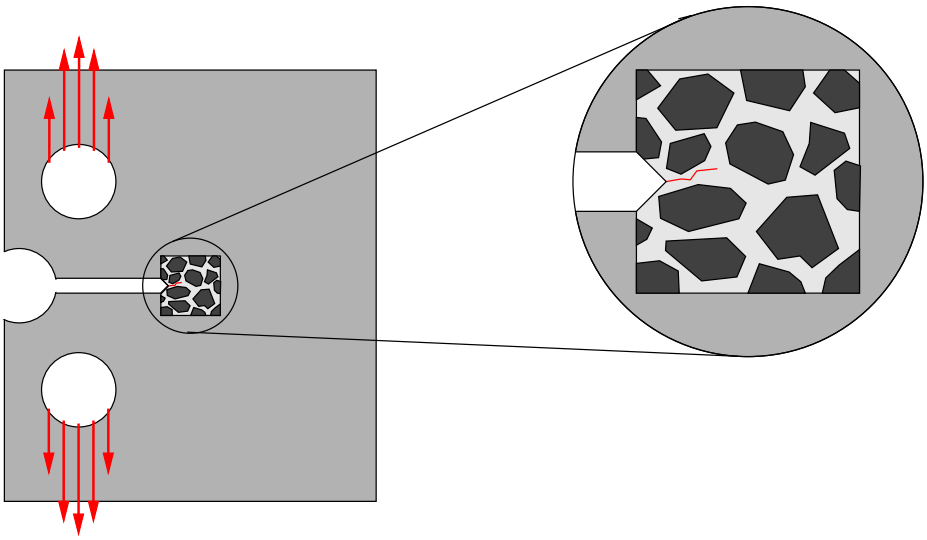

Figure 8.2: Schematic depiction of the arrangement of core and embedding region in an embedded cell model of a tensile test specimen.

Embedding models making use of prescribed properties for the embedding region are not the best choice for homogenization analysis — they may rather be viewed as methods specialized towards localization. On the one hand, this arguably makes them the most versatile and powerful tool for looking in detail at "strong features" in some region of interest. Embedding models of this kind can be used without intrinsic restrictions at or in the vicinity of free surfaces and interfaces, they can handle gradients in composition and loads, and they can be employed for studying the interaction of macrocracks with microstructures[126] following fig. 8.2. It is worth noting that for such models typically it is not of major importance whether the core is a proper RVE or not — embedding models

[126]The requirement of sufficiently separated length scales, compare Section 1.1, does not necessarily apply to embedded models. Care is, however, required, with highly nonlinear analyses, especially with models involving damage, where the inherent perturbations at boundaries between core and embedding region may trigger spurious behavior.

of this type do not involve scale transitions. In fact, it may make sense to use phase arrangements for the core that are known (or suspected) to be critical for the behavior to be studied rather than being representative, in the spirit of a worst case analysis. The core must, however, be of sufficient size for keeping perturbations due to boundary layer effects at a suitably low level in its critical regions.

Other Embedding Strategies, Submodeling Schemes and Related Approaches

Another approach related to embedding uses discrete microstructures in both the core region and in the surrounding material, the latter, however, being discretized by a much coarser FE mesh, see, e.g., Sautter et al. (1993). Such models, which are also referred to as "fine mesh window" approaches (Podgórski, 2011) and are essentially descriptions of full samples or structures that contain a refined mesh in some region(s) of interest, can avoid boundary layers to a considerable extent by using appropriately graded meshes. They tend, however, to be rather expensive computationally due to the need for relatively highly resolved "sacrificial" zones in the embedding region that only serve to insulate the core from the boundary layers (Harper et al., 2012a). Mesh superposition techniques, which use a coarse mesh over the macroscopic model of some structure or sample together with a geometrically independent, much finer mesh in regions of interest (Takano et al., 2001) are conceptually similar to the above modeling strategy.

A closely related approach makes use of submodeling techniques in which an inhomogeneous micromodel is weakly or strongly coupled to a homogeneous macromodel via appropriate coupling conditions (which may be implemented via the boundary conditions of the micromodel), compare, e.g., Heness et al. (1999) or Váradi et al. (1999). Similarly, far-field strains obtained from an unperturbed periodic model subjected to appropriate loads or loading histories may be used as boundary conditions for a region containing a local microstructural perturbation, compare Aboudi and Ryvkin (2012). Such modeling strategies are conceptually related, on the one hand, to embedding models of the type shown in Fig. 8.2 and, on the other hand, to the "inhomogeneous structure models" mentioned in Section 1.5.

Additional Remarks on Embedding Schemes

When a periodic multi-inhomogeneity volume element is used as the core in a self-consistent or quasi-self-consistent embedding scheme, the concomitant relaxation of the periodicity constraints tends to make the overall responses of the embedded configuration more compliant compared to proper periodic homogenization of the periodic arrangement (Bruzzi et al., 2001)[127].

Some analytical methods such as classical and generalized self-consistent schemes, see Section 2.3, can obviously be viewed as embedding schemes that combine relatively simple

[127]In the study mentioned above, the difference between PMA and ECA results is relatively small. Identical responses can be expected from the two types of model if the core takes the form of a proper RVE (so that by definition the boundary conditions do not play a role in the effective behavior) and the embedding material can fully describe the homogenized behavior of the core.

cores with self-consistently defined material behavior of the embedding region. When geometrically more complex cores are considered in ECA-like frameworks, however, numerical engineering methods are best suited for resolving the discrete phase arrangements in the core region, compare Bornert (1996).

The core and embedding regions may be planar, axisymmetric or fully three-dimensional, and symmetries present in the geometries can, as usual, be made us of for reducing the size of the model, compare Xia et al. (2001). Effective and phase averaged stresses and strains from embedded cell models are best evaluated via eqn. (1.4) or its equivalents, and it is typically preferable to use only the central regions of the core for this purpose in order to avoid perturbations from the boundary layers.

All embedding techniques discussed above can also be used in analogy for studying the thermal conduction behavior of inhomogeneous materials.

Chapter 9

Hierarchical and Multi-Scale Models

The micromechanical methods discussed in Chapters 2, 6, and 7 are designed for handling a single scale transition between a lower and a higher length scale ("microscale" and "macroscale"), overall responses being obtained by homogenization and local fields by localization. Many inhomogeneous materials, however, show more than two clearly distinct characteristic length scales, typical examples being laminated and woven composites (compare Section 6.4), materials in which there are well defined clusters of particles, as well as most biomaterials. In such cases an obvious modeling strategy is a hierarchical approach that uses a sequence of scale transitions, i.e., the material response at any given length scale is described on the basis of the homogenized behavior of the next finer one[128]. Figure 9.1 schematically shows such a hierarchical model for a particle-reinforced composite with a clustered mesostructure.

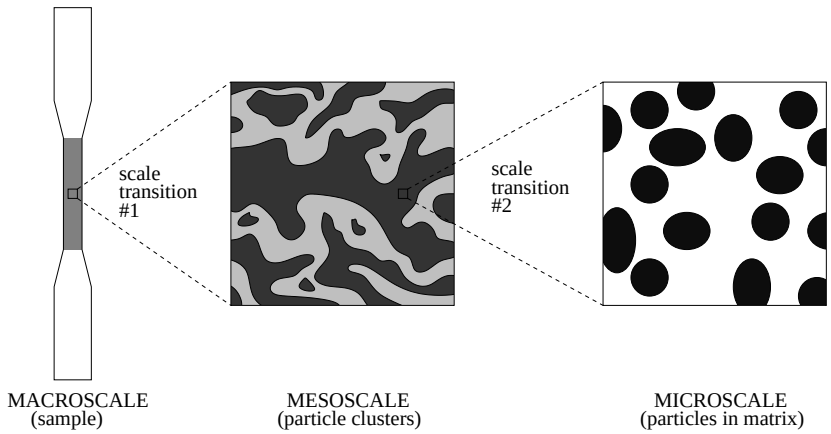

Figure 9.1: Schematic representation of a hierarchical approach to studying a material consisting of clustered inhomogeneities in a matrix. Two scale transitions, macro⟷meso and meso⟷micro, are used.

A hierarchical model can be viewed as involving a sequence of scale transitions, and suitable micromechanical models, i.e., mean-field, unit cell, windowing and, to some extent,

[128]Describing the material behavior at lower length scales by a homogenized model implies that characteristic lengths differ by more than, say, an order of magnitude, so that valid homogenization volumes can be defined (there may, however, be exceptions in the case of linear material behavior). Employing hierarchical approaches within "bands" of more or less continuous distributions of length scales, as can be found, e.g., in some metallic foams with highly disperse cell sizes, requires specialized methods.

embedding approaches, may be used as "building blocks" at any level within hierarchical schemes. Such hierarchical modeling strategies have the additional advantage of allowing the behavior of the constituents at all lower length scales to be assessed via the corresponding localization relations. Multiscaling methods can be classified into concurrent and sequential approaches (Chakraborty and Rahman, 2008; Tadmor and Miller, 2011), with the former requiring the physical problem to be studied simultaneously at all length scales involved.

Among the continuum mechanical hierarchical descriptions of the thermomechanical behavior of inhomogeneous materials reported in the literature, some have combined mean-field methods at the higher length scale with mean-field (Hu et al., 1998; Tszeng, 1998) or periodic microfield approaches (González and LLorca, 2000) at the lower length scale. A common strategy for hierarchical modeling, however, uses Finite Element based unit cell or embedding methods at the topmost length scale, which implies that the homogenized material models describing the lower level(s) of the hierarchy must be proper constitutive laws (i.e., material descriptions that are capable of handling any loading conditions and any loading history) that are evaluated at each integration point of the discretized model. For this purpose, either explicit, micromechanically-based constitutive models may be used or micromechanical models may be run at each integration point, the results of which provide "implicit" descriptions of the local material behavior. The models used for such purposes may be analytical, semi-analytical or numerical.

For the elastic range, generating a micromechanically based constitutive description at each integration point of the "macroscopic" model typically does not pose massive computational requirements, even if different microscopic models are used for different regions of the macromodel; furthermore, in such a setting decomposition techniques may be used to formulate the problems at the finer length scales in such a way that they are well suited for parallel processing, allowing the development of computationally highly efficient multi-scale procedures, see, e.g., Oden and Zohdi (1997). Once the appropriate homogenized elasticity and thermal concentration tensors have been generated any load case can be handled, often in a sequential mode. For simulating the thermomechanical response of inelastic inhomogeneous materials, however, essentially a full micromechanical submodel has to be maintained and solved for at each integration point, which amounts to fully concurrent procedures[129]. Although within such frameworks the use of sophisticated numerical models at the lower length scales tends to be an expensive proposition in terms of computational requirements, this concept has elicited major research interest, especially within the framework of multi-scale models (Belsky et al., 1995; Ghosh et al., 1996; Lee and Ghosh, 1996; Zohdi et al., 1996; Smit et al., 1998; Feyel and Chaboche, 2000; Fish and Shek, 2000; Ibrahimbegović and Markovič, 2003; Moës et al., 2003; Tan et al., 2020). Pertinent overviews were given by Ghosh et al. (2001), Kanouté et al. (2009), Geers et al. (2010) as well as Nguyen et al. (2011).

[129]Some approaches have been reported that aim at decoupling the scales by parameterizing results from microscopic full field analysis and using this data together with an interpolation scheme as an "approximate constitutive model", see, e.g., Terada and Kikuchi (1996), Gänser (1998) or Schrefler et al. (1999). A major challenge in this type of sequential modeling strategy lies in handling the load history and load path dependences required for elastoplastic local behavior of and/or microscopic damage to the constituents. Appropriate representation of general multiaxial stress and/or strain states also tends to be difficult.

It is worth noting that in models of this type (which are often referred to as FE^2 procedures) no explicit material law is used on the macroscale, the full constitutive behavior being determined concurrently at the microscale. Arguably, such approaches at present represent the most sophisticated application of the concepts of continuum micromechanics.

Lower (but by no means negligible) computational costs can be achieved by using mean-field models in lieu of constitutive models at the integration point level. Applications to elastoplastic composites have included incremental Mori–Tanaka methods, see, e.g., Pettermann (1997) and mean-field based versions of the Transformation Field Analysis, compare, e.g., Fish and Shek (1998) or Plankensteiner (2000). In addition, the semi-analytical non-uniform TFA has been employed for this purpose (Michel and Suquet, 2004). Figure 9.2 shows a result obtained by applying a multiscale approach that uses an incremental Mori–Tanaka method, compare Section 2.9, at the integration point level of a two-dimensional meso-scale unit cell model for describing the elastoplastic behavior of a cluster-structured high speed steel. The particle-rich and particle-poor regions used for the description at the mesoscale are treated as particle-reinforced MMCs with appropriate reinforcement volume fractions. Such a model not only predicts macroscopic stress–strain curves, but also allows the mesoscopic distributions of phase averaged microscopic variables to be evaluated, compare (Plankensteiner, 2000). For an example of an Extended Finite Element method at the upper length scale coupled to a semi-analytical model at the lower one see Novák et al. (2012).

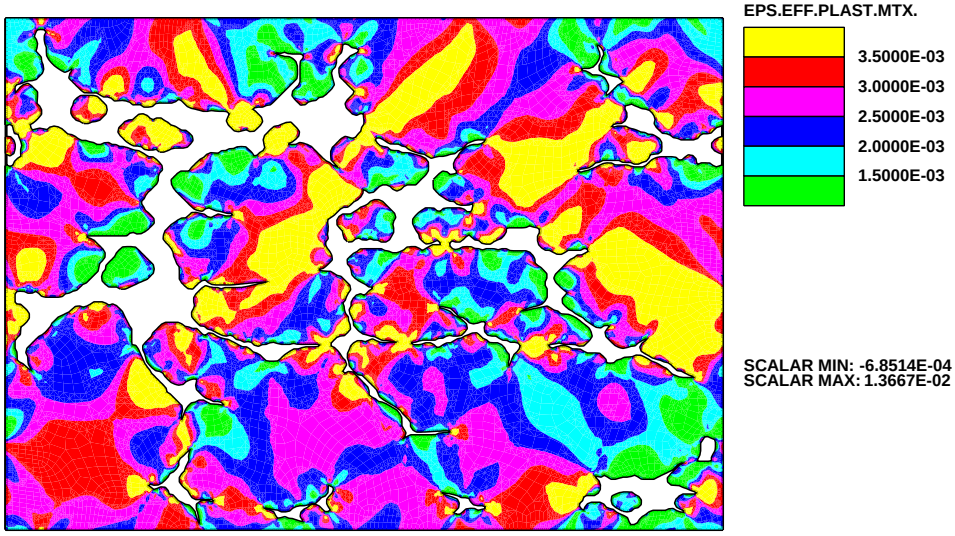

Figure 9.2: Phase averaged microscopic equivalent plastic strains in the matrix within the inhomogeneity-poor regions of a cluster-structured high speed steel under mechanical loading as predicted by a mesoscopic unit cell model combined with an incremental Mori–Tanaka model at the microscale (Plankensteiner, 2000).

Alternatively, multiscale approaches may be rather "loosely coupled", essentially linking together quite different models to obtain an overall result, see, e.g., (Onck and van der Giessen, 1997).

A further development are concurrent multi-scale methods in which the computational domain is adaptively split into regions resolved at the appropriate length scale. In an FE-based hierarchical framework developed by Ghosh et al. (2001) "non-critical" regions are described by continuum elements with pre-homogenized material properties, and for zones of clearly nonlinear behavior PMA models are automatically activated at the integration points to monitor the phase behavior at the microscale. If local behavior exceeding the capabilities of periodic homogenization is detected (e.g., progressive damage, mesoscopic interfaces, free edges), embedded models of the fully resolved microgeometry may be activated at the appropriate positions, compare Raghavan and Ghosh (2004). Such strategies allow detailed studies of critical regions in inhomogeneous materials, e.g., near free edges. In an alternative approach, homogenization models employing generalized continua have been proposed for handling regions close to free surfaces and zones with high local field gradients (Feyel, 2003).

Finally, it is worth noting that hierarchical and multi-scale approaches are not limited to using the "standard" methods of continuum micromechanics as discussed above. Especially the capability of the Finite Element method of handling highly complex constitutive descriptions has been used to build hierarchical approaches that employ, among others, material models based on crystal plasticity (McHugh et al., 1993) and discrete dislocation plasticity (Cleveringa et al., 1997).

The linking of continuum and atomistic descriptions has been an important goal of modeling work for a considerable time, involving, e.g., concurrent homogenization schemes, compare Curtin and Miller (2003) and, for a view on recent and future developments, van der Giessen et al. (2020). The equivalent of homogenization in such settings is often referred to as "upwards linking", that to localization being known as "downward linking".

Chapter 10

Closing Remarks

The research field of continuum micromechanics of materials has enjoyed considerable success in the past four decades in furthering the understanding of the thermomechanical behavior of inhomogeneous materials and in providing predictive tools for engineers and materials scientists. However, its methods are subject to some practical limitations that should be kept in mind when employing them.

All the methods discussed in Chapters 2 to 7 implicitly use the assumption that the constituents of the inhomogeneous material to be studied can be treated as homogeneous at the lower length scale, which, of course, does not necessarily hold. When the length scale of the inhomogeneities in a constituent is much smaller than the length scale of the phase arrangement to be studied, the above assumption is valid and hierarchical as well as multiscale models ("successive homogenization") as discussed in Chapter 9 can be used (Carrère, 2001). However, no rigorous theory appears to be available at present for handling scale transitions in materials that do not fulfill the above requirement (e.g., particle-reinforced composites in which the grain size of the matrix is comparable to or even larger than the size of the particles[130]). Typically the best that can be done in such cases is either to use sufficiently detailed models with resolved microgeometry (potentially, a computationally very expensive proposition) or to employ homogenized phase properties and be aware of the approximation that is introduced.

A major practical difficulty in the use of continuum micromechanics approaches (which in many cases is closely related to the questions mentioned above) has been identifying appropriate constitutive models and obtaining the required material parameters for the constituents. Typically, available data pertain to the behavior of the bulk materials (as measured from homogeneous macroscopic samples), whereas the actual requirement is for parameters and, in some cases, constitutive theories that describe the in-situ response of the constituents at the microscale. For example, with respect to MMCs, on the one hand, there is considerable evidence that classical continuum plasticity theories (in which there is no absolute length scale) cannot adequately describe the behavior of metallic materials in the presence of strong strain gradients, where geometrically necessary dislocations can markedly influence the material behavior (Hutchinson, 2000). On the other hand,

[130] For this special case unit cell or embedding models employing anisotropic or crystal plasticity models for the phases may be used which, however, can become very large when the statistics of grain orientation are accounted for.

it is well known that the presence of reinforcements can lead to accelerated aging and refinement of the grain size in the matrix ("secondary strengthening"). Furthermore, in many cases reasonably accurate material parameters are essentially not available (e.g., strength parameters for most interfaces in inhomogeneous materials). In fact, the dearth of dependable material parameters is one of the reasons why predictions of the strength of inhomogeneous materials by micromechanical methods tend to be a considerable challenge.

Another point that should be kept in mind is that continuum micromechanical descriptions in most cases do not have absolute length scales unless a length scale is introduced explicitly, typically via the constitutive model(s) of one (or more) of the constituents[131]. In this vein, absolute length scales, on the one hand, may be provided explicitly via discrete dislocation models (Cleveringa et al., 1997), via gradient or nonlocal constitutive laws, see, e.g., Tomita et al. (2000) or Niordson and Tvergaard (2001), or via (nonlocal) damage models. On the other hand, they may be introduced in an ad-hoc fashion, e.g., by adjusting the phase material parameters to account for grain sizes via the Hall–Petch effect. Analysts should also be aware that absolute length scales may be introduced inadvertently into a model by mesh dependence effects of discretizing numerical methods, a "classical" example being strain localization due to softening material behavior of a constituent. When hierarchical or multi-scale models are used special care may be necessary to avoid introducing inconsistent length scales at different modeling levels.

In addition it is worth noting that usually the macroscopic responses of inhomogeneous materials (and, as a consequence of eqns. (2.8) to (2.12), the phase averages of the microfields) are much less sensitive to the phase arrangement (and to modeling approximations) than are the distributions of the microfields. Accordingly, whereas good agreement in the overall behavior of a given model with "benchmark" theoretical results or experimental data typically indicates that the phase averages of stresses and strains are described satisfactorily, this does not necessarily imply that the higher statistical moments of the stress and strain distributions (and thus the heterogeneity of these fields) are captured sufficiently accurately.

It is important to be aware that work in the field of micromechanics of materials invariably involves finding viable compromises in terms of the complexity of the models, which, on the one hand, have to be able to account (at least to a reasonably good approximation) for the physical phenomena relevant to the given problem, and, on the other hand, must be sufficiently simple to allow solutions to be obtained within the relevant constraints of time, cost, and computational resources. Obviously, actual problems cannot be solved without recourse to various approximations and tradeoffs — the important point is to be aware of them and to account for them in interpreting and assessing results. It is worth keeping in mind that there is no such thing as a "best micromechanical approach" to all problems.

[131] One important exception are models for studying macroscopic cracks (e.g., via embedded cells), where the crack length does introduce an absolute length scale.
It is worth noting that the behavior of nanocomposites is typically dominated by interfaces (or interphases). Appropriately accounting for this behavior may require the introduction of an absolute length scale. Within the framework of mean-field methods this may be achieved by introducing surface terms into the Eshelby tensor, see, e.g., Duan et al. (2005).

Bibliography

N. Abolfathi, A. Naik, G. Karami, and C. Ulven. A micromechanical characterization of angular bidirectional fibrous composites. *Comput.Mater.Sci.*, 43:1193–1206, 2008. doi:10.1016/j.commatsci.2008.03.017.

J. Aboudi. The generalized method of cells and high-fidelity generalized method of cells micromechanical models — A review. *Mech.Adv.Mater.Struct.*, 11:329–366, 2004. doi:10.1080/15376490490451543.

J. Aboudi. Damage in composites — modeling of imperfect bonding. *Compos.Sci.Technol.*, 28:103–128, 1987. doi:10.1016/0266-3538(87)90093-5.

J. Aboudi. Micromechanical analysis of composites by the method of cells. *Appl.Mech.Rev.*, 42:193–221, 1989. doi:10.1115/1.3152428.

J. Aboudi. *Mechanics of Composite Materials*. Elsevier, Amsterdam, 1991. ISBN 0-444-88452-1.

J. Aboudi. Micromechanical analysis of composites by the method of cells — Update. *Appl.Mech.Rev.*, 49:S83–S91, 1996. doi:10.1115/1.3101981.

J. Aboudi and M. Ryvkin. The effect of localized damage on the behavior of composites with periodic microstructure. *Int.J.Engng.Sci.*, 52:41–55, 2012. doi:10.1016/j.ijengsci.2011.12.001.

D.W. Abueidda, M. Bakir, A.K. Abu Al-Rub, J.S. Bergström, N.A. Sobh, and I. Jasiuk. Mechanical properties of 3D printed polymer cellular materials with triply periodic minimal surface architectures. *Mater.Design*, 122:255–267, 2017. doi:10.1016/j.matdes.2017.03.018.

M.L. Accorsi. A method for modeling microstructural material discontinuities in a finite element analysis. *Int.J.Num.Meth.Engng.*, 26:2187–2197, 1988. doi:10.1002/nme.1620261004.

J.D. Achenbach and H. Zhu. Effect of interfacial zone on mechanical behavior and failure of fiber-reinforced composites. *J.Mech.Phys.Sol.*, 37:381–393, 1989. doi:10.1016/0022-5096(89)90005-7.

K. Acton, C. Sherod, B. Bahmani, and R. Abedi. Effect of volume element geometry on convergence to a representative volume. *J.Risk Uncert.Engng.Syst.B*, 5:030907, 2019.

D.F. Adams and D.A. Crane. Finite element micromechanical analysis of a unidirectional composite including longitudinal shear loading. *Comput.Struct.*, 18:1153–1165, 1984. doi:10.1016/0045-7949(84)90160-3.

D.F. Adams and D.R. Doner. Transverse normal loading of a uni-directional composite. *J.Compos.Mater.*, 1:152–164, 1967. doi:10.1177/002199836700100205.

S.G. Advani and C.L. Tucker. The use of tensors to describe and predict fiber orientation in short fiber composites. *J.Rheol.*, 31:751–784, 1987. doi:10.1122/1.549945.

D.H. Allen and J.W. Lee. The effective thermoelastic properties of whisker-reinforced composites as functions of material forming parameters. In G.J. Weng, M. Taya, and H. Abé, editors, *Micromechanics and Inhomogeneity*, pages 17–40, New York, NY, 1990. Springer-Verlag. doi:10.1007/978-1-4613-8919-4_2.

H. Altendorf and D. Jeulin. Random-walk-based stochastic modeling of three-dimensional fiber systems. *Phys.Rev. E*, 83:041804, 2011. doi:10.1103/PhysRevE.83.041804.

A. Anthoine. Derivation of the in-plane elastic characteristics of masonry through homogenization theory. *Int.J.Sol.Struct.*, 32:137–163, 1995. doi:10.1016/0020-7683(94)00140-R.

T. Antretter. *Micromechanical Modeling of High Speed Steel*. Reihe 18, Nr. 232. VDI–Verlag, Düsseldorf, 1998. ISBN 3-18-323218-9.

S. Aoki, Y. Moriya, K. Kishimoto, and S. Schmauder. Finite element fracture analysis of WC–Co alloys. *Engng.Fract.Mech.*, 55:275–287, 1996. doi:10.1016/0013-7944(96)00021-5.

P. Arbenz, G.H. van Lenthe, U. Mennel, R. Müller, and M. Sala. Multi-level μ-finite element analysis for human bone structures. In B. Kagström, E. Elmroth, J. Dongarra, and J. Wasniewski, editors, *Applied Parallel Computing. State of the Art in Scientific Computing*, pages 240–250, Berlin, 2008. Springer-Verlag. doi:10.1007/978-3-540-75755-9_30.

R.T. Arenburg and J.N. Reddy. Analysis of metal-matrix composite structures — I. Micromechanics constitutive theory. *Comput.Struct.*, 40:1357–1368, 1991. doi:10.1016/0045-7949(91)90407-D.

J.L. Auriault. Upscaling heterogeneous media by asymptotic expansions. *J.Engng.Mech.*, 128:817–822, 2002. doi:10.1061/(ASCE)0733-9399(2002)128:8(817).

J.L. Auriault. Effective macroscopic description for heat conduction in periodic composites. *Int.J.Heat Mass Transf.*, 26:861–869, 1983. doi:10.1016/S0017-9310(83)80110-0.

M. Avellaneda. Iterated homogenization, differential effective medium theory, and applications. *Comm.Pure Appl.Math.*, 40:803–847, 1987. doi:10.1002/cpa.3160400502.

M.S. Axelsen and R. Pyrz. Correlation between fracture toughness and the microstructure morphology in transversely loaded unidirectional composites. In R. Pyrz, editor, *Microstructure–Property Interactions in Composite Materials*, pages 15–26, Dordrecht, 1995. Kluwer Academic Publishers. doi:10.1007/978-94-011-0059-5_2.

A. Ayyar, G.A. Crawford, J.J. Williams, and N. Chawla. Numerical simulation of the effect of particle spatial distribution and strength on tensile behavior of particle reinforced composites. *Comput.Mater.Sci.*, 44:496–506, 2008. doi:10.1016/j.commatsci.2008.04.009.

I. Babuška, B. Andersson, P.J. Smith, and K. Levin. Damage analysis of fiber composites. Part I: Statistical analysis on fiber scale. *Comput.Meth.Appl.Mech.Engng.*, 172:27–77, 1999. doi:10.1016/S0045-7825(98)00225-4.

Y. Bai, C.Z. Dong, and Z.Y. Liu. Effective elastic properties and stress states of doubly periodic array of inclusions with complex shapes by isogeometric boundary element method. *Compos.Struct.*, 128:54–69, 2015. doi:10.1016/j.compstruct.2015.03.061.

D. Balzani, D. Brands, J. Schröder, and C. Carstensen. Sensitivity analysis of statistical measurements for the reconstruction of microstructures based on the minimization of generalized least-square functionals. *Techn.Mech.*, 30:297–315, 2010. URL `https://journals.ub.ovgu.de/index.php/techmech/article/view/800`.

P.K. Banerjee and D.P. Henry. Elastic analysis of three-dimensional solids with fiber inclusions by BEM. *Int.J.Sol.Struct.*, 29:2423–2440, 1992. doi:10.1016/0020-7683(92)90001-A.

L. Banks-Sills and V. Leiderman. Macro-mechanical material model for fiber-reinforced metal matrix composites. *Composites B*, 30:443–452, 1999. doi:10.1016/S1359-8368(99)00018-9.

Y. Bansal and M.J. Pindera. Finite-volume direct averaging micromechanics of heterogeneous materials with elastic-plastic phases. *Int.J.Plast.*, 22:775–825, 2006. doi:10.1016/j.ijplas.2005.04.012.

G. Bao. Damage due to fracture of brittle reinforcements in a ductile matrix. *Acta.metall. mater.*, 40:2547–2555, 1992. doi:10.1016/0956-7151(92)90324-8.

G. Bao, J.W. Hutchinson, and R.M. McMeeking. Particle reinforcement of ductile matrices against plastic flow and creep. *Acta metall.mater.*, 39:1871–1882, 1991. doi:10.1016/0956-7151(91)90156-U.

R.B. Barello and M. Lévesque. Comparison between the relaxation spectra obtained from homogenization models and finite elements simulation for the same composite. *Int.J.Sol.Struct.*, 45:850–867, 2008. doi:10.1016/j.ijsolstr.2007.09.002.

S. Bargmann, B. Klusemann, J. Markmann, J.E. Schnabel, K. Schneider, C. Soyarslan, and J. Wilmers. Generation of 3D representative volume elements for heterogeneous materials: A review. *Prog.Mater.Sci.*, 96:322–384, 2018. doi:10.1016/j.pmatsci.2018.02.003.

B. Barroqueiro, J. Dias-de-Oliveira, J. Pinho-da-Cruz, and A. Andrade-Campos. Practical implementation of asymptotic expansion homogenisation in thermoelasticity using a commercial simulation software. *Compos.Struct.*, 141:117–131, 2016. doi:10.1016/j.compstruct.2016.01.036.

J.F. Barthélémy. Simplified approach to the derivation of the relationship between Hill polarization tensors of transformed problems and applications. *Int.J.Engng.Sci.*, 154: 103326, 2020. doi:10.1016/j.ijengsci.2020.103326.

N.D. Barulich, L.A. Godoy, and P.M. Dardati. A simple procedure to evaluate Cauchy stress tensor at the macro level based on computational micromechanics under general finite strain states. *Mech.Mater.*, 117:73–80, 2018. doi:10.1016/j.mechmat.2017.10.008.

J.L. Bassani, A. Needleman, and E. van der Giessen. Plastic flow in a composite: Comparison of nonlocal continuum and discrete dislocation predictions. *Int.J.Sol.Struct.*, 38: 833–853, 2001. doi:10.1016/S0020-7683(00)00059-7.

V. Belsky, M.W. Beall, J. Fish, M.S. Shephard, and S. Gomaa. Computer-aided multiscale modeling tools for composite materials and structures. *Comput.Syst.Engng.*, 6:213–223, 1995. doi:10.1016/0956-0521(95)00019-V.

Y. Benveniste. A new approach to the application of Mori–Tanaka's theory in composite materials. *Mech.Mater.*, 6:147–157, 1987. doi:10.1016/0167-6636(87)90005-6.

Y. Benveniste. Some remarks on three micromechanical models in composite media. *J.Appl.Mech.*, 57:474–476, 1990. doi:10.1115/1.2892016.

Y. Benveniste and G.J. Dvorak. On a correspondence between mechanical and thermal effects in two-phase composites. In G.J. Weng, M. Taya, and H. Abé, editors, *Micromechanics and Inhomogeneity*, pages 65–82, New York, NY, 1990. Springer-Verlag. doi:10.1007/978-1-4613-8919-4_4.

Y. Benveniste, G.J. Dvorak, and T. Chen. On diagonal and elastic symmetry of the approximate effective stiffness tensor of heterogeneous media. *J.Mech.Phys.Sol.*, 39: 927–946, 1991. doi:10.1016/0022-5096(91)90012-D.

A.A. Benzerga and J. Besson. Plastic potentials for anisotropic porous solids. *Eur.J.Mech. A/Solids*, 20:397–434, 2001. doi:10.1016/S0997-7538(01)01147-0.

M.J. Beran and J. Molyneux. Use of classical variational principles to determine bounds for the effective bulk modulus in heterogeneous media. *Quart.Appl.Math.*, 24:107–118, 1966. doi:10.1090/qam/99925.

S.A. Berggren, D. Lukkassen, A. Meidell, and L. Simula. Some methods for calculating stiffness properties of periodic structures. *Appl.Math*, 2:97–110, 2003. doi:10.1023/A:1026090026531.

J.G. Berryman. Long-wavelength propagation in composite elastic media, II. Ellipsoidal inclusions. *J.Acoust.Soc.Amer.*, 68:1820–1831, 1980. doi:10.1121/1.385172.

J.G. Berryman and P.A. Berge. Critique of two explicit schemes for estimating elastic properties of multiphase composites. *Mech.Mater.*, 22:149–164, 1996. doi:10.1016/0167-6636(95)00035-6.

J.G. Berryman and G.W. Milton. Microgeometry of random composites and porous media. *J. Phys.D*, 21:87–94, 1988. doi:10.1088/0022-3727/21/1/013.

M. Berveiller and A. Zaoui. A simplified self-consistent scheme for the plasticity of two-phase metals. *Res.Mech.Lett.*, 1:119–124, 1981.

A. Bhattacharyya and G.J. Weng. Plasticity of isotropic composites with randomly oriented packeted inclusions. *Int.J.Plast.*, 10:553–578, 1994. doi:10.1016/0749-6419(94)90014-0.

P. Bisegna and R. Luciano. Variational bounds for the overall properties of piezoelectric composites. *J.Mech.Phys.Sol.*, 44:583–602, 1996. doi:10.1016/0022-5096(95)00084-4.

J.E. Bishop, J.M. Emery, R.V. Field, C.R. Weinberger, and D.J. Littlewood. Direct numerical simulations in solid mechanics for understanding the macroscale effects of microscale material variability. *Comput.Mech.Appl.Mech.Engng.*, 287:262–289, 2015. doi:10.1016/j.cma.2015.01.017.

J.F.W. Bishop and R. Hill. A theory of the plastic distortion of a polycrystalline aggregate under combined stress. *London Edinburgh Dublin Phil.Mag.J.Sci.*, 42:414–427, 1951. doi:10.1080/14786445108561065.

B. Bochenek and R. Pyrz. Reconstruction of random microstructures — a stochastic optimization problem. *Comput.Mater.Sci.*, 31:93–112, 2004. doi:10.1016/j.commatsci.2004.01.038.

H.J. Böhm. A short introduction to continuum micromechanics. In H.J. Böhm, editor, *Mechanics of Microstructured Materials*, pages 1–40. Springer-Verlag, CISM Courses and Lectures Vol. 464, 2004. doi:10.1007/978-3-7091-2776-6_1.

H.J. Böhm. Comparison of analytical and numerical models for the thermoelastic behavior of composites reinforced by coated spheres. *Int.J.Engng.Sci.*, 142:216–229, 2019. doi:10.1016/j.ijengsci.2019.06.009.

H.J. Böhm. A comparative study of analytical and numerical models for the elastic behavior of composites reinforced by coated unidirectional fibers. *Int.J.Sol.Struct.*, 264:112093, 2023. doi:10.1016/j.ijsolstr.2022.112093.

H.J. Böhm and W. Han. Comparisons between three-dimensional and two-dimensional multi-particle unit cell models for particle reinforced metal matrix composites. *Modell.Simul.Mater.Sci.Engng.*, 9:47–65, 2001. doi:10.1088/0965-0393/9/2/301.

H.J. Böhm and F.G. Rammerstorfer. Fiber arrangement effects on the microscale stresses of continuously reinforced MMCs. In R. Pyrz, editor, *Microstructure–Property Interactions in Composite Materials*, pages 51–62, Dordrecht, 1995. Kluwer Academic Publishers. doi:10.1007/978-94-011-0059-5_5.

H.J. Böhm and A. Rasool. Effects of particle shape on the thermoelastoplastic behavior of particle reinforced composites. *Int.J.Sol.Struct.*, 87:90–101, 2016. doi:10.1016/j.ijsolstr.2016.02.028.

H.J. Böhm, F.G. Rammerstorfer, and E. Weissenbek. Some simple models for micromechanical investigations of fiber arrangement effects in MMCs. *Comput.Mater.Sci.*, 1: 177–194, 1993. doi:10.1016/0927-0256(93)90010-K.

H.J. Böhm, A. Eckschlager, and W. Han. Modeling of phase arrangement effects in high speed tool steels. In F. Jeglitsch, R. Ebner, and H. Leitner, editors, *Tool Steels in the Next Century*, pages 147–156, Leoben, 1999. Montanuniversität Leoben.

H.J. Böhm, A. Eckschlager, and W. Han. Multi-inclusion unit cell models for metal matrix composites with randomly oriented discontinuous reinforcements. *Comput.Mater.Sci.*, 25:42–53, 2002. doi:10.1016/S0927-0256(02)00248-3.

H.J. Böhm, D.H. Pahr, and T. Daxner. Analytical and numerical methods for modeling the thermomechanical and thermophysical behavior of microstructured materials. In V.V. Silberschmidt, editor, *Computational and Experimental Mechanics of Advanced Materials*, pages 167–223. Springer-Verlag, CISM Courses and Lectures Vol. 514, 2009. doi:10.1007/978-3-211-99685-0_5.

N. Bonfoh, V. Hounkpati, and H. Sabar. New micromechanical approach of the coated inclusion problem: Exact solution and applications. *Comput.Mater.Sci.*, 62:175–183, 2012. doi:10.1016/j.commatsci.2012.05.007.

M. Bornert. Homogénéisation des milieux aléatoires: Bornes et estimations. In M. Bornert, T. Bretheau, and P. Gilormini, editors, *Homogénéisation en mécanique des matériaux 1. Matériaux aléatoires élastiques et milieux périodiques*, pages 133–221, Paris, 2001. Editions Hermès.

M. Bornert. *Morphologie microstructurale et comportement mécanique; charactérisations expérimentales, approches par bornes et estimations autocohérentes généralisées*. PhD thesis, Ecole Nationale des Ponts et Chaussées, Paris, 1996.

M. Bornert and P. Suquet. Propriétés non linéaires des composites: Approches par les potentiels. In M. Bornert, T. Bretheau, and P. Gilormini, editors, *Homogénéisation en mécanique des matériaux 2. Comportements non linéaires et problèmes ouverts*, pages 45–90, Paris, 2001. Editions Hermès.

M. Bornert, E. Hervé, C. Stolz, and A. Zaoui. Self consistent approaches and strain heterogeneities in two-phase elastoplastic materials. *Appl.Mech.Rev.*, 47:66–S76, 1994. doi:10.1115/1.3122824.

M. Bornert, C. Stolz, and A. Zaoui. Morphologically representative pattern-based bounding in elasticity. *J.Mech.Phys.Sol.*, 44:307–331, 1996. doi:10.1016/0022-5096(95)00083-6.

M. Bornert, T. Bretheau, and P. Gilormini, editors. *Homogénéisation en mécanique des matériaux*. Editions Hermès, Paris, 2001. ISBN 2-746-20199-2.

N. Bouhfid, M. Raji, R. Boujmal, H. Essabir, M.O. Bensalah, R. Bouhfid, and A.K. Qaiss. Numerical modeling of hybrid composite materials. In M. Jawaid, M. Thariq, and N. Saba, editors, *Modeling of Damage Processes in Biocomposites, Fibre-Reinforced Composites and Hybrid Composites*, pages 57–101, Cambridge, UK, 2019. Elsevier. doi:10.1016/B978-0-08-102289-4.00005-9.

D. Boussaa. Effective thermoelastic properties of composites with temperature-dependent constituents. *Mech.Mater.*, 43:397–407, 2011. doi:10.1016/j.mechmat.2011.04.004.

S. Boyd and R. Müller. Smooth surface meshing for automated finite element model generation from 3D image data. *J.Biomech.*, 39:1287–1295, 2006. doi:10.1016/j.jbiomech.2005.03.006.

L. Brassart, L. Stainier, I. Doghri, and L. Delannay. Homogenization of elasto-(visco)plastic composites based on an incremental variational principle. *Int.J.Plast.*, 36:86–112, 2012. doi:10.1016/j.ijplas.2012.03.010.

R. Brenner and R. Masson. Improved affine estimates for nonlinear viscoelastic composites. *Eur.J.Mech. A/Solids*, 24:1002–1015, 2005. doi:10.1016/j.euromechsol.2005.06.004.

R. Brenner, O. Castelnau, and P. Gilormini. A modified affine theory for the overall properties of nonlinear composites. *C.R.Acad.Sci.Paris, série IIb*, 329:649–654, 2001. doi:10.1016/S1620-7742(01)01382-4.

L.C. Brinson and W.S. Lin. Comparison of micromechanics methods for effective properties of multiphase viscoelastic composites. *Compos.Struct.*, 41:353–367, 1998. doi:10.1016/S0263-8223(98)00019-1.

S. Brisard and L. Dormieux. FFT-based methods for the mechanics of composites: A general variational framework. *Comput.Mater.Sci.*, 49:663–671, 2010. doi:10.1016/j.commatsci.2010.06.009.

L.M. Brown and W.M. Stobbs. The work-hardening of copper–silica. I. A model based on internal stresses, with no plastic relaxation. *Phil.Mag.*, 23:1185–1199, 1971. doi:10.1080/14786437108217405.

D.A.G. Bruggemann. Berechnung verschiedener physikalischer Konstanten von heterogenen Substanzen. I. Dielektrizitätskonstanten und Leitfähigkeiten der Mischkörper aus isotropen Substanzen. *Ann.Phys.*, 24:636–679, 1935. doi:10.1002/andp.19354160705.

M.S. Bruzzi, P.E. McHugh, F. O'Rourke, and T. Linder. Micromechanical modelling of the static and cyclic loading of an Al 2141-SiC MMC. *Int.J.Plast.*, 17:565–599, 2001. doi:10.1016/S0749-6419(00)00063-2.

I. Bucataru and M.A. Slawinski. Invariant properties for finding distance in space of elasticity tensors. *J.Elast.*, 94:97–114, 2009. doi:10.1007/s10659-008-9186-9.

J.Y. Buffière, P. Cloetens, W. Ludwig, E. Maire, and L. Salvo. In situ X-ray tomography studies of microstructural evolution combined with 3D modeling. *MRS Bull.*, 33:611–619, 2008. doi:10.1557/mrs2008.126.

V.N. Bulsara, R. Talreja, and J. Qu. Damage initiation under transverse loading of unidirectional composites with arbitrarily distributed fibers. *Compos.Sci.Technol.*, 59:673–682, 1999. doi:10.1016/S0266-3538(98)00122-5.

V. Buryachenko. *Micromechanics of Heterogeneous Materials*. Springer-Verlag. Berlin, 2007. ISBN 978-0-387-36827-6.

V. Buryachenko. Critical analysis of generalized Maxwell homogenization schemes and related prospective problems. *Mech.Mater.*, 165:104181, 2022b. doi:10.1016/j.mechmat.2021.104181.

V.A. Buryachenko. General integral equations of micromechanics of heterogeneous materials. *J.Multisc.Comput.Engng.*, 13:11–53, 2015. doi:10.1615/IntJMultCompEng.2014011234.

V.A. Buryachenko. *Local and Nonlocal Micromechanics of Heterogeneous Materials*. Springer-Verlag. Cham, 2022a. ISBN 978-3-030-81783-1.

V.A. Buryachenko. The overall elastoplastic behavior of multiphase materials with isotropic components. *Acta Mech.*, 119:93–117, 1996. doi:10.1007/BF01274241.

V.A. Buryachenko, N.J. Pagano, R.Y. Kim, and J.E. Spowart. Quantitative description and numerical simulation of random microstructures of composites and their elastic moduli. *Int.J.Sol.Struct.*, 40:47–72, 2003. doi:10.1016/S0020-7683(02)00462-6.

J. Byström, N. Jēkabsons, and J. Varna. An evaluation of different models for prediction of elastic properties of woven composites. *Composites B*, 31:7–20, 2000. doi:10.1016/S1359-8368(99)00061-X.

C. Calvo-Jurado and W.J. Parnell. The influence of two-point statistics on the Hashin–Shtrikman bounds for three-phase composites. *J.Comput.Appl.Math.*, 318:354–365, 2017. doi:10.1016/j.cam.2016.08.046.

C.W. Camacho, C.L. Tucker, S. Yalvaç, and R.L. McGee. Stiffness and thermal expansion predictions for hybrid short fiber composites. *Polym.Compos.*, 11:229–239, 1990. doi:10.1002/pc.750110406.

N. Carrère. *Sur l'analyse multiéchelle des matériaux composites à matrice métallique: application au calcul de structure*. PhD thesis, Ecole Polytechnique, Palaiseau, 2001.

M.A.A. Cavalcante, M.J. Pindera, and H. Khatam. Finite-volume micromechanics of periodic materials: Past, present and future. *Composites B*, 43:2521–2543, 2012. doi:10.1016/j.compositesb.2012.02.006.

A. Cazzani and M. Rovati. Extrema of Young's modulus for cubic and transversely isotropic solids. *Int.J.Sol.Struct.*, 40:1713–1744, 2003. doi:10.1016/S0020-7683(02)00668-6.

J.L. Chaboche and P. Kanouté. Sur les approximations "isotrope" et "anisotrope" de l'opérateur tangent pour les méthodes tangentes incrémentale et affine. *C.R.Mécanique*, 331:857–864, 2003. doi:10.1016/j.crme.2003.08.002.

J.L. Chaboche, S. Kruch, J.F. Maire, and T. Pottier. Towards a micromechanics based inelastic and damage modelling of composites. *Int.J.Plast.*, 17:411–439, 2001. doi:10.1016/S0749-6419(00)00056-5.

A. Chakraborty and S. Rahman. Stochastic multiscale models for fracture analysis of functionally graded materials. *Engng.Fract.Mech.*, 75:2062–2068, 2008. doi:10.1016/j.engfracmech.2007.10.013.

N. Charalambakis. Homogenization techniques and micromechanics. A survey and perspectives. *Appl.Mech.Rev.*, 63:030803, 2010. doi:10.1115/1.4001911.

G. Chatzigeorgiou and F. Meraghni. Elastic and inelastic local strain fields in composites with coated fibers or particles: Theory and validation. *Math.Mech.Sol.*, 24:2858–2894, 2019. doi:10.1177/1081286518822695.

N. Chawla and K.K. Chawla. Microstructure based modeling of the deformation behavior of particle reinforced metal matrix composites. *J.Mater.Sci.*, 41:913–925, 2006. doi:10.1007/s10853-006-6572-1.

H.R. Chen, Q.S. Yang, and F.W. Williams. A self-consistent finite element approach to the inclusion problem. *Comput.Mater.Sci.*, 2:301–307, 1994. doi:10.1016/0927-0256(94)90112-0.

Q. Chen, X. Chen, Z. Zhai, and Z. Yang. A new and general formulation of three-dimensional finite-volume micromechanics for particulate reinforced composites with viscoplastic phases. *Composites B*, 85:216–232, 2016. doi:10.1016/j.compositesb.2015.09.014.

T. Chen. Exact moduli and bounds of two-phase composites with coupled multifield linear responses. *J.Mech.Phys.Sol.*, 45:385–398, 1997. doi:10.1016/S0022-5096(96)00092-0.

B. Chiaia, A. Vervuurt, and J.G.M. van Mier. Lattice model evaluation of progressive failure in disordered particle composites. *Engng.Fract.Mech.*, 57:301–318, 1997. doi:10.1016/S0013-7944(97)00011-8.

C.M. Chimani, H.J. Böhm, and F.G. Rammerstorfer. On stress singularities at free edges of bimaterial junctions — A micromechanical study. *Scr.mater.*, 36:943–947, 1997. doi:10.1016/S1359-6462(96)00461-7.

R.M. Christensen. Sufficient symmetry conditions for isotropy of the elastic moduli tensor. *J.Appl.Mech.*, 54:772–777, 1987. doi:10.1115/1.3173115.

R.M. Christensen and K.H. Lo. Solutions for effective shear properties in three phase sphere and cylinder models. *J.Mech.Phys.Sol.*, 27:315–330, 1979. doi:10.1016/0022-5096(79)90032-2.

R.M. Christensen and K.H. Lo. Erratum to Christensen and Lo, 1979. *J.Mech.Phys.Sol.*, 34:639, 1986. doi:10.1016/0022-5096(86)90043-8.

R.M. Christensen, H. Schantz, and J. Shapiro. On the range of validity of the Mori–Tanaka method. *J.Mech.Phys.Sol.*, 40:69–73, 1992. doi:10.1016/0022-5096(92)90240-3.

B.G. Christoff, H. Brito-Santana, S. Talreja, and V. Tita. Development of an ABAQUS™ plug-in to evaluate the fourth-order elasticity tensor of a periodic material via homogenization by the asymptotic expansion method. *Fin.Elem.Anal.Design*, 181:103482, 2020. doi:10.1016/j.finel.2020.103482.

P.W. Chung, K.K. Tamma, and R.R. Namburu. Asymptotic expansion homogenization for heterogeneous media: Computational issues and applications. *Composites A*, 32: 1291–1301, 2001. doi:10.1016/S1359-835X(01)00100-2.

H.H.M. Cleveringa, E. van der Giessen, and A. Needleman. Comparison of discrete dislocation and continuum plasticity predictions for a composite material. *Acta mater.*, 45: 3163–3179, 1997. doi:10.1016/S1359-6454(97)00011-6.

T.W. Clyne and P.J. Withers. *An Introduction to Metal Matrix Composites*. Cambridge University Press, Cambridge, 1993. ISBN 0-521-48357-3.

I. Cohen. Simple algebraic approximations for the effective elastic moduli of cubic arrays of spheres. *J.Mech.Phys.Sol.*, 52:2167–2183, 2004. doi:10.1016/j.jmps.2004.02.008.

D.A. Colera and H.G. Kim. Asymptotic expansion homogenization analysis using two-phase representative volume element for non-periodic composite materials. *Multisc.Sci.Engng.*, 1:130–140, 2019. doi:10.1007/s42493-018-00014-w.

R.D. Cook and W.C. Young. *Advanced Mechanics of Materials*. Mcmillan, London, 1985. ISBN 0-133-96961-4.

W.M.G. Courage and P.J.G Schreurs. Effective material parameters for composites with randomly oriented short fibers. *Comput.Struct.*, 44:1179–1185, 1992. doi:10.1016/0045-7949(92)90361-3.

B.N. Cox and G. Flanagan. Handbook of analytical methods for textile composites. Technical Report NASA–CR–4570, NASA, Washington, DC, 1997.

H.L. Cox. The elasticity and strength of paper and other fibrous materials. *Brit.J.Appl. Phys.*, 3:72–79, 1952. doi:10.1088/0508-3443/3/3/302.

M.E. Cruz and A.T. Patera. A parallel Monte-Carlo finite element procedure for the analysis of multicomponent random media. *Int.J.Num.Meth.Engng.*, 38:1087–1121, 1995. doi:10.1002/nme.1620380703.

J. Cugnoni and M. Galli. Representative volume element size of elastoplastic and elastoviscoplastic particle-reinforced composites with random microstructure. *Comput.Model.Engng.Sci.*, 66:165–185, 2010. doi:10.3970/cmes.2010.066.165.

W.A. Curtin and R.E. Miller. Atomistic/continuum coupling in computational materials science. *Model.Simul.Mater.Sci.Engng.*, 11:R33–R68, 2003. doi:10.1088/0965-0393/11/3/201.

A.S. Dalaq, D.W. Abueidda, R. Abu Al-Rub, and I.M. Jasiuk. Finite element predictions of effective elastic properties of interpenetrating phase composites with architectured sheet reinforcements. *Int.J.Sol.Struct.*, 83:169–182, 2016. doi:10.1016/j.ijsolstr.2016.01.011.

T.D. Dang and B.V. Sankar. Meshless Local Petrov–Galerkin formulation for problems in composite micromechanics. *AIAA J.*, 45:912–921, 2007. doi:10.2514/1.23434.

L.C. Davis. Flow rule for the plastic deformation of particulate metal matrix composites. *Comput.Mater.Sci.*, 6:310–318, 1996. doi:10.1016/0927-0256(96)00044-4.

P.R. Dawson. Computational crystal plasticity. *Int.J.Sol.Struct.*, 37:115–130, 2000. doi:10.1016/S0020-7683(99)00083-9.

T. Daxner. *Multi-Scale Modeling and Simulation of Metallic Foams*. Reihe 18, Nr. 285. VDI–Verlag, Düsseldorf, 2003. ISBN 3-183-28581-5.

T. Daxner, R.D. Bitsche, and H.J. Böhm. Micromechanical models of metallic sponges with hollow struts. In T. Chandra, K. Tsuzaki, M. Militzer, and C. Ravindran, editors, *Thermec 2006*, pages 1857–1862, Trans Tech Publications, Zurich, 2007. Materials Science Forum 539–543. doi:10.4028/www.scientific.net/MSF.539-543.1857.

F. de Francqueville, P. Gilormini, and J. Diani. Representative volume elements for the simulation of isotropic composites highly filled with monosized spheres. *Int.J.Sol.Struct.*, 158:277–286, 2019. doi:10.1016/j.ijsolstr.2018.09.013.

P.H. Dederichs and T. Zeller. Variational treatment of the elastic constants of disordered materials. *Z.Phys.*, 259:103–116, 1973. doi:10.1007/BF01392841.

L. Delannay, I. Doghri, and O. Pierard. Prediction of tension–compression cycles in multiphase steel using a modified mean-field model. *Int.J.Sol.Struct.*, 44:7291–7306, 2007. doi:10.1016/j.ijsolstr.2007.04.013.

V.S. Deshpande, M.F. Ashby, and N.A. Fleck. Foam topology: Bending versus stretching dominated architectures. *Acta mater.*, 49:1035–1040, 2001. doi:10.1016/S1359-6454(00)00379-7.

A. Desmoulins and D.M. Kochmann. Local and nonlocal continuum modeling of inelastic periodic networks applied to stretching-dominated trusses. *Comput.Meth.Appl.Mech.Engng.*, 313:85–105, 2017. doi:10.1016/j.cma.2016.09.027.

S. Diebels, T. Ebinger, and H. Steeb. An anisotropic damage model of foams on the basis of a micromechanical description. *J.Mater.Sci.*, 40:5919–5924, 2005. doi:10.1007/s10853-005-5043-4.

F. Dinzart, H. Sabar, and S. Berbenni. Homogenization of multi-phase composites based on a revisited formulation of the multi-coated inclusion problem. *Int.J.Engng.Sci.*, 100: 136–151, 2016. doi:10.1016/j.ijengsci.2015.12.001.

J. Dirrenberger, S. Forest, and D. Jeulin. Towards gigantic RVE sizes for 3D stochastic fibrous networks. *Int.J.Sol.Struct.*, 51:359–376, 2014. doi:10.1016/j.ijsolstr.2013.10.011.

I. Doghri and C. Friebel. Effective elasto-plastic properties of inclusion-reinforced composites. Study of shape, orientation and cyclic response. *Mech.Mater.*, 37:45–68, 2005. doi:10.1016/j.mechmat.2003.12.007.

I. Doghri and A. Ouaar. Homogenization of two-phase elasto-plastic composite materials and structures. *Int.J.Sol.Struct.*, 40:1681–1712, 2003. doi:10.1016/S0020-7683(03)00013-1.

I. Doghri and L. Tinel. Micromechanical modeling and computation of elasto-plastic materials reinforced with distributed-orientation fibers. *Int.J.Plast.*, 21:1919–1940, 2005. doi:10.1016/j.ijplas.2004.09.003.

M. Dong and S. Schmauder. Modeling of metal matrix composites by a self-consistent embedded cell model. *Acta mater.*, 44:2465–2478, 1996. doi:10.1016/1359-6454(95)00345-2.

A. Drago and M.J. Pindera. A locally exact homogenization theory for periodic microstructures with isotropic phases. *J.Appl.Mech.*, 75:051010, 2008. doi:10.1115/1.2913043.

W. Dreyer, W.H. Müller, and J. Olschewski. An approximate analytical 2D-solution for the stresses and strains in eigenstrained cubic materials. *Acta Mech.*, 136:171–192, 1999. doi:10.1007/BF01179256.

W.J. Drugan and J.R. Willis. A micromechanics-based nonlocal constitutive equation and estimates of representative volume element size for elastic composites. *J.Mech.Phys.Sol.*, 44:497–524, 1996. doi:10.1016/0022-5096(96)00007-5.

D.X. Du and Q.S. Zheng. A further exploration of the interaction direct derivative (IDD) estimate for the effective properties of multiphase composites taking into account inclusion distribution. *Acta Mech.*, 157:61–80, 2002. doi:10.1007/BF01182155.

H.L. Duan, J. Wang, Z.P. Huang, and Z.Y. Luo. Stress concentration tensors of inhomogeneities with interface effects. *Mech.Mater.*, 37:723–736, 2005. doi:10.1016/j.mechmat.2004.07.004.

H.L. Duan, B.L. Karihaloo, J. Wang, and X. Yi. Effective thermal conductivities of heterogeneous media containing multiple inclusions with various spatial distributions. *Phys.Rev. B*, 73:174203, 2006. doi:10.1103/PhysRevB.73.174203.

H.L. Duan, J. Wang, and Z. Huang. Micromechanics of composites with interface effects. *Acta Mech.Sinica*, 38:222025, 2022. doi:10.1007/s10409-022-22025-x.

C.F. Dunant, B. Bary, A.B. Giorla, C. Péniguel, M. Sanahuja, C. Toulemonde, A.B. Tran, F. Willot, and J. Yvonnet. A critical comparison of several numerical methods for computing effective properties of highly heterogeneous materials. *Adv.Engng.Softw.*, 58: 1–12, 2013. doi:10.1016/j.advengsoft.2012.12.002.

M.L. Dunn and H. Ledbetter. Elastic–plastic behavior of textured short-fiber composites. *Acta mater.*, 45:3327–3340, 1997. doi:10.1016/S1359-6454(96)00401-6.

M.L. Dunn and M. Taya. Micromechanics predictions of the effective electroelastic moduli of piezoelectric composites. *Int.J.Sol.Struct.*, 30:161–175, 1993. doi:10.1016/0020-7683(93)90058-F.

D. Duschlbauer. *Computational Simulation of the Thermal Conductivity of MMCs under Consideration of the Inclusion–Matrix Interface*. Reihe 5, Nr. 561. VDI–Verlag, Düsseldorf, 2004. ISBN 3-183-69105-1.

D. Duschlbauer, H.J. Böhm, and H.E. Pettermann. Numerical simulation of the thermal conductivity of MMCs: The effect of thermal interface resistance. *Mater. Sci. Technol.*, 19:1107–1114, 2003a. doi:10.1179/026708303225004305.

D. Duschlbauer, H.E. Pettermann, and H.J. Böhm. Mori–Tanaka based evaluation of inclusion stresses in composites with nonaligned reinforcements. *Scr.mater.*, 48:223–228, 2003b. doi:10.1016/S1359-6462(02)003-1.

D. Duschlbauer, H.J. Böhm, and H.E. Pettermann. Computational simulation of composites reinforced by planar random fibers: Homogenization and localization by unit cell and mean field approaches. *J.Compos.Mater.*, 40:2217–2234, 2006. doi:10.1177/0021998306062317.

D. Duschlbauer, H.E. Pettermann, and H.J. Böhm. Modeling interfacial effects on the thermal conduction behavior of short fiber reinforced composites. *Int.J.Mater.Res.*, 102: 717–728, 2011. doi:10.3139/146.110515.

G.J. Dvorak. *Micromechanics of Composite Materials*. Springer-Verlag, Dordrecht, 2013. ISBN 9-400-79781-8.

G.J. Dvorak. Transformation field analysis of inelastic composite materials. *Proc.Roy.Soc. London*, A437:311–327, 1992. doi:10.1098/rspa.1992.0063.

G.J. Dvorak and Y.A. Bahei-el Din. A bimodal plasticity theory of fibrous composite materials. *Acta Mech.*, 69:219–241, 1987. doi:10.1007/BF01175723.

G.J. Dvorak, T. Chen, and J. Teply. Thermomechanical stress fields in high-temperature fibrous composites. I: Unidirectional laminates. *Compos.Sci.Technol.*, 43:347–358, 1992. doi:10.1016/0266-3538(92)90058-B.

G.J. Dvorak, Y.A. Bahei-el Din, and A.M. Wafa. The modeling of inelastic composite materials with the transformation field analysis. *Modell.Simul.Mater.Sci.Engng.*, 2:571–586, 1994. doi:10.1088/0965-0393/2/3A/011.

M.P. Echlin, W.C. Lenthe, and T.M. Pollock. Three-dimensional sampling of material structure for property modeling and design. *Integ.Mater.Manuf.Innov.*, 3:21, 2014. doi:10.1186/s40192-014-0021-9.

R.F. Eduljee and R.L. McCullough. Elastic properties of composites. In R.W. Cahn, P. Haasen, and E.J. Kramer, editors, *Materials Science and Technology Vol.13: Structure and Properties of Composites*, pages 381–474, Weinheim, 1993. VCH. doi:10.1002/9783527603978.mst0155.

F. El Houdaigui, S. Forest, A.F. Gourgues, and D. Jeulin. On the size of the representative volume element for isotropic elastic copper. In Y.L. Bai and Q.S. Zheng, editors, *IUTAM Symposium on Mechanical Behavior and Micro-Mechanics of Nanostructured Materials*, pages 171–180, Dordrecht, 2007. Springer-Verlag. doi:10.1007/978-1-4020-5624-6_17.

M. El Mouden and A. Molinari. Thermoelastic properties of composites containing ellipsoidal inhomogeneities. *J.Therm.Stresses*, 23:233–255, 2000. doi:10.1080/014957300280425.

J.A. Elliott and A.H. Windle. A dissipative particle dynamics method for modeling the geometrical packing of filler particles in polymer composites. *J.Chem.Phys.*, 113:10367–10376, 2000. doi:10.1063/1.1322636.

O. Eroshkin and I. Tsukrov. On micromechanical modeling of particulate composites with inclusions of various shapes. *Int.J.Sol.Struct.*, 42:409–427, 2005. doi:10.1016/j.ijsolstr.2004.06.045.

J.D. Eshelby. The determination of the elastic field of an ellipsoidal inclusion and related problems. *Proc.Roy.Soc.London*, A241:376–396, 1957. doi:10.1098/rspa.1957.0133.

J.D. Eshelby. The elastic field outside an ellipsoidal inclusion. *Proc.Roy.Soc.London*, A252: 561–569, 1959. doi:10.1098/rspa.1959.0173.

Y. Estrin, S. Arndt, M. Heilmaier, and Y. Bréchet. Deformation behaviour of particle-strengthened alloys: A Voronoi mesh approach. *Acta mater.*, 47:595–606, 1999. doi:10.1016/S1359-6454(98)00362-0.

J. Faleskog and C.F. Shih. Micromechanics of coalescence — I.: Synergistic effects of elasticity, plastic yielding and multi-size-scale voids. *J.Mech.Phys.Sol.*, 45:21–50, 1997. doi:10.1016/S0022-5096(96)00078-6.

G. Fang, B. El Said, D. Ivanov, and S.R. Hallett. Smoothing artificial stress concentrations in voxel-based models of textile composites. *Composites A*, 80:270–284, 2016. doi:10.1016/j.compositesa.2015.10.025.

Y.F. Fangye, N. Miska, and D. Balzani. Automated simulation of voxel-based microstructures based on enhanced finite cell approach. *Arch.Appl.Mech.*, 90:2255–2273, 2020. doi:10.1007/s00419-020-01719-x.

M. Fergoug, A. Parret-Fréaud, N. Feld, B. Marchand, and S. Forest. A general boundary layer corrector for the asymptotic homogenization of elastic linear composite structures. *Compos.Struct.*, 285:115091, 2022. doi:10.1016/j.compstruct.2021.115091.

M. Ferrari. Asymmetry and the high concentration limit of the Mori–Tanaka effective medium theory. *Mech.Mater.*, 11:251–256, 1991. doi:10.1016/0167-6636(91)90006-L.

F. Feyel. A multilevel finite element method (FE^2) to describe the response of highly non-linear structures using generalized continua. *Comput.Meth.Appl.Mech.Engng.*, 192: 3233–3244, 2003. doi:10.1016/S0045-7825(03)00348-7.

F. Feyel and J.L. Chaboche. FE^2 multiscale approach for modelling the elastoviscoplastic behaviour of long fiber SiC/Ti composite materials. *Comput.Meth.Appl.Mech.Engng.*, 183:309–330, 2000. doi:10.1016/S0045-7825(99)00224-8.

S. Firooz, S. Saeb, G. Chatzigeorgiou, F. Meraghni, P. Steinmann, and A. Javili. Systematic study of homogenization and the utility of circular simplified representative volume element. *Math.Mech.Sol.*, 24:2961–2985, 2019. doi:10.1177/1081286518823834.

H.F. Fischmeister and B. Karlsson. Plastizitätseigenschaften grob-zweiphasiger Werkstoffe. *Z.Metallkd.*, 68:311–327, 1977. doi:10.1515/ijmr-1977-680501.

J. Fish and K. Shek. Multiscale analysis of composite materials and structures. *Compos.Sci.Technol.*, 60:2547–2556, 2000. doi:10.1016/S0266-3538(00)00048-8.

J. Fish and K. Shek. Computational plasticity and viscoplasticity for composite materials and structures. *Composites B*, 29:613–619, 1998. doi:10.1016/S1359-8368(98)00015-8.

S. Fliegener, M. Luke, and P. Gumbsch. 3D microstructure modeling of long fiber reinforced thermoplastics. *Compos.Sci.Technol.*, 104:136–145, 2014. doi:10.1016/j.compscitech.2014.09.009.

C. Fond, A. Riccardi, R. Schirrer, and F. Montheillet. Mechanical interaction between spherical inhomogeneities: An assessment of a method based on the equivalent inclusion. *Eur.J.Mech. A/Solids*, 20:59–75, 2001. doi:10.1016/S0997-7538(00)01118-9.

S. Forest, G. Cailletaud, D. Jeulin, F. Feyel, I. Galliet, V. Mounoury, and S. Quilici. Introduction au calcul de microstructures. *Méc.Indust.*, 3:439–456, 2002. URL https://www.sciencedirect.com/science/article/pii/S1296213902011879.

P. Franciosi. Uniformity of the Green operator and Eshelby tensor for hyperboloidal domains in infinite media. *Math.Mech.Sol.*, 25:1610–1642, 2020. doi:10.1177/1081286520911119.

H. Fricke. A mathematical treatment of the electric conductivity and capacity of disperse systems I. The electric conductivity of a suspension of homogeneous spheroids. *Phys.Rev.*, 24:575–587, 1924. doi:10.1103/PhysRev.24.575.

C. Friebel, I. Doghri, and V. Legat. General mean-field homogenization schemes for viscoelastic composites containing multiple phases of coated inclusions. *Int.J.Sol.Struct.*, 43:2513–2541, 2006. doi:10.1016/j.ijsolstr.2005.06.035.

F. Fritzen and T. Böhlke. Periodic three-dimensional mesh generation for particle reinforced composites with application to metal matrix composites. *Int.J.Sol.Struct.*, 48: 706–718, 2011. doi:10.1016/j.ijsolstr.2010.11.010.

F. Fritzen and O. Kunc. Two-stage data driven homogenization for nonlinear solids using a reduced order model. *Eur.J.Mech. A/Solids*, 69:201–220, 2018. doi:10.1016/j.euromechsol.2017.11.007.

F. Fritzen, T. Böhlke, and E. Schnack. Periodic three-dimensional mesh generation for crystalline aggregates based on Voronoi tessellations. *Comput.Mech.*, 43:701–713, 2009. doi:10.1007/s00466-008-0339-2.

S.Y. Fu and B. Lauke. The elastic modulus of misaligned short-fiber-reinforced polymers. *Compos.Sci.Technol.*, 58:389–400, 1998. doi:10.1016/S0266-3538(97)00129-2.

H. Fukuda and T.W. Chou. A probabilistic theory of the strength of short-fibre composites with variable fibre length and orientation. *J.Mater.Sci.*, 17:1003–1007, 1982. doi:10.1007/BF00543519.

H. Fukuda and K. Kawata. Stress and strain fields in short fibre-reinforced composites. *Fibre Sci.Technol.*, 7:129–156, 1974. doi:10.1016/0015-0568(74)90025-6.

J. Gager and H.E. Pettermann. Numerical homogenization of textile composites based on shell element discretization. *Compos.Sci.Technol.*, 72:806–812, 2012. doi:10.1016/j.compscitech.2012.02.009.

M. Galli, J. Botsis, and J. Janczak-Rusch. An elastoplastic three-dimensional homogenization model for particle reinforced composites. *Comput.Mater.Sci.*, 41:312–321, 2008. doi:10.1016/j.commatsci.2007.04.010.

M. Galli, J. Cugnoni, and J. Botsis. Numerical and statistical estimates of the representative volume element of elastoplastic random composites. *Eur.J.Mech. A/Solids*, 33: 31–38, 2012. doi:10.1016/j.euromechsol.2011.07.010.

H.P. Gänser. *Large Strain Behavior of Two-Phase Materials*. Reihe 5, Nr. 528. VDI–Verlag, Düsseldorf, 1998.

H.P. Gänser, F.D. Fischer, and E.A. Werner. Large strain behaviour of two-phase materials with random inclusions. *Comput.Mater.Sci.*, 11:221–226, 1998. doi:10.1016/S0927-0256(98)00007-X.

M. Gărăjeu, J.C. Michel, and P. Suquet. A micromechanical approach of damage in viscoplastic materials by evolution in size, shape and distribution of voids. *Comput.Meth.Appl.Mech.Engng.*, 183:223–246, 2000. doi:10.1016/S0045-7825(99)00220-0.

M.R. Garnich and G. Karami. Finite element micromechanics for stiffness and strength of wavy fiber composites,. *J.Compos.Mater.*, 38:273–292, 2004. doi:10.1177/00219983040392.

D. Garoz, F.A. Gilabert, R.D.B. Sevenois, S.W.F Spronk, and W. Van Paepegem. Consistent application of periodic boundary conditions in implicit and explicit finite element simulations of damage in composites. *Composites B*, 168:254–266, 2019. doi:10.1016/j.compositesb.2018.12.023.

A.C. Gavazzi and D.C. Lagoudas. On the numerical evaluation of Eshelby's tensor and its application to elastoplastic fibrous composites. *Comput.Mech.*, 7:12–19, 1990. doi:10.1007/BF00370053.

M.G.D. Geers, R.A.B. Engelen, and R.J.M. Ubachs. On the numerical modelling of ductile damage with an implicit gradient-enhanced formulation. *Rev.Eur.Elem.Fin.*, 10:173–191, 2001a. doi:10.1080/12506559.2001.11869246.

M.G.D. Geers, V.G. Kouznetsova, and W.A.M. Brekelmans. Gradient enhanced homogenization for the micro–macro scale transition. *J.Physique IV*, 11:145–152, 2001b. doi:10.1051/jp4:2001518.

M.G.D. Geers, V.G. Kouznetsova, and W.A.M. Brekelmans. Multi-scale computational homogenization: Trends and challenges. *J.Comput.Appl.Math.*, 234:2175–2182, 2010. doi:10.1016/j.cam.2009.08.077.

G.M. Genin and V. Birman. Micromechanics and structural response of functionally graded, particulate–matrix, fiber-reinforced composites. *Int.J.Sol.Struct.*, 46:2136–2150, 2009. doi:10.1016/j.ijsolstr.2008.08.010.

A. Ghazavizadeh, M. Haboussi, A. Abdul-Latif, A. Jafari, and H. Bousoura. A general and explicit Eshelby-type estimator for evaluating the equivalent stiffness of multiply coated ellipsoidal heterogeneities. *Int.J.Sol.Struct.*, 171:103–116, 2019. doi:10.1016/j.ijsolstr.2019.04.023.

S. Ghosh and D.V. Kubair. Exterior statistics based boundary conditions for representative volume elements of elastic composites. *J.Mech.Phys.Sol.*, 95:1–24, 2016. doi:10.1016/j.jmps.2016.05.022.

S. Ghosh and S. Moorthy. Three dimensional Voronoi cell finite element model for microstructures with ellipsoidal heterogeneities. *Comput.Mech.*, 34:510–531, 2004. doi:10.1007/s00466-004-0598-5.

S. Ghosh, K.H. Lee, and S. Moorthy. Two scale analysis of heterogeneous elastic-plastic materials with asymptotic homogenization and Voronoi cell finite element model. *Comput.Meth.Appl.Mech.Engng.*, 132:63–116, 1996. doi:10.1016/0045-7825(95)00974-4.

S. Ghosh, K.H. Lee, and P. Raghavan. A multi-level computational model for multi-scale analysis in composite and porous materials. *Int.J.Sol.Struct.*, 38:2335–2385, 2001. doi:10.1016/S0020-7683(00)00167-0.

S. Ghosh, D. Dimiduk, and D. Furrer. Statistically equivalent representative volume elements (SERVE) for material behaviour analysis and multiscale modelling. *Int.Mater.Rev.*, 68:1158–1191, 2023. doi:10.1080/09506608.2023.2246766.

E. Ghossein and M. Lévesque. A fully automated numerical tool for a comprehensive validation of homogenization models and its application to spherical particles reinforced composites. *Int.J.Sol.Struct.*, 49:1387–1398, 2012. doi:10.1016/j.ijsolstr.2012.02.021.

E. Ghossein and M. Lévesque. Random generation of periodic hard ellipsoids based on molecular dynamics: A computationally-efficient algorithm. *J.Comput.Phys.*, 253:471–490, 2013. doi:10.1016/j.jcp.2013.07.004.

L.V. Gibiansky and S. Torquato. Connection between the conductivity and bulk modulus of isotropic composite materials. *Proc.Roy.Soc.London*, A452:253–283, 1996. doi:10.1098/rspa.1996.0015.

L.J. Gibson. The mechanical behavior of cancellous bone. *J.Biomech.*, 18:317–328, 1985. doi:10.1016/0021-9290(85)90287-8.

L.J. Gibson and M.F. Ashby. *Cellular Solids: Structure and Properties*. Pergamon Press, Oxford, 1988. ISBN 0-521-49911-9.

A. Gillman, G. Amadio, K. Matouš, and T.L. Jackson. Third-order thermo-mechanical properties for packs of Platonic solids using statistical micromechanics. *Proc.Roy.Soc.*, A471:20150060, 2015. doi:10.1098/rspa.2015.0060.

P. Gilormini. Insuffisance de l'extension classique du modèle auto-cohérent au comportement non-linéaire. *C.R.Acad.Sci.Paris, série IIb*, 320:115–122, 1995.

S. Giordano. Differential schemes for the elastic characterization of dispersions of randomly oriented ellipsoids. *Eur.J.Mech. A/Solids*, 22:885–902, 2003. doi:10.1016/S0997-7538(03)00091-3.

S. Giordano. Order and disorder in heterogeneous material microstructure: Electric and elastic characterisation of dispersions of pseudo-oriented spheroids. *Int.J.Engng.Sci.*, 43:1033–1058, 2005. doi:10.1016/j.ijengsci.2005.06.002.

A. Giraud, C. Gruescu, D.P. Do, F. Homand, and D. Kondo. Effective thermal conductivity of transversely isotropic media with arbitrary oriented ellipsoidal inhomogeneities. *Int.J.Sol.Struct.*, 44:2627–2647, 2007. doi:10.1016/j.ijsolstr.2006.08.011.

I.M. Gitman. *Representative Volumes and Multi-Scale Modelling of Quasi-Brittle Materials*. PhD thesis, Technische Universiteit te Delft, Delft, 2006.

I.M. Gitman, H. Askes, and L.J. Sluys. Representative volume: Existence and size determination. *Engng.Fract.Mech.*, 74:2518–2534, 2007. doi:10.1016/j.engfracmech.2006.12.021.

R. Glüge, M. Weber, and A. Bertram. Comparison of spherical and cubical statistical volume elements with respect to convergence, anisotropy, and localization behavior. *Comput.Mater.Sci.*, 63:91–104, 2012. doi:10.1016/j.commatsci.2012.05.063.

M. Gologanu, J.B. Leblond, G. Perrin, and J. Devaux. Recent extensions of Gurson's model for porous ductile materials. In P. Suquet, editor, *Continuum Micromechanics*, pages 61–130, Vienna, 1997. Springer-Verlag, CISM Courses and Lectures Vol. 377. doi:10.1007/978-3-7091-2662-2_2.

B. Gommers, I. Verpoest, and P. van Houtte. The Mori–Tanaka method applied to textile composite materials. *Acta mater.*, 46:2223–2235, 1998. doi:10.1016/S1359-6454(97)00296-6.

L. Gong, S. Kyriakides, and N. Triantafyllidis. On the stability of Kelvin cell foams under compressive loads. *J.Mech.Phys.Sol.*, 53:771–794, 2005. doi:10.1016/j.jmps.2004.10.007.

C. González and J. LLorca. A self-consistent approach to the elasto-plastic behavior of two-phase materials including damage. *J.Mech.Phys.Sol.*, 48:675–692, 2000. doi:10.1016/S0022-5096(99)00057-5.

C. González and J. LLorca. Virtual fracture testing of composites: A computational micromechanics approach. *Engng.Fract.Mech.*, 74:1126–1138, 2007. doi:10.1016/j.engfracmech.2006.12.013.

M. Goudarzi and A. Simone. Discrete inclusion model for reinforced composites: Comparative performance analysis and modeling challenges. *Comput.Meth.Appl.Mech.Engng.*, 355:535–557, 2019. doi:10.1016/j.cma.2019.06.026.

J.L. Grenestedt. Influence of wavy imperfections in cell walls on elastic stiffness of cellular solids. *J.Mech.Phys.Sol.*, 46:29–50, 1998. doi:10.1016/S0022-5096(97)00035-5.

D. Gross and T. Seelig. *Bruchmechanik mit einer Einführung in die Mikromechanik*. Springer-Verlag, Berlin, 2001. ISBN 978-3-662-46736.

C. Grufman and F. Ellyin. Numerical modeling of damage susceptibility of an inhomogeneous representative material volume element of polymer composites. *Compos.Sci.Technol.*, 68:650–657, 2008. doi:10.1016/j.compscitech.2007.09.018.

H. Gu, J. Réthore, M.C. Baietto, P. Sainsot, P. Lecomte-Grosbras, C.H. Venner, and A.A. Lubrecht. An efficient MultiGrid solver for the 3D simulation of composite materials. *Comput.Mater.Sci.*, 112:230–237, 2016. doi:10.1016/j.commatsci.2015.10.025.

F.J. Guild and A.J. Kinloch. Modelling the properties of rubber-modified epoxy polymers. *J.Mater.Sci*, 30:1689–1697, 1995. doi:10.1007/BF00351597.

R.E. Guldberg, S.J. Hollister, and G.T. Charras. The accuracy of digital image-based finite element models. *J.Biomech.Engng.*, 120:289–295, 1998. doi:10.1115/1.2798314.

G. Guo, J. Fitoussi, D. Baptiste, N. Sicot, and C. Wolff. Modelling of damage behavior of a short-fiber reinforced composite structure by the finite element analysis using a micro–macro law. *Int.J.Dam.Mech.*, 6:278–299, 1997. doi:10.1177/105678959700600304.

A.L. Gurson. Continuum theory of ductile rupture by void nucleation and growth: Part I — Yield criteria and flow rules for porous ductile media. *J.Engng.Mater.Technol.*, 99: 2–15, 1977. doi:10.1115/1.3443401.

A.A. Gusev. Controlled accuracy finite element estimates for the effective stiffness of composites with spherical inclusions. *Int.J.Sol.Struct.*, 80:227–236, 2016. doi:10.1016/j.ijsolstr.2015.11.006.

A.A. Gusev. Representative volume element size for elastic composites: A numerical study. *J.Mech.Phys.Sol.*, 45:1449–1459, 1997. doi:10.1016/S0022-5096(97)00016-1.

A.A. Gusev, P.J. Hine, and I.M. Ward. Fiber packing and elastic properties of a transversely random unidirectional glass/epoxy composite. *Compos.Sci.Technol.*, 60:535–541, 2000. doi:10.1016/S0266-3538(99)00152-9.

R.M. Haj-Ali and J. Aboudi. Formulation of the high-fidelity generalized method of cells with arbitrary cell geometry for refined micromechanics and damage in composites. *Int.J.Sol.Struct.*, 47:3447–3461, 2010. doi:10.1016/j.ijsolstr.2010.08.022.

J.C. Halpin and J.L. Kardos. The Halpin–Tsai equations: A review. *Polym.Engng.Sci.*, 16:344–351, 1976. doi:10.1002/pen.760160512.

L.T. Harper, C. Qian, T.A. Turner, S. Li, and N.A. Warrior. Representative volume elements for discontinuous carbon fibre composites — Part 1: Boundary conditions. *Compos.Sci.Technol.*, 72:225–234, 2012a. doi:10.1016/j.compscitech.2011.11.006.

L.T. Harper, C. Qian, T.A. Turner, S. Li, and N.A. Warrior. Representative volume elements for discontinuous carbon fibre composites — Part 2: Determining critical size. *Compos.Sci.Technol.*, 72:204–210, 2012b. doi:10.1016/j.compscitech.2011.11.003.

A.M. Harte and J.F. Mc Namara. Use of micromechanical modelling in the material characterisation of overinjected thermoplastic composites. *J.Mater.Process.Technol.*, 173: 376–383, 2006. doi:10.1016/j.jmatprotec.2005.12.010.

R. Hashemi, R. Avazmohammadi, H.M. Shodja, and Weng G.J. Composites with superspherical inhomogeneities. *Phil.Mag.Lett.*, 89:439–451, 2009. doi:10.1080/09500830903019020.

Z. Hashin. The elastic moduli of heterogeneous materials. *J.Appl.Mech.*, 29:143–150, 1962. doi:10.1115/1.3636446.

Z. Hashin. Viscoelastic behavior of heterogeneous media. *J.Appl.Mech.*, 32:630–636, 1965. doi:10.1115/1.3627270.

Z. Hashin. Complex moduli of viscoelastic composites: I. General theory and application to particulate composites. *Int.J.Sol.Struct.*, 6:539–552, 1970. doi:10.1016/0020-7683(70)90029-6.

Z. Hashin. Theory of fiber reinforced materials. Technical Report NASA–CR–1974, NASA, Washington, DC, 1972.

Z. Hashin. Analysis of composite materials — A survey. *J.Appl.Mech.*, 50:481–505, 1983. doi:10.1115/1.3167081.

Z. Hashin. The differential scheme and its application to cracked materials. *J.Mech.Phys. Sol.*, 36:719–733, 1988. doi:10.1016/0022-5096(88)90005-1.

Z. Hashin and B.W. Rosen. The elastic moduli of fiber-reinforced materials. *J.Appl.Mech.*, 31:223–232, 1964. doi:10.1115/1.3629590.

Z. Hashin and S. Shtrikman. Note on a variational approach to the theory of composite elastic materials. *J.Franklin Inst.*, 271:336–341, 1961. doi:10.1016/0016-0032(61)90032-1.

Z. Hashin and S. Shtrikman. A variational approach to the theory of the effective magnetic permeability of multiphase materials. *J.Appl.Phys.*, 33:3125–3131, 1962. doi:10.1063/1.1728579.

Z. Hashin and S. Shtrikman. A variational approach to the theory of the elastic behavior of multiphase materials. *J.Mech.Phys.Sol.*, 11:127–140, 1963. doi:10.1016/0022-5096(63)90060-7.

B. Hassani and E. Hinton. *Homogenization and Structural Topology Optimization*. Springer-Verlag. London, 1999. ISBN 1-447-11229-6.

D.P.H. Hasselman and L.F. Johnson. Effective thermal conductivity of composites with interfacial thermal barrier resistance. *J.Compos.Mater.*, 21:508–515, 1987. doi:10.1177/002199838702100602.

H. Hatta and M. Taya. Equivalent inclusion method for steady state heat conduction in composites. *Int.J.Engng.Sci.*, 24:1159–1172, 1986. doi:10.1016/0020-7225(86)90011-X.

S. Hazanov. Hill condition and overall properties of composites. *Arch.Appl.Mech.*, 68: 385–394, 1998. doi:10.1007/s004190050173.

S. Hazanov and M. Amieur. On overall properties of elastic bodies smaller than the representative volume. *Int.J.Engng.Sci.*, 33:1289–1301, 1995. doi:10.1016/0020-7225(94)00129-8.

S. Hazanov and C. Huet. Order relationships for boundary condition effects in heterogeneous bodies smaller than the representative volume. *J.Mech.Phys.Sol.*, 41:1995–2011, 1994. doi:10.1016/0022-5096(94)90022-1.

Q.C. He and A. Curnier. A more fundamental approach to damaged elastic stress–strain relations. *Int.J.Sol.Struct.*, 32:1433–1457, 1997. doi:10.1016/0020-7683(94)00183-W.

G.L. Heness, B. Ben-Nissan, L.H. Gan, and Y.W. Mai. Development of a finite element micromodel for metal matrix composites. *Comput.Mater.Sci.*, 13:259–269, 1999. doi:10.1016/S0927-0256(98)00127-X.

A. Henkes and H. Wessels. Three-dimensional microstructure generation using generative adversarial neural networks in the context of continuum micromechanics. *Comput.Meth.Appl.Mech.Engng.*, 400:115497, 2022. doi:10.1016/j.cma.2022.115497.

J.J. Hermans. The elastic properties of fiber reinforced materials when the fibers are aligned. *Proc.K.Ned.Akad.Wet.*, B70:1–9, 1967.

E. Hervé and A. Zaoui. Modelling the effective behavior of nonlinear matrix–inclusion composites. *Eur.J.Mech. A/Solids*, 9:505–515, 1990.

E. Hervé and A. Zaoui. n-layered inclusion-based micromechanical modelling. *Int.J. Engng.Sci.*, 31:1–10, 1993. doi:10.1016/0020-7225(93)90059-4.

E. Hervé and A. Zaoui. Elastic behavior of multiply coated fibre-reinforced composites. *Int.J.Engng.Sci.*, 33:1419–1433, 1995. doi:10.1016/0020-7225(95)00008-L.

E. Hervé, C. Stolz, and A. Zaoui. A propos de'l assemblage des sphères composites de Hashin. *C.R.Acad.Sci.Paris, série II*, 313:857–862, 1991.

E. Hervé-Luanco and S. Joannès. Multiscale modelling of transport phenomena for materials with n-layered embedded fibres. Part I: Analytical and numerical-based approaches. *Int.J.Sol.Struct.*, 97–98:625–636, 2016. doi:10.1016/j.ijsolstr.2016.05.015.

P.A. Hessman, F. Welschinger, K. Hornberger, and T. Böhlke. On mean field homogenization schemes for short fiber reinforced composites: Unified formulation, application and benchmark. *Int.J.Sol.Struct.*, 230–231:111141, 2021. doi:10.1016/j.ijsolstr.2021.111141.

R. Hill. A theory of the yielding and plastic flow of anisotropic metals. *Proc.Phys.Soc.London*, 193:281–297, 1948. doi:10.1098/rspa.1948.0045.

R. Hill. The elastic behavior of a crystalline aggregate. *Proc.Phys.Soc.London*, A65:349–354, 1952. doi:10.1088/0370-1298/65/5/307.

R. Hill. Elastic properties of reinforced solids: Some theoretical principles. *J.Mech.Phys.Sol.*, 11:357–372, 1963. doi:10.1016/0022-5096(63)90036-X.

R. Hill. Theory of mechanical properties of fibre-strengthened materials: I. elastic behaviour. *J.Mech.Phys.Sol.*, 12:199–212, 1964. doi:10.1016/0022-5096(64)90019-5.

R. Hill. Continuum micro-mechanics of elastoplastic polycrystals. *J.Mech.Phys.Sol.*, 13:89–101, 1965a. doi:10.1016/0022-5096(65)90023-2.

R. Hill. A self-consistent mechanics of composite materials. *J.Mech.Phys.Sol.*, 13:213–222, 1965b. doi:10.1016/0022-5096(65)90010-4.

R. Hill. The essential structure of constitutive laws for metal composites and polycrystals. *J. Mech. Phys. Sol.*, 15:79–95, 1967. doi:10.1016/0022-5096(67)90018-X.

R. Hill. On constitutive macro-variables for heterogeneous solids at finite strain. *Proc. Roy.Soc.London*, A326:131–147, 1972. doi:10.1098/rspa.1972.0001.

S. Hoffmann. *Computational Homogenization of Short Fiber Reinforced Thermoplastic Materials*. PhD thesis, Universität Kaiserslautern, Kaiserslautern, 2012.

S.J. Hollister, D.P. Fyhrie, K.J. Jepsen, and S.A. Goldstein. Application of homogenization theory to the study of trabecular bone mechanics. *J.Biomech.*, 24:825–839, 1991. doi:10.1016/0021-9290(91)90308-A.

S.J. Hollister, J.M. Brennan, and N. Kikuchi. A homogenization sampling procedure for calculating trabecular bone effective stiffness and tissue level stress. *J.Biomech.*, 27: 433–444, 1994. doi:10.1016/0021-9290(94)90019-1.

S. Holmberg, K. Persson, and H. Petersson. Nonlinear mechanical behaviour and analysis of wood and fibre materials. *Comput.Struct.*, 72:459–480, 1999. doi:10.1016/S0045-7949(98)00331-9.

C.L. Hom and R.M. McMeeking. Plastic flow in ductile materials containing a cubic array of rigid spheres. *Int.J.Plast.*, 7:255–274, 1991. doi:10.1016/0749-6419(91)90035-W.

M. Hori and S. Nemat-Nasser. Double-inclusion model and overall moduli of multi-phase composites. *Mech.Mater.*, 14:189–206, 1993. doi:10.1016/0167-6636(93)90066-Z.

H. Horii and S. Nemat-Nasser. Overall moduli of solids with microcracks: Load induced anisotropy. *Int.J.Sol.Struct.*, 21:731–745, 1985. doi:10.1016/0022-5096(83)90048-0.

G.K. Hu. Composite plasticity based on matrix average second order stress moment. *Int.J.Sol.Struct.*, 34:1007–1015, 1997. doi:10.1016/S0020-7683(96)00044-3.

G.K. Hu and G.J. Weng. The connections between the double-inclusion model and the Ponte Castañeda–Willis, Mori–Tanaka, and Kuster–Toksoz models. *Mech.Mater.*, 32: 495–503, 2000. doi:10.1016/S0167-6636(00)00015-6.

G.K. Hu, G. Guo, and D. Baptiste. A micromechanical model of influence of particle fracture and particle cluster on mechanical properties of metal matrix composites. *Comput.Mater.Sci.*, 9:420–430, 1998. doi:10.1016/S0927-0256(97)00166-3.

G.K. Hu, X.N. Liu, and T.J. Lu. A variational method for nonlinear micropolar composites. *Mech.Mater.*, 37:407–425, 2005. doi:10.1016/j.mechmat.2004.03.006.

J.H. Huang. Some closed-form solutions for effective moduli of composites containing randomly oriented short fibers. *Mater.Sci.Engng. A*, 315:11–20, 2001. doi:10.1016/S0921-5093(01)01212-6.

J.H. Huang and J.S. Yu. Electroelastic Eshelby tensors for an ellipsoidal piezoelectric inclusion. *Compos.Engng.*, 4:1169–1182, 1994. doi:10.1016/0961-9526(95)91290-W.

Y. Huang and K.X. Hu. A generalized self-consistent mechanics method for solids containing elliptical inclusions. *J.Appl.Mech.*, 62:566–572, 1995. doi:10.1115/1.2895982.

Z.M. Huang. A unified micromechanical model for the mechanical properties of two constituent composite materials Part I: Elastic behavior. *J.Thermoplast.Compos.Mater.*, 13:252–271, 2000. doi:10.1177/089270570001300401.

Z.M. Huang and S. Ramakrishna. Micromechanical modeling approaches for the stiffness and strength of knitted fabric composites: A review and comparative study. *Composites A*, 31:479–501, 2000. doi:10.1016/S1359-835X(99)00083-4.

C.O. Huber, M.H. Luxner, S. Kremmer, S. Nogales, H.J. Böhm, and H.E. Pettermann. Forming simulations of MMC components by a micromechanics based hierarchical FEM approach. In J.M.A.C. de Sá and A.D. Santos, editors, *Proceedings of NUMIFORM 2007*, pages 1351–1356, New York, NY, 2007. American Institute of Physics. doi:10.1063/1.2740997.

C. Huet. Application of variational concepts to size effects in elastic heterogeneous bodies. *J.Mech.Phys.Sol.*, 38:813–841, 1990. doi:10.1016/0022-5096(90)90041-2.

C. Huet, P. Navi, and P.E. Roelfstra. A homogenization technique based on Hill's modification theorem. In G.A. Maugin, editor, *Continuum Models and Discrete Systems*, pages 135–143, Harlow, 1990. Longman.

M.I. Hussein, M.J. Leamy, and M. Ruzzene. Dynamics of phononic materials and structures: Historical origins, recent progress, and future outlook. *Appl.Mech.Rev.*, 66:040802, 2014. doi:10.1115/1.4026911.

J.W. Hutchinson. Plasticity on the micron scale. *Int.J.Sol.Struct.*, 37:225–238, 2000. doi:10.1016/S0020-7683(99)00090-6.

J.W. Hutchinson. Elastic-plastic behavior of polycrystalline metals and composites. *Proc. Roy.Soc.London*, A319:247–272, 1970. doi:10.1098/rspa.1970.0177.

A. Ibrahimbegović and D. Markovič. Strong coupling methods in multi-phase and multi-scale modeling of inelastic behavior of heterogeneous structures. *Comput.Meth.Appl.Mech.Engng.*, 192:3089–3107, 2003. doi:10.1016/S0045-7825(03)00342-6.

L. Iorga, Y. Pan, and A.A. Pelegri. Numerical characterization of material elastic properties for random fiber composites. *J.Mech.Mater.Struct.*, 3:1279–1298, 2008. doi:10.2140/jomms.2008.3.1279.

N. Ishikawa, D. Parks, S. Socrate, and M. Kurihara. Micromechanical modeling of ferrite–pearlite steels using finite element unit cell models. *ISIJ Int.*, 40:1170–1179, 2000. doi:10.2355/isijinternational.40.1170.

Y. Ismail, D.M. Yang, and J.Q. Ye. Discrete element method for generating random fibre distributions in micromechanical models for fibre reinforced composite laminates. *Composites B*, 90:485–492, 2016. doi:10.1016/j.compositesb.2016.01.037.

H. Ismar and F. Schröter. Three-dimensional finite element analysis of the mechanical behavior of cross ply-reinforced aluminum. *Mech.Mater.*, 32:329–338, 2000. doi:10.1016/S0167-6636(00)00008-9.

T. Iung and M. Grange. Mechanical behavior of two-phase materials investigated by the finite element method: Necessity of three-dimensional modeling. *Mater.Sci.Engng. A*, 201:L8–L11, 1995. doi:10.1016/0921-5093(95)09891-7.

D.S. Ivanov and S.V. Lomov. Modeling of 2D and 3D woven composites. In P. Irving and C. Soutis, editors, *Polymer Composites in the Aerospace Industry*, pages 23–57. Woodhead Publishing, Duxford, UK, 2020. doi:10.1016/B978-0-08-102679-3.00002-2.

S.K. Iyer, C.J. Lissenden, and S.M. Arnold. Local and overall flow in composites predicted by micromechanics. *Composites B*, 31:327–343, 2000. doi:10.1016/S1359-8368(00)00011-1.

N. Järvstråt. Homogenization and the mechanical behavior of metal composites. In H. Fujiwara, T. Abe, and K. Tanaka, editors, *Residual Stresses — III*, pages 70–75, London, 1992. Elsevier.

N. Järvstråt. An ellipsoidal unit cell for the calculation of micro-stresses in short fibre composites. *Comput.Mater.Sci.*, 1:203–212, 1993. doi:10.1016/0927-0256(93)90012-C.

K. Jayaraman and M.T. Kortschot. Correction to the Fukuda–Kawata Young's modulus theory and the Fukuda–Chou strength theory for short fibre-reinforced composite materials. *J.Mater.Sci.*, 31:2059–2064, 1996. doi:10.1007/BF00356627.

D. Jeulin. Random structure models for homogenization and fracture statistics. In D. Jeulin and M. Ostoja-Starzewski, editors, *Mechanics of Random and Multiscale Microstructures*, pages 33–91, Vienna, 2001. Springer-Verlag, CISM Courses and Lectures Vol. 430. doi:10.1007/978-3-7091-2780-3_2.

M. Jiang, M. Ostoja-Starzewski, and I. Jasiuk. Scale-dependent bounds on effective elastoplastic response of random composites. *J.Mech.Phys.Sol.*, 49:655–673, 2001. doi:10.1016/S0022-5096(00)00034-X.

M. Jiang, I. Jasiuk, and M. Ostoja-Starzewski. Apparent thermal conductivity of periodic two-dimensional composites. *Comput.Mater.Sci.*, 25:329–338, 2002a. doi:10.1016/S0927-0256(02)00234-3.

W.G. Jiang, S.R. Hallett, and M.R. Wisnom. Development of domain superposition technique for the modelling of woven fabric composites. In P.P. Camanho, C.G. Dávila, S.T. Pinho, and J.J.C. Remmers, editors, *Mechanical Response of Composites*, pages 281–291, Berlin, 2008. Springer-Verlag. doi:10.1007/978-1-4020-8584-0_14.

Y. Jiao, F.H. Stillinger, and S. Torquato. Modeling heterogeneous materials via two-point correlation functions: Basic principles. *Phys.Rev. E*, 76:031110, 2007. doi:10.1103/PhysRevE.76.031110.

N. Jiménez Segura, B.L.A. Pichler, and C. Hellmich. Concentration tensors preserving elastic symmetry of multiphase composites. *Mech.Mater.*, 178:104555, 2023. doi:10.1016/j.mechmat.2023.104555.

X. Jin, D. Lyu, X. Zhang, Q. Zhou, Q. Wang, and L.M. Keer. Explicit analytical solutions for a complete set of the Eshelby tensors of an ellipsoidal inclusion. *J.Appl.Mech.*, 83: 121010, 2016. doi:10.1115/1.4034705.

M. Jirásek and S. Rolshoven. Comparison of integral-type nonlocal plasticity models for strain softening materials. *Int.J.Engng.Sci.*, 41:1553–1602, 2003. doi:10.1016/S0020-7225(03)00027-2.

B. Johannesson and O.B. Pedersen. Analytical determination of the average Eshelby tensor for transversely isotropic fiber orientation distributions. *Acta mater.*, 46:3165–3173, 1998. doi:10.1016/S1359-6454(98)00003-2.

R.M. Jones. *Mechanics of Composite Materials*. Taylor & Francis, Philadelphia, PA, 1999. ISBN 1-560-32712-X.

J.W. Ju and L.Z. Sun. Effective elastoplastic behavior of metal matrix composites containing randomly located aligned spheroidal inhomogeneities. Part I: Micromechanics-based formulation. *Int.J.Sol.Struct.*, 38:183–201, 2001. doi:10.1016/S0020-7683(00)00023-8.

J.W. Ju and L.Z. Sun. A novel formulation for the exterior point Eshelby's tensor of an ellipsoidal inclusion. *J.Appl.Mech.*, 66:570–574, 1999. doi:10.1115/1.2791090.

M. Kabel, A. Fink, and M. Schneider. The composite voxel technique for inelastic problems. *Comput.Meth.Appl.Mech.Engng.*, 322:396–418, 2017. doi:10.1016/j.cma.2017.04.025.

M. Kachanov and I. Sevostianov. On quantitative characterization of microstructures and effective properties. *Int.J.Sol.Struct.*, 42:309–336, 2005. doi:10.1016/j.ijsolstr.2004.06.016.

M. Kachanov and I. Sevostianov. *Effective Properties of Heterogeneous Materials*. Springer-Verlag, New York, NY, 2013. ISBN 978-94-007-5714-1.

M. Kachanov and I. Sevostianov. *Micromechanics of Materials, with Applications*. Springer International. Cham, 2018. ISBN 978-3-319-76203-6.

M. Kachanov, I. Tsukrov, and B. Shafiro. Effective moduli of solids with cavities of various shapes. *Appl.Mech.Rev.*, 47:151–S174, 1994. doi:10.1115/1.3122810.

M. Kailasam, N. Aravas, and P. Ponte Castañeda. Porous metals with developing anisotropy: Constitutive models, computational issues and applications to deformation processing. *Comput.Model.Engng.Sci.*, 1:105–118, 2000. doi:10.3970/cmes.2000.001.265.

A.L. Kalamkarov, I.V. Andrianov, and V.V. Danishevs'kyy. Asymptotic homogenization of composite materials and structures. *Appl.Mech.Rev.*, 62:030802, 2009. doi:10.1115/1.3090830.

S. Kammoun, I. Doghri, L. Adam, G. Robert, and L. Delannay. First pseudo-grain failure model for inelastic composites with misaligned short fibers. *Composites A*, 42:1892–1902, 2011. doi:10.1016/j.compositesa.2011.08.013.

S.K. Kanaun. Efficient homogenization techniques for elastic composites: Maxwell scheme vs. effective field method. *Int.J.Engng.Sci.*, 103:19–34, 2016. doi:10.1016/j.ijengsci.2016.03.004.

S.K. Kanaun and V.M. Levin. Effective field method in mechanics of matrix composite materials. In K.Z. Markov, editor, *Recent Advances in Mathematical Modelling of Composite Materials*, pages 1–58, Singapore, 1994. World Scientific. doi:10.1142/9789814354219_0001.

H. Kang and G.W. Milton. Solutions to the Pólya–Szegö conjecture and the weak Eshelby conjecture. *Arch.Rat.Mech.Anal.*, 188:93–116, 2008. doi:10.1007/s00205-007-0087-z.

T. Kanit, S. Forest, I. Gallier, V. Mounoury, and D. Jeulin. Determination of the size of the representative volume element for random composites: Statistical and numerical approach. *Int.J.Sol.Struct.*, 40:3647–3679, 2003. doi:10.1016/S0020-7683(03)00143-4.

T. Kanit, F. N'Guyen, S. Forest, D. Jeulin, M. Reed, and S. Singleton. Apparent and effective physical properties of heterogeneous materials: Representativity of samples of two materials from food industry. *Comput.Meth.Appl.Mech.Engng.*, 195:3960–3982, 2006. doi:10.1016/j.cma.2005.07.022.

P. Kanouté, D.P. Boso, J.L. Chaboche, and B.A. Schrefler. Multiscale methods for composites: A review. *Arch.Comput.Meth.Engng.*, 16:31–75, 2009. doi:10.1007/s11831-008-9028-8.

P. Karimi, A. Malyarenko, M. Ostoja-Starzewski, and X. Zhang. RVE problem: Mathematical aspects and related stochastic mechanics. *Int.J.Engng.Sci.*, 146:103169, 2020. doi:10.1016/j.ijengsci.2019.103169.

P. Kenesei, A. Borbély, and H. Biermann. Microstructure based three-dimensional finite element modeling of particulate reinforced metal matrix composites. *Mater.Sci. Engng. A*, 387:852–856, 2004. doi:10.1016/j.msea.2004.02.076.

E.H. Kerner. The elastic and thermo-elastic properties of composite media. *Proc.Phys.Soc.London*, B69:808–813, 1956. doi:10.1088/0370-1301/69/8/305.

Y.M Khalevitsky and A.V. Konovalov. A gravitational approach to modeling the representative volume geometry of particle reinforced metal matrix composites. *Engng.w.Comput.*, 35:1037–1044, 2019. doi:10.1007/s00366-018-0649-8.

Z.F. Khisaeva and M. Ostoja-Starzewski. On the size of RVE in finite elasticity of random composites. *J.Elast.*, 85:153–173, 2006. doi:10.1007/s10659-006-9076-y.

D.W. Kim, J.H. Lim, and S. Lee. Prediction and validation of the transverse mechanical behavior of unidirectional composites considering interfacial debonding through convolutional neural networks. *Composites B*, 225:109314, 2021. doi:10.1016/j.compositesb.2021.109314.

K. Kitazono, E. Sato, and K. Kuribayashi. Application of mean-field approximation to elastic-plastic behavior for closed cell metal foams. *Acta mater.*, 51:4823–4836, 2003. doi:10.1016/S1359-6454(03)00322-7.

J. Koplik and A. Needleman. Void growth and coalescence in porous plastic solids. *Int.J.Sol.Struct.*, 24:835–853, 1988. doi:10.1016/0020-7683(88)90051-0.

V.G. Kouznetsova, M.G.D. Geers, and W.A.M. Brekelmans. Multi-scale constitutive modeling of heterogeneous materials with a gradient-enhanced computational homogenization scheme. *Int.J.Num.Meth.Engng.*, 54:1235–1260, 2002. doi:10.1002/nme.541.

V.G. Kouznetsova, M.G.D. Geers, and W.A.M. Brekelmans. Multi-scale second-order computational homogenization of multi-phase materials: A nested finite element solution strategy. *Comput.Meth.Appl.Mech.Engng.*, 193:5525–5550, 2004. doi:10.1016/j.cma.2003.12.073.

K. Krabbenhøft, M. Hain, and P. Wriggers. Computation of effective cement paste diffusivities from microtomographic images. In V.V. Kompiš, editor, *Composites with Micro- and Nano-Structure: Computational Modeling and Experiments*, pages 281–297, Berlin, 2008. Springer-Verlag. doi:10.1007/978-1-4020-6975-8_15.

I. Krakovsky and V. Myroshnychenko. Modelling dielectric properties of composites by finite element method. *J.Appl.Phys.*, 92:6743–6748, 2002. doi:10.1063/1.1516837.

A.M. Kraynik and D.A. Reinelt. Elastic-plastic behavior of a Kelvin foam. In D. Weaire, editor, *The Kelvin Problem. Foam Structures of Minimal Surface Area*, pages 93–108, London, 1996. Taylor & Francis.

E. Kröner. Self-consistent scheme and graded disorder in polycrystal elasticity. *J.Phys.F*, 8:2261–2267, 1978. doi:10.1088/0305-4608/8/11/011.

V.I. Kushch. *Micromechanics of Composites: Multipole Expansion Approach*. Butterworth–Heinemann, Kidlington, UK, 2013. ISBN 978-0-12-407683-9.

V.I. Kushch, I. Sevostianov, and L. Mishnaevsky. Stress concentration and the effective stiffness of aligned fiber reinforced composite with anisotropic constituents. *Int.J.Sol.Struct.*, 45:5103–5117, 2008. doi:10.1016/j.ijsolstr.2008.05.009.

G.T. Kuster and M.N. Toksöz. Velocity and attenuation of seismic waves in two-phase media: I. Theoretical formulation. *Geophysics*, 39:587–606, 1974. doi:10.1190/1.1440450.

N. Lahellec and P. Suquet. Effective behavior of linear viscoelastic composites: A time-integration approach. *Int.J.Sol.Struct.*, 44:507–529, 2007. doi:10.1016/j.ijsolstr.2006.04.038.

N. Lahellec and P. Suquet. Effective response and field statistics in elastoplastic and elasto-viscoplastic composites under radial and non-radial loadings. *Int.J.Plast.*, 42:1–30, 2013. doi:10.1016/j.ijplas.2012.09.005.

F. Larsson, K. Runesson, S. Saroukhani, and R. Vafadari. Computational homogenization based on a weak format of microperiodicity for RVE-problems. *Comput.Meth.Appl.Sci.Engng.*, 200:11–26, 2011. doi:10.1016/j.cma.2010.06.023.

E.A. Lazar, J.K. Mason, R.D. McPherson, and D.J. Srolovitz. Complete topology of cells, grains, and bubbles in three-dimensional microstructures. *Phys.Rev.Lett.*, 109:095505, 2012. doi:10.1103/PhysRevLett.109.095505.

H.K. Lee and S. Simunovic. Modeling of progressive damage in aligned and randomly oriented discontinuous fiber polymer matrix composites. *Composites B*, 31:77–86, 2000. doi:10.1016/S1359-8368(99)00070-0.

H.W. Lee, A. Gillman, and K. Matouš. Computing overall elastic constants of polydisperse particular composites from microtomographic data. *J.Mech.Phys.Sol.*, 59:1838–1857, 2011a. doi:10.1016/j.jmps.2011.05.010.

K.H. Lee and S. Ghosh. Small deformation multi-scale analysis of heterogeneous materials with the Voronoi cell finite element model and homogenization theory. *Comput.Mater.Sci.*, 7:131–146, 1996. doi:10.1016/S0927-0256(96)00072-9.

W.J. Lee, Y.J. Kim, N.H. Kang, I.M. Park, and Y.H. Park. Finite-element modeling of the particle clustering effect in a powder-metallurgy-processed ceramic-particle-reinforced metal matrix composite on its mechanical properties. *Mech.Compos.Mater.*, 46:639–648, 2011b. doi:110.1007/s11029-011-9177-y.

G. Legrain, P. Cartraud, I. Perreard, and N. Moës. An X-FEM and level set computational approach for image based modelling: Application to homogenization. *Int.J.Numer.Meth.Engng.*, 86:915–934, 2011. doi:10.1002/nme.3085.

B.A. Lerch, M.E. Melis, and M. Tong. Experimental and analytical analysis of the stress–strain behavior in a $[90/0]_{2S}$ SiC/Ti-15-3 laminate. Technical Report NASA–TM–104470, NASA, 1991.

M. Lévesque, M.D. Gilchrist, N. Bouleau, K. Derrien, and D. Baptiste. Numerical inversion of the Laplace–Carson transform applied to homogenization of randomly reinforced linear viscoelastic media. *Comput.Mech.*, 10:771–789, 2007. doi:10.1007/s00466-006-0138-6.

V.M. Levin. On the coefficients of thermal expansion of heterogeneous materials. *Mech.Sol.*, 2:58–61, 1967.

A. Levy and J.M. Papazian. Elastoplastic finite element analysis of short-fiber-reinforced SiC/Al composites: Effects of thermal treatment. *Acta metall.mater.*, 39:2255–2266, 1991. doi:10.1016/0956-7151(91)90008-O.

H. Li, B. Zhang, and G. Bai. Effect of constructing different unit cells on predicting composite viscoelastic properties. *Compos.Struct.*, 125:459–466, 2015. doi:10.1016/j.compstruct.2015.02.028.

M. Li, S. Ghosh, O. Richmond, H. Weiland, and T.N. Rouns. Three dimensional characterization and modeling of particle reinforced metal matrix composites, Part I: Quantitative description of microstructural morphology. *Mater.Sci.Engng. A*, 265:153–173, 1999. doi:10.1016/S0921-5093(98)01132-0.

S. Li and Z. Zou. The use of central reflection in the formulation of unit cells for micromechanical FEA. *Mech.Mater.*, 43:824–834, 2011. doi:10.1016/j.mechmat.2011.08.014.

S.G. Li. On the nature of periodic traction boundary conditions in micromechanical FE analyses of unit cells. *SIAM J.Appl.Math.*, 77:441–450, 2012. doi:10.1093/imamat/hxr024.

S.G. Li and A. Wongsto. Unit cells for micromechanical analyses of particle-reinforced composites. *Mech.Mater.*, 36:543–572, 2004. doi:10.1016/S0167-6636(03)00062-0.

W. Li and M. Ostoja-Starzewski. Yield of random elastoplastic materials. *J.Mech.Mater.Struct.*, 1:1055–1073, 2006. doi:10.2140/jomms.2006.1.1055.

Y.Y. Li and J.Z. Cui. The multi-scale computational method for the mechanics parameters of the materials with random distribution of multi-scale grains. *Compos.Sci.Technol.*, 65:1447–1458, 2005. doi:10.1016/j.compscitech.2004.12.016.

G. Lielens, P. Pirotte, A. Couniot, F. Dupret, and R. Keunings. Prediction of thermo-mechanical properties for compression-moulded composites. *Composites A*, 29:63–70, 1998. doi:10.1016/S1359-835X(97)00039-0.

D.S. Liu, C.Y. Chen, and D.Y. Chiou. 3-D modeling of a composite material reinforced with multiple thickly coated particles using the infinite element method. *Comput.Model.Engng.Sci.*, 9:179–192, 2005a. doi:10.3970/cmes.2005.009.179.

L. Liu, R.D. James, and P.H. Leo. Periodic inclusion–matrix microstructures with constant field inclusions. *Metall.Mater.Trans.*, 38A:781–787, 2007. doi:10.1007/s11661-006-9019-z.

Y.J. Liu, N. Nishimura, Y. Otani, T. Takahashi, X.L. Chen, and H. Munakata. A fast boundary element method for the analysis of fiber-reinforced composites based on rigid-inclusion model. *J.Appl.Mech.*, 72:115–128, 2005b. doi:10.1115/1.1825436.

J. LLorca. A numerical analysis of the damage mechanisms in metal-matrix composites under cyclic deformation. *Comput.Mater.Sci.*, 7:118–122, 1996. doi:10.1016/S0927-0256(96)00070-5.

M. Lo Cascio, A. Milazzo, and I. Benedetti. Virtual element method for computational homogenization of composite and heterogeneous materials. *Comput.Struct.*, 232:111523, 2020. doi:10.1016/j.compstruct.2019.111523.

S.V. Lomov, D.S. Ivanov, I. Verpoest, M. Zeko, T. Kurashiki, H. Nakai, and S. Hirosawa. Meso-FE modelling of textile composites: Road map, data flow and algorithms. *Compos.Sci.Technol.*, 67:1870–1891, 2006. doi:10.1016/j.compscitech.2006.10.017.

B.D. Lubachevsky, F.H. Stillinger, and E.N. Pinson. Disks vs. spheres: Contrasting properties of random packing. *J.Statist.Phys.*, 64:501–524, 1991. doi:10.1007/BF01048304.

V.A. Lubarda and X. Markenscoff. On the absence of Eshelby property for non-ellipsoidal inclusions. *Int.J.Sol.Struct.*, 35:3405–3411, 1998. doi:10.1016/S0020-7683(98)00025-0.

H.R. Lusti, P.J. Hine, and A.A. Gusev. Direct numerical predictions for the elastic and thermoelastic properties of short fibre composites. *Compos.Sci.Technol.*, 62:1927–1934, 2002. doi:10.1016/S0266-3538(02)00106-9.

M.H. Luxner, J. Stampfl, and H.E. Pettermann. Finite element modeling concepts and linear analyses of 3D regular open cell structures. *J.Mater.Sci.*, 40:5859–5866, 2005. doi:10.1007/s10853-005-5020-y.

F. Maggi, S. Stafford, T.L. Jackson, and J. Buckmaster. Nature of packs used in propellant modeling. *Phys.Rev. E*, 77:046107, 2008. doi:10.1103/PhysRevE.77.046107.

J.M. Mahishi. An integrated micromechanical and macromechanical approach to fracture behavior of fiber-reinforced composites. *Engng.Fract.Mech.*, 25:197–228, 1986. doi:10.1016/0013-7944(86)90218-3.

E. Maire, F. Wattebled, J.Y. Buffière, and G. Peix. Deformation of a metallic foam studied by X-ray computed tomography and finite element calculations. In T.W. Clyne and F. Simancik, editors, *Metal Matrix Composites and Metallic Foams*, pages 68–73, Weinheim, 2000. Wiley–VCH. doi:10.1002/3527606165.ch11.

M. Majewski, M. Kursa, P. Hołobut, and K. Kowalczyk-Gajewska. Micromechanical and numerical analysis of packing and size effects in elastic particulate composites. *Composites*, 124B:158–174, 2017. doi:10.1016/j.compositesb.2017.05.004.

M. Majewski, M. Wichrowski, P. Hołobut, and K. Kowalczyk-Gajewska. Shape and packing effects in particulate composites: Micromechanical modelling and numerical verification. *Arch.Civ.Mech.Engng.*, 22:86, 2022. doi:10.1007/s43452-022-00405-9.

P. Makowski, W. John, G. Kuś, and G. Kokot. Multiscale modeling of the simplified trabecular bone structure. In *Mechanika: Proceedings of the 18th International Conference*, pages 156–161, Kaunas, 2013.

J. Mandel. Généralisation de la théorie de la plasticité de W.T. Koiter. *Int.J.Sol.Struct.*, 1:273–295, 1965. doi:10.1016/0020-7683(65)90034-X.

J. Mandel. *Plasticité classique et viscoplasticité*. CISM lecture notes, vol. 97, Springer–Verlag, Wien, 1972.

C. Mareau and C. Robert. Different composite voxel methods for the numerical homogenization of heterogeneous inelastic materials with FFT-based techniques. *Mech.Mater.*, 105:157–165, 2017. doi:10.1016/j.mechmat.2016.12.002.

S. Marfia and E. Sacco. Multiscale technique for nonlinear analysis of elastoplastic and viscoplastic composites. *Composites B*, 136:241–253, 2018. doi:10.1016/j.compositesb.2017.10.015.

F. Marketz and F.D. Fischer. Micromechanical modelling of stress-assisted martensitic transformation. *Modell.Simul.Mater.Sci.Engng.*, 2:1017–1046, 1994. doi:10.1088/0965-0393/2/5/006.

K. Markov. Elementary micromechanics of heterogeneous media. In K. Markov and L. Preziosi, editors, *Heterogeneous Media: Micromechanics Modeling Methods and Simulations*, pages 1–162, Boston, 2000. Birkhäuser. doi:10.1007/978-1-4612-1332-1_1.

R. Masson. New explicit expressions of the Hill polarization tensor for general anisotropic elastic solids. *Int.J.Sol.Struct.*, 45:757–769, 2008. doi:10.1016/j.ijsolstr.2007.08.035.

R. Masson, M. Bornert, P. Suquet, and A. Zaoui. An affine formulation for the prediction of the effective properties of nonlinear composites and polycrystals. *J.Mech.Phys.Sol.*, 48:1203–1227, 2000. doi:10.1016/S0022-5096(99)00071-X.

C.F. Matt and M.A.E. Cruz. Application of a multiscale finite-element approach to calculate the effective thermal conductivity of particulate media. *Comput.Appl.Math.*, 21: 429–460, 2002.

C.F. Matt and M.A.E. Cruz. Effective thermal conductivity of composite materials with 3-D microstructures and interfacial thermal resistance. *Numer.Heat Transf.*, A53:577–604, 2008. doi:10.1080/10407780701678380.

A.Y. Matveeva, G. Kravchenko, H.J. Böhm, and F.W.J. van Hattum. Investigation of the embedded element technique for modelling wavy CNT composites. *Comput.Mater.Cont.*, 42:1–23, 2014. doi:10.3970/cmc.2014.042.001.

J.C. Maxwell. *A Treatise on Electricity and Magnetism*. Clarendon Press, Oxford, 1873. doi:10.1017/CBO9780511709333.

D.L. McDowell. Modeling and experiments in plasticity. *Int.J.Sol.Struct.*, 37:293–310, 2000. doi:10.1016/S0020-7683(99)00094-3.

P.E. McHugh, R.J. Asaro, and C.F. Shih. Computational modeling of metal-matrix composite materials — I. Isothermal deformation patterns in ideal microstructures. *Acta metall.mater.*, 41:1461–1476, 1993. doi:10.1016/0956-7151(93)90255-Q.

R. McLaughlin. A study of the differential scheme for composite materials. *Int.J.Engng. Sci.*, 15:237–244, 1977. doi:10.1016/0020-7225(77)90058-1.

R. McMeeking and C.L. Hom. Finite element analysis of void growth in elastic-plastic materials. *Int.J.Fract.*, 42:1–19, 1990. doi:10.1007/BF00018610.

C. Meng, W. Heltsley, and D.D. Pollard. Evaluation of the Eshelby solution for the ellipsoidal inclusion and heterogeneity. *Comput.Geosci*, 40:40–48, 2012. doi:10.1016/j.cageo.2011.07.008.

S.D. Mesarovic and J. Padbidri. Minimal kinetic boundary conditions for simulations of disordered microstructures. *Phil.Mag.*, 85:65–78, 2005. doi:10.1080/14786430412331313321.

J.C. Michel and P. Suquet. Computational analysis of nonlinear composite structures using the nonuniform transformation field analysis. *Comput.Meth.Appl.Mech.Engng.*, 193:5477–5502, 2004. doi:10.1016/j.cma.2003.12.071.

J.C. Michel, H. Moulinec, and P. Suquet. Effective properties of composite materials with periodic microstructure: A computational approach. *Comput.Meth.Appl.Mech.Engng.*, 172:109–143, 1999. doi:10.1016/S0045-7825(98)00227-8.

J.C. Michel, H. Moulinec, and P. Suquet. Composites à microstructure périodique. In M. Bornert, T. Bretheau, and P. Gilormini, editors, *Homogénéisation en mécanique des matériaux 1. Matériaux aléatoires élastiques et milieux périodiques*, pages 57–94, Paris, 2001. Editions Hermès.

N.J. Mills, R. Stämpfli, F. Marone, and P.A. Brühwiler. Finite element micromechanics model of impact compression of closed-cell polymeric foams. *Int.J.Sol.Struct.*, 46:677–697, 2009. doi:10.1016/j.ijsolstr.2008.09.012.

T. Miloh and Y. Benveniste. A generalized self-consistent method for the effective conductivity of composites with ellipsoidal inclusions and cracked bodies. *J.Appl.Phys.*, 63: 789–796, 1988. doi:10.1063/1.340071.

G.W. Milton. *The Theory of Composites*. Cambridge University Press, Cambridge, 2002. ISBN 0-521-88125-6.

G.W. Milton. Bounds on the electromagnetic, elastic, and other properties of two-component composites. *Phys.Rev.Lett.*, 46:542–545, 1981. doi:10.1103/PhysRevLett.46.542.

L.L. Mishnaevsky. Three-dimensional numerical testing of microstructures of particle reinforced composites. *Acta mater.*, 52:4177–4188, 2004. doi:10.1016/j.actamat.2004.05.032.

D. Missoum-Benziane, D. Ryckelynck, and F. Chinesta. A new fully coupled two-scales modelling for mechanical problems involving microstructure: The 95/5 technique. *Comput.Meth.Appl.Mech.Engng.*, 196:2325–2337, 2007. doi:10.1016/j.cma.2006.10.013.

B. Mlekusch. Thermoelastic properties of short-fibre-reinforced thermoplastics. *Compos. Sci.Technol.*, 59:911–923, 1999. doi:10.1016/S0266-3538(98)00133-X.

M. Moakher and A.N. Norris. The closest elastic tensor of arbitrary symmetry to an elastic tensor of lower symmetry. *J.Elast.*, 85:215–263, 2006. doi:10.1007/s10659-006-9082-0.

N. Moës, M. Cloirec, P. Cartraud, and J.F. Remacle. A computational approach to handle complex microstructure geometries. *Comput.Meth.Appl.Mech.Engng.*, 192:3163–3177, 2003. doi:10.1016/S0045-7825(03)00346-3.

A. Molinari, G.R. Canova, and S. Ahzi. A self-consistent approach for large deformation viscoplasticity. *Acta metall.*, 35:2983–2984, 1987. doi:10.1016/0001-6160(87)90297-5.

J. Monaghan and D. Brazil. Modeling the sub-surface damage associated with the machining of a particle reinforced MMC. *Comput.Mater.Sci.*, 9:99–107, 1997. doi:10.1016/S0927-0256(97)00063-3.

I. Monetto and W.J. Drugan. A micromechanics-based nonlocal constitutive equation and minimum RVE size estimates for random elastic composites containing aligned spheroidal heterogeneities. *J.Mech.Phys.Sol.*, 57:1578–1595, 2009. doi:10.1016/S0022-5096(03)00103-0.

T. Mori and K. Tanaka. Average stress in matrix and average elastic energy of materials with misfitting inclusions. *Acta metall.*, 21:571–574, 1973. doi:10.1016/0001-6160(73)90064-3.

Z.A. Moschovidis and T. Mura. Two ellipsoidal inhomogeneities by the equivalent inclusion method. *J.Appl.Mech.*, 42:847–852, 1975. doi:10.1115/1.3423718.

O.F. Mossotti. Discussione analitica sull'influenza che l'azione di un mezzo dielettrico ha sulla distribuzione dell'elettricitá alla superficie di piú corpi elettrici disseminati in eso. *Mem.Mat.Fis.Soc.Ital.Sci.Modena*, 24:49–74, 1850.

C. Motz, R. Pippan, A. Ableidinger, H.J. Böhm, and F.G. Rammerstorfer. Deformation and fracture behavior of ductile aluminium foams in the presence of notches under tensile loading. In J. Banhart, M.F. Ashby, and N.A. Fleck, editors, *Cellular Metals and Metal Foaming Technology*, pages 299–304, Bremen, 2001. Verlag MIT Publishing.

H. Moulinec and P. Suquet. A fast numerical method for computing the linear and nonlinear mechanical properties of composites. *C.R.Acad.Sci.Paris, série II*, 318:1417–1423, 1994.

H. Moulinec and P. Suquet. A numerical method for computing the overall response of nonlinear composites with complex microstructure. *Comput.Meth.Appl.Mech.Engng.*, 157:69–94, 1997. doi:10.1016/S0045-7825(97)00218-1.

H. Moussaddy, D. Therriault, and M. Lévesque. Assessment of existing and introduction of a new and robust efficient definition of the representative volume element. *Int.J.Sol.Struct.*, 50:3817–3828, 2013. doi:10.1016/j.ijsolstr.2013.07.016.

W.H. Müller. Mathematical vs. experimental stress analysis of inhomogeneities in solids. *J.Phys.IV*, 6:C1–139–C1–148, 1996. doi:10.1051/jp4:1996114.

T. Mura. *Micromechanics of Defects in Solids*. Martinus Nijhoff, Dordrecht, 1987. ISBN 9-024-73256-5.

T. Nakamura and S. Suresh. Effects of thermal residual stresses and fiber packing on deformation of metal-matrix composites. *Acta metall.mater.*, 41:1665–1681, 1993. doi:10.1016/0956-7151(93)90186-V.

A. Needleman. A continuum model for void nucleation by inclusion debonding. *J.Appl.Mech.*, 54:525–531, 1987. doi:10.1115/1.3173064.

S. Nemat-Nasser. Averaging theorems in finite deformation plasticity. *Mech.Mater.*, 31: 493–523, 1999. doi:10.1016/S0167-6636(98)00073-8.

S. Nemat-Nasser and M. Hori. *Micromechanics: Overall Properties of Heterogeneous Solids*. North–Holland, Amsterdam, 1993. ISBN 0-444-89881-6.

V.D. Nguyen, E. Béchet, C. Geuzaine, and L. Noels. Imposing periodic boundary conditions on arbitrary meshes by polynomial interpolation. *Comput.Mater.Sci.*, 55:390–406, 2012. doi:10.1016/j.commatsci.2011.10.017.

V.D. Nguyen, L. Wu, and L. Noels. Unified treatment of microscopic boundary conditions and efficient algorithms for estimating tangent operators of the homogenized behavior in the computational homogenization method. *Comput.Mech.*, 59:483–505, 2017. doi:10.1007/s00466-016-1358-z.

V.P. Nguyen, M. Stroeven, and L.J. Sluys. Multiscale continuous and discontinuous modeling of heterogeneous materials: A review on recent developments. *J.Multiscal.Model.*, 3:229–270, 2011. doi:10.1142/S1756973711000509.

G.L. Niebur, J.C. Yuen, A.C. Hsia, and T.M. Keaveny. Convergence behavior of high-resolution finite element models of trabecular bone. *J.Biomech.Engng.*, 121:629–635, 1999. doi:10.1115/1.2800865.

C.F. Niordson and V. Tvergaard. Nonlocal plasticity effects on the tensile properties of a metal matrix composite. *Eur.J.Mech. A/Solids*, 20:601–613, 2001. doi:10.1016/S0997-7538(01)01149-4.

S. Nogales. *Numerical Simulation of the Thermal and Thermomechanical Behavior of Metal Matrix Composites*. Reihe 18, Nr. 317. VDI–Verlag, Düsseldorf, 2008. ISBN 3-18-140118-8.

S. Nogales and H.J. Böhm. Modeling of the thermal conductivity and thermomechanical behavior of diamond reinforced composites. *Int.J.Engng.Sci.*, 46:606–619, 2008. doi:10.1016/j.ijengsci.2008.01.011.

A.N. Norris. The isotropic material closest to a given anisotropic material. *J.Mech.Mater. Struct.*, 1:223–238, 2006. doi:10.2140/jomms.2006.1.223.

A.N. Norris. A differential scheme for the effective moduli of composites. *Mech.Mater.*, 4: 1–16, 1985. doi:10.1016/0167-6636(85)90002-X.

D. Nouailhas and G. Cailletaud. Finite element analysis of the mechanical behavior of two-phase single crystal superalloys. *Scr.mater.*, 34:565–571, 1996. doi:10.1016/1359-6462(95)00547-1.

J. Novák, Ł. Kaczmarczyk, P. Grassl, J. Zeman, and C.J. Pearce. A micromechanics-enhanced finite element formulation for modelling heterogeneous materials. *Comput.Meth.Appl.Mech.Engng.*, 201–204:53–64, 2012. doi:10.1016/j.cma.2011.09.003.

J.F. Nye. *Physical Properties of Crystals, Their Representation by Tensors and Matrices*. Clarendon, Oxford, 1957. ISBN 0-198-51165-5.

M. Nygårds. Number of grains necessary to homogenize elastic materials with cubic symmetry. *Mech.Mater.*, 35:1049–1057, 2003. doi:10.1016/S0167-6636(02)00325-3.

R.J. O'Connell and B. Budiansky. Seismic velocities in dry and saturated cracked solids. *J.Geophys.Res.*, 79:5412–5426, 1974. doi:10.1029/JB079i035p05412.

J.T. Oden and T.I. Zohdi. Analysis and adaptive modeling of highly heterogeneous elastic structures. *Comput.Meth.Appl.Mech.Engng.*, 148:367–391, 1997. doi:10.1016/S0045-7825(97)00032-7.

S. Onaka. Averaged Eshelby tensor and elastic strain energy of a superspherical inclusion with uniform eigenstrains. *Phil.Mag.Lett.*, 81:265–272, 2001. doi:10.1080/09500830010019031.

P. Onck and E. van der Giessen. Microstructurally-based modelling of intergranular creep fracture using grain elements. *Mech.Mater.*, 26:109–126, 1997. doi:10.1016/S0167-6636(97)00020-3.

S.M. Oppenheimer and D.C. Dunand. Finite element modeling of creep deformation in cellular materials. *Acta mater.*, 55:3825–3834, 2007. doi:10.1016/j.actamat.2007.02.033.

M. Ostoja-Starzewski. Lattice models in micromechancis. *Appl.Mech.Rev.*, 55:35–60, 2002. doi:10.1115/1.1432990.

M. Ostoja-Starzewski. Material spatial randomness: From statistical to representative volume element. *Probab.Engng.Mech.*, 21:112–131, 2006. doi:10.1016/j.probengmech.2005.07.007.

M. Ostoja-Starzewski. *Microstructural Randomness and Scaling in Mechanics of Materials*. Chapman & Hall, Boca Raton, FL, 2008. ISBN 1-584-88417-7.

M. Ostoja-Starzewski, X. Du, Z.F. Khisaeva, and W. Li. Comparisons of the size of the representative volume element in elastic, plastic, thermoelastic, and permeable random microstructures. *Int.J.Multiscal.Comput.Engng.*, 5:73–82, 2007. doi:10.1615/IntJMultCompEng.v5.i2.10.

T. Ozturk, C. Stein, R. Pokharel, C. Hefferan, H. Tucker, S. Jha, R. John, R.A. Lebenssohn, P. Kenesei, and R.M. Suter. Simulation domain size requirements for elastic response of 3D polycrystalline materials. *Modell.Simul.Mater.Sci.Engng.*, 24:015006, 2016. doi:10.1088/0965-0393/24/1/015006.

D.H. Pahr. *Experimental and Numerical Investigations of Perforated FRP-Laminates*. Reihe 18, Nr. 284. VDI–Verlag, Düsseldorf, 2003. ISBN 3-183-28418-9.

D.H. Pahr and S.M. Arnold. The applicability of the generalized method of cells for analyzing discontinuously reinforced composites. *Composites B*, 33:153–170, 2002. doi:10.1088/0965-0393/24/1/015006.

D.H. Pahr and H.J. Böhm. Assessment of mixed uniform boundary conditions for predicting the mechanical behavior of elastic and inelastic discontinuously reinforced composites. *Comput.Model.Engng.Sci.*, 34:117–136, 2008. doi:10.3970/cmes.2008.034.117.

D.H. Pahr and F.G. Rammerstorfer. Buckling of honeycomb sandwiches: Periodic finite element considerations. *Comput.Model.Engng.Sci.*, 12:229–242, 2006. doi:10.3970/cmes.2006.012.229.

D.H. Pahr and P.K. Zysset. Influence of boundary conditions on computed apparent elastic properties of cancellous bone. *Biomech.Model.Mechanobiol.*, 7:463–476, 2008. doi:10.1007/s10237-007-0109-7.

J. Panyasantisuk, D.H. Pahr, and P.K. Zysset. Effect of boundary conditions on yield properties of human femoral trabecular bone. *Biomech.Model.Mechanobiol.*, 15:1043–1053, 2016. doi:10.1007/s10237-015-0741-6.

S.D. Papka and S. Kyriakides. In-plane compressive response and crushing of honeycomb. *J.Mech.Phys.Sol.*, 42:1499–1532, 1994. doi:10.1016/0022-5096(94)90085-X.

A. Paquin, H. Sabar, and M. Berveiller. Integral formulation and self consistent modelling of elastoviscoplastic behaviour of heterogeneous materials. *Arch.Appl.Mech.*, 69:14–35, 1999. doi:10.1007/s004190050201.

W.J. Parnell. The Eshelby, Hill, moment and concentration tensors for ellipsoidal inhomogeneities in the Newtonian potential problem and linear elastostatics. *J.Elast.*, 125:231–294, 2016. doi:10.1007/s10659-016-9573-6.

W.J. Parnell and C. Calvo-Jurado. On the computation of the Hashin–Shtrikman bounds for transversely isotropic two-phase linear elastic fibre-reinforced composites. *J.Engng.Math.*, 95:295–323, 2015. doi:10.1007/s10665-014-9777-3.

M.V. Pathan, V.L. Tagarielli, S. Patsias, and P.M. Baiz-Villafranca. A new algorithm to generate representative volume elements of composites with cylindrical or spherical fillers. *Composites B*, 110:267–278, 2017. doi:10.1016/j.compositesb.2016.10.078.

C.B. Pedersen and P.J. Withers. Iterative estimates of internal stresses in short-fibre metal matrix composites. *Phil.Mag.*, A65:1217–1233, 1992. doi:10.1080/01418619208201506.

O.B. Pedersen. Thermoelasticity and plasticity of composites — I. Mean field theory. *Acta metall.*, 31:1795–1808, 1983. doi:10.1016/0001-6160(83)90126-8.

C. Pelissou, J. Baccou, Y. Monerie, and F. Perales. Determination of the size of the representative volume element for random quasi-brittle composites. *Int.J.Sol.Struct.*, 46:2842–2855, 2009. doi:10.1016/j.ijsolstr.2009.03.015.

P. Peng, M. Gao, E. Guo, H. Kang, H. Xie, Z. Chen, and T. Wang. Deformation behavior and damage in B_4C_p/6061 Al composites: An actual 3D microstructure based modeling. *Mater.Sci.Engng.A*, 781:139169, 2020. doi:10.1016/j.msea.2020.139169.

X. Peng, S. Tang, N. Hu, and J. Han. Determination of the Eshelby tensor in mean-field schemes for evaluation of mechanical properties of elastoplastic composites. *Int.J.Plast.*, 76:147–165, 2016. doi:10.1016/j.ijplas.2015.07.009.

V. Pensée and Q.C. He. Generalized self-consistent estimation of the apparent isotropic elastic moduli and minimum representative volume element size of heterogeneous media. *Int.J.Sol.Struct.*, 44:2225–2243, 2007. doi:10.1016/j.ijsolstr.2006.07.003.

E.S. Perdahcıoğlu and J.M. Geijselaers. Constitutive modeling of two phase materials using the mean field method of homogenization. *Int.J.Mater.Form.*, 4:93–102, 2011. doi:10.1007/s12289-010-1007-6.

H.E. Pettermann. *Derivation and Finite Element Implementation of Constitutive Material Laws for Multiphase Composites Based on Mori–Tanaka Approaches*. Reihe 18, Nr. 217. VDI–Verlag, Düsseldorf, 1997. ISBN 3-183-21718-X.

H.E. Pettermann and J. Hüsing. Modeling and simulation of relaxation in viscoelastic open cell materials and structures. *Int.J.Sol.Struct.*, 49:2848–2853, 2012. doi:10.1016/j.ijsolstr.2012.04.027.

H.E. Pettermann and S. Suresh. A comprehensive unit cell model: A study of coupled effects in piezoelectric 1–3 composites. *Int.J.Sol.Struct.*, 37:5447–5464, 2000. doi:10.1016/S0020-7683(99)00224-3.

H.E. Pettermann, H.J. Böhm, and F.G. Rammerstorfer. Some direction dependent properties of matrix–inclusion type composites with given reinforcement orientation distributions. *Composites B*, 28:253–265, 1997. doi:10.1016/S1359-8368(96)00055-8.

N. Phan-Thien and G.W. Milton. New third-order bounds on the effective moduli of n-phase composites. *Quart.Appl.Math.*, 41:59–74, 1983. doi:10.1090/qam/700661.

N. Phan-Thien and D.C. Pham. Differential multiphase models for polydispersed spheroidal inclusions: Thermal conductivity and effective viscosity. *Int.J.Engng.Sci.*, 38:73–88, 2000. doi:10.1016/S0020-7225(99)00016-6.

C. Pichler and R. Lackner. Upscaling the viscoelastic properties of highly filled composites: Investigation of matrix–inclusion-type morphologies with power-law viscoelastic material response. *Compos.Sci.Technol.*, 69:2410–2420, 2009. doi:10.1016/j.compscitech.2009.06.008.

O. Pierard, C. Friebel, and I. Doghri. Mean-field homogenization of multi-phase thermo-elastic composites: A general framework and its validation. *Compos.Sci.Technol.*, 64: 1587–1603, 2004. doi:10.1016/j.compscitech.2003.11.009.

O. Pierard, C. González, J. Segurado, J. LLorca, and I. Doghri. Micromechanics of elasto-plastic materials reinforced with ellipsoidal inclusions. *Int.J.Sol.Struct.*, 44:6945–6962, 2007. doi:10.1016/j.ijsolstr.2007.03.019.

A.F. Plankensteiner. *Multiscale Treatment of Heterogeneous Nonlinear Solids and Structures*. Reihe 18, Nr. 248. VDI–Verlag, Düsseldorf, 2000. ISBN 3-183-24818-2.

A.F. Plankensteiner, H.J. Böhm, F.G. Rammerstorfer, V.A. Buryachenko, and G. Hackl. Modeling of layer-structured high speed steel. *Acta mater.*, 45:1875–1887, 1997. doi:10.1016/S1359-6454(96)00327-8.

J. Podgórski. Criterion for angle prediction for the crack in materials with random structure. *Mech.Contr.*, 30:229–233, 2011.

P. Ponte Castañeda. The effective mechanical properties of nonlinear isotropic composites. *J.Mech.Phys.Sol.*, 39:45–71, 1991. doi:10.1016/0022-5096(91)90030-R.

P. Ponte Castañeda. Bounds and estimates for the properties of nonlinear heterogeneous systems. *Phil.Trans.Roy.Soc.*, A340:531–567, 1992. doi:10.1098/rsta.1992.0079.

P. Ponte Castañeda and P. Suquet. Nonlinear composites. In E. van der Giessen and T.Y. Wu, editors, *Advances in Applied Mechanics 34*, pages 171–302, New York, NY, 1998. Academic Press. doi:10.1016/S0065-2156(08)70321-1.

P. Ponte Castañeda and J.R. Willis. The effect of spatial distribution on the effective behavior of composite materials and cracked media. *J.Mech.Phys.Sol.*, 43:1919–1951, 1995. doi:10.1016/0022-5096(95)00058-Q.

A. Pontefisso, M. Zappalorto, and M. Quaresimin. Effectiveness of the random sequential absorption algorithm in the analysis of volume elements with nanoplatelets. *Comput.Mater.Sci.*, 117:511–517, 2016. doi:10.1016/j.commatsci.2016.02.024.

G.L. Povirk, S.R. Nutt, and A. Needleman. Analysis of creep in thermally cycled Al/SiC composites. *Scr.metall.mater.*, 26:461–66, 1992. doi:10.1016/0956-716X(92)90630-W.

C.P. Przybyla and D.L. McDowell. Microstructure-sensitive extreme value probabilities for high-cycle fatigue of Ni-base superalloy IN100. *Int.J.Plast.*, 26:372–384, 2010. doi:10.1016/j.ijplas.2009.08.001.

M. Ptashnyk and B. Seguin. Periodic homogenization and material symmetry in linear elasticity. *J.Elast.*, 124:225–241, 2016. doi:10.1007/s10659-015-9566-x.

S.M. Qidwai, D.M. Turner, S.R. Niezgoda, A.C. Lewis, A.B. Geltmacher, D.J. Rowenhorst, and S.R. Kalidindi. Estimating the response of polycrystalline materials using sets of weighted statistical volume elements. *Acta mater.*, 60:5284–5299, 2012. doi:10.1016/j.actamat.2012.06.026.

Y.P. Qiu and G.J. Weng. A theory of plasticity for porous materials and particle-reinforced composites. *J.Appl.Mech.*, 59:261–268, 1992. doi:10.1115/1.2899515.

J. Qu and M. Cherkaoui. *Fundamentals of Micromechanics of Solids*. John Wiley, New York, NY, 2006. ISBN 0-471-46451-1.

S. Quilici and G. Cailletaud. FE simulation of macro-, meso- and microscales in polycrystalline plasticity. *Comput.Mater.Sci.*, 16:383–390, 1999. doi:10.1016/S0927-0256(99)00081-6.

J.A. Quintanilla. Microstructure and properties of random heterogeneous materials: A review of theoretical results. *Polym.Engng.Sci.*, 39:559–585, 1999. doi:10.1002/pen.11446.

D. Raabe. *Computational Materials Science*. VCH, Weinheim, 1998. ISBN 3-527-29541-0.

F.K.F. Radtke, A. Simone, and L.J. Sluys. A partition of unity finite element method for simulating non-linear debonding and matrix failure in thin fibre composites. *Int.J.Numer.Meth.Engng.*, 86:453–476, 2011. doi:10.1002/nme.3056.

P. Raghavan and S. Ghosh. Adaptive multi-scale modeling of composite materials. *Comput.Model.Engng.Sci.*, 5:151–170, 2004. doi:10.3970/cmes.2004.005.151.

F.G. Rammerstorfer and H.J. Böhm. Finite element methods in micromechanics of composites and foam materials. In B.H.V. Topping, editor, *Computational Mechanics for the Twenty First Century*, pages 145–164, Edinburgh, 2000. Saxe–Coburg Publications.

A. Rasool and H.J. Böhm. Effects of particle shape on the macroscopic and microscopic linear behaviors of particle reinforced composites. *Int.J.Engng.Sci.*, 58:21–34, 2012. doi:10.1016/j.ijengsci.2012.03.022.

C. Redenbach. Microstructure models for cellular materials. *Comput.Mater.Sci.*, 44:1397–1407, 2009. doi:10.1016/j.commatsci.2008.09.018.

T.J. Reiter, G.J. Dvorak, and V. Tvergaard. Micromechanical models for graded composite materials. *J.Mech.Phys.Sol.*, 45:1281–1302, 1997. doi:10.1016/S0022-5096(97)00007-0.

Z.Y. Ren and Q.S. Zheng. Effects of grain sizes, shapes, and distribution on minimum sizes of representative volume elements of cubic polycrystals. *Mech.Mater.*, 36:1217–1229, 2004. doi:10.1016/j.mechmat.2003.11.002.

A. Reuss. Berechnung der Fließgrenze von Mischkristallen auf Grund der Plastizitätsbedingung für Einkristalle. *ZAMM*, 9:49–58, 1929. doi:10.1002/zamm.19290090104.

A. Riccardi and F. Montheillet. A generalized self-consistent method for solids containing randomly oriented spheroidal inclusions. *Acta Mech.*, 133:39–56, 1999. doi:10.1007/BF01179009.

J.R. Rice and D.M. Tracey. On the ductile enlargement of voids in triaxial stress fields. *J.Mech.Phys.Sol.*, 17:201–217, 1969. doi:10.1016/0022-5096(69)90033-7.

M. Rintoul and S. Torquato. Reconstruction of the structure of dispersions. *J.Colloid Interf.Sci.*, 186:467–476, 1997. doi:10.1006/jcis.1996.4675.

A.P. Roberts and E.J. Garboczi. Elastic moduli of model random three-dimensional closed-cell cellular solids. *Acta mater.*, 49:189–197, 2001. doi:10.1016/S1359-6454(00)00314-1.

A.P. Roberts and E.J. Garboczi. Elastic properties of a tungsten–silver composite by reconstruction and computation. *J.Mech.Phys.Sol.*, 47:2029–2055, 1999. doi:10.1016/S0022-5096(99)00016-2.

F. Robitaille, A.C. Long, I.A. Jones, and C.D. Rudd. Automatically generated geometric descriptions of textile and composite unit cells. *Composites A*, 34:303–312, 2003. doi:10.1016/S1359-835X(03)00063-0.

G.J. Rodin. The overall elastic response of materials containing spherical inhomogeneities. *Int.J.Sol.Struct.*, 30:1849–1863, 1993. doi:10.1016/0020-7683(93)90221-R.

G.J. Rodin and G.J. Weng. On reflected interactions in elastic solids containing inhomogeneities. *J.Mech.Phys.Sol.*, 68:197–209, 2014. doi:10.1016/j.jmps.2014.04.001.

R. Roscoe. Isotropic composites with elastic or viscoelastic phases: General bounds for the moduli and solutions for special geometries. *Rheol.Acta*, 12:404–411, 1973. doi:10.1007/BF01502992.

B.W. Rosen and Z. Hashin. Effective thermal expansion coefficients and specific heats of composite materials. *Int.J.Engng.Sci.*, 8:157–173, 1970. doi:10.1016/0020-7225(70)90066-2.

F. Roters, P. Eisenlohr, L. Hantcherli, D.D. Tjahjanto, T.R. Bieler, and D. Raabe. Overview of constitutive laws, kinematics, homogenization and multiscale methods in crystal plasticity finite element modeling: Theory, experiments, applications. *Acta mater.*, 58:1152–1211, 2010. doi:10.1016/j.actamat.2009.10.058.

F. Saadat, V. Birman, S. Thomopoulos, and G. Genin. Effective elastic properties of a composite containing multiple types of anisotropic ellipsoidal inclusions, with application to the attachment of tendon to bone. *J.Mech.Phys.Sol.*, 82:367–377, 2015. doi:10.1016/j.jmps.2015.05.017.

K. Sab. On the homogenization and the simulation of random materials. *Eur.J.Mech. A/Solids*, 11:585–607, 1992.

G. Sachs. Zur Ableitung einer Fließbedingung. *Z.VDI*, 72:734–736, 1928.

I. Saiki, K. Terada, K. Ikeda, and M. Hori. Appropriate number of unit cells in a representative volume element for micro-structural bifurcation encountered in a multi-scale modeling. *Comput.Meth.Appl.Mech.Engng.*, 191:2561–2585, 2002. doi:10.1016/S0045-7825(01)00413-3.

V. Salit and D. Gross. On the convergence of the iterative self-consistent embedded cell model. *Comput.Mater.Sci.*, 81:199–204, 2014. doi:10.1016/j.commatsci.2013.08.014.

M. Salmi, F. Auslender, M. Bornert, and M. Fogli. Apparent and effective mechanical properties of linear matrix–inclusion random composites: Improved bounds for the effective behavior. *Int.J.Sol.Struct.*, 49:1195–1211, 2012. doi:10.1016/j.ijsolstr.2012.01.018.

W. Sanders and L.J. Gibson. Mechanics of hollow sphere foams. *Mater.Sci.Engng. A*, 347: 70–85, 2003. doi:10.1016/S0921-5093(02)00583-X.

A. Sangani and W. Lu. Elastic coefficients of composites containing spherical inclusions in a periodic array. *J.Mech.Phys.Sol.*, 35:1–21, 1987. doi:10.1016/0022-5096(87)90024-X.

A. Sangani and G. Mo. Elastic interactions in particulate composites with perfect as well as imperfect interfaces. *J.Mech.Phys.Sol.*, 45:2001–2031, 1997. doi:10.1016/S0022-5096(97)00025-2.

S.P. Santosa and T. Wierzbicki. On the modeling of crush behavior of a closed-cell aluminum foam structure. *J.Mech.Phys.Sol.*, 46:645–669, 1998. doi:10.1016/S0022-5096(97)00082-3.

M. Sautter, C. Dietrich, M.H. Poech, S. Schmauder, and H.F. Fischmeister. Finite element modelling of a transverse-loaded fibre composite: Effects of section size and net density. *Comput.Mater.Sci.*, 1:225–233, 1993. doi:10.1016/0927-0256(93)90014-E.

D. Savvas, G. Stefanou, and M. Papadrakakis. Determination of RVE size for random composites with local volume fraction variation. *Comput.Meth.Appl.Mech.Engng.*, 305: 340–358, 2016. doi:10.1016/j.cma.2016.03.002.

R.A. Schapery. Approximate methods of transform inversion in viscoelastic stress analysis. In *Proceedings of the Fourth US National Congress on Applied Mechanics*, pages 1075–1085, New York, NY, 1962. ASME.

R.A. Schapery. Viscoelastic behavior and analysis of composite materials. In G.P. Sendeckyj, editor, *Mechanics of Composite Materials 2*, pages 84–168, New York, NY, 1974. Academic Press.

L. Scheunemann, D. Balzani, D. Brands, and J. Schröder. Design of 3D statistically similar representative volume elements based on Minkowski functionals. *Mech.Mater.*, 90:185–201, 2015. doi:10.1016/j.mechmat.2015.03.005.

J. Schjødt-Thomsen and R. Pyrz. Influence of statistical cell description on the local strain and overall properties of cellular materials. In S. Ghosh, J.M. Castro, and J.K. Lee, editors, *Proceedings of NUMIFORM 2004*, pages 1630–1635, Melville, NY, 2004. American Institute of Physics. doi:10.1063/1.1766763.

S. Schmauder, J. Wulf, T. Steinkopff, and H. Fischmeister. Micromechanics of plasticity and damage in an Al/SiC metal matrix composite. In A. Pineau and A. Zaoui, editors, *Micromechanics of Plasticity and Damage of Multiphase Materials*, pages 255–262, Dordrecht, 1996. Kluwer. doi:10.1007/978-94-009-1756-9_32.

K. Schneider, B. Klusemann, and S. Bargmann. Fully periodic RVEs for technologically relevant composites: Not worth the effort! *J.Mech.Mater.Struct.*, 12:471–484, 2017. doi:10.2140/jomms.2017.12.471.

M. Schneider. The sequential addition and migration method to generate representative volume elements for the homogenization of short fiber reinforced plastics. *Comput.Mech.*, 59:247–263, 2017. doi:10.1007/s00466-016-1350-7.

M. Schneider. A review of nonlinear FFT-based computational homogenization methods. *Acta Mech.*, 232:2051–2100, 2021. doi:10.1007/s00707-021-02962-1.

M. Schneider. Superaccurate effective elastic moduli via postprocessing in computational homogenization. *Int.J.Num.Meth.Engng.*, 123:4119–4135, 2022. doi:10.1002/nme.7002.

M. Schneider, M. Josien, and F. Otto. Representative volume elements for matrix–inclusion composites — A computational study on the effects of an improper treatment of particles intersecting the boundary and the benefits of periodizing the ensemble. *J.Mech.Phys.Sol.*, 158:104652, 2022. doi:10.1016/j.jmps.2021.104652.

P.J. Schneider and D.H. Eberly. *Geometric Tools for Computer Graphics*. Morgan–Kaufmann, San Francisco, 2003. ISBN 1-558-60594-0.

B.A. Schrefler, M. Lefik, and U. Galvanetto. Correctors in a beam model for unidirectional composites. *Compos.Mater.Struct.*, 4:159–190, 1997. doi:10.1080/10759419708945879.

B.A. Schrefler, U. Galvanetto, C. Pellegrino, and F. Ohmenhäuser. Global non-linear behavior of periodic composite materials. In H.A. Mang and F.G. Rammerstorfer, editors, *Discretization Methods in Structural Mechanics*, pages 265–272, Dordrecht, 1999. Kluwer. doi:10.1007/978-94-011-4589-3_31.

J. Segurado, J. LLorca, and C. González. On the accuracy of mean-field approaches to simulate the plastic deformation of composites. *Scr.mater.*, 46:525–529, 2002a. doi:10.1016/S1359-6462(02)00027-1.

J. Segurado, E. Parteder, A. Plankensteiner, and H.J. Böhm. Micromechanical studies of the densification of porous molybdenum. *Mater.Sci.Engng. A*, 333:270–278, 2002b. doi:10.1016/S0921-5093(01)01853-6.

J. Segurado, C. González, and J. LLorca. A numerical investigation of the effect of particle clustering on the mechanical properties of composites. *Acta mater.*, 51:2355–2369, 2003. doi:10.1016/S1359-6454(03)00043-0.

A. Selmi, I. Doghri, and L. Adam. Micromechanical simulation of biaxial yield, hardening and plastic flow in short glass fiber reinforced polyamide. *Int.J.Mech.Sci.*, 53:696–706, 2011. doi:10.1016/j.ijmecsci.2011.06.002.

I. Sevostianov. On the shape of effective inclusion in the Maxwell homogenization scheme for anisotropic elastic composites. *Mech.Mater.*, 75:45–59, 2014. doi:10.1016/j.mechmat.2014.03.003.

I. Sevostianov and A. Giraud. Generalization of Maxwell homogenization scheme for elastic material containing inhomogeneities of diverse shape. *Int.J.Engng.Sci.*, 64:23–36, 2013. doi:10.1016/j.ijengsci.2012.12.004.

I. Sevostianov and M. Kachanov. Explicit cross-property correlations for anisotropic two-phase composite materials. *J.Mech.Phys.Sol.*, 50:253–282, 2002. doi:10.1016/S0022-5096(01)00051-5.

I. Sevostianov and M. Kachanov. Effect of interphase layers on the overall elastic and conductive properties of matrix composites. Application to nanosize inclusion. *Int.J.Sol.Struct.*, 44:1304–1315, 2007a. doi:10.1016/j.ijsolstr.2006.06.020.

I. Sevostianov and M. Kachanov. Elastic fields generated by inhomogeneities: Far-field asymptotics, its shape dependence and relation to the effective elastic properties. *Int.J.Sol.Struct.*, 48:2340–2348, 2011. doi:10.1016/j.ijsolstr.2011.04.014.

I. Sevostianov and M. Kachanov. On some controversial issues in effective field approaches to the problem of overall elastic properties. *Mech.Mater.*, 69:93–105, 2014. doi:10.1016/j.mechmat.2013.09.010.

I. Sevostianov and M. Kachanov. Compliance tensors of ellipsoidal inclusions. *Int.J.Fract.*, 96:L3–L7, 1999. doi:10.1023/A:1018712913071.

I. Sevostianov, M. Kachanov, and T. Zohdi. On computation of the compliance and stiffness contribution tensors to non ellipsoidal inhomogeneities. *Int.J.Sol.Struct.*, 45:4375–4383, 2008. doi:10.1016/j.ijsolstr.2008.03.020.

I. Sevostianov, S.G. Mogilevskaya, and V.I. Kushch. Maxwell's methodology of estimating effective properties: Alive and well. *Int.J.Sol.Struct.*, 140:35–88, 2019. doi:10.1016/j.ijengsci.2019.05.001.

Z. Shan and A.M. Gokhale. Micromechanics of complex three-dimensional microstructures. *Acta mater.*, 49:2001–2015, 2001. doi:10.1016/S1359-6454(01)00093-3.

A.S. Shedbale, I.V. Singh, and B.K. Mishra. Heterogeneous and homogenized models for predicting the indentation response of particle reinforced metal matrix composites. *Int.J.Mech.Mater.Design*, 13:531–552, 2017. doi:10.1007/s10999-016-9352-3.

H. Shen and L.C. Brinson. A numerical investigation of the effect of boundary conditions and representative volume element size for porous titanium. *J.Mech.Mater.Struct.*, 1: 1179–1204, 2006. doi:10.2140/jomms.2006.1.1179.

H. Shen and C.J. Lissenden. 3D finite element analysis of particle-reinforced aluminum. *Mater.Sci.Engng. A*, 338:271–281, 2002. doi:10.1016/S0921-5093(02)00094-1.

L. Shen and S. Yi. An effective inclusion model for effective moduli of heterogeneous materials with ellipsoidal inhomogeneities. *Int.J.Sol.Struct.*, 38:5789–5805, 2001. doi:10.1016/S0020-7683(00)00370-X.

P. Sheng, J. Zhang, and Z. Ji. An advanced 3D modeling method for concrete-like particle-reinforced composites with high volume fraction of randomly distributed particles. *Compos.Sci.Technol.*, 134:26–35, 2016. doi:10.1016/j.compscitech.2016.08.009.

M.S. Shephard, M.W. Beall, R. Garimella, and R. Wentorf. Automatic construction of 3/D models in multiple scale analysis. *Comput.Mech.*, 17:196–207, 1995. doi:10.1007/BF00364081.

M. Sherburn. *Geometrical and Mechanical Modelling of Textiles*. PhD thesis, University of Nottingham, Nottingham, 2007.

D.L. Shi, X.Q. Feng, Y.Y. Huang, K.C. Hwang, and H. Gao. The effect of nanotube waviness and agglomeration on the elastic property of carbon nanotube-reinforced composites. *J.Engng.Mater.Technol.*, 126:250–257, 2004. doi:10.1115/1.1751182.

V. Shulmeister, M.W.D. van der Burg, E. van der Giessen, and R. Marissen. A numerical study of large deformations of low-density elastomeric open-cell foams. *Mech.Mater.*, 30: 125–140, 1998. doi:10.1016/S0167-6636(98)00033-7.

T. Siegmund, F.D. Fischer, and E.A. Werner. Microstructure characterization and FE-modeling of plastic flow in a duplex steel. In R. Pyrz, editor, *Microstructure–Property Interactions in Composite Materials*, pages 349–360, Dordrecht, 1995. Kluwer Academic Publishers. doi:10.1007/978-94-011-0059-5_29.

T. Siegmund, R. Cipra, J. Liakus, B. Wang, M. LaForest, and A. Fatz. Processing–microstructure–property relationships in short fiber reinforced carbon–carbon composite system. In H.J. Böhm, editor, *Mechanics of Microstructured Materials*, pages 235–258. Springer-Verlag, CISM Courses and Lectures Vol. 464, 2004. doi:10.1007/978-3-7091-2776-6_7.

S. Sihn and A.K. Roy. Modeling and prediction of bulk properties of open-cell carbon foam. *J.Mech.Phys.Sol.*, 52:167–191, 2005. doi:10.1016/S0022-5096(03)00072-3.

V.V. Silberschmidt and E.A. Werner. Analyses of thermal stresses' evolution in ferritic–austenitic duplex steels. In Y. Tanigawa, R.B. Hetnarski, and N. Noda, editors, *Thermal Stresses 2001*, pages 327–330, Osaka, 2001. Osaka Prefecture University.

N. Silnutzer. *Effective Constants of Statistically Homogeneous Materials*. PhD thesis, University of Pennsylvania, Philadelphia, PA, 1972.

A.E. Simone and L.J. Gibson. Effects of solid distribution on the stiffness and strength of metallic foams. *Acta mater.*, 46:2139–2150, 1998. doi:10.1016/S1359-6454(97)00421-7.

R.J.M. Smit, W.A.M. Brekelmans, and H.E.H. Meijer. Prediction of the mechanical behavior of non-linear heterogeneous systems by multi-level finite element modeling. *Comput.Meth.Appl.Mech.Engng.*, 155:181–192, 1998. doi:10.1016/S0045-7825(97)00139-4.

S. Soghrati, A.M. Aragón, C.A. Duarte, and P.H. Geubelle. An interface-enriched generalized FEM for problems with discontinuous gradient fields. *Int.J.Numer.Meth.Engng.*, 89:991–1008, 2012. doi:10.1002/nme.3273.

G. Soni, R. Singh, M. Mitra, and B. Falzon. Modelling matrix damage and fibre–matrix interfacial decohesion in composite laminates via a multi-fibre multi-layer representative volume element (M^2RVE). *Int.J.Sol.Struct.*, 51:449–461, 2014. doi:10.1016/j.ijsolstr.2013.10.018.

N.J. Sørensen. A planar type analysis for the elastic-plastic behaviour of continuous fibre-reinforced metal-matrix composites under longitudinal shearing and combined loading. *Int.J.Sol.Struct.*, 29:867–877, 1992. doi:10.1016/0020-7683(92)90022-L.

N.J. Sørensen, S. Suresh, V. Tvergaard, and A. Needleman. Effects of reinforcement orientation on the tensile response of metal matrix composites. *Mater.Sci.Engng. A*, 197:1–10, 1995. doi:10.1016/0921-5093(94)09739-9.

C. Soyarslan, S. Bargmann, M. Pradas, and J. Weissmüller. 3D stochastic bicontinuous microstructures: Generation, topology and elasticity. *Acta mater.*, 149:326–340, 2018. doi:10.1016/j.actamat.2018.01.005.

M. Stroeven, H. Askes, and L.J. Sluys. Numerical determination of representative volumes for granular materials. *Comput.Meth.Appl.Mech.Engng.*, 193:3221–3238, 2004. doi:10.1016/j.cma.2003.09.023.

N. Sukumar, D.L. Chopp, N. Moës, and T. Belytschko. Modeling holes and inclusions by level sets in the extended finite element method. *Comput.Meth.Appl.Mech.Engng.*, 190: 6183–6900, 2001. doi:10.1016/S0045-7825(01)00215-8.

R.M. Sullivan and L.J. Ghosn. Shear moduli for non-isotropic, open cell foam using a general elongated Kelvin foam model. *Int.J.Engng.Sci.*, 47:990–1001, 2009. doi:10.1016/j.ijengsci.2009.05.005.

P. Suquet. Elements of homogenization for inelastic solid mechanics. In E. Sanchez-Palencia and A. Zaoui, editors, *Homogenization Techniques in Composite Media*, pages 194–278, Berlin, 1987. Springer-Verlag.

P. Suquet. Overall properties of nonlinear composites: A modified secant moduli theory and its link with Ponte Castañeda's nonlinear variational procedure. *C.R.Acad.Sci.Paris, série IIb*, 320:563–571, 1995.

P. Suquet. Effective properties of nonlinear composites. In P. Suquet, editor, *Continuum Micromechanics*, pages 197–264, Vienna, 1997. Springer-Verlag. doi:10.1007/978-3-7091-2662-2_4.

T. Suzuki and P.K.L. Yu. Complex elastic wave band structures in three-dimensional periodic elastic media. *J.Mech.Phys.Sol.*, 46:115–138, 1998. doi:10.1016/S0022-5096(97)00023-9.

S. Swaminathan and S. Ghosh. Statistically equivalent representative volume elements for unidirectional composite microstructures: Part II — With interfacial debonding. *J.Compos.Mater.*, 40:605–621, 2006. doi:10.1177/0021998305055274.

S. Swaminathan, S. Ghosh, and N.J. Pagano. Statistically equivalent representative volume elements for unidirectional composite microstructures: Part I — Without damage. *J.Compos.Mater.*, 40:583–604, 2006. doi:10.1177/0021998305055273.

E.B. Tadmor and R.E. Miller. *Modeling Materials: Continuum, Atomistic and Multiscale Techniques*. Cambridge University Press, Cambridge, 2011. ISBN 0-521-85698-1.

N. Takano, M. Zako, and T. Okazaki. Efficient modeling of microscopic heterogeneity and local crack in composite materials by finite element mesh superposition method. *JSME Int.J.Srs.A*, 44:602–609, 2001. doi:10.1299/jsmea.44.602.

D.R.S. Talbot and J.R. Willis. Variational principles for inhomogeneous non-linear media. *J.Appl.Math.*, 35:39–54, 1985. doi:10.1093/imamat/35.1.39.

D.R.S. Talbot and J.R. Willis. Upper and lower bounds for the overall response of an elastoplastic composite. *Mech.Mater.*, 28:1–8, 1998. doi:10.1016/S0167-6636(97)00012-4.

V.B.C. Tan, K. Raju, and H.P. Lee. Direct FE^2 for concurrent multilevel modelling of heterogeneous structures. *Comput.Meth.Appl.Mech.Engng.*, 360:112694, 2020. doi:10.1016/j.cma.2019.112694.

G.P. Tandon and G.J. Weng. The effect of aspect ratio of inclusions on the elastic properties of unidirectionally aligned composites. *Polym.Compos.*, 5:327–333, 1984. doi:10.1002/pc.750050413.

G.P. Tandon and G.J. Weng. Average stress in the matrix and effective moduli of randomly oriented composites. *Compos.Sci.Technol.*, 27:111–132, 1986. doi:10.1016/0266-3538(86)90067-9.

G.P. Tandon and G.J. Weng. A theory of particle-reinforced plasticity. *J.Appl.Mech.*, 55: 126–135, 1988. doi:10.1115/1.3173618.

T. Tang and W. Yu. A variational asymptotic micromechanics model for predicting conductivities of composite materials. *J.Mech.Mater.Struct.*, 2:1813–1830, 2007. doi:10.2140/jomms.2007.2.1813.

T. Tang and W. Yu. Asymptotic approach to initial yielding surface and elastoplasticity of heterogeneous materials. *Mech.Adv.Mater.Struct.*, 18:244–254, 2011. doi:10.1080/15376494.2010.483324.

X. Tang and J.D. Whitcomb. General techniques for exploiting periodicity and symmetries in micromechanics analysis of textile composites. *J.Compos.Mater.*, 37:1167–1189, 2003. doi:10.1177/00219983030370130.

M. Tashkinov. Multipoint stochastic approach to localization of microscale elastic behavior of random heterogeneous media. *Comput.Struct.*, 249:106474, 2021. doi:10.1016/j.compstruc.2020.106474.

M. Taya and T. Mori. Dislocations punched-out around a short fiber in MMC subjected to uniform temperature change. *Acta metall.*, 35:155–162, 1987. doi:10.1016/0001-6160(87)90224-0.

M. Taya, W.D. Armstrong, M.L. Dunn, and T. Mori. Analytical study on dimensional changes in thermally cycled metal matrix composites. *Mater.Sci.Engng. A*, 143:143–154, 1991. doi:10.1016/0921-5093(91)90734-5.

G. Taylor. Plastic strain in metals. *J.Inst.Metals*, 62:307–324, 1938.

C. Tekoğlu, L.J. Gibson, T. Pardoen, and P.R. Onck. Size effects in foams: Experiments and modeling. *Prog.Mater.Sci.*, 56:109–138, 2011. doi:10.1016/j.pmatsci.2010.06.001.

I. Temizer and P. Wriggers. Homogenization in finite thermoelasticity. *J.Mech.Phys.Sol.*, 59:344–372, 2011. doi:10.1016/j.jmps.2010.10.004.

I. Temizer, T. Wu, and P. Wriggers. On the optimality of the window method in computational homogenization. *Int.J.Engng.Sci.*, 64:66–73, 2013. doi:10.1016/j.ijengsci.2012.12.007.

J.L. Teply and G.J. Dvorak. Bounds on overall instantaneous properties of elastic-plastic composites. *J.Mech.Phys.Sol.*, 36:29–58, 1988. doi:10.1016/0022-5096(88)90019-1.

K. Terada and N. Kikuchi. Microstructural design of composites using the homogenization method and digital images. *Mater.Sci.Res.Int.*, 2:65–72, 1996. doi:10.2472/jsms.45.6Appendix_65.

K. Terada, T. Miura, and N. Kikuchi. Digital image-based modeling applied to the homogenization analysis of composite materials. *Comput.Mech.*, 20:331–346, 1997. doi:10.1007/s004660050255.

K. Terada, M. Hori, T. Kyoya, and N. Kikuchi. Simulation of the multi-scale convergence in computational homogenization approach. *Int.J.Sol.Struct.*, 37:2285–2311, 2000. doi:10.1016/S0020-7683(98)00341-2.

K. Terada, I. Saiki, K. Matsui, and Y. Yamakawa. Two-scale kinematics and linearization for simultaneous two-scale analysis of periodic heterogeneous solids at finite strain. *Comput.Meth.Appl.Mech.Engng.*, 192:3531–3563, 2003. doi:10.1016/S0045-7825(03)00365-7.

W. Tian, L. Qi, J. Zhou, J. Liang, and Y. Ma. Representative volume element for composites reinforced by spatially randomly oriented discontinuous fibers and its applications. *Compos.Struct.*, 131:366–373, 2015. doi:10.1016/j.compstruct.2015.05.014.

K. Tohgo and T.W. Chou. Incremental theory of particulate-reinforced composites including debonding damage. *JSME Int.J.Srs.A*, 39:389–397, 1996. doi:10.1299/jsmea1993.39.3_389.

Y. Tomita, Y. Higa, and T. Fujimoto. Modeling and estimation of deformation behavior of particle reinforced metal-matrix composite. *Int.J.Mech.Sci.*, 42:2249–2260, 2000. doi:10.1016/S0020-7403(00)00006-0.

S. Torquato. *Random Heterogeneous Media*. Springer-Verlag, New York, NY, 2002. ISBN 1-475-76357-3.

S. Torquato. Random heterogeneous media: Microstructure and improved bounds on effective properties. *Appl.Mech.Rev.*, 44:37–75, 1991. doi:10.1115/1.3119494.

S. Torquato. Effective stiffness tensor of composite media: I. Exact series expansions. *J.Mech.Phys.Sol.*, 45:1421–1448, 1997. doi:10.1016/S0022-5096(97)00019-7.

S. Torquato. Effective stiffness tensor of composite media: II. Applications to isotropic dispersions. *J.Mech.Phys.Sol.*, 46:1411–1440, 1998a. doi:10.1016/S0022-5096(97)00083-5.

S. Torquato. Morphology and effective properties of disordered heterogeneous media. *Int.J.Sol.Struct.*, 35:2385–2406, 1998b. doi:10.1016/S0020-7683(97)00142-X.

S. Torquato and S. Hyun. Effective-medium approximation for composite media: Realizable single-scale dispersions. *J.Appl.Phys.*, 89:1725–1729, 2001. doi:10.1063/1.1336523.

S. Torquato and F. Lado. Improved bounds on the effective moduli of random arrays of cylinders. *J.Appl.Mech.*, 59:1–6, 1992. doi:10.1115/1.2899429.

S. Torquato and D.M. Rintoul. Effect of the interface on the properties of composite media. *Phys.Rev.Lett.*, 75:4067–4070, 1995. doi:10.1103/PhysRevLett.75.4067.

S. Torquato, C.L.Y. Yeong, M.D. Rintoul, D. Milius, and L.A. Aksay. Characterizing the structure and mechanical properties of interpenetrating boron carbide/aluminum multiphase composites. *J.Amer.Ceram.Soc.*, 82:1263–1268, 1999. doi:10.1111/j.1151-2916.1999.tb01905.x.

C. Toulemonde, R. Masson, and J. El Gharib. Modeling the effective elastic behavior of composites: A mixed finite element and homogenization approach. *C.R.Mécanique*, 336: 275–282, 2008. doi:10.1016/j.crme.2007.11.024.

D. Trias. *Analysis and Simulation of Transverse Random Fracture of Long Fibre Reinforced Composites*. PhD thesis, Universitat de Girona, Girona, 2005.

D. Trias, J. Costa, A. Turon, and J.F. Hurtado. Determination of the critical size of a statistical representative volume element (SRVE) for carbon reinforced polymers. *Acta mater.*, 54:3471–3484, 2006. doi:10.1016/j.actamat.2006.03.042.

A. Trofimov, B. Drach, and I. Sevostianov. Effective elastic properties of composites with particles of polyhedral shapes. *Int.J.Sol.Struct.*, 120:157–170, 2017. doi:10.1016/j.ijsolstr.2017.04.037.

T.C. Tszeng. The effects of particle clustering on the mechanical behavior of particle reinforced composites. *Composites B*, 29:299–308, 1998. doi:10.1016/S1359-8368(97)00031-0.

C.L. Tucker and E. Liang. Stiffness predictions for unidirectional short-fiber composites: Review and evaluation. *Compos.Sci.Technol.*, 59:655–671, 1999. doi:10.1016/S0266-3538(98)00120-1.

V. Tvergaard. Debonding of short fibres among particulates in a metal matrix composite. *Int.J.Sol.Struct.*, 40:6957–6967, 2003. doi:10.1016/S0020-7683(03)00347-0.

V. Tvergaard. Analysis of tensile properties for a whisker-reinforced metal-matrix composite. *Acta metall.mater.*, 38:185–194, 1990. doi:10.1016/0956-7151(90)90048-L.

V. Tvergaard. Fibre debonding and breakage in a whisker-reinforced metal. *Mater.Sci. Engng. A*, 190:215–222, 1994. doi:10.1016/0921-5093(95)80005-0.

V. Tvergaard. Effect of void size difference on growth and cavitation instabilities. *J.Mech.Phys.Sol.*, 44:1237–1253, 1996. doi:10.1016/0022-5096(96)00032-4.

V. Tvergaard and A. Needleman. Analysis of the cup-cone fracture in a round tensile bar. *Acta metall.*, 32:157–169, 1984. doi:10.1016/0001-6160(84)90213-X.

A.J. Urbański. Unified, finite element based approach to the problem of homogenisation of structural members with periodic microstructure. In W. Wunderlich, editor, *Solids, Structures and Coupled Problems in Engineering*, Munich, 1999. TU München.

S. Vajjhala, A.M. Kraynik, and L.J. Gibson. A cellular solid model for modulus reduction due to resorption of trabeculae in bone. *J.Biomech.Engng.*, 122:511–515, 2000. doi:10.1115/1.1289996.

E. van der Giessen and V. Tvergaard. Development of final creep failure in polycrystalline aggregates. *Acta metall.mater.*, 42:952–973, 1994. doi:10.1016/0956-7151(94)90290-9.

E. van der Giessen, P.A. Schultz, N. Bertin, V.V. Bulatov, W. Cai, G. Csányi, S.M. Foiles, M.G.D. Geers, C. González, M. Hütter, W.K. Kim, D.M. Kochmann, J. LLorca, A.E. Mattson, J. Rottler, S. Shluger, R.B. Sills, I. Steinbach, A. Strachan, and Tadmor E.B. Roadmap on multiscale materials modeling. *Model.Simul.Mater.Sci.Engng.*, 42:043001, 2020. doi:10.1088/1361-651X/ab7150.

B. van Rietbergen, R. Müller, D. Ulrich, P. Rüegsegger, and R. Huiskes. Tissue stresses and strain in trabeculae of a canine proximal femur can be quantified from computer reconstructions. *J.Biomech.*, 32:165–173, 1999. doi:10.1016/S0021-9290(98)00150-X.

K. Váradi, Z. Néder, K. Friedrich, and J. Flöck. Finite-element analysis of a polymer composite subjected to ball indentation. *Compos.Sci.Technol.*, 59:271–281, 1999. doi:10.1016/S0266-3538(98)00066-9.

T.J. Vaughan and C.T. McCarthy. A combined experimental–numerical approach for generating statistically equivalent fibre distributions for high strength laminated composite materials. *Compos.Sci.Technol.*, 70:291–297, 2010. doi:10.1016/j.compscitech.2009.10.020.

F. Vazeille and L. Laberge Lebel. Envelope enrichment method for homogenization of non-periodic structures. *Compos.Struct.*, 329:117819, 2024. doi:10.1016/j.compstruct.2023.117819.

A.S. Viglin. A quantitative measure of the texture of a polycrystalline material–texture function. *Sov.Phys.Solid State*, 2:2195–2207, 1961.

E.N. Vilchevskaya, V.I. Kushch, M. Kachanov, and I. Sevostianov. Effective properties of periodic composites: Irrelevance of one particle homogenization techniques. *Mech.Mater.*, 159:103918, 2021. doi:10.1016/j.mechmat.2021.103918.

W. Voigt. Über die Beziehung zwischen den beiden Elasticitäts-Constanten isotroper Körper. *Ann.Phys.*, 38:573–587, 1889. doi:10.1002/andp.18892741206.

W.K. Vonach. *A General Solution to the Wrinkling Problem of Sandwiches*. Reihe 18, Nr. 268. VDI–Verlag, Düsseldorf, 2001. ISBN 3-183-26818-3.

K. Wakashima, H. Tsukamoto, and B.H. Choi. Elastic and thermoelastic properties of metal matrix composites with discontinuous fibers or particles: Theoretical guidelines toward materials tailoring. In *The Korea–Japan Metals Symposium on Composite Materials*, pages 102–115, Seoul, 1988. The Korean Institute of Metals.

L.J. Walpole. On bounds for the overall elastic moduli of inhomogeneous systems — I. *J.Mech.Phys.Sol.*, 14:151–162, 1966. doi:10.1016/0022-5096(66)90035-4.

J. Wang, J.H. Andreasen, and B.L. Karihaloo. The solution of an inhomogeneity in a finite plane region and its application to composite materials. *Compos.Sci.Technol.*, 60:75–82, 2000. doi:10.1016/S0266-3538(99)00103-7.

R. Wang, L. Zhang, D. Hu, C. Liu, X. Shen, C. Cho, and B. Li. A novel approach to impose periodic boundary condition on braided composite RVE model based on RPIM. *Compos.Struct.*, 163:77–88, 2017. doi:0.1016/j.compstruct.2016.12.032.

X. Wang, Z. Guan, S. Du, G. Han, and M. Zhang. A long-range force based random method for generating anisotropic 2D fiber arrangement statistically equivalent to real composites. *Compos.Sci.Technol.*, 180:33–43, 2019. doi:10.1016/j.compscitech.2019.05.013.

Y.C. Wang and Z.M. Huang. Bridging tensor with an imperfect interphase. *Eur.J.Mech. A/Solids*, 56:73–91, 2016. doi:10.1016/j.euromechsol.2015.10.006.

Y.C. Wang and Z.M. Huang. Analytical micromechanics models for elastoplastic behavior of long fibrous composites: A critical review and comparative study. *Materials*, 11: ma11101919, 2018. doi:10.3390/ma11101919.

Y.U. Wang, Y.M. Jin, and A.G. Khachaturyan. Phase field microelasticity theory and modelling of elastically and structurally inhomogeneous solid. *J.Appl.Phys.*, 92:1351–1360, 2002. doi:10.1063/1.1492859.

Z. Wang, R.J. Oelkers, K.C. Lee, and F.T. Fisher. Annular coated inclusion model and applications for polymer nancomposites — Part II: Cylindrical inclusions. *Mech.Mater.*, 101:59–60, 2016. doi:10.1016/j.mechmat.2016.07.005.

Z.Y. Wang, H.T. Zhang, and Y.T. Chou. Characteristics of the elastic field of a rigid line inhomogeneity. *J.Appl.Mech.*, 52:818–822, 1985. doi:10.1115/1.3169152.

W.E. Warren and A.M. Kraynik. The nonlinear elastic behavior of open-cell foams. *J.Appl.Mech.*, 58:376–381, 1991. doi:10.1115/1.2897196.

D.F. Watt, X.Q. Xu, and D.J. Lloyd. Effects of particle morphology and spacing on the strain fields in a plastically deforming matrix. *Acta mater.*, 44:789–799, 1996. doi:10.1016/1359-6454(95)00209-X.

D. Weaire and R. Phelan. A counter-example to Kelvin's conjecture on minimal surfaces. *Phil.Mag.Lett.*, 69:107–110, 1994. doi:10.1080/09500839408241577.

G. Wei and S.F. Edwards. Effective elastic properties of composites of ellipsoids (I). Nearly spherical inclusions. *Physica A*, 264:388–403, 1999. doi:10.1016/S0378-4371(98)00465-8.

D. Weidt and L. Figiel. Finite strain compressive behavior of CNT/epoxy nanocomposites: 2D versus 3D RVE-based modelling. *Comput.Mater.Sci.*, 82:298–309, 2014. doi:10.1016/j.commatsci.2013.10.001.

E. Weissenbek. *Finite Element Modelling of Discontinuously Reinforced Metal Matrix Composites*. Reihe 18, Nr. 164. VDI–Verlag, Düsseldorf, 1994. ISBN 3-18-316418-3.

E. Weissenbek, H.J. Böhm, and F.G. Rammerstorfer. Micromechanical investigations of arrangement effects in particle reinforced metal matrix composites. *Comput.Mater.Sci.*, 3:263–278, 1994. doi:10.1016/0927-0256(94)90141-4.

E. Weissenbek, H.E. Pettermann, and S. Suresh. Elasto-plastic deformation of compositionally graded metal-ceramic composites. *Acta mater.*, 45:3401–3417, 1997. doi:10.1016/S1359-6454(96)00403-X.

E.W. Weisstein. Sphere packing, 2000. URL `http://mathworld.wolfram.com/SpherePacking.html`.

G.J. Weng. The theoretical connection between Mori–Tanaka theory and the Hashin–Shtrikman–Walpole bounds. *Int.J.Engng.Sci.*, 28:1111–1120, 1990. doi:10.1016/0020-7225(90)90111-U.

O. Wiener. Die Theorie des Mischkörpers für das Feld der stationären Strömung. *Abh.Math-Phys.Kl.Königl.Sächs.Ges.Wiss.*, 32:509–604, 1912.

J.R. Willis. The overall response of nonlinear composite media. *Eur.J.Mech. A/Solids*, 19: S165–S184, 2000.

J.R. Willis. Bounds and self-consistent estimates for the overall moduli of anisotropic composites. *J.Mech.Phys.Sol.*, 25:185–202, 1977. doi:10.1016/0022-5096(77)90022-9.

J. Wippler, S. Fünfschilling, F. Fritzen, T. Böhlke, and M.F. Hoffmann. Homogenization of the thermoelastic properties of silicon nitride. *Acta mater.*, 59:6029–6038, 2011. doi:10.1016/j.actamat.2011.06.011.

P.J. Withers. The determination of the elastic field of an ellipsoidal inclusion in a transversely isotropic medium, and its relevance to composite materials. *Phil.Mag.*, A59: 759–781, 1989. doi:10.1080/01418618908209819.

P.J. Withers, W.M. Stobbs, and O.B. Pedersen. The application of the Eshelby method of internal stress determination to short fibre metal matrix composites. *Acta metall.*, 37: 3061–3084, 1989. doi:10.1016/0001-6160(89)90341-6.

L.A. Wittig and D.H. Allen. Modeling the effect of oxidation on damage in SiC/Ti-15-3 metal matrix composites. *J.Engng.Mater.Technol.*, 116:421–427, 1994. doi:10.1115/1.2904308.

L. Wu, L. Noels, L. Adam, and I. Doghri. A combined incremental–secant mean-field homogenization scheme with per-phase residual strains for elasto-plastic composites. *Int.J.Plast.*, 51:80–102, 2013. doi:10.1016/j.ijplas.2013.06.006.

T.T. Wu. The effect of inclusion shape on the elastic moduli of a two-phase material. *Int.J.Sol.Struct.*, 2:1–8, 1966. doi:10.1016/0020-7683(66)90002-3.

J. Wulf, T. Steinkopff, and H. Fischmeister. FE-simulation of crack paths in the real microstructure of an Al(6061)/SiC composite. *Acta mater.*, 44:1765–1779, 1996. doi:10.1016/1359-6454(95)00328-2.

Z. Xia, Y. Zhang, and F. Ellyin. A unified periodical boundary conditions for representative volume elements of composites and applications. *Int.J.Sol.Struct.*, 40:1907–1921, 2003. doi:10.1016/S1359-6454(00)00317-7.

Z.H. Xia, W.A. Curtin, and P.W.M. Peters. Multiscale modeling of failure in metal matrix composites. *Acta mater.*, 49:273–287, 2001. doi:10.1016/S1359-6454(00)00317-7.

F.X. Xu and X. Chen. Stochastic homogenization of random elastic multi-phase composites and size quantification of representative volume element. *Mech.Mater.*, 41:174–186, 2009. doi:10.1016/j.mechmat.2008.09.002.

Q.S. Yang, L. Tang, and H.R. Chen. Self-consistent finite element method: A new method of predicting effective properties of inclusion media. *Fin.Elem.Anal.Design*, 17:247–257, 1994. doi:10.1016/0168-874X(94)90001-9.

Q.S. Yang, X. Tao, and H. Yang. A stepping scheme for predicting effective properties of the multi-inclusion composites. *Int.J.Engng.Sci.*, 45:997–1006, 2007. doi:10.1016/j.ijengsci.2007.07.005.

Y.M. Yi, S.H. Park, and S.K. Youn. Asymptotic homogenization of viscoelastic composites with periodic microstructures. *Int.J.Sol.Struct.*, 35:2039–2055, 1998. doi:10.1016/S0020-7683(97)00166-2.

P.G. Young, T.B.H. Beresford-West, S.R.L. Coward, B. Notarberardino, B. Walker, and A. Abdul-Aziz. An efficient approach to converting three-dimensional image data into highly accurate computational models. *Phil.Trans.Roy.Soc.London*, A366:3155–3173, 2008. doi:10.1098/rsta.2008.0090.

S. Youssef, E. Maire, and R. Gaertner. Finite element modelling of the actual structure of cellular materials determined by X-ray tomography. *Acta mater.*, 53:719–730, 2005. doi:10.1016/j.actamat.2004.10.024.

W. Yu and T. Tang. Variational asymptotic method for unit cell homogenization of periodically heterogeneous materials. *Int.J.Sol.Struct.*, 44:3738–3755, 2007. doi:10.1016/j.ijsolstr.2006.10.020.

J. Yvonnet. *Computational Homogenization of Heterogeneous Materials with Finite Elements*. Springer-Verlag, Cham, 2019. ISBN 978-3-030-18382-0.

J. Zangenberg and P. Brøndsted. Quantitative study on the statistical properties of fibre architecture of genuine and numerical composite microstructures. *Composites A*, 47: 124–134, 2013. doi:10.1016/j.compositesa.2012.11.015.

A. Zaoui. Plasticité: Approches en champ moyen. In M. Bornert, T. Bretheau, and P. Gilormini, editors, *Homogénéisation en mécanique des matériaux 2. Comportements non linéaires et problèmes ouverts*, pages 17–44, Paris, 2001. Editions Hermès.

A. Zaoui. Continuum micromechanics: Survey. *J.Engng.Mech.*, 128:808–816, 2002. doi:10.1061/(ASCE)0733-9399(2002)128:8(808).

J. Zeman. *Analysis of Composite Materials with Random Microstructure*. PhD thesis, Czech Technical University, Prague, 2003.

J. Zeman and M. Šejnoha. Numerical evaluation of effective elastic properties of graphite fiber tow impregnated by polymer matrix. *J.Mech.Phys.Sol.*, 49:69–90, 2001. doi:10.1016/S0022-5096(00)00027-2.

J. Zeman and M. Šejnoha. From random microstructures to representative volume elements. *Modell.Simul.Mater.Sci.Engng.*, 15:S325–S335, 2007. doi:10.1088/0965-0393/15/4/S01.

C.M. Zener. *Elasticity and Anelasticity of Metals*. University of Chicago Press, Chicago, IL, 1948. ISBN 0-226-98054-5.

H. Zhang, P. Sheng, J. Zhang, and Z. Ji. Realistic 3D modeling of concrete composites with randomly distributed aggregates by using aggregate expansion method. *Constr.Buildg.Mater.*, 225:927–240, 2019. doi:10.1016/j.conbuildmat.2019.07.190.

J. Zhang and M. Ostoja-Starzewski. Mesoscale bounds in viscoelasticity of random composites. *Mech.Res.Comm.*, 68:98–104, 2015. doi:10.1016/j.mechrescom.2015.05.005.

R. Zhang and R. Guo. Modeling of progressive debonding of interphase–matrix interface cracks in particle reinforced composites using VCFEM composites. *Engng.Fract.Mech.*, 248:107734, 2021. doi:10.1016/j.engfracmech.2021.107734.

X.X. Zhang, B.L. Xiao, H. Andrä, and Z.Y. Ma. Homogenization of the average thermo-elastoplastic properties of particle reinforced metal matrix composites: The minimum representative volume element. *Compos.Struct.*, 113:459–4681, 2014. doi:10.1016/j.compstruct.2014.03.048.

Q.S. Zheng, Z.H. Zhao, and D.X. Du. Irreducible structure, symmetry and average of Eshelby's tensor fields in isotropic elasticity. *J.Mech.Phys.Sol.*, 54:368–383, 2006. doi:10.1016/j.jmps.2005.08.012.

S.J. Zhou and W.A. Curtin. Failure of fiber composites: A lattice Green function model. *Acta metall.mater.*, 43:3093–3104, 1995. doi:10.1016/0956-7151(95)00003-E.

H.X. Zhu, J.F. Knott, and N.J. Mills. Analysis of the elastic properties of open-cell foams with tetrakaidecahedral cells. *J.Mech.Phys.Sol.*, 45:319–343, 1997. doi:10.1016/S0022-5096(96)00090-7.

R.W. Zimmerman. Hashin–Shtrikman bounds on the Poisson ratio of a composite material. *Mech.Res.Comm.*, 19:563–569, 1992. doi:10.1016/0093-6413(92)90085-O.

T.I. Zohdi. Constrained inverse formulations in random material design. *Comput.Meth.Appl.Mech.Engng.*, 192:3179–3194, 2003. doi:10.1016/S0045-7825(03)00345-1.

T.I. Zohdi and P. Wriggers. A model for simulating the deterioration of structural-scale material responses of microheterogeneous solids. *Comput.Meth.Appl.Mech.Engng.*, 190: 2803–2823, 2001. doi:10.1016/S0045-7825(00)00367-4.

T.I. Zohdi, J.T. Oden, and G.J. Rodin. Hierarchical modeling of heterogeneous bodies. *Comput.Meth.Appl.Mech.Engng.*, 138:273–289, 1996. doi:10.1016/S0045-7825(96)01106-1.